UNIVERSIDAD DE CHILE
FACULTAD DE CIENCIAS FÍSICAS Y MATEMÁTICAS
DEPARTAMENTO DE FÍSICA

DISSIPATIVE MAGNETIZATION TEXTURES INDUCED BY SPIN-TRANSFER TORQUES AND ALTERNATING MAGNETIC FIELDS

TESIS PARA OPTAR AL GRADO DE DOCTOR EN CIENCIAS, MENCIÓN FÍSICA

ALEJANDRO OSVALDO LEÓN VEGA

PROFESOR GUÍA:
MARCEL G. CLERC GAVILÁN

MIEMBROS DE LA COMISIÓN:
REMBERT DUINE
DORA ALTBIR DRULLINSKY
ALEJANDRO VALDIVIA HEPP
ÁLVARO NÚÑEZ VÁSQUEZ

SANTIAGO DE CHILE
2016

DISSIPATIVE MAGNETIZATION TEXTURES INDUCED BY SPIN-TRANSFER TORQUES AND ALTERNATING MAGNETIC FIELDS

Los materiales ferromagnéticos a escala nanométrica pueden ser manipulados mediante torques por transferencia de espín y/o campos magnéticos oscilatorios. El torque por transferencia de espín es el resultado de la interacción entre los espines de un material ferromagnético y los espines de una corriente eléctrica que fluye por él. El objetivo de la presente tesis es investigar las dinámicas de la magnetización inducidas mediante torques por transferencia de espín y campos magnéticos oscilatorios.

En el primer capítulo se exponen la motivación del presente estudio, los objetivos y los principales resultados. Los capítulos dos y tres de este trabajo introducen la descripción micromagnética de la magnetización y los conceptos y métodos de la física no lineal, respectivamente. En el cuarto capítulo se motivan y discuten de manera general los resultados de la presente investigación, mientras que el quinto capítulo presenta las conclusiones generales de la tesis. Los cinco capítulos siguientes (apéndices A, B, C, D y E) presentan los detalles de nuestros resultados, en formato de publicación. En el Capítulo A, se describen estados tipo patrón de la magnetización inducidos mediante torques por transferencia de espín. Estas texturas, periódicas en el espacio, son descritas mediante ecuaciones para las envolventes de los modos críticos. En el Capítulo B, se estudia la equivalencia entre el efecto de torque por transferencia de espín y los sistemas macroscópicos con inyección de energía modulada en el tiempo. En particular se demuestra que un ferromagneto forzado mediante torques por transferencia de espín exhibe los mismos estados que un medio ferromagnético rotado mecánicamente. Empleando esta equivalencia, se logra predecir texturas tales como patrones y estados localizados. En el Capítulo C, se analizan los efectos de una corriente de espín-polarizado alternante en la dinámica de la magnetización. Como resultado de este estudio, se demuestra analítica y numéricamente la existencia de una resonancia sub-armónica, y se comprueba numéricamente la emergencia de estados similares a ondas de Faraday y solitones. En el Capítulo D, se estudian sistemas macroscópicos en presencia de un forzamiento que oscila en el tiempo. Mediante un modelo fenomenológico para la envolvente de las oscilaciones, se predice y caracteriza un nuevo tipo de estado fuera del equilibrio, este es un pulso que se propaga sobre fondos periódicos. Estas soluciones se caracterizan por un incremento localizado y viajero de la amplitud del estado patrón que las soporta. Se determina que el mecanismo mediante el cual emergen los pulsos es una inestabilidad de Andronov-Hopf sub-crítica. Estos comportamientos son estudiados en un hilo magnético forzado por un campo magnético que oscila en el tiempo. En el Capítulo E, se estudian oscilaciones de patrones bidimensionales, inducidas mediante torques por transferencia de espín. Se comprueba numéricamente que los mecanismos que originan las oscilaciones son una bifurcación homoclina y una inestabilidad de Andronov-Hopf. Finalmente, el Apéndice F presenta dos actas de conferencia con resultados complementarios desarrollados en la tesis.

DISSIPATIVE MAGNETIZATION TEXTURES INDUCED BY SPIN-TRANSFER TORQUES AND ALTERNATING MAGNETIC FIELDS

Spin-transfer torques and oscillatory magnetic fields permit manipulating ferromagnetic materials at nanoscales. The spin-transfer effect is based on the interaction between the spins of a ferromagnetic material and the spins of an electric current flowing through it. The aim of this thesis is to investigate magnetization dynamics induced by spin-transfer torques and oscillatory magnetic fields. In particular we study the formation of dissipative structures, that is, states or dynamical behaviors of dissipative systems that can attract initial conditions in phase space.

In the first Chapter we present the motivation, objectives and results of this thesis. Chapters two and three introduce the micromagnetic description of magnetization and the concepts and methods of nonlinear physics, respectively. In the fourth Chapter we motivate and discuss our results in general terms, while we present our general conclusions in Chapter five.

The appendix Chapters A, B, C, D and E present in detail the results of this thesis in publication format. Chapter A describes magnetic pattern states driven by spin-transfer torques. Patterns are spatially periodic textures, and they are usually described by equations for the spatial mode envelopes. In Chapter B, we studied the equivalence between spin-transfer torque driven nanomagnets and macroscopic systems with time dependent injections of energy. In particular, we demonstrated that ferromagnets driven by spin-transfer torques exhibit the same type of states as a mechanically rotated magnetic film. This equivalence permitted us to predict a vast variety of magnetic textures such as patterns and localized states. In Chapter C we analyzed the magnetization dynamics for the case of alternating spin-polarized electric currents. As a result of this study, the existence of a sub-harmonic resonance was demonstrated. Numerically, Faraday-like waves and solitons were observed. In Chapter D, we studied parametrically driven one-dimensional media. Based on a phenomenological model for the oscillation envelope, we predicted and characterized a new type of state, namely a traveling pulse on a periodic background. This solution is characterized by a localized increment of the pattern amplitude. We elucidated the formation mechanism of this state, which is a subcritical Andronov-Hopf instability of a spatially periodic texture. These behaviors are exemplified on a ferromagnetic wire driven by an alternating magnetic field. In Chapter E, we studied oscillatory two-dimensional patterns induced by spin-transfer torques, which emerge through a homoclinic bifurcation and an Andronov-Hopf instability.

Finally, Appendix F presents two conference proceedings.

Dedicado al amor de mi vida, a mi maravillosa esposa Ana Belén Castañeda Jara, por hacerme feliz cada día.

Te amo Belencita.

Agradecimientos

Quisiera comenzar agradeciendo al director de esta tesis, profesor Marcel Clerc, por los innumerables esfuerzos invertidos en mi formación. Gracias Marcel por haberme mostrado la belleza de las ideas simples, el poder que otorgan la constancia y la perseverancia, y el valor de la creatividad. Estaré profundamente agradecido de todo lo que aprendí de Marcel durante estos cuatro años.

Gracias a mi papá por ser mi primer y gran ejemplo a seguir, por inculcarme la rigurosidad, la pasión por los estudios, por la justicia, pero por sobre todo, el amor por la familia. Te amo papá. Gracias también a mi mamá, por ser mi amiga y consejera, por comprenderme y apoyarme incondicionalmente, en particular a lo largo de esta tesis. Gracias mamá por ser un manantial de paz y alegría. Te amo mamá. Gracias a mis hermanos Pipe, Tobi y Mati, son mis mejores amigos; a ustedes gracias por cada momento que disfrutamos juntos. Los amo.

Gracias también a mi Belencita, que además de ser mi señora y mi compañera de aventuras, me enseñó a superar las frustraciones y a ser feliz. Gracias por estar presente en cada idea, cálculo y simulación. Todo mi trabajo va dedicado a ti mi Belencita. Gracias también a mis suegros y mi cuñada Anais, por acogerme como uno más de su bello hogar; los quiero.

Gracias al profesor Álvaro Núñez, su visión fresca y creativa de la física fue un estímulo constante en mi trabajo de tesis, y sus consejos resultaron siempre asertivos. Gracias al profesor David Laroze, que me enseñó las virtudes del trabajo en equipo, las ventajas de las simulaciones numéricas de alta precisión y la belleza del norte de Chile. Gracias al profesor Saliya Coulibaly, quien me recibió en dos oportunidades en su equipo de investigación en Francia y enseñó poderosas técnicas computacionales.

Gracias de corazón a mi mejor amiga, Dani Mancilla, por su invaluable apoyo a lo largo de esta tesis, y por ser una sabia consejera y una cómplice alegre. Recordaré con nostalgia nuestras conversaciones sobre física y pedagogía, siempre con café en mano. Te quiero Dani. Gracias a mis amigos Vincent y su señora Nazek, por su apoyo durante esta tesis, son excelentes científicos, y sobre todo excelentes personas. Los quiero amigos. Agradezco a mis amigos Ulises y Diego, por las enriquecedoras conversaciones sobre matemáticas, física y biología. Gracias a Jaime (Chuki) por el apoyo incondicional y por enseñarme a valorar los problemas en su justa medida. Por todos los buenos momentos y el apoyo recibido durante mi tesis, agradezco a Nicolas Perinet, Mario Wilson, Mónica García, Estefanía Vidal, Ignacio Bordeu, Camila Horvath, Ana Cabanas y Roberto Troncoso.

Finally, I would like to thank the evaluation committee for their time and dedication.

x

Tabla de contenido

Capítulo 1

Introduction

The possibility to couple and uncouple degrees of freedom associated to different physical properties has always attracted the attention of physicists, because it permits developing a more general understanding of interactions in nature and also because it allows generating useful technological applications. Some examples are the transfer of momentum from electromagnetic fields to mechanical objects (radiation pressure [31]), transfer of energy from a magnetic medium to its crystal lattice (magnetization relaxation [72]), electric field induced by friction (materials charging by rubbing [31]), among others. More recent appealing examples in nano-magnetism include *spintronics* [53] or spin electronics, a recent branch of science that studies and exploits the interaction between spins of conduction electrons and of ferromagnetic media; *spin-caloritronics* [5], where electric charge, spin, energy and entropy interact; *spin-currents induced by mechanical rotations* [3, 56]; *anti-ferromagnetic spintronics* [61] which is similar to spintronics but uses anti-ferromagnetic media as the building blocks for devices; and the interaction between *topological magnetization structures* [38], such as skyrmions, and spins of electric currents. Hence, this is an exciting time for studying non-equilibrium magnetism at nano-scales, for explaining and predicting novel physical effects emerging from the interaction of mechanical, electrical and magnetic degrees of freedom of electrons, and for proposing fresh technological applications of all the above mentioned effects.

The *giant-magneto-resistance* [72] and the *spin-transfer torque* [74, 6] are two remarkable spintronic effects. When an electric current traverses a multilayer structure composed by two or more ferromagentic materials, the electric resistance depends on the relative orientation of the magnetizations, this phenomenon is the giant-magneto resistance. On the other hand, a spin-transfer torque appears when an electric current transfers spin-angular momentum to a ferromagnet. Understanding spin-transfer torques involves challenges from both the microscopic and the macroscopic approaches, due to the highly nonlinear magnetization dynamics that emerges as the result of collective quantum mechanical interactions. Indeed, spin-transfer torques generate microwave magnetic oscillations [41, 73, 46], magnetization switching [46], chaos [7], stationary smooth textures [82, 42, 49], vortex lattices [81, 29], localized states [51, 48], and domain walls movement [39]. Moreover, the technological applications promised by the spin-transfer torque effect are also appealing [70]. For instance it is possible to use the spin-transfer torque to write information in magnetic random access

memories, MRAM, and the generation of spin-waves with gigahertz frequencies to transmit information.

Following the widespread goal of coupling different types of degrees of freedom and making analogies between different physical systems, in this thesis we study magnetization dynamics using the concepts and tools of Nonlinear Physics, which permits us to find similarities between systems governed by different equations, such as vibrated fluids, driven granular media, and forced optical systems [25]. In this context, we found that the mathematical form of the spin-transfer torque is equivalent to the pseudo torque that appears when a rotating reference frame is considered. Using this idea, we conceived an equivalence between macroscopic systems driven by time-dependent forces and spintronics, even if the electric current is continuous. This equivalence implies that under some reasonable approximations both types of systems obey the same equations and exhibit the same type of dynamical behaviors. Furthermore, the equivalence predicts localized states, usually known as *dissipative solitons*, and spatially periodic textures or *patterns*. Figure 1.1 shows the magnetization profiles of these two states. We also investigate magnetic media forced by alternating magnetic fields and spin-transfer torques that oscillate on time, and we compare the dynamical responses of these systems.

Next section presents in more detail the aims of this research work.

1.1.   Objectives and main results of the thesis

The general goal of this thesis is to study the formation of dissipative states, such as spatially periodic textures and localized states, in ferromagnetic media driven by spin-transfer torques and alternating magnetic fields. In particular:

(A) To study the formation of magnetization textures induced by continuous spin-polarized currents—spin transfer torques—. As a result of this analysis, we found and characterized analytically a wide variety of states known as *superlattices*, which are textures composed by several spatial modes [see Fig. 1.1(b)].

(B) To study the relation between spin-transfer torque induced textures and dynamics exhibited by other non equilibrium systems. As a result of this work, we found an equivalence between macroscopic systems with a time-dependent forcing and the ferromagnetic materials driven by spin-transfer torques. Figure 1.1(a) shows a magnetic dissipative soliton, which is one of the predictions resulting from the equivalence.

(C) To study the formation of textures when the spin-polarized current oscillates in time. We found the conditions of the sub-harmonic resonance known as *parametric instability*, and we obtained a reduced model for the magnetization excitation which permits us to predict localized states and textures.

(D) To analyze instabilities of magnetization patterns in magnetic wires driven by alternating magnetic fields. As a result of this study, we found and characterized traveling pulses on a periodic background. This state is shown in Fig. 1.1(c). We also demonstrated that the pulses are a general phenomenon of systems with a time-dependent injection of energy.
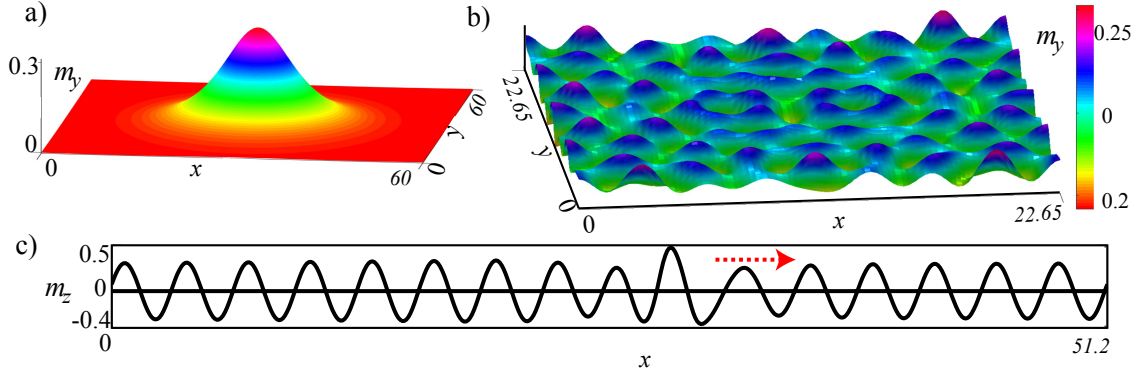
Figura 1.1: Magnetization textures induced by spin-transfer torques and oscillatory magnetic fields. (a) *Soliton* are localized excitations. (b) *Pattern* are spatially periodic textures. (c) *Traveling pulses on periodic backgrounds* are localized increments of a wave envelope.

(E) To study the dissipative structures that emerge when the stationary two-dimensional patterns shown in Fig. 1.1(b) become unstable. As result of this study, we found oscillatory patterns that alternate their shape and we revealed the mechanisms that originate such states, namely an Andronov-Hopf instability and a homoclinic bifurcation.

1.2.   Organization of the document

The thesis is organized as follows. Chapter 2 describes the magnetization dynamics at nano-scales. We present a brief introduction to ferromagnetic media from the classical and continuous approach known as *micromagnetism*, which describes the behavior of the averaged magnetic moment density, that is, the magnetization. This chapter also introduces the Landau-Lifshitz-Gilbert equation—a paradigmatic model that described the temporal evolution of the magnetization—, time-dependent forcing and the spin-transfer effect.

In Chapter 3 we introduce the concepts and methods of nonlinear physics that permitted us to analyze the Landau-Lifshitz-Gilbert equation. In particular we describe commonly observed bifurcations—qualitative changes in the phase space—and the amplitude equation method that reduces the number of degrees of freedom of the system under study.

The general discussions and conclusions of the results of the thesis are presented in chapters 4 and 5, respectively.

Appendix Chapters A, B, C, D, and E present the details of our results. Each chapter is devoted to one of the research objectives described in the previous section.

Appendix F presents two conference proceedings.

Capítulo 2

Magnetization Dynamics at nanoscales

Ferromagnetic materials at nano-scales are described in the classical continuum approach—kown as micromagnetic theory—by the magnetic moment density *magnetization* $\mathbf{M}$ [22]

$$\mathbf{M} \equiv \frac{\sum_j \mathbf{S}_j}{\sum_j \Delta V_j},$$

where $\mathbf{S}_j$ represents the averaged magnetic moment in a region or domain of volume ΔV_j. The sum is over all the magnetic domains. In the continuum approach, the spatial variations of the magnetization field $\mathbf{M}$ must be slow, that is, the magnetization is constant at the scales of a few atoms or molecules, and the average magnetic moment $d\mathbf{S}$ in a volume dV can be approximated by $d\mathbf{S} = \mathbf{M}dV$. For spatial scales smaller than the *exchange length*, l_{ex}, which is a material property and it usually takes values between $3-7$ nm, the magnetization can be assumed constant [22]. The exchange length is a relevant quantity in magnetism and its precise definition will be given later on this chapter.

In thermodynamic equilibrium, the magnetization is stationary and its spatial configuration depends on material properties and applied magnetic fields [57]. In the next subsection we review the dominant physical effects that determine the equilibrium magnetization.

2.1. Magnetic Energy

Ferromagnetic Exchange.- At a quantum mechanical level, neighbor spins $\hat{s}_k$ interact through an *exchange* Hamiltonian of the form [72]

$$\hat{H}_{ex} = -2J\hat{s}_1 \cdot \hat{s}_2,$$

where J is the exchange constant, and it depends on the overlap of spatial wave function of electrons. One the one hand, if the exchange constant is positive, then the minimum energy is obtained for spins pointing in the same direction. This is the case of ferromagnetic media, where spins tend to align and a net magnetic momentum appears. The macroscopic

description of a system of magnetic moments is conducted using the magnetization $\mathbf{M}$. On the other hand, when J is negative, the minimum energy configuration is obtained when the spins are antiparallel. In that case the material is an antiferromagnet, and it has zero magnetization. Along this work, we focus only on ferromagnetic media.

The magnetization is result of quantum mechanical interactions. However, a classical Hamiltonian description can be proposed after replacing the spin operators $\hat{s}_k$ by classical magnetic moments $\mathbf{S}_k$ of magnitude S. We consider a simple cubic lattice of localized magnetic moments. The position $\mathbf{r_k} \equiv \mathbf{r}(k)$ of each magnetic moment $\mathbf{S}_k$ is labeled by the discrete index k. Then, we have

$$H_{ex} = -J \sum_k \sum_j \mathbf{S}_k \cdot \mathbf{S}_j,$$

where the discrete index j labels the nearest-neighbors spins around $\mathbf{S}_k$.

$$H_{ex} = -J \sum_k \sum_j (\mathbf{S}_k \cdot \mathbf{S}_j + \frac{1}{2}\mathbf{S}_k^2 - \frac{1}{2}\mathbf{S}_k^2 + \frac{1}{2}\mathbf{S}_j^2 - \frac{1}{2}\mathbf{S}_j^2) = \frac{J}{2} \sum_k \sum_j (\mathbf{S}_k - \mathbf{S}_j)^2 + H_0,$$

where $H_0 = -(J/2) \sum_k \sum_j [\mathbf{S}_k^2 + \mathbf{S}_j^2]$. Using a Taylor series $\mathbf{S}_j \approx \mathbf{S}_k + a(\mathbf{e_{j,k}} \cdot \nabla)\mathbf{S}_k$, where the unit vector $\mathbf{e_{j,k}} \equiv (\mathbf{r_j} - \mathbf{r_k})/a$ accounts for the direction between neighbor spins, and the lattice constant a is the distance between nearest-neighbors spins. Then,

$$H_{ex} = \frac{Ja^2}{2} \sum_k \sum_j [(\mathbf{e_{j,k}} \cdot \nabla)\mathbf{S}_k]^2 + H_0,$$

Let us write the magnetic momentum in terms of the unit vector $\mathbf{s}$, that is $\mathbf{S}_k = S\mathbf{s}_k = S(s_{x,k}\mathbf{e_x} + s_{y,k}\mathbf{e_y} + s_{z,k}\mathbf{e_z})$ in Cartesian coordinates, where $\{\mathbf{e_x}, \mathbf{e_y}, \mathbf{e_z}\}$ are the unit vectors along the $\{x, y, z\}$ axes. Summing over the j index yields

$$H_{ex} = Ja^2 S^2 \sum_k \left[(\nabla s_{x,k})^2 + (\nabla s_{y,k})^2 + (\nabla s_{z,k})^2\right] + H_0.$$

Considering the continuum limit $\sum_k \sim \iiint$, $a^3 \sim dV$ and $\mathbf{s}_k \sim \mathbf{s}(\mathbf{r})$, where dV is the volume element. Then we have

$$H_{ex} = \iiint_V \frac{JS^2}{a} \left[(\nabla s_x)^2 + (\nabla s_y)^2 + (\nabla s_z)^2\right] dV + H_0,$$

eliminating the constant H_0, which is proportional to the volume of the ferromagnet V and the spin magnitude square, that is $H_0 \sim VS^2$. We obtain [57]

$$H_{ex} = \iiint_V \frac{A}{M_s^2}|\nabla \mathbf{M}|^2,$$

where the integration domain is the ferromagnet and $\mathbf{M} = M_s\mathbf{s}$ is the magnetization. The magnetization norm $M_s \equiv |\mathbf{M}|$ is the *saturation magnetization*. In the continuum limit the ferromagnetic exchange favors smooth textures. Furthermore, at nano-scales the exchange interaction is dominant and favors the parallel orientation of spins. Then the exchange interaction only permits rotation of the magnetization, while its norm $|\mathbf{M}| = M_s$ is constant [57].

For instance, for Iron, Cobalt and Nickel the values [1] of $\mu_0 M_s$, where μ_0 is the vacuum permeability, are $\mu_0 M_s = 2{,}16$ T, $\mu_0 M_s = 1{,}82$ T and $\mu_0 M_s = 0{,}62$ T [22, 8], respectively. The norm conservation permits one to study the magnetization in different representations such as spherical or stereographic coordinates. Moreover, $|\nabla \mathbf{M}|^2 \equiv (\nabla M_x)^2 + (\nabla M_y)^2 + (\nabla M_z)^2$, and $\{M_x, M_y, M_z\}$ are the Cartesian components of the vector $\mathbf{M}$. The parameter $A \approx cJS^2/a$ is the *exchange stiffness constant* [22, 8]. The parameter c is of order one, and it accounts for the details of the lattice [22, 8]. In the case of the simple cubic lattice studied here, we have $c = 1$. For example, for Iron, Cobalt and Nickel [8] $A \approx 1{,}5 \ 10^{-11}$ J/m. This constant permits one to define the exchange length as

$$l_{ex} \equiv \sqrt{\frac{2A}{\mu_0 M_s^2}}.$$

The exchange lengths for Iron, Cobalt and Nickel are 2,8 nm, 3,4 nm, and 9,9 nm [8], respectively.

Zeeman effect.- Another relevant interaction is the Zeeman effect [72], and it couples the magnetization with an external magnetic field $\mathbf{H_0}$ through the Zeeman Hamiltonian, H_z, given by

$$H_z = -\iiint_V \mu_0 \mathbf{H_0} \cdot \mathbf{M},$$

which is minimized when the magnetization points parallel to the external field. Since the magnetization aligns with external magnetic fields, it is posible to manipulate the magnetic state of materials by means of magnetic field pulses. During the last decades, this excitation mechanism has been the key to record information in magnetic memories.

Magnetostatic fields.- Magnetization generates an irrotational magnetic field $\mathbf{H}_D$, usually known as magnetostic or demagnetizing field. This field can be written as the gradient of a scalar potential $\mathbf{H}_D = -\nabla \Phi$, where [22]

$$\Phi(\mathbf{r}) = \frac{1}{4\pi} \int_V \frac{\rho_m(\mathbf{r}')}{|\mathbf{r} - \mathbf{r}'|} dV' + \frac{1}{4\pi} \int_{\partial V} \frac{\sigma_m(\mathbf{r}')}{|\mathbf{r} - \mathbf{r}'|} dS',$$

where $\rho_m \equiv -\nabla \cdot \mathbf{M}$ and $\sigma_m = \mathbf{M} \cdot \mathbf{n_{out}}$ are the the volumetric and surface magnetic density, respectively, and $\mathbf{n_{out}}$ is the outward normal vector at the material surface.

The Hamiltonian H_D that describes the interaction between the magnetization and the magnetostatic field is [57]

$$H_D = -\iiint_V \mu_0 \frac{\mathbf{H}_D \cdot \mathbf{M}}{2}.$$

---

[1] It is usual to multiply the magnetization by the vacuum permeability to obtain units of magnetic field $B = \mu_0 M$, that is, Tesla [T].

When the magnetization close to the sample surfaces is not important, the magnetic medium is usually considered an uniformly magnetized infinite plane. In that case the magnetostatic energy can be simplified to

$$H_D \approx \mu_0 \iiint_V \frac{1}{2} M_z^2,$$

which is a shape anisotropy for the system. This simplification is known as the *thin film approximation*. This is a rough approximation when the surface magnetic density σ_m is non negligible in the lateral borders, that is, when an important part of the magnetization lies on the sample plane. Moreover, several magnetization configuration are far from the uniform limit. However, the use of the simplified form is widespread in literature because it permits one to work with local energy contributions, and therefore analytic calculations and numerical simulations become more accessible.

Magnetocrystalline anisotropies.- Materials are not necessarily isotropic, furthermore, the crystalline structure and the coupling between spin and the spatial part of the wave function usually generate one or more preferred directions for the magnetization. The Hamiltonian used to describe the magnetocrystalline anisotropy depends on the material. However, a very commonly observed type of anisotropy is known as *uniaxial anisotropy*, and at leading order this anisotropy is modeled as [8]

$$H_{ani} = -\mu_0 \iiint_V \frac{\beta}{2} \left(\mathbf{k} \cdot \mathbf{M} \right)^2,$$

where β is an anisotropy constant, and H_{ani} is the Hamiltonian of the uniaxial anisotropy. This energy favors configurations along the unit vector $\mathbf{k}$ when β is positive. In that case, the direction of $\mathbf{k}$ is named an *easy axis*. When β is negative, the minimum energy state is the magnetization direction in the plain perpendicular to $\mathbf{k}$. In this case, the system has a *hard axis* along $\mathbf{k}$ or an *easy plane* perpendicular to $\mathbf{k}$.

Total Magnetic energy.- In general, the magnetic configuration is the result of the competition among all the above mentioned effects. Indeed, the stationary magnetic equilibria are minima of the following magnetic energy [57]

$$E = \iiint_V \left(\frac{A}{M_s^2} |\nabla \mathbf{M}|^2 - \mu_0 \mathbf{H_0} \cdot \mathbf{M} - \frac{\mu_0}{2} \mathbf{H}_D \cdot \mathbf{M} - \mu_0 \frac{\beta}{2} \left(\mathbf{k} \cdot \mathbf{M} \right)^2 \right) dV, \qquad (2.1)$$

where V is the volume of the ferromagnetic media. Several other terms can be added to the Eq. (2.1) to model border anisotropies, chirality, impurities, among other effects.

The study of equilibrium magnetizations at nano-scales is based on the minimization of this energy with the norm conservation constraint $|\mathbf{M}| = M_s$. The temporal evolution of the magnetization requires a dynamical equation. In the next section we introduce Landau-Lifshitz and Landau-Lifshitz-Gilbert equations which governs the dynamics of the magnetization.

2.2. Landau-Lifshitz and Landau-Lifshitz-Gilbert equations

The model that describes the magnetization evolution was proposed in 1935 by Landau and Lifshitz, and since then, this equation has proved to be an excellent model to describe a vast variety of phenomena, including ferromagnetic resonance, magnetization switching, and precessional dynamics (see [57] and references therein). The phenomenological equation proposed in 1935 is known as *Landau-Lifshitz* equation, and it is based on two basic considerations: the norm conservation of the magnetization $|\mathbf{M}| = M_s$ and the temporal evolution of the magnetic energy, that contains a conservative and a dissipative part. The norm conservation $\partial_t |\mathbf{M}|^2 = 2\mathbf{M} \cdot \partial_t \mathbf{M} = 0$ requires $\mathbf{M}$ and $\partial_t \mathbf{M}$ to be orthogonal.

Regarding the temporal evolution of the magnetic energy, let us start by the simple case of the Hamiltonian motions of the magnetization. The energy conservation implies that $\delta E / \delta \mathbf{M}$ and $\partial_t \mathbf{M}$ are orthogonal, that is

$$\frac{\mathrm{d}E}{\mathrm{d}t} = \iiint_V \frac{\delta E}{\delta \mathbf{M}} \cdot \partial_t \mathbf{M} \equiv 0 \Rightarrow \partial_t \mathbf{M} = \mathbf{f}(\mathbf{M}) \times \frac{\delta E}{\delta \mathbf{M}},$$

since the magnetization norm is conserved, the vector function $\mathbf{f}$ must be proportional to $\mathbf{M}$,

$$\Rightarrow \partial_t \mathbf{M} = [f(\mathbf{M})\,\mathbf{M}] \times \frac{\delta E}{\delta \mathbf{M}} \approx \gamma_{LL} \mathbf{M} \times \frac{\delta E}{\delta \mathbf{M}},$$

where the scalar function $f(\mathbf{M})$ could depend on the magnetization and its gradients, and it was approximated by its leading order contribution $f(\mathbf{M}) \approx \gamma_{LL}$. Hence, the precessional motion of the magnetization is modeled by a torque simultaneously perpendicular to the magnetization and to the energy gradients $\delta E / \delta \mathbf{M}$ [57]. It is worth noting that the conservative magnetization equation is similar to the torque acting over loops of electric currents in classical electromagnetism [75]. This equation can also be motivated from quantum mechanics [72], because the expectation value of the spin operator, $<\mathbf{s}> \equiv <\psi|\mathbf{s}|\psi>$, evolves as $\partial_t <\mathbf{s}> = -\gamma_s <\mathbf{s}> \times \mathbf{B}$, where $\mathbf{B}$ is an external field and γ_s is a gyromagnetic constant.

In brief, the magnetization dynamics admits a conservative torque that generates oscillations around the energy gradient $\delta E / \delta \mathbf{M}$. In the case of dissipative dynamics, a torque with projection over $\delta E / \delta \mathbf{M}$ should be added to account for energy losses. In particular the dissipation torque should have the form [57]

$$\frac{\delta E}{\delta \mathbf{M}} - \left(\mathbf{M} \cdot \frac{\delta E}{\delta \mathbf{M}} \right) \frac{\mathbf{M}}{M_s^2} = \frac{1}{M_s^2} \mathbf{M} \times \left(\mathbf{M} \times \frac{\delta E}{\delta \mathbf{M}} \right),$$

where the projection of the dissipation torque on the magnetization has been subtracted to ensure norm conservation [57]. Combining the precessional and dissipation torques, one obtains the well-known *Landau-Lifshitz* (LL) equation

$$\boxed{\partial_t \mathbf{M} = -\gamma_{LL} \mathbf{M} \times \mathbf{H}_{\text{eff}} - \frac{\alpha \gamma_{LL}}{M_s} \mathbf{M} \times (\mathbf{M} \times \mathbf{H}_{\text{eff}})} \tag{2.2}$$

where $\gamma_{LL} \sim 2.2 \cdot 10^5$ m/(As) is the gyromagnetic constant [57], and it is the ratio between the magnetic moment and the angular momentum. The coefficient α is a phenomenological damping parameter. The typical values of α are in the range $10^{-3} - 10^{-2}$. The effective field is given by

$$\mathbf{H}_{\text{eff}} \equiv -\frac{1}{\mu_0}\left(\frac{\delta E}{\delta \mathbf{M}}\right) = \mathbf{H_0} + \beta\,(\mathbf{k}\cdot\mathbf{M})\,\mathbf{k} + \mathbf{H_D} + \frac{2A}{\mu_0 M_s^2}\nabla^2\mathbf{M} \qquad (2.3)$$

The magnetic energy decreases to its minima[2] at a rate proportional to α

$$\frac{\mathrm{d}E}{\mathrm{d}t} = -\frac{\alpha\mu_0\gamma_{LL}}{M_s}\iiint_V |\mathbf{M}\times\mathbf{h}_{\text{eff}}|^2\mathrm{d}V.$$

Then, the dissipation torque decreases the energy monotonically. The magnetization that minimizes the energy ($\mathrm{d}E/\mathrm{d}t = 0$) satisfies the *Brown* equation [57, 8]

$$\mathbf{M}\times\mathbf{H}_{\text{eff}} = 0.$$

In 1955 Gilbert wrote the dissipation vector in terms of the temporal derivative of the magnetization [8, 30], that is,

$$\boxed{\partial_t\mathbf{M} = -\gamma_G\mathbf{M}\times\mathbf{H}_{\text{eff}} + \frac{\alpha}{M_s}\mathbf{M}\times\partial_t\mathbf{M},} \qquad (2.4)$$

where $\gamma_G = (1 + \alpha^2)\gamma_{LL}$. This equation is known as the *Landau-Lifshitz-Gilbert* (LLG) equation. Gilbert dissipation decreases the magnetic energy until it reaches a stationary equilibrium $\partial_t\mathbf{M} = 0$,

$$\frac{\mathrm{d}E}{\mathrm{d}t} = -\frac{\alpha\mu_0}{\gamma_G M_s}\iiint_V |\partial_t\mathbf{M}|^2\mathrm{d}V.$$

Both Landau-Lifshitz and Landau-Lifshitz-Gilbert equations are mathematically equivalent [57] and widely used in the literature nowadays.

An important issue is the *magnetization boundary conditions*. Neumann boundary condition are often used, and the magnetization derivative with respect to the direction of the outward normal of the sample is zero, that is $\partial\mathbf{M}/\partial(\mathbf{r}\cdot\mathbf{n_{out}}) = 0$. It can be demonstrated [8] that Neumann boundary condition is satisfied by equilibrium magnetization configurations— it is necessary to minimize the magnetic energy of Eq. (2.1)— and then it is the natural choice for the non-equilibrium process.

In brief, the magnetization will evolve until it reaches a stationary equilibrium that minimizes the energy, according to the Landau-Lifshitz equation. The manipulation of the magnetization can be performed by considering a forcing mechanism in Eq.(2.4), such as

---

[2]Unless the magnetic field depends on time $\mathbf{H_0}(t)$.

magnetic field pulses, alternating magnetic fields, spin-polarized electric current, thermally induced spin-currents, and mechanical rotations. The next two sections introduce the effect of a magnetic field that oscillates in time and a spin-polarized electric current.

2.3. Oscillatory magnetic fields as a driving mechanism

Let us focus on a magnetic wire of length L along the z-axis. The magnetization obeys the dimensionless Landau-Lifshitz-Gilbert equation,

$$\frac{\partial \mathbf{m}}{\partial t} = -\mathbf{m} \times \mathbf{h}_{\text{eff}} + \alpha \mathbf{m} \times \frac{\partial \mathbf{m}}{\partial t} \tag{2.5}$$

where the effective field is

$$\mathbf{h}_{\text{eff}} \equiv -\frac{1}{\mu_0 M_s^2} \frac{\delta E_w}{\delta \mathbf{m}} = h\mathbf{e}_x - \beta m_z \mathbf{e}_z + \partial_{zz}\mathbf{m},$$

the external magnetic field is $\mathbf{h}$, and the term proportional to β accounts for the anisotropy of the wire. E_w is the energy of the wire. We focus on the case $\beta > 0$ for which z is a hard axis and x-y is an easy plane.

The Eq. (2.5) has two trivial states, $\mathbf{m} = \pm\mathbf{e}_x$. We concentrate here on the magnetization dynamics near the state $\mathbf{m} = \mathbf{e}_x$, which is favored by the Zeeman energy when $h > 0$. Due to the norm conservation, only the Cartesian components of the magnetization (m_y, m_z) will be dynamical, and $m_x = [1 - m_y^2 - m_z^2]^{1/2} \approx 1 - (m_y^2 + m_z^2)/2$ will be a slave variable.

For a constant external field $h = H_0$ and negligible damping $\alpha = 0$, the Eq. (2.5) reduces to a Hamiltonian oscillator. Moreover, the macrospin or uniform magnetization dynamics of (m_y, m_z) is given by

$$\frac{\mathrm{d}}{\mathrm{d}t} \begin{pmatrix} m_y \\ m_z \end{pmatrix} \approx \begin{bmatrix} 0 & -H_0 - \beta \\ H_0 & 0 \end{bmatrix} \begin{pmatrix} m_y \\ m_z \end{pmatrix},$$

or equivalently

$$\frac{\mathrm{d}^2 m_y}{\mathrm{d}t^2} = -H_0 \left(H_0 + \beta \right) m_y,$$

which predicts oscillations of the form

$$\begin{pmatrix} m_y \\ m_z \end{pmatrix} = A_0 e^{i\omega_0 t} \begin{pmatrix} \sqrt{H_0 + \beta} \\ -i\sqrt{H_0} \end{pmatrix} + c.c.,$$

where $\omega_0 = \sqrt{H_0(H_0 + \beta)}$ is the natural frequency, and $c.c.$ stands the complex conjugate. For H_0 of order one and wires with easy plane anisotropy ($CsNiF_3$ for instance) the natural frequency is $\omega_0 \sim 100$ GHz. The constant A_0 is the amplitude of the oscillations and it depends on the initial conditions.

In presence of dissipation, the magnetization behaves as a damped oscillator and therefore it will converge to the energy minimum $\mathbf{m} = \mathbf{e}_x$. The use of an an oscillatory field of the form

$h = H_0 + h_0 \cos(\omega t)$ permits injecting energy and exciting the system. A particularly efficient mechanism is based on the use a alternating field with twice the natural frequency of the system [2, 18, 79, 80, 50], that is, $\omega = 2(\omega_0 + \nu)$, where ν is a small detuning. Figure 2.1 shows two types of responses of the magnetization to an oscillatory field, namely a soliton and a pattern. Dissipative solitons are particle-like states described by a few parameters—position, oscillation phase, maximum amplitude, and width—and they are asymptotic connections to the uniform state $\mathbf{e}_x$,

$$\lim_{z \to \pm\infty} \mathbf{m} = \mathbf{e}_x.$$

This property implies that solitons are stable only if their background $\mathbf{e}_x$ is also stable. On the other hand, patterns, or nonlinear waves, can emerge as the result of an instability, that is, small perturbations around the $\mathbf{m} = \mathbf{e}_x$ state grow with a well defined wavelength and frequency [see Fig. 2.1(b)]. The analytic description of this system is left to the subsection 3.3.2, where approximate expressions for solitons and patterns are given.

2.4. Spin-transfer torque as a driving mechanism

In 1996, Slonczewski [74] and Berger [6] demonstrated that electric currents can transfer spin-angular momentum to a ferromagnetic layer. This effect is known as the *spin-transfer torque* and it based on the interaction between spins of an electric current and spins of magnetic media. The spin-transfer torque has two important dynamical effects on the magnetization, namely self-oscillations at gigahertz frequencies [41, 73, 46] and magnetic switching [46]. Both behaviors could generate technological advances in the fields of information transmission and
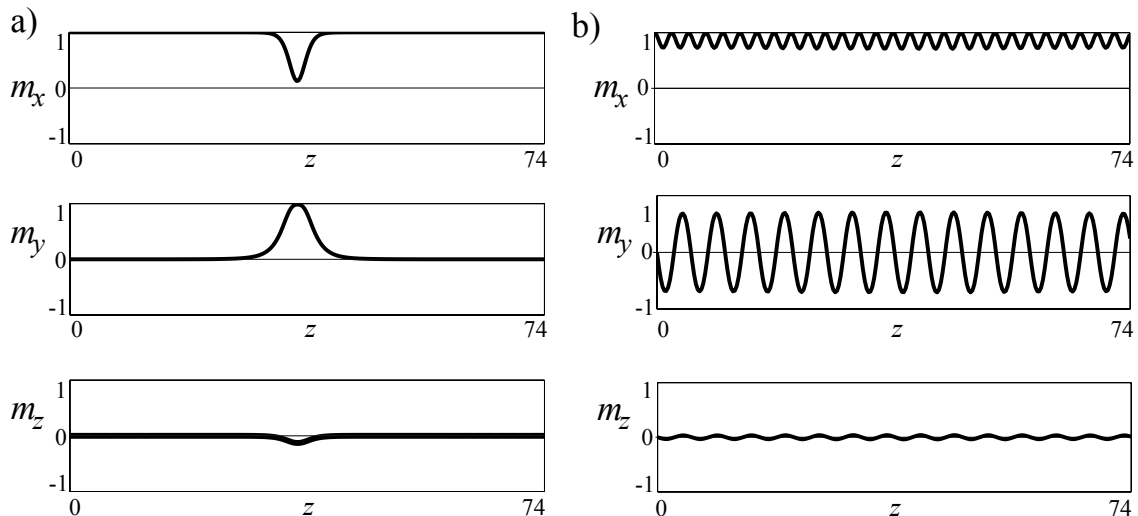
Figura 2.1: Dissipative structures induced by the alternating field. (a) A Soliton appears for negative detuning, and they are a localized structure. (b) Patterns or Faraday-type waves emerge for positive detuning and they are extended (and usually periodic) spatial structures. Equation (2.5) was integrated using periodic boundary conditions and the following parameter values: $H_0 = 3$, $\alpha = 0{,}05$, $\beta = 20$, the detuning and alternating filed are $\nu^{sol} = -0{,}4497$, $h_0^{sol} = 1{,}127$ for the soliton and $\nu^{patt} = 2$ and $h_0^{patt} = 1{,}53$ for the pattern.

recording.

From the microscopic point of view, the conduction electrons become spin-polarized when they transverse a magnetic medium [75]. Such net spin-polarization of the electric current interacts with the magnetization of another layer, which is *free* to evolve. The next two subsections describe each process.

2.4.1. Spin-polarization of an electric current

Let us consider *one electron inside a box of volume V in presence of a magnetic field*. The electron energy E given by

$$E = E_k \pm E_m = \frac{\hbar^2 k^2}{2m_{\mathrm{e}}} \pm E_m,$$

where k is the wavenumber, m_{e} is the electron mass, and $\{E_k, E_m\}$ are the kinetic and Zeeman energies, respectively. If the magnetic moment of the electron points parallel to the magnetic field, it will have a smaller Zeeman energy E_m, and therefore a larger kinetic energy E_k, which increases the number of available states [75]. Indeed, the density of states $g(E)$ for an electron with a defined spin orientation grows as $g(E) \sim E^{1/2}$

$$g(E) = \frac{\mathrm{d}}{\mathrm{d}E} \left(\frac{4\pi k^3}{3k_0^3} \right) = \frac{V}{4\pi^2} \left(\frac{2m_{\mathrm{e}}}{\hbar^2} \right)^{3/2} \sqrt{E},$$

where $V = L^3$ is the volume and $k_0 = 2\pi/L$ is a normalization factor. Moreover, we can define a density of states for electrons with magnetic moment pointing along ($\uparrow$) and against ($\downarrow$) the magnetic field [75]

$$g_\uparrow(E) \equiv g(E_k[\uparrow]) = g(E + E_m),$$

$$g_\downarrow(E) \equiv g(E_k[\downarrow]) = g(E - E_m),$$

Hence, an electron with magnetic moment pointing parallel to the magnetic field has more available states.

In the case of an *ideal gas of electrons in presence of a magnetic field in thermodynamic equilibrium*, the number of particles at a state with energy E is given by the Fermi-Dirac distribution

$$f(E) = \frac{1}{\mathrm{e}^{(E-\mu)/k_B T} + 1},$$

where μ is the chemical potential. A low temperatures ($T \ll \mu/k_B$), almost all the states with energy below the Fermi level[3] are occupied. Then, if electrons have their magnetic moment along the magnetic field, they will have more available states at a given energy, and (almost) each one of those states will be occupied with an electron. Hence, the magnetic field

---

[3]The Fermi level is the largest single energy level occupied by a electron at zero temperature. In the case of electric currents, most of the transport is done by electrons close the Fermi level.

increases the number of electrons with magnetic moment along the magnetization direction. This polarization of the ideal gas is usually described in terms of the polarization factor [75]

$$P(E) \equiv \frac{g_\uparrow(E) - g_\downarrow(E)}{g_\uparrow(E) + g_\downarrow(E)}.$$

The above description of a spin-polarized ideal gas of electrons can be used as a toy model to understand the *polarization of an electric current traversing ferromagnetic materials*. In this idealization, conduction electrons interact with a magnetic field—the magnetization of the media— and the result is a band-splitting into two channels, namely the majority electrons that point along the magnetization, and the minority electrons that point against the magnetization. The polarization of the current is given by the number of states available at the Fermi level [75]

$$P_{\text{current}} \equiv P(E_F) = \frac{g_\uparrow(E_F) - g_\downarrow(E_F)}{g_\uparrow(E_F) + g_\downarrow(E_F)}.$$

In more realistic descriptions, the density of states can have contributions from different bands [76], and therefore the splitting due to the magnetization affects the number of electrons in each channel and, at the same time, the scattering processes between different bands become spin-dependent. The result is an increment in the resistance of the minority electrons due to the scattering process. A complete description of spin-dependent transport processes, particularly in transition metals, can be found in the book *Magnetism* of J. Stöhr and H. C Siegmann, Ref. [76].

2.4.2. Spin-transfer torque (STT)

Let us consider a spin-valve device. Spin-valves are metallic multilayer structures composed by at least two ferromagnets separated by a non-magnetic spacer. Usual lateral dimensions are in the range $50 - 200$ nm. An electric current transverses spin-valves perpendicularly to the plane of the layers. This type of setup is known as a Current-Perpendicular to plane device (CPP). Figure 2.2 shows a typical spin-valve, where a magnetization $\mathbf{M}$ is *fixed* and another one $\mathbf{m}$ is *free* to evolve in time.

The magnetization $\mathbf{M}$ filters or polarizes the spins of the electric current, and its orientation is maintained constant by means of the coupling with an antiferromagnetic anchoring, obtained the use of a thick material (one order of magnitude thicker than the free film typically), or large magnetic anisotropies. The other layer is free to evolve according to an appropriate Landau-Lifshitz-Gilbert equation. Moreover, as the result of the electric current that becomes spin-polarized after traversing the fixed layer, the equation for the normalized magnetization $\mathbf{m}$ has an additional torque, which is the *spin-transfer torque* [57].

According to the discussion of the last subsection, after the current passes through the fixed layer, it is spin-polarized and then it has a net magnetic moment $\mathbf{n}_{\text{in}}$, which is proportional to the angular momentum per electron $\hbar/2$ and to the number of electrons traversing the

media per unit of time I/e. All the transport details, such as the efficiency of the polarizer (the P_{current} coefficient) and spin-dependent superficial scattering, can be summarized in a factor f. Then $\mathbf{n}_{\text{in}}$ has the following form [85]

$$\mathbf{n}_{\text{in}} = f\frac{\hbar}{2}\frac{I}{e}\mathbf{M},$$

After the current traverses the free layer, only the component parallel to $\mathbf{m}$ of the incoming magnetic moment is present [85]

$$\mathbf{n}_{\text{out}} = f\frac{\hbar}{2}\frac{I}{e}\left(\mathbf{M}\cdot\mathbf{m}\right)\mathbf{m}.$$

The difference between the polarization of the electric current is absorbed by the ferromagnetic material. Indeed, the angular momentum conservation takes the form [85]

$$\tau + \mathbf{n}_{\text{out}} - \mathbf{n}_{\text{in}} = 0, \tag{2.6}$$

where τ is the total torque applied by the electric current to the ferromagnetic medium. Subtracting the final and initial magnetic moments and using the mathematical relation $\mathbf{A}\times(\mathbf{B}\times\mathbf{C}) = (\mathbf{A}\cdot\mathbf{C})\mathbf{B} - (\mathbf{A}\cdot\mathbf{B})\mathbf{C}$ one obtains

$$\mathbf{n}_{\text{in}} - \mathbf{n}_{\text{out}} = f\frac{\hbar}{2}\frac{I}{e}\left[\mathbf{M} - (\mathbf{M}\cdot\mathbf{m})\mathbf{m}\right] = f\frac{\hbar}{2}\frac{I}{e}\left[\mathbf{M}\mathbf{m}^2 - (\mathbf{M}\cdot\mathbf{m})\mathbf{m}\right] = f\frac{\hbar}{2}\frac{I}{e}\left[\mathbf{m}\times(\mathbf{M}\times\mathbf{m})\right].$$

Then, the torque acting on the ferromagnetic medium per unit of volume $\tau_{\text{STT}} \equiv \tau/V$ is given by [74, 70, 57, 86, 87]

$$\boxed{\tau_{\text{STT}} \equiv \frac{\tau}{V} = g\mathbf{m}\times(\mathbf{m}\times\mathbf{M}).} \tag{2.7}$$
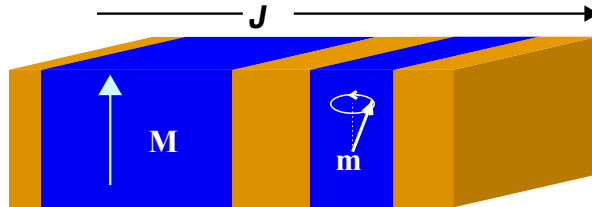

Figura 2.2: Spin-valve structure. The two blue (dark) layers are ferromagnetic films. One magnet has a fixed magnetization $\mathbf{M}$, and it is used to polarize the electric current. The magnetization $\mathbf{m}$ is free to evolve according to the Landau-Lifshitz-Gilbert equation with an additional term that accounts for the spin-polarized current. Usually, the fixed layer is ticker than the free magnet, for instance in the experiment of Kiselev and coworkers [41], their thickness are 40 nm and 3 nm, respectively. The thickness of the spacer between ferromagnets is usually about 10 nm, which permits to neglect the RKKY [72] and the dipolar interactions between $\mathbf{M}$ and $\mathbf{m}$. The rest of the structure is composed by non-magnetic metals, which permits to dissipate most of Joule heating, see Refs. [89, 33, 34, 88, 32] for a detailed discussion on Joule heating in spin-valves and magnetic nanowires.

where the prefactor is [85]

$$g = f\left(\mathbf{m} \cdot \mathbf{M}\right) \frac{1}{V} \frac{\hbar}{2} \frac{I}{|e|} = f\left(\mathbf{m} \cdot \mathbf{M}\right) \frac{\hbar}{2} \frac{J}{|e|d}, \tag{2.8}$$

and d is the ferromagnet width. The f function, which accounts for the microscopic details of electronic transport, is known as the angular dependence of the spin-transfer torque, and it has the general form of [86, 87]

$$f\left(\mathbf{m} \cdot \mathbf{M}\right) = \frac{q_+}{A + B\mathbf{m} \cdot \mathbf{M}} + \frac{q_-}{A - B\mathbf{m} \cdot \mathbf{M}}, \tag{2.9}$$

where the parameters $\{q_+, q_-, A, B\}$ account for spin-dependent transport process [86, 87]. The simplest approximation for the angular dependence is to consider f as a constant, $f = \eta_0$, this is known as the *sine-approximation*. This approximation is widely used in literature. Furthermore, the sine-approximation simplifies analytic calculations and it also provides better agreement than the full g function for certain devices [87, 47, 40].

The magnetization dynamics in presence of spin-polarized currents are studied by adding the torque (2.7) to the Landau-Lifshitz-Gilbert Eq. (2.4). It is worth noting that the spin-polarized current has a different dynamical effect on the magnetization, because it injects and dissipates energy depending on both the value of the electric current J and the magnetic configuration. Then, a spin-transfer torque is different from the precessional torque and the Gilbert dissipation.

2.5. Spin-transfer driven nanopillar with in-plane polarizer and in plane magnetic field

We present here the particular configuration that we studied in this thesis. Let us consider a free layer driven by a spin-polarized current and an external magnetic field. There are several possible orientations for the fixed magnetization $\mathbf{M}$ and the external magnetic field $\mathbf{H_0}$, the case in which both vectors point along a single in-plane direction deserves special attention, because the external field and the spin-transfer torque can enforce each other or have an opposite effect. Accordingly, we choose the fixed layer magnetization and the external field to point along the x-axis (see Fig. 2.3).

We use the following adimensionalization $t \to t/(\gamma M_s)$, $\mathbf{r} \to l_{ex}\mathbf{r}$. Moreover, we normalize the magnetization vector $\mathbf{m} \equiv \mathbf{m}/M_s$ and all[4] the fields $\mathbf{h_j} = \mathbf{H_j}/M_s$ by the saturation magnetization M_s. Then, the magnetic energy per unit of area is

$$E_m = \iint \left[-h_0 m_x - \frac{\beta_x}{2}m_x^2 + \frac{\beta_z}{2}m_z^2 + \frac{|\nabla\mathbf{m}|^2}{2}\right] \mathrm{d}x\mathrm{d}y, \tag{2.10}$$

and the Landau-Lifshitz-Gilbert equation becomes the *Landau-Lifshitz-Gilbert-Slonczewski* equation (LLGS)

$$\boxed{\partial_t\mathbf{m} = -\mathbf{m} \times \mathbf{h}_{\text{eff}} + g\mathbf{m} \times (\mathbf{m} \times \mathbf{e}_x) + \alpha\mathbf{m} \times \partial_t\mathbf{m},} \tag{2.11}$$

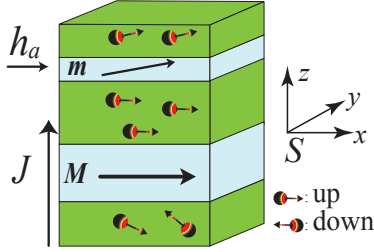[4]The exchange, external, magnetocrystalline and magnetostatic fields.

Figura 2.3: Nanopillar with in plain polarizer. We focus on the configuration where both the polarization magnetization $\mathbf{M}$ and the external field $\mathbf{h_0}$ lie in the x-axis.

where the effective field is

$$\mathbf{h}_{\text{eff}} = \left(h_0 + \beta_x m_x\right)\mathbf{e}_x - \beta_z m_z \mathbf{e}_z + \nabla^2 \mathbf{m}. \tag{2.12}$$

The parameter g is negative for electrons flowing from the fixed to the free layer. The coefficients β_x and β_z are the anisotropy constants for the x-axis (easy axis) and the z-axis (hard axis).

The model has two trivial equilibria, they are $\mathbf{m} = \pm\mathbf{e}_x$. They are named the parallel (+) and the antiparallel (-) states, because of the relative orientations between the fixed magnetization $\mathbf{M}$ and the equilibrium of the free magnetization $\mathbf{m}$.

Justification of the minimal model Eq. (2.11).- For the sake of simplicity we have included only the dominant order effects. However, it is possible to consider several other torques, that account for thermal fluctuations, nonlocal dipolar fields, border anisotropy, Oersted fields, eddy currents, the polycristalline nature of the free layer, the angular dependence of the spin-transfer and field-like spin-transfer torques. On the one hand such a complete approach could give rise to more realistic and detailed simulations and obtain a better agreement with experiments; one the other hand, it will be hard to obtain simple analytic approximations, analogies and explanations. Indeed, Equation (2.11) is a balance between simple enough to admit the use of several perturbation methods—modal decomposition, stability analysis, weakly nonlinear analysis, among others—and at the same time, it is complicated enough to predict complex dynamics such as chaotic states.

In this scenario, it is a natural strategy to start studying the simple model first, and to analyze more realistic equations later on.

2.5.1. LLGS equation in Cartesian representation

A straightforward decomposition of the magnetization vector is the Cartesian representation,

$$\mathbf{m} = m_x\mathbf{e}_x + m_y\mathbf{e}_y + m_z\mathbf{e_z}.$$

Replacing the above expression into Eq. (2.11), one obtains

$$
\begin{aligned}
\partial_t m_x &= \left(\alpha\left[h_0 + \beta_x m_x + \nabla^2 m_x\right] - g\right)\left[m_y^2 + m_z^2\right] + \mathrm{d}_{zy} + \beta_z m_z m_y \\
&\quad + \alpha\beta_z m_x m_z^2 - \alpha m_x\left(m_z\nabla^2 m_z + m_y\nabla^2 m_y\right), \\
\partial_t m_y &= -(h_0 + \alpha g)m_z + (g - \alpha h_0)m_x m_y - (\beta_x + \beta_z)m_x m_z - \alpha m_y(\beta_x m_x^2 - \beta_z m_z^2) \\
&\quad + \mathrm{d}_{xz} + \alpha m_x \mathrm{d}_{xy} + \alpha m_z \mathrm{d}_{zy}, \\
\partial_t m_z &= (h_0 + \alpha g)m_y + (g - \alpha h_0)m_x m_z + \beta_x m_x m_y - \alpha m_z\left(\beta_z m_y^2 + (\beta_x + \beta_z)m_x^2\right) \\
&\quad + \mathrm{d}_{yx} + \alpha m_x \mathrm{d}_{xz} + \alpha m_y \mathrm{d}_{yz},
\end{aligned}
\tag{2.13}
$$

where $\mathrm{d}_{ab} = m_a\nabla^2 m_b - m_b\nabla^2 m_a$. The above set of equations has to be integrated considering the norm conservation constrain $m_x^2 + m_y^2 + m_z^2 = 1$.

The numerical errors generated by the integration of the Cartesian representation could deviate the magnetization norm from 1. To avoid this problem, it is possible to implement several routines (see [57] and references therein). Another possibility to surpass the norm conservation problem is to represent the magnetization using only two variables. In the next subsection we introduce two useful decomposition of the magnetization vector, namely the spherical and steoregraphic representations.

2.5.2. LLGS equation in spherical representation

The spherical angles are the natural variables to describe the motions on the spherical surface [57]. Let us introduce the following change of variables illustrated on the Fig. 2.5.1

$$
\mathbf{m} = \sin(\theta)\left[\cos(\phi)\,\mathbf{e}_x + \sin(\phi)\,\mathbf{e}_y\right] + \cos(\theta)\,\mathbf{e_z}.
$$

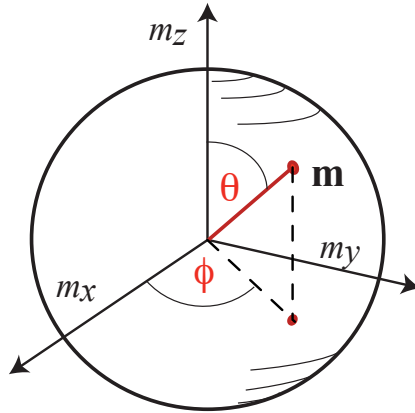Replacing this decomposition in Eq. (2.11), one obtains after straightforward calculations

Figura 2.4: Spherical representation of the magnetization. In this representation, spherical angles are used to label the magnetization space.

$$\partial_\tau \theta = -(h_0 + \alpha g)\sin(\phi) - \frac{\beta_x}{2}\sin(\theta)\sin(2\phi) + (\alpha h_0 - g)\cos(\phi)\cos(\theta)$$
$$+ \frac{\alpha}{2}\sin(2\theta)\left[\beta_z + \beta_x \cos^2(\phi)\right] + 2\cos(\theta)\nabla\phi \cdot \nabla\theta$$
$$+ \sin(\theta)\nabla^2\phi + \alpha\nabla^2\theta - \frac{\alpha}{2}\sin(2\theta)(\nabla\phi)^2, \tag{2.14}$$

$$\sin(\theta)\partial_\tau\phi = (g - \alpha h_0)\sin(\phi) - \alpha\frac{\beta_x}{2}\sin(\theta)\sin(2\phi) - (\alpha g + h_0)\cos(\phi)\cos(\theta)$$
$$- \frac{1}{2}\sin(2\theta)\left[\beta_z + \beta_x \cos^2(\phi)\right] + 2\alpha\cos(\theta)\nabla\phi \cdot \nabla\theta$$
$$+ \alpha\sin(\theta)\nabla^2\phi - \nabla^2\theta + \frac{1}{2}\sin(2\theta)(\nabla\phi)^2, \tag{2.15}$$

where the re-normalized time is $\tau = (1 + \alpha^2)t$. It is worth noting that the use of spherical coordinates allows to represent the magnetization space with spherical angles $\{\theta, \phi\}$. On the other hand, the physical space is labeled by the position vector, $\mathbf{r} = x\mathbf{e}_x + y\mathbf{e}_y$, which is decomposed in the Cartesian axes.

There are three disadvantages of the spherical decomposition. The first one is the coordinate singularity at $\sin(\theta) = 0$. This implies that the magnetization motion cannot include points in the vecinity of the north and south poles. The second problem is the $\phi \to \phi + 2\pi n_\phi$ and $\theta \to \theta + 2\pi n_\theta$ invariances, because a discontinuity in the angles $\{\theta, \phi\}$ will generate errors when calculating the spatial derivatives. This drawback is easily surpassed using continuous functions as initial conditions, or calculating spatial derivatives in the Cartesian representation and then projecting over the spherical variables. The third problem is that trigonometric functions decrease the numerical calculation speed.

2.5.3. LLGS equation in stereographic representation

The stereographic [57, 43] representation is shown in Fig. 2.5.3(a), and it consist on a the projection of the spherical surface on a complex equatorial plane through [see 2.5.3(b)]

$$\psi = \frac{m_y + \mathrm{i}m_z}{1 + m_x}. \tag{2.16}$$

The complex field ψ quantifies the deviations from the parallel state. The Cartesian magnetization components can be expressed in terms of ψ

$$(m_x, m_y, m_z) = \frac{1}{1 + |\psi|^2}\left(1 - |\psi|^2, \psi + \bar{\psi}, \mathrm{i}\left[\bar{\psi} - \psi\right]\right). \tag{2.17}$$

Replacing the above stereographic representation in the LLGS equation, after straightforward calculation one obtains
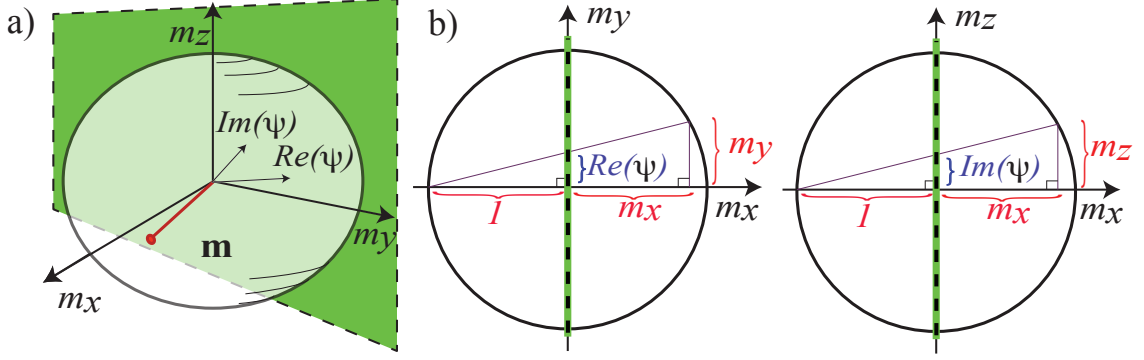
Figura 2.5: Stereographic representation of the magnetization. (a) The spherical surface is mapped to a equatorial complex plane. (b) Stereographic change of variables.

$$(i + \alpha) \partial_T \psi = (ig - h_0) \psi - \frac{\beta_z}{2} \left(\psi - \overline{\psi} \right) \frac{1 + \psi^2}{1 + |\psi|^2} - \beta_x \psi \frac{1 - |\psi|^2}{1 + |\psi|^2} + \nabla^2 \psi - 2 \frac{\overline{\psi}}{1 + |\psi|^2} \left(\nabla \psi \right)^2.$$
(2.18)

This is a *Generalized complex Ginzburg-Landau* equation. Ginzburg-Landau models appear in several contexts, in particular they are used to describe the envelopes of nonlinear waves in dissipative media. Indeed, the use of the stereographic representation facilitates the comparison between magnetization dynamics and dynamics of a wide variety of physical systems.

When the angular dependence of the spin-transfer torque is considered, the g factor is replaced by $g\left(|\psi|^2\right)$.

The equation for the complex field ψ can be decomposed using the real and imaginary parts of ψ. Replacing $\psi = u + iv$ into Eq. (2.18) yields

$$
\begin{aligned}
\partial_t u &= \left(g - \alpha h_0 + \alpha \nabla^2\right) u + \left(\nabla^2 - h_0 - \alpha g\right) v \\
&+ \frac{\alpha \beta_x u^3 + (\beta_x + \beta_z) v^3 + 2 (v - \alpha u) \left\{ (\nabla u)^2 - (\nabla v)^2 \right\} - 4 \nabla u \cdot \nabla v \, (u + \alpha v)}{1 + u^2 + v^2} \\
&+ \frac{-\alpha \beta_x u - (\beta_x + \beta_z) v + (\beta_x - \beta_z) u^2 v + \alpha (\beta_x + 2\beta_z) u v^2}{1 + u^2 + v^2}, \\
\partial_t v &= \left(h_0 + \alpha g - \nabla^2\right) u + \left(g - \alpha h_0 + \alpha \nabla^2\right) v \\
&+ \frac{-\beta_x u^3 + \alpha (\beta_x + \beta_z) v^3 + 2 (u + \alpha v) \left\{ (\nabla u)^2 - (\nabla v)^2 \right\} + 4 \nabla u \cdot \nabla v \, (v - \alpha u)}{1 + u^2 + v^2} \\
&+ \frac{\beta_x u - \alpha (\beta_x + \beta_z) v + \alpha (\beta_x - \beta_z) u^2 v - (\beta_x + 2\beta_z) u v^2}{1 + u^2 + v^2}.
\end{aligned}
$$
(2.19)

(2.20)

The change of variables $\{m_x, m_y, m_z\} \rightarrow \{u = Re\left(\psi\right), v = Im\left(\psi\right)\}$ can be very efficient to simulate because the stereographic representation automatically preserves the magnetization norm. Furthermore, the functions involved are not trigonometric as in the case of spherical

coordinates. A disadvantage of stereographic representation is that the antiparallel state $\mathbf{m} \equiv -\mathbf{e_x}$ is mapped to infinity, thus dynamics close to this state are not accurately described.

Capítulo 3

Mathematical methods to study nonlinear magnetization dynamics

Physical systems kept out of thermodynamic equilibrium self-organize into dissipative structures [25, 77, 66]. Even if the dissipative states emerge in different branches of science, they usually have similar features, such as intrinsic lengths and frequencies. This regularity in the morphogenesis processes of physical systems is beyond nano-magnetism, and it motivates the quest for a universal theory for pattern formation in non-equilibrium systems. There are three well-known general approaches to study such systems, they are discrete maps [62], cellular automata [4, 71], and differential equations [25, 77]. In the first case, the state of the system is described by continuous variables that evolve in discrete time steps. In the second case, the dynamical object is known as cellular automaton, and it has a discrete phase space and evolves in discrete steps. Both approaches are ideal to model inherently discrete systems, and they are efficient to simulate complex dynamics. The third approach, differential equations, is based on differential and integral calculus, and it has demonstrated the capacity to model, explain and predict several phenomena in a wide spectrum of ares of knowledge. The treatment of nonlinear differential equations can be conducted in a unified framework known as *bifurcation theory* [25, 77, 66]. A bifurcation is a qualitative change in the phase space of the system [66], and then it is responsible for all the qualitative aspects of the dynamical behavior. Moreover, in complicated systems that involve partial differential equations of several variables, a few transformations of variables usually permit one to obtain a reduced representation of the dynamics at the onset of the bifurcation. This minimal representation takes the form of one or a few variables—known as order parameters [66]— that satisfy simple equations—normal forms [25, 77, 66]—and they allow one to explain and predict various phenomena. Even if in some cases the normal form is difficult to derive[1], it is still possible to obtain a deep insight by means of phenomenological models based on normal forms and the symmetries of the system.

In this thesis, we study ferromagnetic media forced by spin-polarized currents and alternating magnetic fields by means of differential equations. This approach is the natural one

---

[1]For instance, some states are highly nonlinear and therefore perturbation analysis is not admissible. In this situation the derivation of a normal form is more complicated.

to study continuous ferromagnetic media at nano-scales, where the exchange interaction is dominant and it smooths the magnetization textures. Moreover, we use bifurcation theory to predict states, to find analytic expressions for equilibria, and to characterize the phases diagram. On the one hand, this viewpoint permits us to use well known analytic methods of *nonlinear physics* to characterize magnetic systems, and on the other hand, we find analogies between the magnetization dynamic and other physical systems, such as vibrated fluids, driven optical media, fluid mixtures heated from bellow, to mention a few.

The rest of this section introduces briefly concepts and methods of nonlinear science, as well as the most commonly observed bifurcations by means of well-known prototype models.

3.1. Equilibrium and Stability

Let us consider a physical system described by the following dimensionless model

$$\frac{\mathrm{d}u}{\mathrm{d}t} = f(u), \tag{3.1}$$

where $u = u(t)$ is a real-valued function of time, and it accounts for the dynamics of the system. The equilibria (also known as *fixed points*, or *steady states*) of Eq. (3.1) satisfy $\mathrm{d}u/\mathrm{d}t = 0$. Lets u_0 denote one of those solutions. An important property of states is their capacity to attract or repeal nearby trajectories. We consider the decomposition $u(t) = u_0 + \delta u(t)$, where δu is a small perturbation function, to verify if state u_0 attracts it neighborhood or not. At dominant order the perturbation δu obeys the equation

$$\frac{\mathrm{d}\delta u}{\mathrm{d}t} = \frac{\mathrm{d}f}{\mathrm{d}u}(u_0)\,\delta u.$$

The solution of the above equation takes the form $\delta u = \delta u(0)\mathrm{e}^{\lambda t}$, where the quantity $\lambda = (\mathrm{d}f/\mathrm{d}u)(u_0)$ is the *eigenvalue* [77] of the state and it measures the growth ($\lambda > 0$) or decay ($\lambda < 0$) rate of perturbations. The general (approximate) solution of the model (3.1) close to u_0 is at dominant order

$$u(t) = u_0 + \delta u(0)\mathrm{e}^{\lambda t}.$$

If $\lambda < 0$, then nearby trajectories converge exponentially to u_0. In that case, the state u_0 is said to be an *attractor* or an *asymptotically stable* equilibrium. On the other hand, if $\lambda > 0$ the perturbations grow and trajectories move away from the *unstable* state u_0. In the critical situation $\lambda = 0$, the equilibrium is named a *marginally stable state* [66]. The capacity of marginally stable points to attract or repeal nearby orbits is only accessible by nonlinear analysis.

Let us review now the case of *vector equations*, where the state of the system is described by two or more independent real-valued functions of time.

Vector equations.- We analyze here the vector state function $\mathbf{u} = \mathbf{u}(t)$ that obeys the following equation

$$\frac{\mathrm{d}\mathbf{u}}{\mathrm{d}t} = \mathbf{f}(\mathbf{u}). \tag{3.2}$$

Let's name one of the steady states of the above model as $\mathbf{u}_0$. We study the dynamics of the perturbations about this state by replacing the ansatz $\mathbf{u} = \mathbf{u}_0 + \delta\mathbf{u}$ in Eq. (3.2). At linear order on the perturbation $\delta\mathbf{u}$ we have

$$\frac{\mathrm{d}\delta\mathbf{u}}{\mathrm{d}t} = \left[\frac{\partial\mathbf{f}}{\partial\mathbf{u}}\left(\mathbf{u}_0\right)\right] \cdot \delta\mathbf{u},$$

where the matrix $[\partial\mathbf{f}/\partial\mathbf{u}\left(\mathbf{u}_0\right)]$ is the Jacobian of $\mathbf{f}$ evaluated on the equilibrium $\mathbf{u}_0$. Since the perturbation $\delta\mathbf{u}$ obeys the former linear equation, its solution is

$$\delta\mathbf{u} = \mathrm{e}^{\lambda t}\mathbf{v},$$

replacing this formula in model (3.2) one obtains

$$\left[\frac{\partial\mathbf{f}}{\partial\mathbf{u}}\left(\mathbf{u}_0\right) - \lambda\mathbb{I}\right]\mathbf{v} = 0,$$

where $\mathbb{I}$ is the identity matrix. Such problem is soluble when

$$\det\left(\left[\frac{\partial\mathbf{f}}{\partial\mathbf{u}}\right]\left(\mathbf{u}_0\right) - \lambda\mathbb{I}\right) = 0, \tag{3.3}$$

where det is the determinant. The expression (3.3) is known as the characteristic polynomial equation or *characteristic equation* [77]. Notice that the left-hand side of Eq. (3.3) is a polynomial function of λ, which has N a priory complex roots, where N is the number of components of vector $\mathbf{u}$. Figure 3.1 shows typical plots of eigenvalues in the complex plane, this type of figure is usually known as the stability *spectrum* of the state $\mathbf{u_0}$. For vector equations, the stability of a state is determined by the real part of the eigenvalues because the imaginary part only generates oscillations at frequencies $\omega = \mathrm{Im}(\lambda)$, that is

$$\delta\mathbf{u} = \sum_j \underbrace{\mathrm{e}^{\mathrm{Re}(\lambda_j)t}}_{\text{decay/growth}} \underbrace{\mathrm{e}^{\mathrm{iIm}(\lambda_j)t}}_{\text{oscillations}} \mathbf{v}_j,$$

where $\{\lambda_j\}_{j=1}^N$ are the eigenvalues and $\{\mathbf{v}_j\}_{j=1}^N$ are their respective eigenvectors. If there is an eigenvalue with positive real part, then there is a direction of the phase space in which perturbations grow. In that case, the equilibrium $\mathbf{u_0}$ is unstable [77]. If all the eigenvalues have negative real part [see Fig. 3.1(a)], then the state is stable [77].

Let us consider a single control parameter ε. In general, the eigenvalues depend on the control parameter $\lambda = \lambda(\varepsilon)$, and then a change of sign of the real part of one eigenvalue can be expected. This change in the stability of a state when a control parameter is increased or decreased is an *instability*. Instabilities are examples of *bifurcations*. The eigenvector associated to the eigenvalue $\mathrm{Re}(\lambda) = 0$ is named a *critical mode*, and its direction defines a *center subspace* in the phase space. In a similar manner, we can define the unstable subspace or manifold, as the subspace spanned by the eigenvectors satisfying $\mathrm{Re}(\lambda) > 0$ [66, 84][2]. Moreover, at the onset of the instability the eigenvalue of the critical mode is small, $\mathrm{Re}(\lambda) \approx 0$,

---

[2]Some books name *unstable subspace* to the space spanned by the eigenvectors satisfying $\mathrm{Re}(\lambda) > 0$ and *unstable manifold* to the geometric deformation of the unstable subspace due to nonlinearities. Here we use both expressions as synonyms
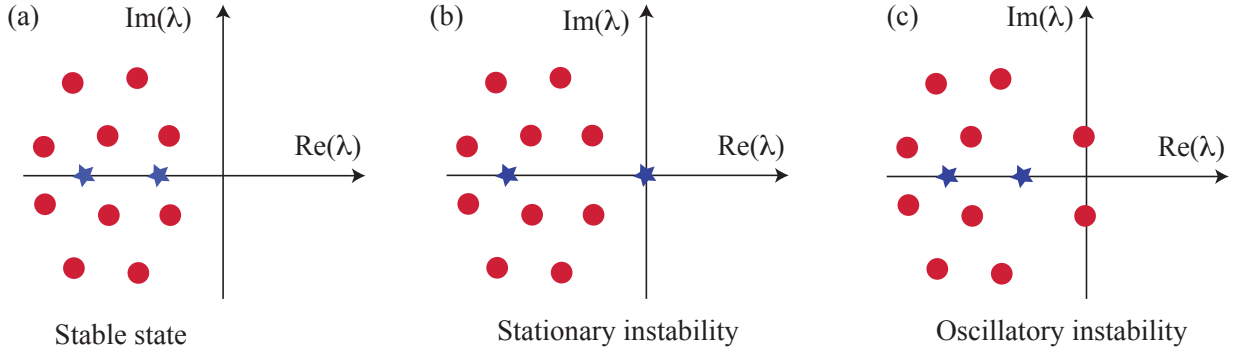
(a) Im(λ) Re(λ)	(b) Im(λ) Re(λ)	(c) Im(λ) Re(λ)
Stable state	Stationary instability	Oscillatory instability

Figura 3.1: Stability spectra. The plots show the growth or decay rate λ of perturbations $\delta\mathbf{u} = e^{\lambda t}\mathbf{v}$ around an equilibrium $\mathbf{u_0}$. (a) Stable states are characterized by having all their eigenvalues with negative real part, $\mathrm{Re}(\lambda) < 0$. The general destabilization mechanisms are the stationary and the oscillatory instabilities, shown in (b) and (c), respectively. When a stationary instability takes place, one eigenvalue is zero $\lambda = 0$ for a critical value of a control parameter $\varepsilon = \varepsilon_c$ [see (b)]. When the control parameter is further increased $\varepsilon > \varepsilon_c$, the critical eigenvalue becomes positive $\lambda > 0$ which exponentially increases the amplitude of perturbations along the *critical mode*. In the case of oscillatory instabilities, also known as *Andronov-Hopf* instabilities, two complex conjugate eigenvalue cross the imaginary axis and destabilize the equilibrium. The imaginary part of the eigenvalue is an intrinsic frequency $\omega = \mathrm{Im}(\lambda)$. This frequency plays a key role in the generation of self-oscillations in magnetism.

and then the *center manifold* is characterized by a slow evolution. The rest of the phase space is spanned by the other eigenvalues, this zone is the *stable manifold*, and in this region the evolution is much faster than in the central manifold. This behavior at the onset of the instability is known as a *temporal scales separation*; and it means that one or a few degrees of freedom are dynamical while all the other evolve fast and become slave modes [66]. Separation of scales permits one to describe the system at long times in terms of a few relevant variables known as *order parameters* [66].

Other definitions of stability.- The linear stability analysis conducted above is an example of *asymptotic stability* [66]. When an equilibrium is asymptotically stable, all trajectories that were close enough to the equilibrium at the initial time will converge to it, that is $\mathbf{u}(t) \to \mathbf{u_0}$ if $t \to \infty$. Another definition is the one of the *Lyapunov stability* [66]. A solution $\mathbf{u_0}$ of a system is said to be Lyapunov stable if all trajectories that were close enough to the equilibrium at the initial time will remain close it. In other words,

$$(\forall \varepsilon > 0)\,(\exists \delta > 0)\,(\forall t > 0)\,|\mathbf{u}(0) - \mathbf{u_0}| \le \delta \Rightarrow |\mathbf{u}(t) - \mathbf{u_0}| \le \varepsilon,$$

where the symbols $\forall$ and $\exists$ are read as *for every* and *exist*, respectively. In the rest of this document we use the phrases *asymptotically stable* and *stable* as synonyms (unless explicitly mentioned).

The next two sections are devoted to studying some bifurcations and instabilities.

3.2. Bifurcations in Ordinary Differential Equations

Changes in a control parameter ε typically induce qualitatively different dynamical behaviors. The transition between these behaviors is named *bifurcation* [77, 66]. Bifurcations can generate or destroy steady states and/or change their stability.

3.2.1. Saddle-Node bifurcation

The Saddle-node bifurcation is responsible for the emergence of new equilibria, and the simplest equation that exhibits this mechanism is (*saddle-node normal form*) [25, 77]

$$\frac{\mathrm{d}u}{\mathrm{d}t} = \varepsilon - u^2, \tag{3.4}$$

Notice that there are two stationary states, namely $u_\pm = \pm\sqrt{\varepsilon}$, when ε is positive. On the other hand, for negative values of ε there is no equilibrium. Figure 3.2 shows these two states as function of the control parameter ε, this type of plot is known as *bifurcation diagram* [77]. The control parameter ε is called *bifurcation parameter* because it tunes the bifurcation (for $\varepsilon \leq 0$ there are no equilibrium, while for $\varepsilon \geq 0$ there are two equilibria).

The linear stability of each state is obtained by introducing a perturbation $u_\pm = \pm\sqrt{\varepsilon} + \delta u e^{\lambda t}$, replacing this ansatz in Eq (3.4), and linearizing around the perturbation δu, we obtain

$$\lambda_\pm = \mp 2\sqrt{\varepsilon}$$

$$\Rightarrow u_\pm(t) = \pm\sqrt{\varepsilon} + \delta u(0) e^{\mp 2\sqrt{\varepsilon}t},$$

therefore, the state u_- is unstable because the perturbations around it grow, while u_+ is stable because the nearby perturbations decay.

An interesting feature of the saddle-Node bifurcation is the existence of a *ghost* [77], that is, for small and negative values of ε, the dynamics around the origin of the phase space is slow, and typical evolution times scale as $\Delta t \sim |\varepsilon|^{-1/2}$. Then, in short experimental recordings and numerical simulations, it is possible to observe trajectories close to the unstable state u_0.
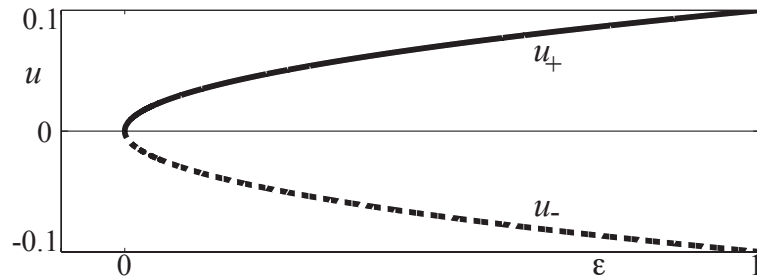

Figura 3.2: Saddle-Node bifurcation. This diagram shows the emergence of two solutions $u_\pm = \pm\sqrt{\varepsilon}$. The state u_+ (solid line) is stable while u_- is unstable (dashed line).

In several systems exhibiting the creation of two states, it is possible to construct a transformation from the original set of equations to the Saddle-Node normal form (3.4). In such case, u represents a relevant variable that accounts for a *critical mode*, that type of variable is known as *order parameters*. Critical modes can be stationary and uniform, stationary and non-uniform, or even non-stationary non-uniform. Some recent examples of saddle-node bifurcations include creation pulses [50, 27], localized patterns [10, 9] and oscillations in systems driven by time-dependent forces [13, 19]. The generality behind the saddle-node bifurcation renders it a *general mechanism*, often called *universal* or *robust phenomenon*, for the emergence of states.

3.2.2. Pitchfork bifurcation

Bifurcations can also involve the destabilization of states. Let us consider the following prototype model (*pitchfork normal form*) [25, 77]

$$\frac{\mathrm{d}u}{\mathrm{d}t} = \varepsilon u - u^3,\tag{3.5}$$

This systems has three steady states, namely $u_0 = 0$, and $u_\pm = \pm\sqrt{\varepsilon}$. The two last equilibria exist only for $\varepsilon \geq 0$, as shown in the bifurcation diagram of Fig. 3.3.

The stability analysis of the trivial state $u_0 = 0$ is quite simple, because its eigenvalue is

$$\lambda_0 = \varepsilon$$

$$\Rightarrow u(t) = \delta u(0)\mathrm{e}^{\varepsilon t}.$$

Then, the trivial state is stable for negative values of ε, while it is unstable for $\varepsilon > 0$. Perturbing close to the $u_\pm$ states, $u = \pm\sqrt{\varepsilon} + \delta u \mathrm{e}^{\lambda t}$, we obtain

$$\lambda_\pm = -2\varepsilon$$

$$\Rightarrow u_\pm(t) = \pm\sqrt{\varepsilon} + \delta u(0)\mathrm{e}^{-2\varepsilon t},$$

Then, both $u_\pm$ states are stable. The stability of u_- and u_+ must be the same because the Eq. (3.5) is invariant to reflection in the order parameter, that is $u \to -u$.

As it occurs for the Saddle-Node bifurcation, the variable u can account for the amplitude of a wide variety of modes, such as spatially periodic patterns, oscillations, uniform states, localized states, to mention a few.
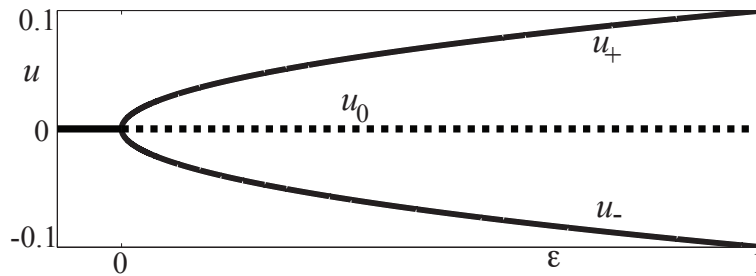

Figura 3.3: Pitchfork bifurcation. The diagram shows the trivial state $u_0 = 0$, which is stable for $\varepsilon < 0$ and unstable for $\varepsilon > 0$, and the stable solutions $u_\pm = \pm\sqrt{\varepsilon}$.
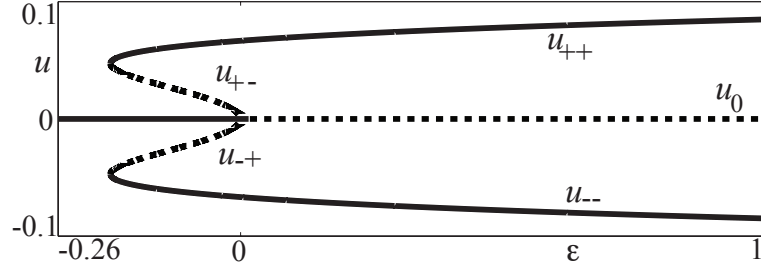
Figura 3.4: Cubic-Quintic stationary bifurcation. The bifurcation diagram shows the five steady states of Eq. (3.6), for $\nu = 1$. This diagram is characterized by biestability, that is, both u_{++}, u_0 and u_{--} are stable for $-\nu^2/4 \leq \varepsilon \leq 0$. The states u_{+-} and u_{-+} are unstable.

Supercritical and subcritical bifurcations.-   In the example of Eq. (3.5) the sign of the nonlinearity is negative, and therefore there is a continuous transition between the stable states u_0 and $u_\pm$ at $\varepsilon = 0$. This type of bifurcation is known as *supercritical* [77], or *second order phase transition*, because the new equilibria $u_\pm$ emerge after the trivial state u_0 is unstable, that is, when the bifurcation parameter surpasses the critical value $\varepsilon = 0$. However, in several systems the cubic nonlinearity has a positive sign. In that case, the bifurcation is described by the (*cubic-quintic equation*)

$$\frac{\mathrm{d}u}{\mathrm{d}t} = \varepsilon u + \nu u^3 - u^5, \tag{3.6}$$

where ν controls the sign of the cubic nonlinearity. A fifth order term was added to ensure saturation (the state of the system should not go to infinity). The equilibria are $u_0 = 0$ and

$$u_{\pm\pm} = \pm\sqrt{\frac{\nu}{2} \pm \frac{1}{2}\sqrt{\nu^2 + 4\varepsilon}}.$$

The bifurcation diagram of this equation is shown in Fig. 3.4, as this figure illustrates, the new states emerge before the trivial states becomes unstable. This bifurcation is known as *subcritical* [77], or *first order phase transition*, and it is characterized by exhibiting hysteresis loops.

A brief remark on bifurcations of reversible systems.-   The saddle-node and pitchfork equations described above are one variable first order equations and then they do not exhibit oscillations. A similar analysis can be conducted for *time-reversible* systems after replacing the first order derivative by a second order one, $\mathrm{d}/\mathrm{d}t \to \mathrm{d}^2/\mathrm{d}t^2$, to obtain the symmetry $t \to -t$. The stability analysis of time-reversible systems is quite similar to the one presented previously; indeed, asymptotically stable points studied here become Lyapunov stable in the reversible case and perturbations oscillate around the stable state; analogically unstable points studied here remain unstable in the reversible case, and perturbations around the unstable states, known as *hyperbolic points*.

Another interesting case is the one of the *perturbed time-reversible systems*, which typically take the form of driven damped oscillators. In the next subsection we study an example of that type of systems, and the well-known *Andronov-Hopf* [77] bifurcation that appears as the result of the balance between injection and dissipation of energy.

3.2.3. Andronov-Hopf bifurcation

Hamiltonian systems exhibit a family of oscillatory Lyapunov stable states—oscillatory orbits—parametrized continuously by a one or a few conserved quantities. In the case of dissipative systems, the balance between injection and dissipation of energy admits usually one isolated stable oscillatory state, known as *limit-cycle* or *self-oscillation*. Stable self-oscillations attract initial conditions that are close enough to them in the phase space. There are three main mechanisms that originate limit-cycles[3], namely the saddle-node bifurcation, the homoclinic bifurcation and the Andronov-Hopf instability. The two first cases are usually complicated to characterize because the trajectories are large and a perturbation analysis is not accurate, thus we review here the Andronov-Hopf instability, which admits a simple mathematical treatment.

Let us consider the Van der Pol model [77, 25]

$$\frac{\mathrm{d}^2 u}{\mathrm{d}t^2} = -\omega_0^2 u + 2\varepsilon \frac{\mathrm{d}u}{\mathrm{d}t} - u^2 \frac{\mathrm{d}u}{\mathrm{d}t}, \tag{3.7}$$

where the first term of the right-hand side of Eq. (3.7) accounts for oscillations at frequency ω_0, the second term is a linear dissipation for $\varepsilon < 0$ and a linear gain for $\varepsilon > 0$. The third term represents nonlinear damping. Notice that the time-reversion symmetry, $t \to -t$, is broken by both linear and nonlinear terms. The simplicity of this model renders it an ideal example to study limit-cycles in other contexts. Indeed, analogies between the Van der Pol equation and ferromagnets driven by spin-transfer torques have been established [73].

The Van der Pol oscillator admits only one steady state, $u_0 = 0$, and its eigenvalues are

$$\lambda = \varepsilon \pm \sqrt{\varepsilon^2 - \omega_0^2} \approx \varepsilon \pm \mathrm{i}\omega_0.$$

Figure 3.5(a) shows those eigenvalues. For $\varepsilon < 0$, the $u_0 = 0$ state is stable and the system

---

[3]Sometimes, another bifurcation, known as Infinite period-bifurcation [77], is considered. However this is not commonly observed.
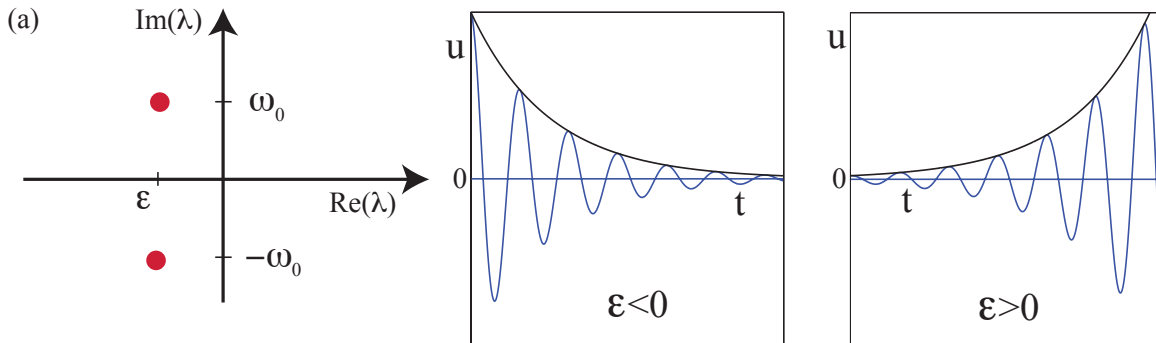

Figura 3.5: Andronov-Hopf instability. (a) Eigenvalues. (b) Decay $\varepsilon = -0{,}1$, and $\omega_0 = 1$. (c) Decay $\varepsilon = 0{,}1$, and $\omega_0 = 1$.

exhibits damped oscillations. On the other hand, if $\varepsilon > 0$, then oscillations increase their amplitude [see Fig. 3.5(c)]. At $\varepsilon = 0$, the *Andronov-Hopf instability* takes place. As the result of this instability, trajectories initially close to the stationary state $u_0 = 0$ grow in an oscillatory fashion until the nonlinearity of the equation saturates the oscillation envelope. This decay for $\varepsilon < 0$ and growth for $\varepsilon > 0$ of the oscillation envelops is an example of scales separation. Indeed, there is a fast time scale $\sim e^{i\omega_0 t}$, and a slow scale at which the oscillation amplitude $A(t)$ evolves. Furthermore the general solution of this system can be written as

$$u = A(t)e^{i\omega_0 t} + \bar{A}(t)e^{-i\omega_0 t} + W(A, \bar{A}, t),$$

where the two first terms are the solution to the linear part of the equation, and W is a small nonlinear correction that depends on polynomials of the amplitudes $(A, \bar{A})$. The function W is constructed so as to satisfy the equation and at cubic order it reads

$$W = c_{3,0}A^3 e^{3i\omega_0 t} + c_{2,1}A|A|^2 e^{i\omega_0 t} + c_{1,2}\bar{A}|A|^2 e^{-i\omega_0 t} + c_{0,3}\bar{A}^3 e^{-3i\omega_0 t},$$

where the $c_{j,k}$ coefficients have to be determined. This ansatz can be replaced in the Van der Pol model, and after straightforward calculations[4] one obtains at leading order

$$2i\omega_0 \frac{dA}{dt}e^{i\omega_0 t} - \omega_0^2 A e^{i\omega_0 t} - 2i\omega_0 \frac{d\bar{A}}{dt}e^{-i\omega_0 t} - \omega_0^2 \bar{A}e^{-i\omega_0 t} - 9\omega_0^2 c_{3,0}A^3 e^{3i\omega_0 t} - 9\omega_0^2 c_{0,3}\bar{A}^3 e^{-3i\omega_0 t}$$
$$= -\omega_0^2 \left(Ae^{i\omega_0 t} + \bar{A}e^{-i\omega_0 t}\right) + 2i\omega_0\varepsilon \left(Ae^{i\omega_0 t} - \bar{A}e^{-i\omega_0 t}\right) - i\omega_0 A^3 e^{3i\omega_0 t} + i\omega_0 \bar{A}^3 e^{-3i\omega_0 t}$$
$$-i\omega_0 |A|^2 \left(Ae^{i\omega_0 t} - \bar{A}e^{-i\omega_0 t}\right) - \omega_0^2 c_{3,0}A^3 e^{3i\omega_0 t} - \omega_0^2 c_{0,3}\bar{A}^3 e^{-3i\omega_0 t}. \tag{3.8}$$

Notice that A and dA/dt are slow functions of time, that is, these functions are approximately constants for time scales of order $2\pi/\omega_0$. Due to the orthogonality of trigonometric functions in Fourier space, we can decompose the above equation in the basis $\{e^{3i\omega_0 t}, e^{i\omega_0 t}, e^{-i\omega_0 t}, e^{-3i\omega_0 t}\}$. Equating the terms proportional to $e^{i\omega_0 t}$ one obtains

$$\boxed{\frac{dA}{dt} = \varepsilon A - \frac{1}{2}A|A|^2.}$$

This model is the well known *Ginzburg-Landau equation* [66] with real coefficients[5]. The calculation conducted above is an example of *weakly nonlinear analysis* [25], and it permits obtaining analytic expressions for the self-oscillation and approximate solutions for the Van der Pol equation. Furthermore, the stationary equilibrium of the envelope A and its corresponding oscillatory state in the original variable u are given by

$$A = \sqrt{2\varepsilon}e^{i\phi_0},$$

$$u \approx 2\sqrt{2\varepsilon}\cos(\omega_0 t + \phi_0),$$

where ϕ_0 is an oscillation phase.

---

[4]Let us assume that $\varepsilon \ll 1$ and that A is a slowly varying small function of time, that is $|dA/dt| \ll |A| \ll 1$. Given this scaling,
   only the dominant order terms in dA/dt and ε will be considered.
   [5]The coefficients are real because the nonlinear term of the Van der Pol equation is proportional to du/dt, that is, it breaks the time-reversion symmetry. In more general cases other terms appear, such as u^3 and $u(du/dt)^2$, and the coefficients of the Ginzburg-Landau equation will be complex.

In an analog manner, projecting Eq. (3.8) on the Fourier functions $\{\mathrm{e}^{3\mathrm{i}\omega_0 t}, \mathrm{e}^{-3\mathrm{i}\omega_0 t}\}$ permits obtaining the unknown coefficients $\{c_{3,0}, c_{0,3}\}$. Note that the terms proportional to $\{c_{3,0}, c_{0,3}\}$ are necessary to be included in the Ansatz to balance the nonlinearities of Eq. (3.8); otherwise, the Ansatz is not a solution. On the other hand, the terms proportional $\{c_{2,1}, c_{1,2}\}$ not necessary because they do not appear in the projection equation. Then, we can eliminate those terms by choosing $c_{2,1} = c_{1,2} = 0$.

3.3.   Bifurcations in Partial Differential Equations

We extend here our analysis to fields $u = u(t, x)$ that depend on time and one spatial coordinate x. This type of systems can also exhibit saddle-node, pitchfork and Andronov-Hopf bifurcations [25]. Moreover, for homogeneous and isotropic systems, that is, systems that are invariant to spatial translations $x \to x + \Delta x$ and spatial reflection $x \to -x$, the three above mentioned bifurcations take the following forms

$$\partial_t u = \varepsilon - u^2 + \partial_{xx} u,$$
$$\partial_t u = \varepsilon u - u^3 + \partial_{xx} u,$$
$$\partial_{tt} u = -\omega_0^2 u + 2\varepsilon \partial_t u - u^2 \partial_t u + \partial_{xx} u,$$

where ∂_t and ∂_x are the partial derivatives for time and space, respectively. The Laplacian operator accounts for diffusion or transport processes in the first order equations and dispersion in the second order equations. In that case, the homogeneous stationary equilibria of each model are the same states discussed in the previous subsections. The stability analysis should consider perturbations with different wavelengths k, that is,

$$\delta \mathbf{u} = \mathrm{e}^{\lambda t + \mathrm{i}kx} \mathbf{v}.$$

It is possible, however, to demonstrate that the critical modes responsible for the destabilization of the system—*leading modes*—are homogeneous $k = 0$. Hence, all the results of the saddle-node, pitchfork and Andronovh-Hopf bifurcations remain equal for typical space dependent systems, where the spatial coupling is a Laplacian.

The situation changes drastically when the sign of the Laplacian is negative, because in this situation the system exhibits non-uniform states. In the next subsection we study a prototype model known as the *Swift-Hohenberg equation* where the diffusion coefficient is negative. In that case the system self-organizes into *patterns*, which are spatially periodic textures [35].

3.3.1.   Spatial instability

Lets consider the following model (*Swift-Hohenberg equation*) [25, 66]

$$\partial_t u = \varepsilon u - u^3 - (q^2 + \partial_{xx})^2 u. \tag{3.9}$$

This equation has three homogeneous stationary states, $u_0 = 0$, $u_\pm = \pm(\varepsilon - q^4)^{1/2}$. The stability of the first solution u_0 is given by the following eigenvalues [see Fig. 3.6(a)]

$$\lambda = \varepsilon - (q^2 - k^2)^2, \tag{3.10}$$

where k is the wavelength of the perturbation. As Fig. 3.6(a) illustrates, perturbations decay exponentially for $\varepsilon < 0$, independently of their wavelength. However, perturbations with wavenumber q are suppress in a slow rate $\lambda(q) = \varepsilon$. On the other hand, for positive values of ε, the mode with wavenumber q will increase its amplitude and destabilize the u_0 state. This bifurcation is known as *spatial instability*, *Turing instability* in the context of chemical media, and *modulational instability* in optics. Spatial instabilities are responsible for the emergence of patterns.

The scales separation between fast and slow modes, as illustrated by Eq. 3.10, permits one to study the envelope of the pattern for times $\tau \sim 1/\varepsilon$. Let us consider an ansatz similar to the one used for the Andronov-Hopf instability,

$$u(x,t) = A(t)e^{iqx} + \bar{A}(t)e^{-iqx} + W(A, \bar{A}, x), \tag{3.11}$$

where A is a slowly varying amplitude (the envelope of the spatial mode with wavenumber q), and W is a small nonlinear correction of general form

$$W = c_{3,0}A^3 e^{3iqx} + c_{2,1}A|A|^2 e^{iqx} + c_{1,2}\bar{A}|A|^2 e^{-iqx} + c_{0,3}\bar{A}^3 e^{-3iqx}.$$

Let us assume that the parameter ε and the amplitude A are small. Replacing the ansatz (3.11) in Eq. (3.9) one obtains the following expression at dominant order

$$\frac{dA}{dt}e^{iqx} + \frac{d\bar{A}}{dt}e^{-iqx} = \varepsilon A e^{iqx} + \varepsilon \bar{A}e^{-iqx} + 8c_{3,0}A^3 e^{3iqx}$$
$$+ \quad 8c_{0,3}\bar{A}^3 e^{-3iqx} - \left(A^3 e^{3iqx} + 3A|A|^2 e^{iqx} + 3\bar{A}|A|^2 e^{-iqx} + \bar{A}^3 e^{-3iqx}\right). \tag{3.12}$$

This equation can be separated into four equations by projecting over the Fourier series

$$\{e^{3iqx}, e^{iqx}, e^{-iqx}, e^{-3iqx}\}.$$

These projections allow one to find both the dynamics of $A(t)$ and the form of the correction W,
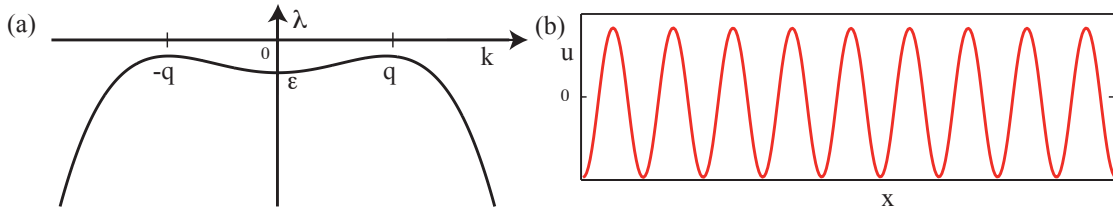
$$\frac{dA}{dt} = \varepsilon A - 3|A|^2 A,$$

Figura 3.6: Spatial instability in the Swift-Hohenberg equation. (a) Eigenvalue curve as function of the wavenumber k. There are two maxima at $k = \pm q$. (b) Pattern solution for $\varepsilon > 0$.

$$\frac{\mathrm{d}\bar{A}}{\mathrm{d}t} = \varepsilon\bar{A} - 3|A|^2\bar{A},$$

$$c_{3,0} = c_{0,3} = \frac{1}{8}.$$

Then, the pattern amplitude obeys the real Ginzburg-Landau equation. This model has known steady states $A_0 = (\varepsilon/3)^{1/2}\mathrm{e}^{\mathrm{i}\phi_0}$, where ϕ_0 is a real constant. Then the pattern solution $u_p(x)$ reads at leading order

$$u_p(x) = 2\sqrt{\frac{\varepsilon}{3}}\cos(qx + \phi_0).$$

3.3.2. Instabilities in systems driven by time-dependent forces

Here we discuss *parametrically driven system*, which are characterized by a response frequency that is a half of the forcing frequency, that is, their dynamics is approximately $u \sim A\mathrm{e}^{\mathrm{i}\frac{\omega}{2}t} + c.c$, where ω is the driving frequency. An example of a parametrically driven system is a magnetic medium forced at twice its natural frequency. This type of system exhibits a *parametric resonance* and several instabilities.

We consider the same model presented in Sec. 2.3, that is, a wire along the z-axis. The magnetization is governed by the following model

$$\frac{\partial\mathbf{m}}{\partial t} = -\mathbf{m} \times [h\mathbf{e}_x - \beta m_z\mathbf{e}_z + \partial_{ZZ}\mathbf{m}] + \alpha\mathbf{m} \times \frac{\partial\mathbf{m}}{\partial t}, \qquad (3.13)$$

where the external field is given by $h(t) = H_0 + h_0\cos(2[\omega_0 + \nu]t)$, and ν is a detuning between half the forcing frequency and the natural frequency. To grasp the dynamics of the Eq. (3.13), it is convenient to approximate it by the leading order contributions

$$\begin{aligned}
\frac{\partial}{\partial t}\begin{pmatrix} m_y \\ m_z \end{pmatrix} &\approx \begin{bmatrix} 0 & \partial_{ZZ} - H_0 - \beta \\ H_0 - \partial_{ZZ} & 0 \end{bmatrix}\begin{pmatrix} m_y \\ m_z \end{pmatrix} \\
&+ \frac{h_0}{2}\left(\mathrm{e}^{2\mathrm{i}(\omega_0+\nu)t} + \mathrm{e}^{-2\mathrm{i}(\omega_0+\nu)t}\right)\begin{bmatrix} 0 & -1 \\ 1 & 0 \end{bmatrix}\begin{pmatrix} m_y \\ m_z \end{pmatrix} \\
&+ \frac{\beta}{2}(m_y^2 + m_z^2)\begin{pmatrix} m_z \\ 0 \end{pmatrix} - \alpha\begin{bmatrix} H_0 & 0 \\ 0 & H_0 + \beta \end{bmatrix}\begin{pmatrix} m_y \\ m_z \end{pmatrix}.
\end{aligned} \qquad (3.14)$$

We considered only the dominant order terms[6] in this equation. To describe the behavior of the oscillator, it is convenient to use the oscillation amplitude $B(t, Z)$ as variable [79, 80, 50, 12, 11, 14]

$$\begin{pmatrix} m_y \\ m_z \end{pmatrix} = B(t, Z)\mathrm{e}^{\mathrm{i}\omega_0 t}\mathbf{u} + c.c. + \mathbf{W}, \qquad (3.15)$$

where B represents a slowly varying oscillation envelope, that is $|\partial_{zz}B| \sim |\partial_t B| \ll |B| \ll 1$ and $\mathbf{W} = \mathbf{W}(B, \bar{B}, \partial_{ZZ}B, \partial_{ZZ}\bar{B}, t)$ is a correction that comes from the nonlinear nature of

---

[6]This is equivalent to consider that operators, variables, and parameter scale as $h_0 \sim \alpha \sim \nu \sim m_y^2 \sim m_z^2 \sim \partial_{ZZ} \ll 1$. and $\partial_t \sim H_0 \sim \beta$ or order 1. Then, terms such as $\alpha m_z^2 m_y$ and $m_y m_z \partial_{ZZ} m_z$ are higher order corrections and we neglect them. Indeed, you can formalize the all the calculations by introducing an expansion parameter and expressing all quantities in terms of this parameter.

the problem, and it scales as $|\mathbf{W}| \sim |B|^3$. Replacing the above Ansatz in Eq. (3.14), and linearizing around the correction $\mathbf{W}$, one obtains

$$
\begin{aligned}
\hat{L}\mathbf{W} = {}& \partial_t B \mathbf{u} + (\partial_{ZZ} - \mathrm{i}\alpha\omega_0)\, B\mathrm{e}^{\mathrm{i}\omega_0 t} \begin{pmatrix} \mathrm{i}\sqrt{H_0} \\ \sqrt{H_0 + \beta} \end{pmatrix} \\
& + \ \mathrm{i}\frac{\beta}{2}\sqrt{H_0}\,(4H_0 + \beta)\, B|B|^2 \mathrm{e}^{\mathrm{i}\omega_0 t} \begin{pmatrix} 1 \\ 0 \end{pmatrix} + B^3 \mathrm{e}^{3\mathrm{i}\omega_0 t}\mathbf{f}_{ct} \\
& - \ \frac{h_0}{2}\bar{B}\mathrm{e}^{2\mathrm{i}\nu t}\mathrm{e}^{\mathrm{i}\omega_0 t} \begin{pmatrix} -\mathrm{i}\sqrt{H_0} \\ \sqrt{H_0 + \beta} \end{pmatrix} + c.c.,
\end{aligned}
\tag{3.16}
$$

where the vector $\mathbf{f}_{ct}$ collects all the constant of the cubic term B^3, and the linear operator $\hat{L}$ is

$$
\hat{L} = \begin{bmatrix} -\partial_t & -H_0 - \beta \\ H_0 & -\partial_t \end{bmatrix}.
$$

The linear equation $\hat{L}\mathbf{W} = \mathbf{g}_{\mathbf{rhs}}$ for the unknown $\mathbf{W}$, where $\mathbf{g}_{\mathbf{rhs}}$ is the right-hand side of Eq. (3.16), can be solved only if $\mathbf{g}_{\mathbf{rhs}}$ is in the image of the operator $\hat{L}$. By the Freedholm alternative [66], the equation $\hat{L}\mathbf{W} = \mathbf{g}_{\mathbf{rhs}}$ can be solved if $\mathbf{g}_{\mathbf{rhs}}$ is orthogonal to the elements of the Kernel of the adjoint operator $\hat{L}^\dagger$. We define the inner product of functions space

$$
(\mathbf{f}, \mathbf{g}) \equiv \frac{\omega_0}{2\pi} \int_{t_0}^{t_0 + 2\pi/\omega_0} (\bar{\mathbf{f}} \cdot \mathbf{g})\, \mathrm{d}t,
$$

where the symbol $\cdot$ denotes the inner product of vectors with complex components, i.e. the dot product of $\mathbb{C}^2$, and $\bar{\mathbf{f}}$ is the complex conjugate of the vector $\mathbf{f}$. Then the operator $\hat{L}^\dagger$ adjoin to $\hat{L}$ is given by

$$
\hat{L}^\dagger = \begin{bmatrix} \partial_t & H_0 \\ -H_0 - \beta & \partial_t \end{bmatrix}.
$$

The kernel of $\hat{L}^\dagger$ is given by $\hat{L}^\dagger \left[\mathrm{e}^{\mathrm{i}\omega_0 t}\mathbf{v}\right] = \hat{L}^\dagger \left[\mathrm{e}^{-\mathrm{i}\omega_0 t}\bar{\mathbf{v}}\right] = 0$, where $\mathbf{v} = (\sqrt{H_0}, \mathrm{i}\sqrt{H_0 + \beta})^T$, and the symbol ^{T} stands for the transpose. Then projecting the right hand side of Eq. (3.16) over $\mathrm{e}^{\mathrm{i}\omega_0 t}\mathbf{v}$ and equaling to zero, after straightforward calculations one obtains

$$
\begin{aligned}
2\omega_0 \partial_t B = {}& -\mathrm{i}\frac{\beta}{2}(\omega_0^2 + 3H_0^2)B|B|^2 - \mathrm{i}(2H_0 + \beta)\partial_{ZZ}B \\
& - \ \alpha\omega_0(2H_0 + \beta)B + \mathrm{i}\frac{\beta h_0}{2}\mathrm{e}^{2\mathrm{i}\nu t}\bar{B}.
\end{aligned}
\tag{3.17}
$$

Introducing the following normalization for the envelope

$$
B(t, Z) = \sqrt{\frac{4\omega_0}{\beta\,(\omega_0^2 + 3H_0^2)}}\, A(t, Z)\mathrm{e}^{\mathrm{i}\nu t + \mathrm{i}\pi/4},
$$

in Eq. (3.17), we obtain

$$
\boxed{\partial_t A = -\mathrm{i}\left(\nu A + |A|^2 A + \partial_{zz}A\right) - \mu A + \gamma \bar{A},}
\tag{3.18}
$$

where $\mu \equiv \alpha \left(2H_0 + \beta\right)/2$ and $\gamma \equiv \beta h_0/(4\omega_0)$ account for the dissipation and the parametric injection, respectively. The spatial coordinate z is $z \equiv \sqrt{2\omega_0/(2H_0 + \beta)}Z$. This is the well-known *parametrically driven, damped nonlinear Schrödinger* equation (PDNLS) [13, 11]. This model describes several systems, such as vibrated fluids [58], parametrically driven optical resonators [52], spin-transfer nano-oscillators [48, 19], among others.

It is worth noting that the equation (3.18) is quite simple or minimal, because it considers only one term for each physical effect involved (frequency, nonlinearity, disspersion, dissipation and injection). This simplicity renders the PDNLS equation a very general model that explains and predicts dynamics in a wide variety of physical systems.

Solutions of the PDNLS equation.- There are two natural decompositions for the complex amplitude A of the PDNLS equation, they are the real and imaginary parts $A = u + iv$, and the modulus and phase $A = Re^{i\phi}$. In the first case we have

$$\partial_t u = (\gamma - \mu)u + (\nu + \partial_{xx})v + v(u^2 + v^2),$$
$$\partial_t v = -(\nu + \partial_{xx})u - (\gamma + \mu)v - u(u^2 + v^2). \tag{3.19}$$

The stability of the trivial state $u = v = 0$ is determined by its eigenvalues

$$\lambda_{\pm} = -\mu \pm \sqrt{\gamma^2 - (\nu - k^2)^2}, \tag{3.20}$$

which describes two bifurcations, the first one is a stationary instability that takes place when $\gamma \geq \sqrt{\nu^2 + \mu^2}$. The zone of the parameter space where the trivial equilibrium $A = 0$ is unstable because of this stationary instability is known as Arnold tongue (see Fig. 3.7).

Spatially periodic textures.- When injection of energy surpasses dissipation $\gamma \geq \mu$ and the detuning is possitive $\nu \geq 0$, the eigenvalue λ_+ can be positive, and then the $A = 0$ state becomes unstable. This bifurcation induces patterns with wavenumber $\sqrt{\nu}$. It is possible to
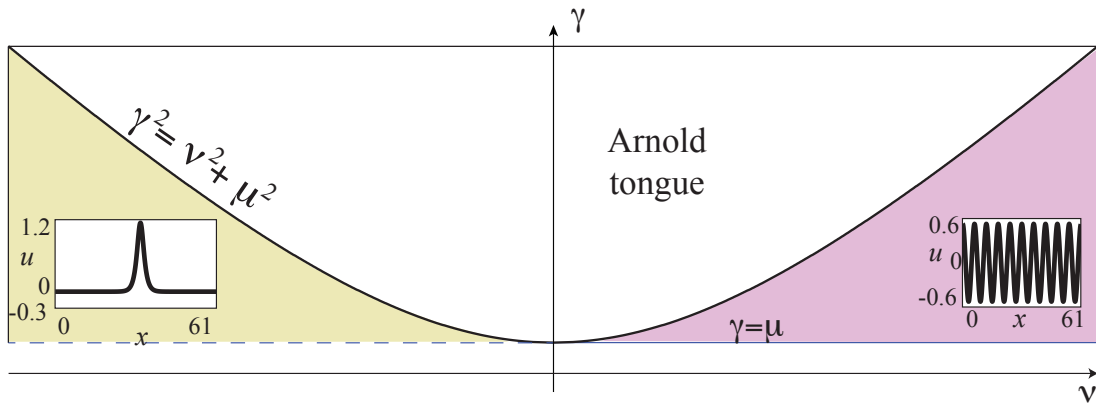

Figura 3.7: Bifurcation diagram of the PDNLS model. The insets show dissipative solitons and patterns obtained from Eq. (3.19). Parameter values are $\gamma = 0{,}5$, $\mu = 0{,}45$, and $\nu = -0{,}5$ and $\nu = 1$ for solitons and patterns, respectively.

characterize the emergence of patterns in the weakly nonlinear regime in analogy to what was done for the Swift-Hohenberg equation in last subsection. Indeed, introducing the ansatz[7]

$$
\begin{pmatrix} u \\ v \end{pmatrix} = T \mathrm{e}^{\mathrm{i}\sqrt{\nu}x} \begin{pmatrix} 1 \\ 0 \end{pmatrix} - \frac{3}{2\mu} T|T|^2 \mathrm{e}^{\mathrm{i}\sqrt{\nu}x} \begin{pmatrix} 0 \\ 1 \end{pmatrix} + \frac{T^3}{8\nu} \mathrm{e}^{3\mathrm{i}\sqrt{\nu}x} \begin{pmatrix} 1 \\ 0 \end{pmatrix} + c.c. + ..., \tag{3.21}
$$

in Eq. (3.19), where T stands for the envelope of the pattern, one obtains the amplitude equation [23]

$$
\partial_t T = (\gamma - \mu)T - \frac{9}{2\mu} T|T|^4. \tag{3.22}
$$

It is worth noting that the amplitude equation does not contain cubic nonlinearities. This is because the nonlinear saturation of a pattern is induced by dissipation, and there is no cubic dissipation. Equation (3.22) predicts the formation of a stable pattern for $\gamma \geq \mu$. The inset of Fig. 3.7 shows this solution, which at leading order reads $A \approx 2(2\mu(\gamma - \mu)/9)^{1/4} \cos(\sqrt{\nu}x)$.

Localized states.- In the modulus and phase representation, $A = R\mathrm{e}^{\mathrm{i}\phi}$, the PDNLS model becomes

$$
\begin{aligned}
\partial_t R &= -\mu R + 2\partial_x R \partial_x \phi + R\partial_{xx}\phi + \gamma R \cos(2\phi), & (3.23) \\
R\partial_t \phi &= -\nu R - R^3 - \partial_{xx}R + R(\partial_x \phi)^2 - \gamma R \sin(2\phi), & (3.24)
\end{aligned}
$$

which admits the following localized states solution

$$
\begin{aligned}
\sin(2\phi_s) &= \mu/\gamma, \\
R_s(x) &= \sqrt{2\delta}\,\mathrm{sech}(\sqrt{\delta}[x - x_0]),
\end{aligned} \tag{3.25}
$$

where $\delta = -\nu + \sqrt{\gamma^2 - \mu^2}$, and x_0 is the soliton position. This is a particle-like stationary solution in the PDNLS model, and it represents a localized oscillatory state in the Landau-Lifshitz-Gilbert equation [cf. Fig. 2.1(a)]. In 2011, it was demonstrated that the the uniform phase soliton given by formula (3.25) is stable only for systems with small lateral dimensions [15, 21, 20, 17]. Indeed, for system size above a critical value, the phase variable ϕ_s becomes a function of space [15].

3.3.3. Galerkin Expansions

The analytic methods studied in the previous sections are valid at the onset of a bifurcation or resonance. However, in several other cases it is not possible to describe a phenomenon in terms of a normal form, because there is not a suitable expansion parameter, or because the

---

[7]A general ansatz should consider several higher order corrections. Those higher order terms are nonlinear in the amplitude T and its complex conjugate, $\bar{T}$, and they can be separated in terms of order three and five in the amplitude $|T|$. The ansatz presented here considers a particular form of the cubic nonlinear correction, which was obtained after replacing the general ansatz in the PDNLS equation and balancing the cubic order terms.

state of the system is highly nonlinear, or just due to the large number of spatial modes involved. In such cases, it is possible to conduct a modal decomposition where the equations are projected into one or a few arbitrarily selected modes. This type of projection is known as the *Garlerkin expansion* [67], and it does not require a bifurcation, solvability condition, or an expansion parameter.

Let us consider the following partial differential equation

$$\partial_t \mathbf{u} = \mathbf{f}\left(\mathbf{r}, \mathbf{u}, \nabla^2 \mathbf{u}\right),$$

where $\mathbf{f}$ is in general a function of space coordinates $\mathbf{r}$, and $\mathbf{u}$ is system variable. We introduce an Ansatz of the form

$$\mathbf{u} = \sum_{j=1}^{N} A_j(t) \mathbf{g}_j\left(\mathbf{r}\right),$$

where $\{\mathbf{g}_j\}_{j=1}^{N}$ is an appropriate set of orthonormal functions for a given inner product $(\mathbf{g}_j, \mathbf{g}_k) = \delta_{jk}$. Such variables are usually chosen motivated by experimental or numerical results. $\{A_j\}_{j=1}^{N}$ are time dependent amplitudes associated to the corresponding modes. Replacing the ansatz in the equation for $\mathbf{u}$, and projecting over $\mathbf{g}_k$, we obtain the following set of equations

$$\frac{\mathrm{d}A_k}{\mathrm{d}t} = (\mathbf{f}', \mathbf{g}_k),$$

where $\mathbf{f}'$ is the function $\mathbf{f}$ evaluated on the ansatz [67]. Let us mention a few remarks about this kind of expansions,

- This modal decomposition does not require separation of spatiotemporal scales. Indeed, the spatial modes $\{\mathbf{g}_j\}_{j=1}^{N}$ are arbitrarily chosen. Then, it is necessary to have some previous knowledge about the solutions.
- If the function $\mathbf{f}$ is nonlinear, then a nonlinear correction $\mathbf{W}$ should be added to the ansatz. Since this is not usually done in Galerkin expansions, the Galerkin method can be less precise than normal forms.
- In the normal form approach, the solvability condition completely determines the structure of the amplitude equations[8]. For instance, the equations for most spatial instabilities take the form of *relaxation equations*. On the other hand, Galerkin expansions do not have such constrains. This permits one to describe a wide variety of behaviors, such as chaos and oscillations, that are prohibited for some normal forms [60].
- We have described here the simplest type of Galerkin expansion. This method can be generalized in several ways [67], for instance it is possible to use spatio-temporal modes $\mathbf{g}_j = \mathbf{g}_j(t, \mathbf{r})$ and slowly varying space dependent amplitudes $A_j = A_j(t, \mathbf{r})$.

---

[8]Solvability condition is usually written as $\hat{L}\mathbf{W} = \mathbf{g_{rhs}}$, where $\mathbf{W}$ is a nonlinear correction and the function $\mathbf{g_{rhs}}$ depends on the amplitude of the critical modes. The form of all the admissible terms of amplitude equations is determined by the linear operator $\hat{L}$. Thus, the nonlinear behavior of a system strongly depends on its linear behavior at the bifurcation point. See Ref. [28] for more details.

Some examples of Galerkin expansions can be found in Refs. [60, 36, 63, 44, 16], where the complicated spatiotemporal behavior is represented in terms of the relevant modes.

3.4. Numerical methods to study nonlinear magnetization dynamics

It is well-known that several differential equations are non-integrable, that is, their solutions cannot be expressed in terms of integrals. Indeed, a wide variety of systems exhibit chaos, an universal behavior where the predictability is restricted to short times [77]. This motivates the use of numerical methods to solve differential equations. Moreover, the numerical exploration of a model can be seen as a *numerical experiment*, and it permits one to discover new types of solutions and to develop a deep intuition about complicated equations.

There are several methods to conduct numerical integration. We present here a commonly used scheme based on a Runge-Kutta algorithm for the temporal evolution and finite differences for the space discretization. This is, perhaps, one the the simplest numerical integration strategies, and at the same time, this method provides both precision and efficiency for most equations.

Runge-Kutta algorithm for temporal integration Let us consider the following first order differential equation

$$\frac{d\mathbf{u}}{dt} = \mathbf{f}(t, \mathbf{u}),$$

where the N-components vector $\mathbf{u} \in \mathbb{R}^N$ is a function of time. Time evolves in discrete steps, $t \to t_n$, where n is an integer number. The evolution of the function $\mathbf{u_n} \equiv \mathbf{u}(t_n)$ can be obtained by means of a Taylor expansion of the form $\mathbf{u_{n+1}} \approx \mathbf{u_n} + dt\mathbf{f}(t, \mathbf{u_n}) + O(dt^2)$, where the step size is $dt \equiv t_{n+1} - t_n$. A more precise expression can be obtained by combining several Taylor expansions—explicit method—, among them let us mention the *fifth order Runge-Kutta scheme*

$$\mathbf{u_{n+1}} = \mathbf{u_n} + \frac{37}{378}\mathbf{k_1} + \frac{250}{621}\mathbf{k_3} + \frac{125}{594}\mathbf{k_4} + \frac{512}{1771}\mathbf{k_6} + O(dt^6),$$

where the $\mathbf{k_j}$ vectors are given by [68]

$$\mathbf{k_1} = dt\mathbf{f}\left(t_n, \mathbf{u_n}\right),$$

$$\mathbf{k_2} = dt\mathbf{f}\left(t_n + \frac{1}{5}dt, \mathbf{u_n} + \frac{1}{5}\mathbf{k_1}\right),$$

$$\mathbf{k_3} = dt\mathbf{f}\left(t_n + \frac{3}{10}dt, \mathbf{u_n} + \frac{3}{40}\mathbf{k_1} + \frac{9}{40}\mathbf{k_2}\right),$$

$$\mathbf{k_4} = dt\mathbf{f}\left(t_n + \frac{3}{5}dt, \mathbf{u_n} + \frac{3}{10}\mathbf{k_1} - \frac{9}{10}\mathbf{k_2} + \frac{6}{5}\mathbf{k_3}\right),$$

$$\mathbf{k_5} = \mathrm{d}t\mathbf{f}\left(t_n + \mathrm{d}t, \mathbf{u_n} - \frac{11}{54}\mathbf{k_1} + \frac{5}{2}\mathbf{k_2} - \frac{70}{27}\mathbf{k_3} + \frac{35}{27}\mathbf{k_4}\right),$$

$$\mathbf{k_6} = \mathrm{d}t\mathbf{f}\left(t_n + \frac{7}{8}\mathrm{d}t, \mathbf{u_n} + \frac{1631}{55296}\mathbf{k_1} + \frac{175}{512}\mathbf{k_2} + \frac{575}{13824}\mathbf{k_3} + \frac{44275}{110592}\mathbf{k_4} + \frac{253}{4096}\mathbf{k_5}\right).$$

This choice of coefficients to sum Taylor expansions is known as Cash-Karp parameters [68]. The above scheme can be used to integrate a set of ordinary differential equations using a constant step size $\mathrm{d}t$. However, the characteristic time scale in which out of equilibrium systems evolve strongly depends on the control parameters and states. Then, it is much more efficient to adapt the step size to obtain a desired integration error. Numerical errors can be estimated by comparing the results of two Runge-Kutta routines of different orders. For instance, along this thesis we estimate errors by comparing the $\mathbf{u_{n+1}}$ functions obtained from both a fourth and a fifth orders Runge-Kutta schemes (see Ref. [68] for the detail implementation).

It is worth noting that the variable step-size fifth order Runge-Kutta algorithm is only one example of the several routines for the integration of differential equations. Other methods are the symplectic, predictor corrector, and Runge-Kutta schemes of order four or six [68]. However, for most dissipative physical systems the variable step-size fifth order Runge-Kutta algorithm is both efficient and accurate.

Finite differences for spatial discretization   Let us discretize the spatial coordinate x into a set of positions, $x_j = j\Delta x$, where the index $j = 0, 1, 2...$ takes discrete values and it labels positions. The constant Δx stand for the distance between two adjacent positions $\Delta x = x_{j+1} - x_j$. Functions of space $f = f(x)$ also become discretized $f_j = f(x_j)$. This scheme is known as finite differences, and it permits to approximate the derivative and laplacian operators by the following expressions [37]

$$\frac{1}{60}f_{i+3} - \frac{3}{20}f_{i+2} + \frac{3}{4}f_{i+1} - \frac{3}{4}f_{i-1} + \frac{3}{20}f_{i-2} - \frac{1}{60}f_{i-3} = \mathrm{d}x \cdot \partial_x f_i + \frac{\mathrm{d}x^7}{140}f_i^{(7)},$$

$$\frac{1}{90}f_{i+3} - \frac{3}{20}f_{i+2} + \frac{3}{2}f_{i+1} - \frac{49}{18}f_i + \frac{3}{2}f_{i-1} - \frac{3}{20}f_{i-2} + \frac{1}{90}f_{i-3} = \mathrm{d}x^2 \cdot \partial_{xx} f_i + \frac{\mathrm{d}x^8}{560}f_i^{(8)}.$$

Notice that if $f_i^{(8)} \sim 1$ and $\mathrm{d}x \sim 0.1$, then the last term of the right-hand side of the laplacian expression is of order $\mathrm{d}x^8 f_i^{(8)}/560 \sim 10^{-11}$.

Capítulo 4

Discussion

We present here a general motivation and discussion of the main results of this thesis, while all details are presented in Chapters A, B, C, D, and E. Those five chapters are the manuscripts generated by this research work.

4.1. Ferromagnetic layer in presence of a direct spin-polarized electric current

Let us consider the spin-valve described in Sec. 2.5. The free magnetization obeys the Landau-Lifshitz-Gilbert equation, that takes the following form in the stereographic representation (see subsection 2.5.3)

$$
(i + \alpha) \, \partial_T \psi = (ig - h_0) \, \psi - \frac{\beta_z}{2} \left(\psi - \overline{\psi} \right) \frac{1 + \psi^2}{1 + |\psi|^2} - \beta_x \psi \frac{1 - |\psi|^2}{1 + |\psi|^2} + \nabla^2 \psi - 2 \frac{\overline{\psi}}{1 + |\psi|^2} \left(\nabla \psi \right)^2 ,
$$
(4.1)

where the complex field $\psi = (m_y + im_z)/(1 + m_x)$ accounts for deviations from the parallel state $\mathbf{m} = \mathbf{e_x}$. The parameters h_0 and g are the external field along the x-axis and the spin-polarized electric current with polarization direction on the x-axis, respectively. The coefficients $\{\beta_x, \beta_z\}$ are the anisotropy constants for the x-axis (easy axis) and the z-axis (hard axis). The phenomenological coefficient α is Gilbert's damping.

A particularly interesting limit of model (4.1) is obtained under the following assumptions:

- The deviations from the parallel state $\psi = 0$ are small ($\psi \ll 1$). This permits us to consider only the dominant nonlinearity—third order terms—and neglect higher order nonlinearities.

- The magnetization varies slowly in space, that is $|\nabla^2 \psi| \ll k|\nabla \psi| \ll 1$, where k is a

characteristic wavenumber. This allows considering just one dispersion term

$$\nabla^2\psi - 2\frac{\overline{\psi}}{1+|\psi|^2}\left(\nabla\psi\right)^2 \approx \nabla^2\psi.$$

- We assume that the perpendicular anisotropy coefficient β_z is small, which is valid for devices where the perpendicular magnetocristalyne anisotropy partially cancels the demagnetization effect (see [69] and references therein),

$$\frac{\beta_z}{2}\left(\psi - \overline{\psi}\right)\frac{1+\psi^2}{1+|\psi|^2} \approx \frac{\beta_z}{2}\left(\psi - \overline{\psi}\right).$$

- In common devices composed by hard magnetic materials, the dissipation and spin-transfer torque coefficients are small, $\alpha \sim |g| \ll 1$, while the in-plane anisotropy coefficient β_x and the external field h_0 are of order 1.

Under these assumptions, Eq. (4.1) is approximated by

$$i\partial_T\psi \approx (ig - h_0[1 + i\alpha])\,\psi - \frac{\beta_z}{2}\left(\psi - \overline{\psi}\right) - \beta_x\psi\left(1 + i\alpha - 2|\psi|^2\right) + \nabla^2\psi.$$

The above equation scales as $|\psi|^2 \sim \nabla^2 \sim \alpha \sim |g| \ll 1$ and $h_0 \sim \beta_x \sim 1$. Introducing a change of variables for the amplitude $A \equiv \psi e^{i\pi/4}/\sqrt{2\beta_x + \beta_z} \approx \psi e^{i\pi/4}/\sqrt{2\beta_x}$, the above equation takes the form of the well-known *parametrically driven, damped nonlinear Schrödinger* model (see subsection 3.3.2)

$$\partial_t A = -i\left(\nu A + A|A|^2 + \nabla^2 A\right) - \mu A + \gamma\bar{A},$$

where the parameter $\nu \equiv -h_a - \beta_x - \beta_z/2 \approx -h_a - \beta_x$ is the analog of the detuning between half the forcing frequency and the response frequency in parametrically driven systems. Moreover, $\mu \equiv -g - \alpha\nu \approx -g$ is the dissipation, and $\gamma \equiv \beta_z/2$ accounts for the parametric injection. The PDNLS model is a paradigmatic equation for macroscopic systems at the onset of the subharmonic 2:1 resonance. This resonance is responsible for the destabilization of $A = 0$ state, and for the creation of localized states and patterns.

Pattern formation.- Since the PDNLS model is a limit of the Landau-Lifshitz-Gilbert equation, one expects to observe patterns and localized states in the numerical simulations of the magnetic equations. Indeed, in the regions of the parameter space where the PDNLS scaling applies, several dissipative states emerge, such as spatially periodic patterns, dissipative solitons, breathers, non-monotonic domain walls, stationary uniform equilibria, to mention a few.

In the case of patterns, the PDNLS limit predicts the formation of textures as the result of a spatial instability. The particular shape of patterns is not obvious and it strongly depends on the nonlinearities. To adequately understand the formation of textures, we used the method of amplitude equations (see subsection 3.3.1) to derive approximate analytic expressions for a wide variety of patterns and to study their linear stability. For small negative applied fields, $-4(\beta_x + \beta_z/2) < h_0 < -\beta_x - \beta_z/2$, we found the following magnetization stable equilibrium

$$m_y \approx 2\left[\frac{4\beta_z(\beta_z/2 + g)}{(6\beta_x + 3\beta_z - 2q^2)^2}\right]^{1/4}\cos\left(\mathbf{q}\cdot\mathbf{r}\right),$$

$$m_z \approx -m_y,$$

$$m_x \approx 1 - \frac{m_y^2 + m_z^2}{2},$$

where $q \equiv |\mathbf{q}| = \sqrt{\nu} = \sqrt{-h_0 - \beta_x - \beta_z/2}$ is the wavenumber. For larger negative fields $h_0 < -4(\beta_x + \beta_z/2)$, the magnetization is composed by the sum of several spatial modes (cosine functions) oriented along the directions admitted by the boundary conditions. This type of pattern is usually called a *superlattice* [35], because it is composed by several modes (8 independent modes, for instance). The transition that occurs at $h_0 = -4(\beta_x + \beta_z/2)$, where a pattern with one mode interchanges stability with a superlattice, is a *roll-superllatice* bifurcation. It is worth noting that the patterns amplitude grows as $(g - g_c)^{1/4}$, where $g_c = -\beta_z/2$. It is not usual to observe this growth law in pattern forming systems, where the envelopes typically grow following a square root law. Note also that the critical value of the electric current is fixed by the perpendicular anisotropy coefficient β_z. Then, systems where the magnetocrystaline anisotropy partially cancels the demagnetization are the best experimental setups to study our predictions [69]. The results in pattern formation are presented in detail in Chapter A.

Parametric equivalence.- Patterns are just one example of the states exhibited by ferromagnetic layers driven by the spin-transfer torque. Some other examples include localized states, uniform equilibria, and domain walls. Chapter B is devoted to the study of such structures in one and two spatial dimensions.

A natural question is, why do parametrically driven systems and spin-valve devices exhibit similar states? Or, why is the PDNLS model a limit of the magnetization equation? From the mathematical point of view, the answer is quite simple, *the perpendicular anisotropy breaks the rotational invariance in the (m_y, m_z) plane in the same way as a time-modulated injection of energy in an oscillator breaks the time-translation symmetry*. Hence, both systems can distinguish the phase of their order parameter A. At leading order, this symmetry-breaking produces a term of the form $\gamma \bar{A}$ in the equations of both systems.

If the $\gamma \bar{A}$ term comes from the anisotropy effect, which is the role of the spin-transfer torque? Spin-transfer torques just permit us to separate the effective parameters μ and ν. Indeed, some magnetic systems that do not have spin-polarized currents are also described by the PDNLS equation. However, since the dissipation coefficient must be positive in the PDNLS model, $\mu = -\alpha\nu > 0$, the detuning must be negative which forbids the existence of patterns. Then, spin-transfer torques permits one to recover the whole parameter space of parametrically driven damped systems.

From a physical viewpoint, the rotational symmetry breaking induced by the perpendicular anisotropy implies that systems that mechanical rotations can generate a parametric injection of energy. Using this simple idea, we constructed the equivalence between magnetic films that rotate mechanically and free layers. The equivalence between this two types of systems is described in detail in Chapter B.

An angular velocity Ω_0 of rotating plates causes a spin-transfer torque term of the form $g \sim \alpha\Omega_0$, then the mechanical rotations needs to reach angular velocities in the terahertz

range to produce the same effect as a spin-transfer torque of order $g \sim \alpha$. Then, it is not meaningful to study experimentally the effects of spin-transfer torques through rotating plates. However, this equivalence permitted us to find simple analogies and to explain the existence of dissipative solitons and patterns.

4.2. Ferromagnetic layer in presence of an alternating spin-polarized electric current

In the previous section we showed that a direct electric current generates states that are usually found in parametrically driven systems. This motivates the following questions: can we induce sub-harmonic resonances by means of an alternating electric current (a time-varying spin-transfer torque)? What dissipative states emerge as the consequence of this forcing mechanism? How do these states compare to those predicted by the parametric equivalence? In this section we answer those questions.

Let us start mentioning that a direct electric current can generate self-oscillations. This subject has been intensively studied during the last two decades (see [57] and references therein). The emergence of self-oscillations is easily understood by means of the linearized Landau-Lifshitz-Gilbert equation. Let us write the LLGS equation in terms of one of its components,

$$\frac{\mathrm{d}^2 m_y}{\mathrm{d}t^2} = -\omega^2 m_y - 2\tilde{\mu}\frac{\mathrm{d}m_y}{\mathrm{d}t},$$

where $\omega^2 = (1 + \alpha^2)\left[(h_0 + \beta_x)(\beta_z + h_0 + \beta_x) + g^2\right]$, $\tilde{\mu} = \alpha(h_0 + \beta_x + \beta_z/2) - g$, and $m_y = \mathbf{m} \cdot \mathbf{e}_y$. This is the equation of a damped oscillator, where the coefficients ω and $\tilde{\mu}$ are the natural frequency and the dissipation, respectively. Moreover, the stability spectrum of this system is given by

$$\lambda^2 + 2\tilde{\mu}\lambda + \omega^2 = 0,$$

which predicts a stationary instability when frequency ω becomes a complex number, that is when $(h_0 + \beta_x + \beta_z/2)^2 + g^2 - (\beta_z/2)^2 = 0$. Another instability takes place when the dissipation changes its sing at $\alpha(h + 1/2) - g = 0$. This instability is the Andronov-Hopf bifurcation, and it generates a similar dynamics to those exhibited by the Van der Pol oscillator; indeed, at linear order both equations are the same. Using the same methods presented in subsection 3.2.3 one could analytically characterize the oscillation by means of a slowly varying envelope B and higher order corrections $W(B, \bar{B})$,

$$m_y(t) = B(t)\mathrm{e}^{\mathrm{i}\omega t} + \bar{B}(t)\mathrm{e}^{\mathrm{i}\omega t} + W(t, B, \bar{B}).$$

The oscillation envelope B obeys the Complex-Ginzburg-Landau equation

$$\frac{\mathrm{d}B}{\mathrm{d}t} = \tilde{\mu}B + \eta B|B|^2,$$

where the parameter η is complex and its real part accounts for nonlinear dissipation and the imaginary part comes from the magnetic energy.

Let us consider a spin-polarized electric current with both a direct and an alternating contribution,

$$g(t) = g_0 + g_1 \sin(\omega t),$$

where g_0 is the continuous part of the current and it will generate self-oscillations through an Andronov-Hopf instability; and the parameter g_1 accounts for the oscillatory part of the spin-transfer effect, and this term will generate the parametric injection of energy with forcing frequency $\omega = 2(\omega_0 + \nu)$, and natural frequency $\omega_0^2 = (1 + \alpha^2)\left[(h_0 + \beta_x)(\beta_z + h_0 + \beta_x) + g_0^2\right]$. Then, our attempt will be to couple the alternating current g_1 to the self-oscillations favored by g_0. To understand the effect of the alternating current we introduce the following ansatz

$$m_y = m_{y,0} e^{i(\omega_0 + \nu)t} A(\mathbf{r}, t) + c.c. + W_y,$$

we replace this ansatz in the Landau-Lifshitz-Gilbert equation and after some straightforward calculations, one gets

$$\frac{\partial A}{\partial t} = -i\nu A - i\left|A\right|^2 A - \mu A + \gamma \bar{A} - i\nabla'^2 A,$$

where $\mu = \alpha\left(h + \frac{1}{2}\right) - g_0$ stands for linear dissipation, and $\gamma = \alpha g_1 / [4\sqrt{(h_0 + \beta_x)(h_0 + \beta_x + 2\beta_z)}]$ represents the forcing amplitude, and the operator ∇' is a normalization of the spatial derivatives, $\nabla' = [(2h_0 + \beta_x + \beta_z)/(2\omega_0)]^{1/2}\nabla$.

Hence, alternating currents can produce sub-harmonic resonance. Since this resonance is mathematically described by the PDNLS model, this system exhibits localized states and patterns. Those states are described in detail in Chapter C.

In brief, dissipative solitons and patterns can be induced by two mechanisms, namely a purely direct current and a current that combines a direct and an alternating contribution. Moreover, the states generated by both mechanisms are described by the same equation, the PNDLS model. However, there are differences between these two cases. The first one is that most of the states induced by the direct current are stationary states (static magnetic configurations), while all the states induced by the alternating current oscillate with the frequency ω_0. A second difference is that in the case of an alternating current, all the relevant parameters of the PDNLS equation—that is injection, dissipation and detuning—are controlled by the electric current. On the other hand, in the case of the parametric equivalence the injection amplitude is fixed by a device property—the total perpendicular anisotropy $\gamma = -\beta_z/2$—while the detuning is controlled by the external field. Then, the spin-transfer effect only permits us to manipulate dissipation coefficient μ in the parametric equivalence.

4.3. Traveling pulse on periodic patterns

The Andronov-Hopf instability of a uniform state generates limit-cycles and dissipative waves. In the last case, waves can be extended or localized, and they can be standing or traveling. From a theoretical point of view, the oscillation amplitude is governed by a

Ginzburg-Landau equation, which usually permits the characterization of waves, pulses and holes (see review [1] and references therein). On the other hand, the Andronov-Hopf instability of stationary textures can induce localized standing waves surrounded by the stationary pattern, traveling structures, among other behaviors. In this section we discuss a traveling pulse that propagates on a periodic pattern, this pulse is the result of a subcritical Andronov-Hopf instability of a Faraday-type pattern.

Let us follow the approach of Coullet and Iooss [24], and consider the differential equation,

$$\partial_t \mathbf{u} = \mathbf{f}\left(\mathbf{u}, \partial_x \mathbf{u}, \partial_{xx} \mathbf{u}\right), \tag{4.2}$$

which admits two symmetries: spatial reflection $x \to -x$ and spatial translation $x \to x + \Delta x$. In addition, we assume that model (4.2) has a spatially periodic patterns $\mathbf{u}_p(x) = \mathbf{u}_p(x + 2\pi/q)$ as solution, where q is the pattern wavenumber. The stability around this state is obtain by perturbing the pattern with a small function $\delta \mathbf{u}(t, x)$ which obeys the linear equation

$$\partial_t \delta \mathbf{u} = \left[\frac{\partial \mathbf{f}}{\partial \mathbf{u}}\left(\mathbf{u}_p, \partial_x \mathbf{u}_p, \partial_{xx} \mathbf{u}_p\right)\right] \delta \mathbf{u}, \tag{4.3}$$

where $[\partial \mathbf{f}/\partial \mathbf{u}\left(\mathbf{u}_p, \partial_x \mathbf{u}_p, \partial_{xx} \mathbf{u}_p\right)]$ is the Jacobian matrix of $\mathbf{f}$ evaluated in the pattern state. Equation (4.3) is a space-dependent eigenvalue problem, and the temporal evolution of the perturbation $\delta \mathbf{u}$ can be reduced to an exponential function, that is $\delta \mathbf{u}(t, x) = e^{\lambda t} \mathbf{v}(x)$, where the eigenvalue λ can be a real or a complex number [24]. Increasing or decreasing a control parameter can produce a change of sign in the real part of one eigenvalue λ_c. In this scenario perturbations grow with a well defined spatial structure given by the eigenfunction $\mathbf{v}_c(x)$, and possibly a frequency if $\mathrm{Im}(\lambda_c) \neq 0$. Hence, patterns display similar instabilities compared to those of uniform states, namely stationary and oscillatory instabilities[1]. At the onset of the Andronov-Hopf instability of the pattern, several states can emerge: standing waves, traveling waves, and localized waves; the system could also reach another equilibrium far from the pattern solution.

Andronov-Hopf instability of Faraday-type waves.- Let us consider the specific case of parametrically driven systems. Close to the sub-harmonic resonance, the oscillation envelope obeys the PNDLS equation, which exhibits patterns or Faraday-type waves (see subsection 3.3.2). The PDNLS model is valid when spatial variations of the envelope are slow ($|\partial_{xx}A| \ll |\partial_x A| \ll |A| \ll 1$). If the pattern wavelength is smaller, then the PDNLS model might be corrected to account for the fast spatial variations of the order parameter. One possible amended-PDNLS equation (APDNLS) is

$$\partial_t A = -\mathrm{i}\left(\nu A + |A|^2 A + \partial_{xx} A\right) - \mu A + \gamma \bar{A} + \mathrm{i}\delta \bar{A}\left(\partial_x A\right)^2, \tag{4.4}$$

---

[1]Patterns in an infinite medium—or in a system with periodic boundary conditions—are a continuous family of solutions parametrized by a constant phase ϕ_0, $\mathbf{u}_p(x + \phi_0)$. The phase is a neutral mode associated to the space translation invariance. At the onset of a pattern instability, the phase usually becomes a dynamical variable that couples to the unstable modes. This generates drifts or changes in the wavelength of the pattern [24]. Then, even if pattern instabilities are similar to the bifurcations of uniform states, the phase increases the center manifold and then a rich variety of structures can be expected.
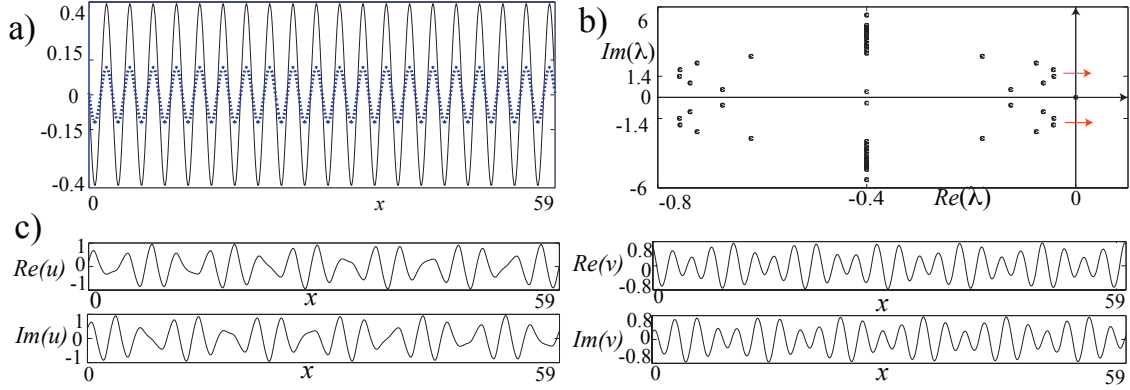
Figura 4.1: Andronov-Hopf instability of a pattern. (a) Stationary pattern state of the APDNLS Eq. (4.4), where solid and dashed lines account for the real and imaginary parts of $A = u + iv$, respectively. (b) Stability spectrum of the pattern. Two complex conjugate eigenvalues are close to the imaginary axis, those eigenvalues are responsible for the destabilization of the pattern state. Note that there is a zero eigenvalue, $\lambda = 0$, which comes from the neutral mode $x \to x + \Delta x$. (c) Eigenfunctions corresponding to the critical modes of the Andronov-Hopf instability. The eigenfunctions break the reflection symmetry $x \to -x$.

where the last term of Eq. (4.4) is phenomenological and it was introduced to account for non-negligible spatial gradients. Moreover, this term emerges naturally in magnetic media [see Eq. (4.1) for instance]. Since the term proportional to δ is nonlinear, it cannot change the instabilities of the state $A = 0$. Then both the PDNLS and the APDNLS model exhibit a spatial instability for $\nu > 0$ and $\gamma \geq \mu$.

Figure 4.1(a) shows the pattern state obtained from Eq. (4.4). The stability analysis of this equilibrium is shown in Fig. 4.1(b). As this figure illustrates, the pattern is close to an Andronov-Hopf instability. The eigenfunctions of the bifurcation (of the critical eigenvalues) are shown in Fig. 4.1(c). According to Coullet and Iooss [24], the Andronov-Hopf instability of the pattern can be described by Ginzburg-Landau amplitude equations coupled to a phase equation. In our case, the critical modes break the spatial reflection invariance, which produces a right and a left-traveling wave. The direct numerical integration of the model (4.4) reveals that the traveling waves emerge subcritically—there is an abrupt passage from the
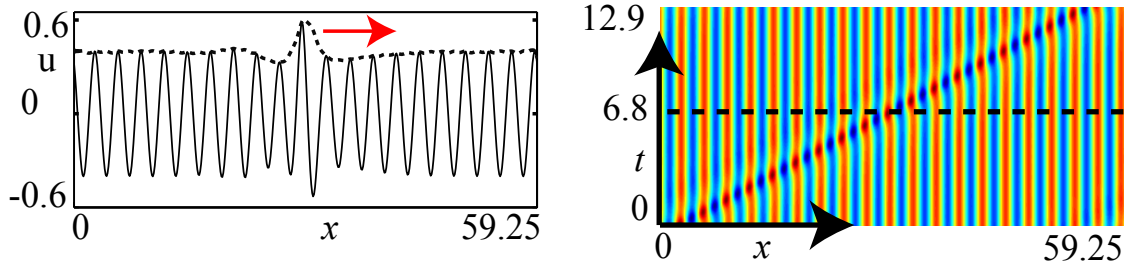
Figura 4.2: Traveling pulse on a periodic background. The left panel shows the profile of the pulse numerically calculated from from Eq. (4.4), where $u = \mathrm{Re}(A)$. The right panel shows the spatiotemporal diagram of the traveling state; the dashed line of the diagram shows the moment when the graphic of the left was obtained.

stationary pattern to the traveling waves. Close to the transition, localized states are observed (see Fig. 4.2). Those pulses are the analog of the Ginzburg-Landau stationary pulses [78, 1]

An example of a pulse traveling in a periodic background is presented in Chapter D, where a ferromagnetic wire is driven by an oscillatory magnetic field.

4.4. Limit-cycles of two-dimensional patterns

Spin-transfer torques induce stationary patterns in magnetic films [49]. Those patterns are stabilized by an electric current that transfers angular momentum from the fixed magnetization to the free one. Then decreasing the electric current will cause a loose of stability of the stationary textures. In this section we study the self-oscillations that emerge when patterns are unstable.

The typical magnetization behavior that we have observed for current values where stationary patterns are unstable is shown in Fig. 4.3. This figure illustrates a texture that alternates between quasi-vertical and quasi-horizontal rolls in time. This is an example of an *alternating pattern*. This type of patterns have been studied in fluid convection [60, 36, 63, 45, 59, 83, 65, 54, 55, 26], and vertically vibrated fluids [64].

Some analytic methods of nonlinear science, such as amplitude equations, cannot account for the permanent dynamics alternating patterns. Indeed, if the pattern amplitude is calculated at the onset of a spatial instability, one typically obtains a relaxation equation which fails to predict oscillatory instabilities. This drawback of singular approaches (such as the one described in Ref. [28]) motivates the use of a more general analytic description in terms of some relevant spatial modes, that is, a Galerkin expansion (see subsection 3.3.3 and Ref. [60]). The selection of spatial modes is usually motivated by numerical simulations and experimental observations, then the spatiotemporal dynamics is projected into those modes to obtain a set of time-dependent amplitudes.
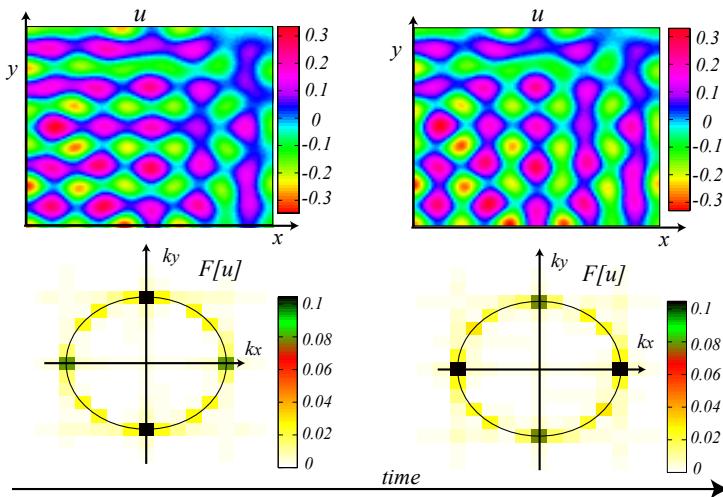
Figura 4.3: Alternating patterns. Oscillatory textures composed by two or more dominant modes. The envelopes of the modes oscillate (alternate) between large and small values, which gives the appearance of a patterns that alternate their shape. The top panel shows the profile of the real part of A as function of space at two times, while the lower panel shows the corresponding spatial Fourier spectra.

By means of an appropriate Galerkin expansion, we transformed the LLGS equation into a set of four ordinary differential equations. This permitted us to conduct efficient numerical simulations and observe trajectories in the reduced phase space. We also determined that there are two bifurcations that create alternating pattern in spin-valve systems, namely an Andronov-Hopf instability and a homoclinic bifurcation. The details of this subject are presented in Chapter E.

Capítulo 5

Conclusions

The control of ferromagnetic media at nano-scales has attracted considerable attention during last decades. The physical description of ferromagnets has several challenging issues, from two perspectives: the microscopic approach (transport phenomena) and the dynamical systems approach (magnetization dynamics).

In this theses, we have studied the nonlinear magnetization dynamics of a spin-valve by means of the Landau-Lifshitz-Gilbert-Slonczesky equation. Using concepts and methods of nonlinear science, we showed in Sec. 4.1 that the form of the spin-transfer torque is equivalent to a non-inertial force, and that a perpendicular anisotropy is equivalent to a time-modulated injection of energy (parametric injection). This simple idea allowed us to predict a plethora of states usually found in macroscopic systems with dissipation and parametric injection of energy, such as uniform equilibria, stationary solitons, oscillatory solitons, spatially periodic patterns, stationary domain walls, moving domain walls, among others. Hence, a ferromagnetic film forced by a direct spin-polarized current belongs to the family of parametrically driven systems. In addition we studied the coupling between the magnetic self-oscillations induced by a direct spin-polarized current and an alternating current. A sub-harmonic resonance was found for forcing frequencies close to twice the self-oscillation frequency. The aforementioned dynamical behaviors increase the versatility of the spin-transfer torque as a mechanism for controlling the magnetization. Furthermore, the observed multistability of spin-transfer torque driven systems could allow the use of spin-valves as memory units with several information states.

Physical systems self-organize into Faraday-type patterns and dissipative solitons at the onset of the sub-harmonic resonance. Such states emerge in several contexts, in particular, we have demonstrated here that such states also emerge in spin-valves. However, the instabilities of patterns and dissipative solitons are less known. In this context we studied the subcritical Andronov-Hopf instability of a one-dimensional Faraday-type wave by means of a phenomenological model for the oscillation envelope. We found traveling pulses on patterns, which are localized increments of the pattern amplitude. We also determined that nonlinear gradients are a necessary ingredient to observe pulses. We provided an example of this behavior in a magnetic wire driven by an oscillatory magnetic field. We expect that this type of solutions will be observed in other systems with nonlinear gradients, such as degenerate

optical parametric oscillators and vibrated fluids.

We studied the emergence of oscillatory two-dimensional patterns in spin-valves. Those states appear in regions of the parameter space where the stationary patterns are unstable. By means of direct numerical simulations we showed that there are two mechanisms or routes that generate oscillatory patterns in this magnetic system, they are an Andronov-Hopf oscillation of stationary patterns and a global bifurcation known as homonclinic bifurcation.

In brief, the interaction of spins of conduction electrons with other degrees of freedom produce several effects. Some of those effects permit controlling the magnetization and then they promise to generate novel technological applications. However, an essential preliminary step is to predict and characterize the possible behaviors of the magnetization. This thesis is an effort in such direction. We used a simplified magnetization equation to observe and characterize several states, and to compare this systems with other ones. We expect that some of our results will be tested experimentally and/or by means of realistic micromagnetic simulations in near the future. However, since most of the predicted states are result of resonances or instabilities, one expects to observed them—perhaps with quantitative changes and in a slightly different region of the parameter space—independently of the microscopic details

Bibliografía

[1] I S Aranson and L Kramer. The world of the complex Ginzburg-Landau equation. *Reviews of Modern Physics*, 74(1):99, 2002.

[2] I V Barashenkov, M M Bogdan, and V I Korobov. Stability diagram of the phase-locked solitons in the parametrically driven, damped nonlinear Schrödinger equation. *EPL (Europhysics Letters)*, 15(2):113, 1991.

[3] S J Barnett. Magnetization by rotation. *Physical Review*, 1915.

[4] Chopard Bastien and Droz Michel. Cellular automata modeling of physical systems. *Cellular automata modeling of physical systems*, 1998.

[5] Gerrit E W Bauer, Eiji Saitoh, and Bart J van Wees. Spin caloritronics. *Nature Publishing Group*, 11(5):391–399, May 2012.

[6] L Berger. Emission of spin waves by a magnetic multilayer traversed by a current. *Physical Review B*, 54(13):9353, 1996.

[7] D Berkov and N Gorn. Transition From the Macrospin to Chaotic Behavior by a Spin-Torque Driven Magnetization Precession of a Square Nanoelement. *Physical Review B*, 71(5):052403, February 2005.

[8] Giorgio Bertotti. *Hysteresis in magnetism: for physicists, materials scientists, and engineers*. Academic press, 1998.

[9] U Bortolozzo, M Clerc, C Falcón, S Residori, and R Rojas. Localized States in Bistable Pattern-Forming Systems. *Physical Review Letters*, 96(21):214501, May 2006.

[10] M Clerc, D Escaff, and V Kenkre. Patterns and localized structures in population dynamics. *Physical Review E*, 72(5):056217, November 2005.

[11] M G Clerc, S Coulibaly, and D Laroze. Localized states beyond the asymptotic parametrically driven amplitude equation. *Physical Review E*, 77(5):056209, May 2008.

[12] M G Clerc, S Coulibaly, and D Laroze. Nonvariational Ising–Bloch transition in parametrically driven systems. *International Journal of Bifurcation and Chaos*, 19(08):2717–2726, 2009.

[13] M G Clerc, S Coulibaly, and D Laroze. Parametrically Driven Instability in Quasi-Reversal Systems. *International Journal of Bifurcation and Chaos*, 19(10):3525–3532, 2009.

[14] M G Clerc, S Coulibaly, and D Laroze. Localized waves in a parametrically driven magnetic nanowire. *EPL (Europhysics Letters)*, 97(3):30006, February 2012.

[15] Marcel Clerc, Saliya Coulibaly, Mónica Garcia-Ñustes, and Yair Zárate. Dissipative Localized States with Shieldlike Phase Structure. *Physical Review Letters*, 107(25):254102, December 2011.

[16] Marcel Clerc, Cristián Fernández-Oto, and Saliya Coulibaly. Pinning-depinning transition of fronts between standing waves. *Physical Review E*, 87(1):012901, January 2013.

[17] Marcel G Clerc, Saliya Coulibaly, Mónica A Garcia-Ñustes, and Yair Zárate. Transverse phase shielding solitons in the degenerated optical parametric oscillator. *Optics Communications*, 354:163–167, November 2015.

[18] Marcel G Clerc, Saliya Coulibaly, and David Laroze. Localized states and non-variational Ising–Bloch transition of a parametrically driven easy-plane ferromagnetic wire. *Physica D: Nonlinear Phenomena*, 239(1-2):72–86, January 2010.

[19] Marcel G Clerc, Saliya Coulibaly, David Laroze, Alejandro O León, and Álvaro S Núñez. Alternating spin-polarized current induces parametric resonance in spin valves. *Physical Review B*, 91(22):224426, June 2015.

[20] Marcel G Clerc, Mónica A Garcia-Ñustes, and Yair Zárate. Propagative phase shielding solitons in inhomogeneous media. *Physica D: Nonlinear Phenomena*, 269:86–93, February 2014.

[21] Marcel G Clerc, Mónica A Garcia-Ñustes, Yair Zárate, and Saliya Coulibaly. Phase shielding soliton in parametrically driven systems. *Physical Review E*, 87(5):052915, May 2013.

[22] John MD Coey. *Magnetism and magnetic materials*. Cambridge University Press, 2010.

[23] P Coullet, T Frisch, and G Sonnino. Dispersion-induced patterns. *Physical Review E*, 49:2087–2090, 1994.

[24] P Coullet and G Iooss. Instabilities of one-dimensional cellular patterns. *Physical Review Letters*, 64(8):866–869, 1990.

[25] M C Cross and Hohenberg, P.C. Pattern-Formation Outside of Equilibrium. *Reviews of Modern Physics*, 65(3):851–1112, July 1993.

[26] Surajit Dan, Pinaki Pal, and Krishna Kumar. Low-Prandtl-number Rayleigh-Bénard convection with stress-free boundaries. *The European Physical Journal B*, 87(11):278, November 2014.

[27] O Descalzi, M Argentina, and E Tirapegui. Saddle-node bifurcation: Appearance mechanism of pulses in the subcritical complex Ginzburg-Landau equation. *Physical Review E*, 67(1):015601, January 2003.

[28] C Elphick, E Tirapegui, M E Brachet, P Coullet, and G Iooss. A simple global characterization for normal forms of singular vector fields. *Physica D: Nonlinear Phenomena*, 29(1):95–127, 1987.

[29] Yuri Gaididei, Oleksii M Volkov, Volodymyr P Kravchuk, and Denis D Sheka. Magnetic vortex-antivortex crystals generated by spin-polarized current. *Physical Review B*, 86(14):144401, October 2012.

[30] T L Gilbert. Classics in Magnetics A Phenomenological Theory of Damping in Ferromagnetic Materials. *Magnetics, IEEE Transactions on*, 40(6):3443–3449, November 2004.

[31] Walter Greiner. *Classical electrodynamics*. Springer Science & Business Media, 2012.

[32] S S Ha, K J Lee, and C Y You. Effect of the resistance-area product on the temperature increase of nanopillar for spin torque magnetic memory. *Current Applied Physics*, 2010.

[33] S S Ha and C Y You. Validity of the analytic expression for the temperature of Joule heated nano-wire. *Journal of Magnetics*, 2007.

[34] Seung-Seok Ha and Chun-Yeol You. Tendency of temperature on nano-pillar for spin transfer torque memory. *physica status solidi (a)*, 204(12):3962–3965, December 2007.

[35] Rebecca B Hoyle. *Pattern formation: an introduction to methods*. Cambridge University Press, 2006.

[36] B Huke and M Lücke. Roll, square, and cross-roll convection in ferrofluids. *Journal of Magnetism and Magnetic Materials*, 289:264–267, March 2005.

[37] James M Hyman and Bernard Larrouturou. The numerical differentiation of discrete functions using polynomial interpolation methods. *Applied Mathematics and Computation*, 10:487–506, 1982.

[38] Junichi Iwasaki, Masahito Mochizuki, and Naoto Nagaosa. Current-induced skyrmion dynamics in constrictedgeometries. pages 1–6, September 2013.

[39] A V Khvalkovskiy, K A Zvezdin, Ya V Gorbunov, V Cros, J Grollier, A Fert, and A K Zvezdin. High Domain Wall Velocities due to Spin Currents Perpendicular to the Plane. *Physical Review Letters*, 102(6):067206, February 2009.

[40] Woojin Kim, Woojin Kim, Seo-Won Lee, Seo-Won Lee, Kyung-Jin Lee, and Kyung-Jin Lee. Micromagnetic modelling on magnetization dynamics in nanopillars driven by spin-transfer torque. *Journal of Physics D: Applied Physics*, 44(38):384001, September 2011.

[41] S I Kiselev, J C Sankey, I N Krivorotov, N C Emley, R J Schoelkopf, R A Buhrman, and D C Ralph. Microwave oscillations of a nanomagnet driven by a spin-polarized current. *Nature*, 425(6956):380–383, 2003.

[42] Volodymyr P Kravchuk, Oleksii M Volkov, Denis D Sheka, and Yuri Gaididei. Periodic magnetization structures generated by transverse spin current in magnetic nanowires. *Physical Review B*, 87(22):224402, June 2013.

[43] M Lakshmanan. The fascinating world of the Landau-Lifshitz-Gilbert equation: an overview. *Philosophical Transactions of the Royal Society A: Mathematical, Physical and Engineering Sciences*, 369(1939):1280–1300, February 2011.

[44] D Laroze, P G Siddheshwar, and H Pleiner. Commun Nonlinear Sci Numer Simulat. *Communications in Nonlinear Science and Numerical Simulation*, 18(9):2436–2447, September 2013.

[45] P Le Gal, A Pocheau, and V Croquette. Square versus roll pattern at convective threshold. *Physical Review Letters*, 1985.

[46] Kyung-Jin Lee, Alina Deac, Olivier Redon, Jean-Pierre Nozières, and Bernard Dieny. Excitations of incoherent spin-waves due to spin-transfer torque. *Nature Materials*, 3(12):877–881, November 2004.

[47] Seo-Won Lee and Kyung-Jin Lee. Effect of Angular Dependence of Spin-Transfer Torque on Zero-Field Microwave Oscillation in Symmetric Spin-Valves. *Magnetics, IEEE Transactions on*, 46(6):2349–2352.

[48] Alejandro O León and Marcel G Clerc. Spin-transfer-driven nano-oscillators are equivalent to parametric resonators. *Physical Review B*, 91(1):014411, January 2015.

[49] Alejandro O León, Marcel G Clerc, and Saliya Coulibaly. Dissipative structures induced by spin-transfer torques in nanopillars. *Physical Review E*, 89(2):022908, February 2014.

[50] Alejandro O León, Marcel G Clerc, and Saliya Coulibaly. Traveling pulse on a periodic background in parametrically driven systems. *Physical Review E*, 91(5):050901, May 2015.

[51] Zai-Dong Li, Qiu-Yan Li, Lu Li, and W Liu. Soliton solution for the spin current in a ferromagnetic nanowire. *Physical Review E*, 76(2):026605, August 2007.

[52] Stefano Longhi. Stable multipulse states in a nonlinear dispersive cavity with parametric gain. *Physical Review E*, 53:5520–5522, 1996.

[53] Sadamichi Maekawa. *Concepts in spin electronics*, volume 4. Oxford University Press Oxford, UK, 2006.

[54] P Maity, K Kumar, and P Pal. Homoclinic bifurcations in low-Prandtl-number Rayleigh-Bénard convection with uniform rotation. *EPL (Europhysics Letters)*, 103(6):64003, October 2013.

[55] Priyanka Maity and Krishna Kumar. Zero-Prandtl-number convection with slow rotation. *Physics of Fluids*, 26(10):104103, October 2014.

[56] Mamoru Matsuo, Jun'ichi Ieda, Kazuya Harii, Eiji Saitoh, and Sadamichi Maekawa. Mechanical generation of spin current by spin-rotation coupling. *Physical Review B*, 87(18):180402, May 2013.

[57] Isaak D Mayergoyz, Isaak D Mayergoyz, Giorgio Bertotti, Giorgio Bertotti, Claudio Serpico, and Claudio Serpico. *Nonlinear magnetization dynamics in nanosystems*. Elsevier, 2009.

[58] J W Miles. Parametrically excited solitary waves. *Journal of Fluid Mechanics*, 1984.

[59] E Moses and V Steinberg. Competing patterns in a convective binary mixture. *Physical Review Letters*, 1986.

[60] H W Müller and M Lücke. Competition between roll and square convection patterns in binary mixtures. *Physical Review A*, 1988.

[61] A S Nuñez, R A Duine, Paul Haney, and A H MacDonald. Theory of spin torques and giant magnetoresistance in antiferromagnetic metals. *Physical Review B*, 73(21):214426, June 2006.

[62] Edward Ott. *Chaos in dynamical systems*. Cambridge university press, 2002.

[63] Pinaki Pal, Krishna Kumar, Priyanka Maity, and Syamal Kumar Dana. Pattern dynamics near inverse homoclinic bifurcation in fluids. *Physical Review E*, 87(2):023001, February 2013.

[64] Nicolas Périnet, Damir Juric, and Laurette S Tuckerman. Alternating Hexagonal and Striped Patterns in Faraday Surface Waves. *Physical Review Letters*, 109(16):164501, October 2012.

[65] Hirdesh K Pharasi and Krishna Kumar. Oscillatory instability and fluid patterns in low-Prandtl-number Rayleigh-Bénard convection with uniform rotation. *Physics of Fluids*, 25(10):104105, 2013.

[66] Len M Pismen. *Patterns and interfaces in dissipative dynamics*. Springer Science & Business Media, 2006.

[67] Andrei D Polyanin and Valentin F Zaitsev. *Handbook of exact solutions for ordinary differential equations*, volume 1. Boca Raton: CRC Press,| c1995, 1995.

[68] William H Press, Saul A Teukolsky, William T Vetterling, and Brian P Flannery. *Numerical recipes in C*, volume 2. Cambridge university press Cambridge, 1996.

[69] D C Ralph, Y T Cui, L Q Liu, T Moriyama, C Wang, and R A Buhrman. Spin-transfer torque in nanoscale magnetic devices. *Philosophical Transactions of the Royal Society A: Mathematical, Physical and Engineering Sciences*, 369(1951):3617–3630, August 2011.

[70] D C Ralph and M D Stiles. Spin transfer torques. *Journal of Magnetism and Magnetic Materials*, 320(7):1190–1216, April 2008.

[71] Alejandro Salcido. *Cellular Automata: Innovative Modelling for Science and Engineering.* InTech, 2011.

[72] Ralph Skomski. *Simple models of magnetism.* Oxford Univ. Press, 2008.

[73] A Slavin and V Tiberkevich. Nonlinear Auto-Oscillator Theory of Microwave Generation by Spin-Polarized Current. *Magnetics, IEEE Transactions on*, 45(4):1875–1918.

[74] John C Slonczewski. Current-driven excitation of magnetic multilayers. *Journal of Magnetism and Magnetic Materials*, 159(1):L1–L7, 1996.

[75] Daniel D Stancil and Anil Prabhakar. *Spin waves*, volume 1047. Springer, 2009.

[76] Joachim Stöhr and Hans Christoph Siegmann. *Magnetism.* Springer, 2006.

[77] Steven H Strogatz. Nonlinear dynamics and chaos: with applications to physics, biology, chemistry, and engineering, 2014.

[78] O Thual and S Fauve. Localized Structures Generated by Subcritical Instabilities. *Journal De Physique*, 49(11):1829–1833, November 1988.

[79] D Urzagasti, D Laroze, and M G Clerc. Two-soliton precession state in a parametrically driven magnetic wire. *Journal of Applied . . .* , 2012.

[80] D Urzagasti, D Laroze, M G Clerc, and H Pleiner. Breather soliton solutions in a parametrically driven magnetic wire. *EPL (Europhysics Letters)*, 104(4):40001, December 2013.

[81] Oleksii M Volkov, Volodymyr P Kravchuk, Denis D Sheka, and Yuri Gaididei. Spin-transfer torque and current-induced vortex superlattices in nanomagnets. *Physical Review B*, 84(5):052404, August 2011.

[82] Oleksii M Volkov, Volodymyr P Kravchuk, Denis D Sheka, Franz G Mertens, and Yuri Gaididei. Periodic magnetic structures generated by spin–polarized currents in nanostripes. *Applied Physics Letters*, 103(22):222401, 2013.

[83] S Weggler, B Huke, and M Lücke. Roll and square convection in binary liquids: A few-mode Galerkin model. *Physical Review E*, 81(1):016309, January 2010.

[84] Stephen Wiggins. *Global bifurcations and chaos: analytical methods*, volume 73. Springer Science & Business Media, 2013.

[85] Jiang Xiao. *Spin-transfer Torque in Magnetic Nanostructures.* PhD thesis, May 2006.

[86] Jiang Xiao, A Zangwill, and M Stiles. Boltzmann test of Slonczewski's theory of spin-transfer torque. *Physical Review B*, 70(17):172405, November 2004.

[87] Jiang Xiao, A Zangwill, and M Stiles. Macrospin models of spin transfer dynamics. *Physical Review B*, 72(1):014446, July 2005.

[88] Chun-Yeol You, Seung-Seok Ha, and Hyun-Woo Lee. ARTICLE IN PRESS. *Journal of Magnetism and Magnetic Materials*, 321(21):3589–3594, August 2009.

[89] Chun-Yeol You, In Mo Sung, and Byung-Kyu Joe. Analytic expression for the temperature of the current-heated nanowire for the current-induced domain wall motion. *Applied Physics Letters*, 89(22):222513, 2006.

Apéndice A

Dissipative structures induced by spin-transfer torques in nanopillars

This chapter presents our results in pattern formation in a ferromagnetic layer driven by spin-transfer torques.

Dissipative structures induced by spin-transfer torques in nanopillars

Alejandro O. León[*] and Marcel G. Clerc[†]

Departamento de Física, Facultad de Ciencias Físicas y Matemáticas, Universidad de Chile, Casilla 487-3, Santiago, Chile

Saliya Coulibaly[‡]

*Laboratoire de Physique des Lasers, Atomes et Molécules, CNRS UMR 8523, Université des Sciences et Technologies de Lille - 59655
Villeneuve d'Ascq Cedex, France*

Macroscopic magnetic systems subjected to external forcing exhibit complex spatiotemporal behaviors as result of dissipative self-organization. Pattern formation from a uniform magnetization state, induced by the combination of a spin-polarized current and an external magnetic field, is studied for spin-transfer nano-oscillator devices. The system is described in the continuous limit by the Landau-Lifshitz-Gilbert equation. The bifurcation diagram of the quintessence parallel state, as a function of the external field and current, is elucidated. We have shown analytically that this state exhibits a spatial supercritical quintic bifurcation, which generates in two spatial dimensions a family of stationary stripes, squares, and superlattice states. Analytically, we have characterized their respective stabilities and bifurcations, which are controlled by a single dimensionless parameter. This scenario is confirmed numerically.

PACS number(s): 05.45.Yv, 89.75.Kd

I. INTRODUCTION

Macroscopic systems maintained out of equilibrium, under the influence of injection and dissipation of energy and momenta, are characterized by exhibiting self-structuring phenomena [1–5]. In the course of the last decades, much effort has been devoted to the study of pattern formation or dissipative structures arising in diverse branches of natural sciences (see the textbooks [4–7] and the references therein). These patterns are the result of the interplay between the linear gain and the nonlinear saturation mechanisms. In many physical systems, these structures emerge as a spatial instability of a uniform state when a control parameter is changed and surpasses a critical value, which usually corresponds to an imbalance of forces. Thus, these bifurcations correspond to spontaneous symmetry breaking [3,8]. Near the instability there is a separation of time scales between the evolution of critical and slave spatial modes, whose amplitudes grow or decrease exponentially, respectively. This separation of scales reduces the dynamics into a few spatial modes, which lead the behavior of the system under study (see [1–4,8–10]). Close to the spatial instability, a unified description of pattern formation can be achieved with the method of amplitude equations.

In one-dimensional extended systems, the dynamics at the onset of bifurcation are generally described by a complex amplitude. The magnitude of the amplitude, at equilibrium, satisfies a power law as a function of the bifurcation parameter [11].

The above scenario changes drastically in two spatial dimensions as result of spatial isotropy. A large number of critical modes can be activated, which correspond to the stripe patterns with different orientations, initially creating several domains separated by local and extended defects. Later on, domains and defects evolve until they reach an equilibrium state [2,2–5]. Near the bifurcation, these equilibria are formed by combinations of a few spatial modes, such as stripes, squares, and hexagons [3,4,8]. Far from the spatial bifurcation, the equilibria observed are more elaborate structures such as quasipatterns [12,13], superlattices [8], and labyrinths [14]. All these stationary states are composed by a large number of modes. The fundamental tools for the understanding of these states are the theory of groups, defects interactions, and amplitude equations.

The control of magnetization in ferromagnetic nanopillars has been the subject of intensive study in recent years [15–17] for its technological applications, such as magnetic sensors, magnetic read heads, data memory, magnetic switching, and spin transistors. In such devices, an electric current J applied through the spin-valve transfers spin angular momentum to a ferromagnetic layer from another film with fixed magnetization. This effect is known as the spin-transfer torque [18–22]. When the direct current overcomes a critical value, spin-transfer torque switches the magnetization and/or carries it into a stable precession in the radio-frequency domain. Recently, it has been shown that large precessional magnetic motions can be destabilized by patternlike perturbations in nanopillars [23]. Figure 1(a) represents schematically a spin-valve structure composed by two magnetic layers (dark layers), the free and the fixed one, separated by a metallic nonmagnetic spacer (light layers).

Most of previous research has focused on the study of uniform magnetization dynamics. This approach is known as the macrospin approximation [21]. A natural question that arises is whether the spin-transfer process is capable of generating self-organized stationary structures from an homogeneous current. This phase transition can become important because it generates nonuniform stationary configurations for parameter values where the parallel state was predicted to be stable by the macrospin model.

The aim of this manuscript is to characterize the formation of patterns from a uniform magnetization state in one and two spatial dimensions in spin-transfer nano-oscillators induced

[*]aoleon@dfi.uchile.cl
[†]marcel@dfi.uchile.cl
[‡]saliya.coulibaly@univ-lille1.fr
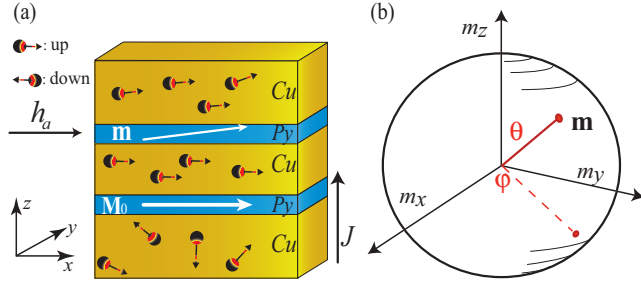
(a)

(b)

FIG. 1. (Color online) Nanopillar device. (a) Schematic representation of the spin-transfer torque nano-oscillator setup. The dark (blue) and light (yellow) layers represent magnetic and nonmagnetic metal films, respectively. Electrons are depicted schematically with their respective spins. J and h_a are the electric current through the spin valve and the external magnetic field, both effects are parallel to the easy axes of the ferromagnetic layer under study. $\mathbf{M}_o$ stands for the magnetization of the fixed layer. (b) Spherical representation of the magnetization $\mathbf{m}$.

by the combination of a spin-polarized current and an external magnetic field.

The system is described in the continuous limit by the Landau-Lifshitz-Gilbert equation with a spin-transfer torque term. Through a linear analysis we characterize entirely the bifurcation diagram of the parallel state submitted to an external magnetic field. Based on amplitude equations we show that the system has a quintic supercritical bifurcation. In two spatial dimensions, we observe the emergence of stripes or superlattices at the onset of the bifurcation. Analytically, we characterize the respective bifurcation diagram, which is controlled by a single parameter. This scenario is qualitatively and quantitatively verified numerically.

The manuscript is organized as follows. In Sec. II, the dynamics of the free magnetic layer in the spin-valve with spin-polarized current are described theoretically. The bifurcation diagram of the one-dimensional configuration is studied in Sec. III. The spatial bifurcation exhibited by the system is characterized by means of amplitude equations. The patterns in the two-dimensional configuration are studied in Sec. IV. The dynamics of four-modes and their conjugates are analyzed in detail. Our conclusions and remarks are left to the final section.

II. SPIN VALVE WITH SPIN-TRANSFER TORQUE

Let us consider a nanopillar device with pinned layer magnetization along the positive x axis as depicted by Fig. 1(a). The energy E of the free magnetic layer has the form [24]

$$E = \tfrac{1}{2}\mu_0 M_s^2 (\nabla \mathbf{m})^2 + \tfrac{1}{2}\mu_0 M_s^2 \beta_z (\mathbf{m} \cdot \hat{\mathbf{z}})^2$$
$$- \tfrac{1}{2}\mu_0 M_s^2 \beta_x (\mathbf{m} \cdot \hat{\mathbf{x}})^2 - \mu_0 M_s^2 \mathbf{m} \cdot \mathbf{h_a}, \qquad (1)$$

where $\mathbf{M}(\mathbf{r},t)$ is the magnetization in the free magnetic layer and $\{\mathbf{r},t\}$ stand for the spatial and temporal coordinates, respectively. $\mathbf{m}(\mathbf{r},t) = \mathbf{M}/M_s$ is the unitary magnetization vector, M_S is the saturation magnetization. β_x and β_z are combinations of the normalized anisotropy and demagnetization constants with respect to the appropriate axes, where β_x (β_z) favors (disfavors) the free magnetization in the x axis (z axis). $\mu_0 M_s^2/2$ is the shape anisotropy energy of the thin film, and $\mathbf{h_a} = h_a \hat{x}$ is the

external magnetic field that we set to point along the x axis [see Fig. 1(a)]. The gradient operator is $\nabla \equiv \hat{\mathbf{x}}\partial_X + \hat{\mathbf{y}}\partial_Y + \hat{\mathbf{z}}\partial_Z$ and distances are nondimensionalized with respect to the exchange length $l_{\text{ex}} \equiv \sqrt{2A/(\mu_0 M_s^2)}$ where A is the exchange coupling in the ferromagnet.

The dynamics of the magnetization of this free layer can then be described by the Landau-Lifshitz-Gilbert equation (LLG) under the influence of a spin-transfer torque term [25]

$$\frac{\partial \mathbf{m}}{\partial t} = \frac{\gamma}{M_s}\mathbf{m} \times \frac{\delta E}{\delta \mathbf{m}} + g\,\mathbf{m} \times (\mathbf{m} \times \hat{\mathbf{x}}) + \alpha \mathbf{m} \times \frac{\partial \mathbf{m}}{\partial t}, \qquad (2)$$

with

$$\frac{\delta E}{\delta \mathbf{m}} = -\frac{1}{2}\mu_0 M_s^2 [(h_a + \beta_x m_x)\hat{x} - \beta_z m_z \hat{z} + \nabla^2 \mathbf{m}], \qquad (3)$$

and γ is the gyromagnetic ratio. The spin-transfer torque coefficient is defined by $g \equiv \mathcal{P}(\hbar/2)(J/d|e|)f(\mathbf{m} \cdot \hat{\mathbf{x}})$, where $\mathcal{P}$ describes the electron polarization at the interface between the magnet and the spacer, J the current density, d the thickness of the layer, and e the electric charge. The parameter g is negative when the electrons flow from the fixed to the free layer. The first term of the right-hand side of Eq. (2) accounts for precessions, the second one gives account of the spin-transfer effect and the last one is the Gilbert damping, which accounts for dissipation of the energy. The parameter α rules the intensity of the damping. We note that in the present analysis the nonlocal effects of demagnetization fields have been approximated by a renormalization of the anisotropy coefficients. This simplifies drastically the equations, allowing us to have access to analytical calculations. Moreover, we have considered this approach because it is a good approximation for thin film systems with dimensions in the nanometer range [26] and also in the case where the magnetization has small deformations with respect to the uniform state [24].

The dynamics of LLG are characterized by the conservation of the magnitude of magnetization $\|\mathbf{m}\|$, since $\mathbf{m}$ and $\partial_t \mathbf{m}$ are perpendicular. Hence, the dynamics of Eq. (2) consist of rotations of $\mathbf{m}$. The LLG model, Eq. (2), admits two natural steady and uniform states: $\mathbf{m} = \pm\hat{x}$, which represent a free magnetization that is parallel (+) or antiparallel (−) to the fixed magnetization $\mathbf{M}_0$ [see Fig. 1(a)]. Both states correspond to extrema of energy Eq. (1). Hereafter, for the sake of simplicity, we will consider the following scaling and dimensioning of units $\mu_0 M_s^2/2 = 1$, $\gamma/M_s = 1$ and $\|\mathbf{m}\| = 1$ without loss of generality.

The specific form of the angular dependence of spin-transfer function $f(\mathbf{m} \cdot \hat{x})$ is sensitive to all the spin-transport parameters and much theoretical effort has been involved in establishing its relation with microscopic properties [18,27–30]. For the sake of simplicity, we consider the case $f \simeq 1$, which is valid for certain types of nanopillars [31,32].

A. Spherical representation of LLG model

Due to the conservation of the magnitude of the free magnetization, the numerical integration of Eq. (2) in the Cartesian representation for the magnetization can be a nontrivial task. Let us introduce the following spherical representation of the free magnetization

$$\mathbf{m} = \sin\theta(\cos\varphi\hat{x} + \sin\varphi\hat{y}) + \cos\theta\hat{z}, \qquad (4)$$

where the angles are outlined in Fig. 1(b) and the north pole lies on the m_z axis. Introducing the previous representation in Eq. (2), one obtains the following set of equations

$$\partial_\tau \theta = \sin\theta \nabla^2\varphi + 2\cos\theta \nabla\varphi \cdot \nabla\theta + \alpha\nabla^2\theta$$
$$- \frac{\alpha}{2}\sin 2\theta(\nabla\varphi)^2 - (h_a + \alpha g)\sin\varphi$$
$$- \frac{\beta_x}{2}\sin\theta \sin 2\varphi + (\alpha h_a - g)\cos\varphi\cos\theta$$
$$+ \frac{\alpha}{2}\sin 2\theta[\beta_z + \beta_x \cos^2\varphi],$$

$$\sin\theta\,\partial_\tau\varphi = \alpha\sin\theta\nabla^2\varphi + 2\alpha\cos\theta\nabla\varphi\cdot\nabla\theta - \nabla^2\theta$$
$$+ \frac{1}{2}\sin 2\theta(\nabla\varphi)^2 + (g - \alpha h_a)\sin\varphi$$
$$- \alpha\frac{\beta_x}{2}\sin\theta\sin 2\varphi - (\alpha g + h_a)\cos\varphi\cos\theta$$
$$- \frac{1}{2}\sin 2\theta[\beta_z + \beta_x\cos^2\varphi], \quad (5)$$

where $\tau = t/(1 + \alpha^2)$. To complement the theoretical study of the dynamics exhibited by the nanopillar, we have conducted numerical simulations with the spherical representation of Eq. (5) in order to preserve the magnitude of the magnetization. In all numerical simulations performed throughout this work, the space is discretized with finite differences where spatial differential operators are approximated with centered schemes of order 6. The magnetization for each element of the grid is obtained by solving Eq. (5) by means of a fourth-order Runge-Kutta algorithm. With this discretization, each volume of the layer interacts with twelve of its neighbors through the ferromagnetic exchange torque. Notice that the nonlocal demagnetization is not a mechanism of spatial coupling, because it has been approximated by the hard-axis anisotropy term proportional to β_z in Eq. (1).

Numerical simulations have also been conducted with stereographic representation [33], an alternative method that guarantees the preservation of the magnitude of **m**. The results provided by both representations are equal. Both Periodic and Neumann boundary conditions are used.

III. ONE-DIMENSIONAL NANOPILLAR

The parallel state, $\mathbf{m} \equiv \mathbf{m_p} = \hat{x}$, is a trivial steady state of LLG equation. Since the external magnetic field is parallel to the easy axis, $\mathbf{h_a} = h_a\hat{x}$, $h_a > 0$ will produce a torque that favors the parallel configuration. On the other hand, fields pointing against $\hat{x}$ will stabilize the antiparallel state. For near-parallel configurations, electric current flowing from the fixed to the free layer, $g < 0$, will contribute to the stabilization of the parallel state. Therefore, the self-organization dynamics appears as a balance between two opposite effects: the current stabilizing the parallel state and the external field destabilizing it. In this section, we analyze the bifurcation diagram of the parallel state in the one-dimensional configuration.

A. Linear stability analysis of parallel state

The parallel state in the spherical representation takes the form $(\theta,\varphi) = (\pi/2,0)$. To study the dynamics around the

parallel state we consider a perturbated state of the form

$$\begin{pmatrix}\theta(x,t)\\\varphi(x,t)\end{pmatrix} = \begin{pmatrix}\pi/2\\0\end{pmatrix} + \begin{pmatrix}\delta\theta_k(t)\\\delta\varphi_k(t)\end{pmatrix}e^{ikx} + \text{c.c.},$$

where the small amplitudes $\{\delta\theta_k(t),\delta\varphi_k(t)\}$ account for Fourier modes and the symbol c.c. represents the complex conjugate. Considering the above perturbation in Eq. (5) at linear order, we obtain

$$\frac{d}{dt}\begin{pmatrix}\delta\theta_k\\\delta\varphi_k\end{pmatrix} = \begin{bmatrix}g - \alpha a & -(a - \beta_z + \alpha g)\\a + \alpha g & g - \alpha(a - \beta_z)\end{bmatrix}\begin{pmatrix}\delta\theta_k\\\delta\varphi_k\end{pmatrix}, \quad (6)$$

with $a \equiv h_a + \beta_x + \beta_z + k^2$. Introducing an eigenmode ansatz $\delta\theta_k(t) = \delta\theta_k e^{\lambda t}$ and $\delta\varphi_k(t) = \delta\varphi_k e^{\lambda t}$, we find the following characteristic polynomial

$$\lambda^2 + b\lambda + c = 0, \quad (7)$$

where

$$b \equiv \alpha(2a - \beta_z) - 2g,$$
$$c \equiv (g - \alpha a)(g - \alpha(a - \beta_z)) + (a + \alpha g)(a + \alpha g - \beta_z).$$

For simplicity we study first the parameter region where the inhomogeneous perturbations decay and the bifurcating mode is homogeneous ($k = 0$). If $b = 0$ and $c > 0$, then the system exhibits an Andronov-Hopf bifurcation [34]. In the space of parameters $\{g,h_a\}$ the Andronov-Hopf instability curve is represented by the tilted straight line (see Fig. 2). Then, the parallel state becomes unstable through an oscillatory precession with frequency $\sqrt{c}$. This type of dynamics has
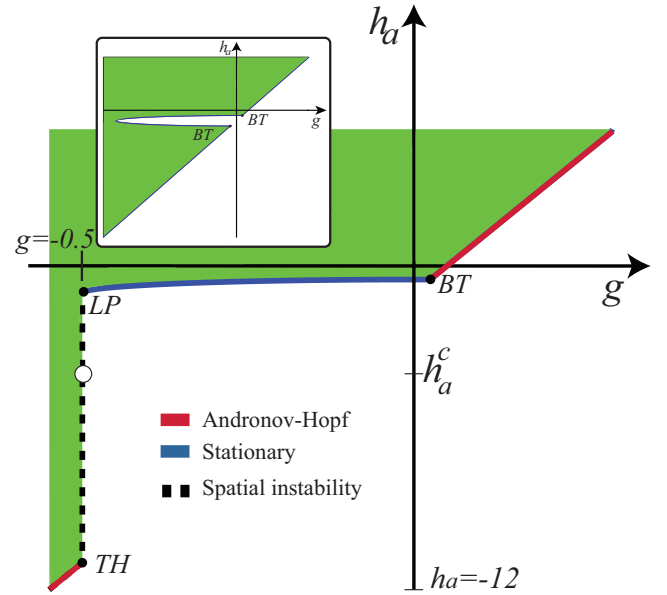

FIG. 2. (Color online) Bifurcation diagram of parallel state in the parameters space $\{g,h_a\}$. The parallel state is stable in the dark region. The thick diagonal line accounts for the Andronov-Hopf bifurcation. The horizontal curve realizes stationary instability. $\{BT,LP,TH\}$ represent the codimension two points associated to Bogdanov-Takens, Lifshitz-point, and Turing-Hopf instabilities, respectively. The vertical dashed line accounts for the spatial instability curve. The inset represents the bifurcation diagram in the case where spatial effects are ignored.

been reported on a nanopillar, where the frequency is typically of the order of the microwave [20].

In the case where the parameter c vanishes and $b \neq 0$, the system exhibits a stationary bifurcation for the parallel state [34]. This instability is characterized by a curve in the $\{g,h_a\}$ plane (see the inset in Fig. 2). In this region of the parameters space, the parallel state becomes unstable and eventually saturates into other states. Simultaneous confluence of a stationary instability and Andronov-Hopf bifurcation is a codimension two point, usually called Bogdanov-Takens [35]. This instability is characterized by two eigenvalues simultaneously crossing the origin of the complex plane with a single associated eigenvector. At this point we have $b = c = 0$. This point in the $\{g,h_a\}$ plane is denoted BT in Fig. 2. In other terms, since we have ignored the spatial dependences, the system exhibits two Bogdanov-Takens points as illustrated in the inset of Fig. 2. It is important to note that the experimental report made in Ref. [20] is performed around the Bogdanov-Takens point. In addition, this bifurcation diagram clearly emphasizes that when both the magnetic field and the spin-polarized current are positive, they favor and disfavor the parallel state $\mathbf{m_p}$.

The above scenario changes drastically when spatial effects are considered, $k \neq 0$, i.e., when one considers the exchange processes. The eigenvalues will become a function of wave number, $\lambda(k)$. The typical curve of the growth rate as a function of wave number [Re($\lambda(k)$)] and the dispersion relation [Im($\lambda(k)$)] are illustrated in Fig. 3(a). Note that the maximum Re(λ) has no-null wave number (k_c). Then changing the parameters of the system, it can exhibit a spatial instability, which analytically corresponds to impose the condition [3]

$$\left.\frac{\partial \lambda}{\partial k}\right|_{k=k_c} = 0, \quad \left.\frac{\partial^2 \lambda}{\partial^2 k}\right|_{k=k_c} < 0, \quad \text{and} \quad \lambda(k_c) = 0.$$

The first relation determines the critical wave number and the other the respective condition of instability. Applying the above conditions, we find the following length and critical condition

$$k_c^2 = -h_a - \left(\beta_x + \frac{\beta_z}{2}\right),$$

$$g_c = -\frac{\beta_z}{2}.$$

(8)

Since $k_c^2 \geqslant 0$, the external field must point against the parallel equilibrium for this bifurcation. The expression above corresponds to a vertical segment on the $\{g,h_a\}$ plane, which is represented by the dashed line of Fig. 2. In that zone, the external field h_a destabilizes the parallel state and $g < 0$ favors it through the current transport the magnetic moment from the fixed layer. The instability occurs when the current is not strong enough to balance with the external field and maintain the magnetization parallel. The emergence of a spatial instability with a divergent wavelength is generated from a Lifshitz point [3,36]. This critical point is characterized by the confluence of stationary instability and a spatial bifurcation. This is a codimension three point introduced for phase transitions in helicoidal ferromagnetic states [36]. Figure 2 represents this point with the symbol LP. Analogously spatial instability may coincide with the Andronov-Hopf bifurcation at a point of
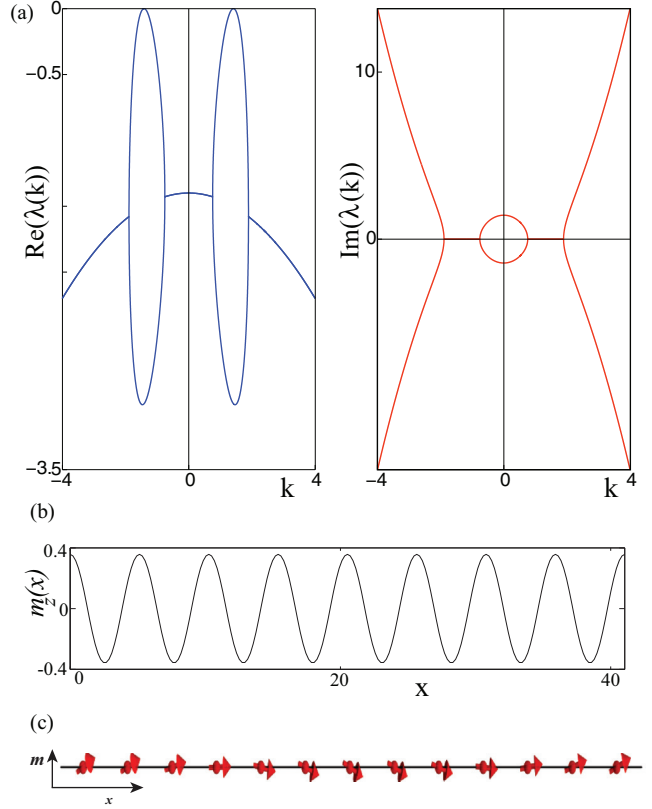

FIG. 3. (Color online) (a) Growth rate as a function of wave number [Re($\lambda(k)$)] and the dispersion relation [Im($\lambda(k)$)]. (b) $m_z(x)$ for the parameter values $g = -0.4976$, $h_a = -2.5$, $\beta_x = 0.5$, $\beta_z = 1$, $\alpha = 0.05$. The size of the box is chosen to admit 8 wavelengths. (c) Spin representation of one wavelength of the above state.

codimension two, which is usually denominated Turing-Hopf point [37,38]. Around this point the system is characterized by the emergence of waves. Figure 2 depicts this point by the symbol TH.

In physical units, the wavelength is $\Lambda = 2\pi l_{ex}/\sqrt{|h_a| - \beta_x - \beta_z/2}$. Notice that the parameter h_a permits the wavelength to vary between the the size of the device and the exchange length l_{ex}, in this last situation the continuous description becomes questionable.

When one crosses the dashed vertical line, the parallel state $\mathbf{m_p}$ becomes unstable giving rise to the appearance of a spatial pattern. Figure 3(b) shows an example of the observed stationary pattern. In order to understand this pattern analytically in Sec. III B we will carry out a weakly nonlinear analysis close to the spatial instability. This nonlinear analysis is based on the amplitude equations method [9].

B. Weakly nonlinear analysis

To characterize the dynamics of the pattern close to the spatial instability, we consider the following approximation for the free magnetization

$$\begin{pmatrix} \theta \\ \varphi \end{pmatrix} \approx \begin{pmatrix} \pi/2 \\ 0 \end{pmatrix} + [T(x,t)e^{ik_c x} + \bar{T}(x,t)e^{-ik_c x}]\begin{pmatrix} 1 \\ 1 \end{pmatrix},$$

(9)

where $\epsilon \equiv g - g_c$ is the bifurcation parameter. $T(x,t)$ describes the slowly varying amplitude of the critical spatial mode $\mathbf{m_c}(x)$, which corresponds in a Cartesian representation to the vector

$$\mathbf{m_c} = \begin{pmatrix} 1 \\ T(x,t)e^{ik_cx} + \bar{T}(x,t)e^{-ik_cx} \\ -T(x,t)e^{ik_cx} - \bar{T}(x,t)e^{-ik_cx} \end{pmatrix}, \qquad (10)$$

$\bar{T}$ stands for the complex conjugate of T, and h.o.t. accounts for the higher-order corrections. Introducing the above ansatz Eq. (9) in Eq. (5), and imposing a solvability condition after calculations we obtain (quintic real Ginzburg-Landau equation)

$$\partial_t T = \epsilon T - \frac{\left(6\beta_x + 3\beta_z - 2k_c^2\right)^2}{4\beta_z} T|T|^4 + \frac{4k_c^2}{\beta_z}\partial_{xx}T. \quad (11)$$

To obtain this equation we have considered the following scaling $T \sim \epsilon^{1/4}$, $\partial_t \sim \epsilon$, and $\partial_x \sim \epsilon^{1/2}$. Then, this amplitude equation is of order $\epsilon^{5/4}$ and the corrections are of order $\epsilon^{7/4}$. Then the characteristic time scale of patterns will be ϵ^{-1}, or, in physical units of $[\gamma M_s(g - g_c)]^{-1}$. Equation (12) has uniform solutions of the form

$$T(x,t) = \left[4\beta_z \frac{(g - g_c)}{\left(6\beta_x + 3\beta_z - 2k_c^2\right)^2}\right]^{1/4}, \qquad (12)$$

which represents the pattern amplitude as a function of the physical parameters. Note that this amplitude increases with 1/4 power of the bifurcation parameter, $|T| \sim \epsilon^{1/4}$. Numerically from the LLG equation Eq. (5), we have verified this prediction. Indeed, we have represented in Fig. 4 the amplitude of the pattern (dotted) and formula Eq. (12). As can be seen from this figure, the two results are in good agreement. Far from the threshold the numerical and analytical results start to disagree. The higher-order terms are responsible for this difference.

Generically, the amplitude of the patterns near the spatial bifurcation follows a power law of the square root type [3,11], due to the cubic nonlinearity. However, in the nanopillar oscillator the pattern is controlled by the quintic nonlinearity. Although supercritical quintic bifurcations are less common than supercritical cubic instabilities in the context of parametric

instabilities such bifurcations are generic [39,40] and even this has been reported experimentally [41].

Note that the coefficient of the quintic term is modified with the external magnetic field, h_a through its dependence on k_c (cf. Eqs. 8). There is a critical value of the external magnetic field,

$$h_a^c = -4\left(\beta_x + \frac{\beta_z}{2}\right), \qquad (13)$$

for which the quintic coefficient vanishes. The dynamics around this point is led by the seventh nonlinearity in the amplitude equation. Notwithstanding, the quintic coefficient always is semidefined positives, that is the spatial instability is always supercritical.

Notice that the parallel state is related with antiparallel one through the transformation $(g,h_a,\varphi) \rightarrow (-g,-h_a,\varphi + \pi)$. Therefore, the antiparallel state of the free magnetization has a analogous phase diagram to the parallel state with the opposite sign of the external magnetic field and spin-polarized current.

IV. DYNAMICS IN TWO DIMENSIONS: STRIPES AND SUPERLATTICES

Let us consider a spatial transversal extension of the nanopillar in two dimensions, then the magnetization becomes a field defined in the xy plane, $\mathbf{m}(x,y,t)$. The stability analysis presented in Sec. III remains valid, where the only instability that is modified is the spatial one, due to the presence of an infinite number of critical spatial modes with wave number $|\mathbf{k}| = k_c$. Figures 5 and 7 show the typical pattern observed at the onset of the spatial bifurcation. Unexpectedly, the observed pattern near the bifurcation reveals a greater spatial complexity in comparison to those usually reported at the onset of the spatial instability such as stripes, squares, and hexagons patterns [1–5]. Figure 5 illustrates the number of coupled
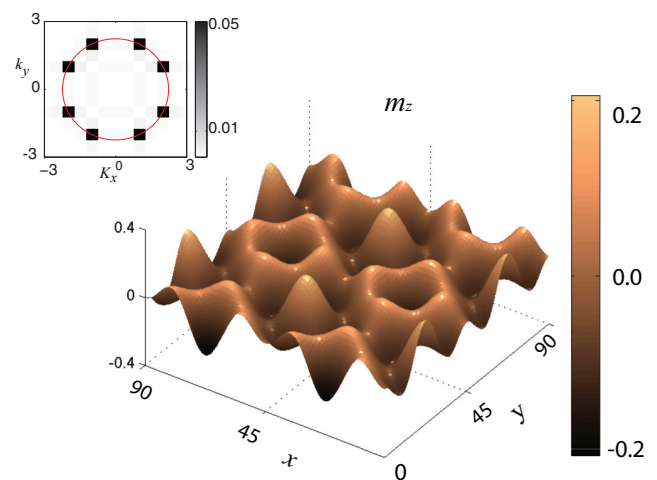

FIG. 4. Pattern amplitude as a function of the spin-polarized current. Points are obtained by numerical simulations of the LLG model for $h_a = -2.5$, $\beta_x = 0.5$, $\beta_z = 1$, and $\alpha = 0.05$. The total length of the simulation box is chosen to admit 8 critical wavelengths. The dotted curve is a fit with a power law where the exponent found is 0.25.

FIG. 5. (Color online) The component m_z of the magnetization in a 90×90 grid, it was obtained by numerical simulations of the LLG model for $g = -0.4999$, $h_a = -6$, $\beta_x = 0.5$, $\beta_z = 1$, and $\alpha = 0.05$. The space is divided into squares of lateral dimension $dx = 0.141\,195$. The inset shows the Fourier transform of m_z, and the circumference shows the critical wavelength k_c.

modes, which corresponds to four spatial modes and their respective conjugate modes. These types of patterns are usually denominated as superlattices [8]. In order to understand the emergence of these patterns analogously to the study that we have conducted on one spatial dimension, we will carry out a weakly nonlinear analysis.

A. Amplitude equations

In two spatial dimensions, the linear stability analysis is similar to those presented in Sec. III. The perturbation of the parallel state reads

$$\begin{pmatrix} \theta(\mathbf{r},t) \\ \varphi(\mathbf{r},t) \end{pmatrix} = \begin{pmatrix} \pi/2 \\ 0 \end{pmatrix} + \begin{pmatrix} \delta\theta_k(t) \\ \delta\varphi_k(t) \end{pmatrix} e^{i\mathbf{k}\cdot\mathbf{r}} + \text{c.c.},$$

where $\mathbf{r} = (x,y)$ stands for the transverse coordinates of the free magnetic layer. Then we obtain the same characteristic polynomial (7) where k is replaced by $|\mathbf{k}|$. Imposing the conditions of spatial instability we obtain

$$|\mathbf{k}_c|^2 = -h_a - \left(\beta_x + \frac{\beta_z}{2}\right), \quad g_c = -\frac{\beta_z}{2}. \quad (14)$$

Therefore, all spatial modes having the same magnitude $|k_c|$ are critical modes.

To study the dynamics of these critical modes we have considered the following ansatz

$$\begin{pmatrix} \theta \\ \varphi \end{pmatrix} = \begin{pmatrix} \pi/2 \\ 0 \end{pmatrix} + R \sum_{j=1}^{N} A_j(\mathbf{r},\epsilon t) e^{i\mathbf{k}_c^j \cdot \mathbf{r}} \begin{pmatrix} 1 \\ 1 \end{pmatrix} + \text{c.c.} + \text{h.o.t.},$$
$$(15)$$

where A_j accounts for the amplitude of the critical spatial mode $\mathbf{k}_c^j$, which we assume is a slow variable in space and time, and N stands for the number of critical spatial modes. Finally, R is a characteristic scale for the amplitude of the patterns given by

$$R = \sqrt[4]{\frac{4\beta_z\epsilon}{(6\beta_x + 3\beta_z - 2q^2)^2}}. \quad (16)$$

Introducing the above ansatz (15) in Eq. (5), and imposing the condition of solubility after straightforward calculations we obtain the following set of amplitude equations (coupled Newell-Whitehead-Segel equations [2,3,42])

$$\partial_t A_j = A_j - A_j|A_j|^4 - \frac{8}{3}\frac{1}{1-D}A_j\sum_{l\neq j}^{N}|A_l|^4$$

$$+ \hat{L}_{nws}(\nabla_j)A_j - \frac{8}{3}\frac{2-3D}{1-D}A_j|A_j|^2\sum_{l\neq j}^{N}|A_l|^2$$

$$- 8A_j \sum_{l\neq j, m\neq j, m\neq l}^{N}|A_l|^2|A_m|^2, \quad (17)$$

with

$$\hat{L}_{nws}(\nabla_j) \equiv \frac{4}{\beta_z}\left(|k_c|\frac{\partial}{\partial x_{\|_j}} - \frac{i}{2}\frac{\partial^2}{\partial x_{\perp_j}^2}\right)^2 \quad (18)$$

is the spatial operator, $\{x_{\|_j}, x_{\perp_j}\}$ are, respectively, the longitudinal and the transverse coordinates with respect to the vector $\mathbf{k}_c^j$ and

$$D \equiv \frac{2}{3}\frac{q^2}{2\beta_x + \beta_z} = \frac{2|h_a| - 2\beta_x - \beta_z}{6\beta_x + 3\beta_z}. \quad (19)$$

Note that there is only one parameter, D, which characterizes the dynamics of the system. The above set of equations have derived considering the scaling $|A_j| \sim \epsilon^{1/4}$, $\partial_t \sim \epsilon$, $x_{\|} \sim \epsilon^{-1/2}x$, and $x_{\perp_j} \sim \epsilon^{-1/4}x$. Equation (17) accounts for the dynamics of all critical modes. Nevertheless, the size effects discretizing and privilege certain critical modes [8].

B. Size effects in the pattern formation

In the case of considering Neumann boundary conditions, and transverse dimensions L_x and L_y, respectively, the critical spatial modes compatible with the boundary conditions have the form $\mathbf{k}_c^{m,n} = (\pi m/L_x, \pi n/L_y)$ with $\{m,n\}$ integer numbers. Therefore the critical spatial modes must satisfy the relation

$$\pi^2\left(\frac{m^2}{L_x^2} + \frac{n^2}{L_y^2}\right) = |h_a| - \left(\beta_x + \frac{\beta_z}{2}\right). \quad (20)$$

As a result of this discretization—owing to size effects—few couplings between patterns are allowed, such as one mode (stripe pattern), two modes (square pattern), four modes (superlattice pattern), six modes (superlattice pattern), and so forth, and their respective conjugates. Hence, the number of critical modes considered in ansatz (15) are such that $N = 1, 2, 4, 6, 8, 12, \ldots$. Patterns generated by an odd number of critical modes such as hexagons (three modes and their conjugates) are not observed because the system has no quadratic terms [2,3]. These terms are not allowed in the LLG equation due to the symmetries $\varphi \to -\varphi$ and $\theta \to -\theta$.

The relevant question that emerges is: how can we understand the observed equilibria at the onset of the bifurcation? To resolve this question one must study the stability of the stripe state. If this state is unstable then for symmetry reasons the system will display squares or superlattices equilibrium state, consistent with the boundary conditions. In the next section, we will perform the stability analysis of the stripe pattern when one considers few coupled modes and their respective conjugate modes.

C. Bifurcation diagram

To clarify the phase diagram we consider the dynamics of four modes and their complex conjugates ($N = 4$) in ansatz (15), and neglecting their spatial coupling, then the amplitude of these modes satisfies

$$\partial_t A_1 = A_1 - \frac{8}{3}\frac{2-3D}{1-D}A_1|A_1|^2(|A_2|^2 + |A_3|^2 + |A_4|^2)$$

$$- A_1(|A_1|^4 + 8(|A_2|^2|A_3|^2 + |A_3|^2|A_4|^2$$

$$+ |A_2|^2|A_4|^2)) - \frac{8}{3}\frac{1}{1-D}A_1(|A_2|^4 + |A_3|^4 + |A_4|^4).$$
$$(21)$$

The equations for the other amplitudes are obtained just by interchanging the indexes, for instance, $\partial_t A_2$ is obtained with the replacement $(1,2,3,4) \rightarrow (2,1,3,4)$. Notice that the bifurcation diagram is characterized entirely by the line $D \geqslant 0$. This parameter describes the competition between the external magnetic field, anisotropies, exchange, and the critical spin-polarized current. Since the coefficients of the above set of equations are real, then only the magnitudes of the amplitudes are coupled and their respective phases are completely decoupled. Hence, the effective dynamical system that accounts for the pattern formation is of dimension 4.

The above set of equations admits four types of equilibria, one describes the stripe patterns $|A_1| \neq 0$, $A_k = 0$ ($k = \{2,3,4\}$), rhombs $|A_1| = |A_2| \neq 0$, $A_3 = A_4 = 0$, hexagons $|A_1| = |A_2| = |A_3| \neq 0$, $A_4 = 0$, and finally the the superlattice. The superlattice pattern is composed by the four modes $|A_1| = |A_2| = |A_3| = |A_4| = 1$

This superlattice pattern is illustrated in Fig. 5. On the other hand, the stripe patterns correspond to a nonzero amplitude while the other amplitudes are zero, for example $A_1 = 1$, and $A_2 = A_3 = A_4 = 0$. This pattern corresponds to a rolls structure in the $\mathbf{k}_1$ direction.

To study the stability of the stripe pattern, we consider the following perturbation $A_1 = 1 + \chi_1(t)$, $A_2 = \chi_2(t)$, $A_3 = \chi_3(t)$, $A_4 = \chi_4(t)$ ($\chi_i \ll 1$) and linearizing with respect to the perturbation we get

$$\partial_t \chi_1 = -4\chi_1, \quad \partial_t \chi_2 = -\frac{5+3D}{3(1-D)}\chi_2,$$

$$\partial_t \chi_3 = -\frac{5+3D}{3(1-D)}\chi_3, \quad \partial_t \chi_4 = -\frac{5+3D}{3(1-D)}\chi_4.$$

Then for $D < 1$ ($D > 1$) the stripe pattern is stable (unstable), and for $D > 1$ the system exhibits stable superlattice patterns. The corresponding bifurcation diagram of the system is shown in Fig. 6. For $D = 1$, the quintic saturation vanishes and higher-order nonlinearities are required. Associated with $D = 1$, the system has an external magnetic field value h_a^c, which is highlighted in Fig. 3.

If one performs the same analysis with $N = 2,6,8,12, \ldots$ modes the stability analysis obtained is exactly the same. Hence, Fig. 6 sketches the bifurcation diagram of the system and Fig. 7 illustrates the observed patterns for $D > 1$. Thus, the region closer to stationary instability—the Lifshitz point—exhibits striped patterns whose saturating mechanism is given by the anisotropies β_x and β_z. In contrast, when $|h_a| > |h_a^c|$
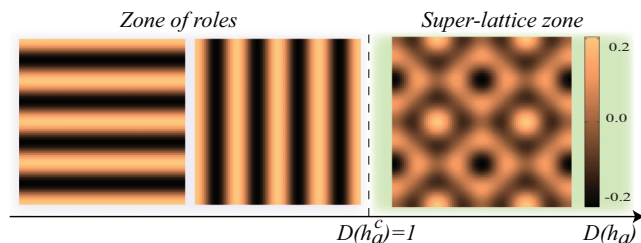

FIG. 6. (Color online) Bifurcation diagram for four-mode models (21). In the left part ($D < 1$), only rolls are stable. For $D > 1$, the four-modes state is stable. A more general scenario for $D > 1$ is illustrated in Fig. 7.
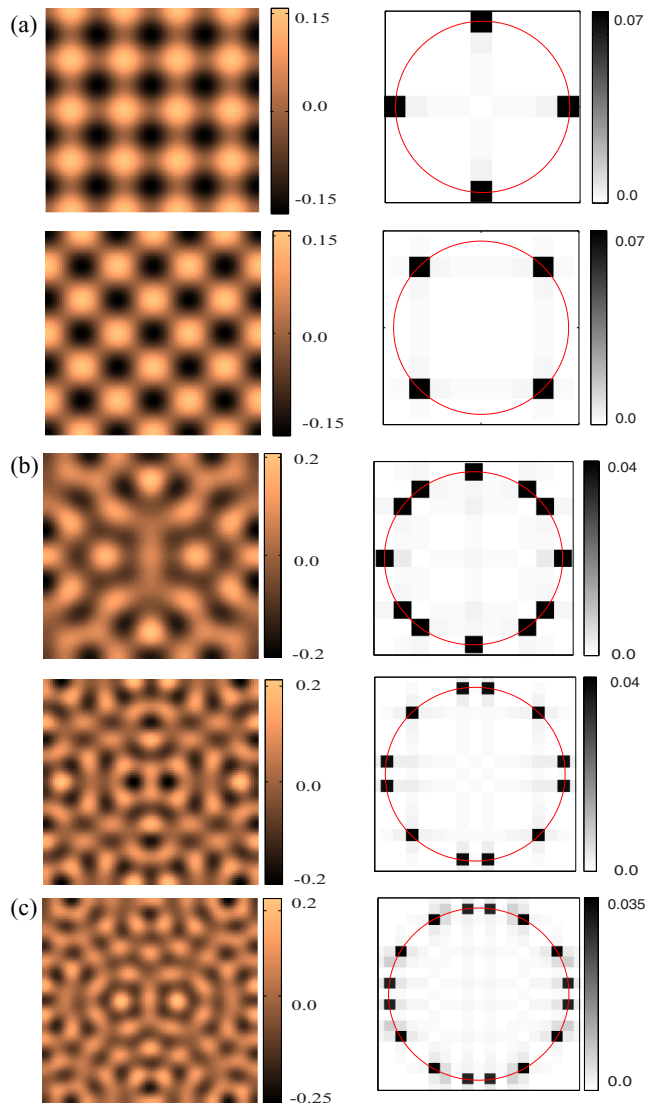

FIG. 7. (Color online) The system size selects the stability of the stationary equilibria for $D > 1$. (a) Squares. The top (down) solution is obtained with $dx = 0.126\,289$ ($dx = 0.133\,949$). (b) Superhexagons. A $dx = 0.157\,861$ ($dx = 0.223\,25$) was used for the top (down) state. (c) Eight-mode superlattices, $dx = 0.254\,543$. The other parameters are the same that we considered in Fig. 5.

the system exhibits superlattice patterns. Since large negative magnetic fields penalize configurations near the parallel state, then all admitted modes grow. Pattern solutions obtained for the same parameters that were used on Fig. 5. The exchange free energy term grows as $(\nabla \mathbf{m})^2 \sim q^2 |A_j|^2 \sim |h_a||A_j|^2$, then it makes the superlattices saturate. As one continues increasing the bifurcation parameter ϵ, by means of decreasing the modulus of the spin-polarized current g, patterns exhibit complex spatiotemporal behavior. Work in this direction is in progress.

V. CONCLUSIONS AND REMARKS

Macroscopic magnetic systems subjected to external forcing exhibit self-organization phenomena as a result of

injection, transport, and dissipation of energy and momenta. For extended systems, natural self-organization states are spatial structures. In this work, we have studied the formation of spatial patterns from a uniform magnetization state in one and two spatial dimensions in a spin-transfer nano-oscillator induced by the competition of a spin-polarized current and an external magnetic field. This system is described in the continuous limit by the Landau-Lifshitz-Gilbert equation. This model incorporates the uniaxial anisotropy, the demagnetization in thin film approximation, the ferromagnetic exchange that provides the spatial coupling, the dissipation, and a spin-transfer torque term. The bifurcation diagram of the parallel state to external magnetic field is revealed. It is important to note that the bifurcation diagram of the antiparallel state is similar to that exhibited by the parallel state, since the parallel state is related with the antiparallel one through the transformation $(g, h_a, \varphi) \rightarrow (-g, -h_a, \varphi + \pi)$.

We have shown analytically that the parallel state has a spatial supercritical quintic bifurcation. Numerical simulations at the onset of spatial bifurcation verify these theoretical results. In addition, we have determined that there is a critical value for the external magnetic field, h_a^c, in which the transition becomes seventh type. For $|h_a| < |h_a^c|$, the dominant mechanism that makes the pattern saturate is the anisotropy, however for $|h_a| > |h_a^c|$, the mechanism that drives the dynamics is the ferromagnetic exchange. In two spatial dimensions the system shows the emergence of stripe patterns or superlattices at the onset of bifurcations. Analytically, we have characterized its respective bifurcation diagram, which is characterized by a single control parameter, which

accounts for the competition between the external magnetic field, anisotropy, exchange, and the critical spin-polarized current. This scenario is confirmed numerically. Therefore, when the anisotropy is the dominant mechanism ($|h_a| < |h_a^c|$) the system exhibits striped patterns, however, in the case of the exchange driving the dynamics ($|h_a| > |h_a^c|$), the system presents superlattice as stable equilibria. Indeed, exchange favors the formation of more complicated structures.

For typical experimental setups, the anisotropies are about $\beta_x = 0.5$ and $\beta_z = 1$, and the exchange length is of the order of 3.5 nm. Then for external fields of magnitude $H_a = M_s|h_a| = 1.5 M_s$, the wavelength of the pattern is typically of order $\Lambda = 30$ nm. One expects that self-organization exhibited in this study persists for generalizations or variations of model (2). For instance, the angular dependence of g [18,27–32] or the use tensor form of magnetization damping [43] could change the saturation mechanisms of patterns for some geometries and materials, due to the inclusion of other terms. Work in this direction is in progress.

[1] G. Nicolis and I. Prigogine, *Self-Organization in Non Equilibrium Systems* (Wiley, New York, 1977).

[2] L. M. Pismen, *Patterns and Interfaces in Dissipative Dynamics* (Springer, Berlin, 2006).

[3] M. C. Cross and P. C. Hohenberg, Rev. Mod. Phys. **65**, 851 (1993).

[4] M. Cross and H. Greenside, *Pattern Formation and Dynamics in Nonequilibrium Systems* (Cambridge University Press, New York, 2009).

[5] M. I. Rabinovich, A. B. Ezersky, and P. D. Weidman, *The Dynamics of Patterns* (World Scientic, Singapore, 2000).

[6] G. Nicolis, *Introduction to Nonlinear Science* (Cambridge University Press, Cambridge, 1995).

[7] P. Ball, *The Self-Made Tapestry: Pattern Formation in Nature* (Oxford University Press, New York, 1999).

[8] R. B. Hoyle, *Pattern Formation: An Introduction to Methods* (Cambridge University Press, Cambridge, 2006).

[9] A. C. Newell, T. Passot, and J. Lega, Ann. Rev. Fluid Mech. **25**, 399 (1993).

[10] I. Ortega, M. G. Clerc, C. Falcon, and N. Mujica, Phys. Rev. E **81**, 046208 (2010).

[11] L. Landau, C. R. Acad. Sci. USSR **44**, 311 (1944).

[12] W. S. Edwards and S. Fauve, Phys. Rev. E **47**, R788 (1993).

[13] E. Pampaloni, P. L. Ramazza, S. Residori, and F. T. Arecchi, Phys. Rev. Lett. **74**, 258 (1995).

[14] M. Le Berre, E. Ressayre, A. Tallet, Y. Pomeau, and L. Di Menza, Phys. Rev. E **66**, 026203 (2002).

[15] B. Georges, J. Grollier, M. Darques, V. Cros, C. Deranlot, B. Marcilhac, G. Faini, and A. Fert, Phys. Rev. Lett. **101**, 017201 (2008).

[16] Z. Yang, S. Zhang, and Y. C. Li, Phys. Rev. Lett. **99**, 134101 (2007).

[17] D. Li, Y. Zhou, C. Zhou, and B. Hu, Phys. Rev. B **83**, 174424 (2011); and references therein.

[18] J. C. Slonczewski, J. Magn. Magn. Mater. **159**, L1 (1996).

[19] L. Berger, Phys. Rev. B **54**, 9353 (1996).

[20] S. I. Kiselev, J. C. Sankey, I. N. Krivorotov, N. C. Emley, R. J. Schoelkopf, R. A. Buhrman, and D. C. Ralph, Nature (London) **425**, 380 (2003).

[21] D. C. Ralph and M. D. Stiles, J. Magn. Magn. Mater. **320**, 1190 (2008).

[22] G. Bertotti, C. Serpico, I. D. Mayergoyz, A. Magni, M. d'Aquino, and R. Bonin, Phys. Rev. Lett. **94**, 127206 (2005).

[23] R. Bonin, M. d'Aquino, G. Bertotti, C. Serpico, and I. D. Mayergoyz, Eur. Phys. J. B **85**, 47 (2012).

[24] I. D. Mayergoyz, G. Bertotti, and C. Serpico, *Nonlinear Magnetization Dynamics in Nanosystems* (Elsevier, Oxford, 2009).

[25] Z. Li and S. Zhang, Phys. Rev. B **68**, 024404 (2003); J. Z. Sun, *ibid.* **62**, 570 (2000); X. Waintal, E. B. Myers, P. W. Brouwer,

and D. C. Ralph, *ibid*. **62**, 12317 (2000); M. D. Stiles and A. Zangwill, *ibid*. **66**, 014407 (2002).

[26] G. Gioia and R. D. James, Proc. R. Soc. Lond. A **453**, 213 (1997).

[27] J. C. Slonczewski, J. Magn. Magn. Mater. **247**, 324 (2002).

[28] J. Xiao, A. Zangwill, and M. D. Stiles, Phys. Rev. B **70**, 172405 (2004).

[29] J. Xiao, A. Zangwill, and M. D. Stiles, Phys. Rev. B **72**, 014446 (2005).

[30] J. Barnas, A. Fert, M. Gmitra, I. Weymann, and V. K. Dugaev, Phys. Rev. B **72**, 024426 (2005).

[31] S.-W. Lee and K.-J. Lee, IEEE Trans. Magn. **46**, 2349 (2010).

[32] W. Kim, S.-W. Lee, and K.-J. Lee, J. Phys. D **44**, 384001 (2011).

[33] M. Lakshmanan, Phil. Trans. R. Soc. A **369**, 1280 (2011).

[34] E. Atlee Jackson, *Perspectives of Nonlinear Dynamics* (Cambridge University Press, New York, 1989), Vol. 1.

[35] Y. Kuznetsov, *Elements of Applied Bifurcation Theory*, 2nd ed. (Springer, New York, 2004).

[36] R. M. Hornreich and M. Luban, Phys. Rev. Lett. **35**, 1678 (1975).

[37] P. Glansdorff and I. Prigogine, *Thermodynamic Theory of Structure, Stability, and Fluctuations* (Wiley, New York, 1974).

[38] A. De Wit, D. Lima, G. Dewel, and P. Borckmans, Phys. Rev. E **54**, 261 (1996).

[39] P. Coullet, T. Frisch, and G. Sonnino, Phys. Rev. E **49**, 2087 (1994).

[40] G. Agez, M. G. Clerc, E. Louvergneaux, and R. G. Rojas, Phys. Rev. E **87**, 042919 (2013).

[41] F. Petrelis, S. Aumaitre, and S. Fauve, Phys. Rev. Lett. **94**, 070603 (2005).

[42] B. A. Malomed, A. A. Nepomnyashchy, and M. I. Tribelsky, Phys. Rev. A **42**, 7244 (1990).

[43] V. L. Safonov, J. Appl. Phys. **91**, 8653 (2002).

Apéndice B

Spin-transfer-driven nano-oscillators are equivalent to parametric resonators

This chapter presents the equivalence between a ferromagnetic film driven by spin-transfer torques and systems driven by a time-dependent forcing.

Spin-transfer-driven nano-oscillators are equivalent to parametric resonators

Alejandro O. León[*] and Marcel G. Clerc[†]

Departamento de Física, Facultad de Ciencias Físicas y Matemáticas, Universidad de Chile, Casilla 487-3, Santiago, Chile

The equivalence between different physical systems permits us to transfer knowledge between them and to characterize the universal nature of their dynamics. We demonstrate that a nanopillar driven by a spin-transfer torque is equivalent to a rotating magnetic plate, which permits us to consider the nanopillar as a macroscopic system under a time-modulated injection of energy, that is, a simple parametric resonator. This equivalence allows us to characterize the phases diagram and to predict magnetic states and dynamical behaviors, such as solitons, stationary textures, and oscillatory localized states, among others. Numerical simulations confirm these predictions.

I. INTRODUCTION

Current-driven magnetization dynamics have attracted much attention in recent years because of both the rich phenomenology that emerges and the promising applications in memory technology [1]. A remarkable example occurs when a direct spin-polarized current applies a torque to nanoscale ferromagnets, an effect known as spin-transfer torque [2,3]. This effect has been confirmed experimentally [4–9], and, in particular, the observation of magnetization reversal caused by spin-transfer torques was reported in Refs. [6,7,10,11]. Spin-transfer effects are usually studied in the metallic multilayer nanopillar, or spin-valve, depicted in Fig. 1(a), where two magnetic films (light layers), the *free* and the *fixed*, are separated by a nonmagnetic spacer (darker layer). In such a nanopillar, an electric current J applied through the spin-valve transfers spin angular momentum from the film with *fixed* magnetization to the *free* ferromagnetic layer.

When the direct current overcomes a critical value, the spin-transfer torque destabilizes the state in which both magnetizations point parallel, and the free magnetization switches or precesses in the microwave-frequency domain. Most scientific efforts have focused on this regime, in which the free magnetization behaves as a self-oscillator with negative damping [12]. Another interesting case is when there is an external field that disfavors the parallel state and the spin-polarized current favors it; under this regime, it is expected that the system will generate complex dynamics as a result of both opposing effects.

The aim of this article is to show that nanopillars under the effect of a spin-polarized direct electric current exhibit the same dynamics present in systems with a time-modulated injection of energy, known as parametric systems [13]. Parametric systems oscillate at half of the forcing frequency, a phenomenon known as parametric resonance. Examples of parametric systems include a layer of water oscillating vertically [14], localized structures in nonlinear lattices [15], light pulses in optical fibers [16], optical parametric oscillators [17], and easy-plane ferromagnetic materials exposed to an oscillatory magnetic field [18].

To understand the parametric nature of the spin-transfer-driven nanopillars, we put in evidence that this system is equivalent to a simple rotating magnetic plate subjected to a constant magnetic field applied in the rotation direction [see Fig. 1(b)], where the electric current intensity on the nanopillar corresponds to the angular velocity in the equivalent rotational system. We analytically show that the magnetization dynamic of a nanopillar under the effect of a spin-transfer torque is well described by *the parametrically driven, damped nonlinear Schrödinger equation* (PDNLS). This equation is the paradigmatic model of parametric systems with small injection and dissipation of energy [19]. Based on this model we predict that the spin-transfer torque generates equilibria, solitons, oscillons, patterns, propagative walls between symmetric periodic structures, and complex behaviors, among others. Numerical simulations of the Landau-Lifshitz-Gilbert equation confirm these theoretical predictions.

The manuscript is organized as follows. In the next section we present the nanopillar and the equation of motion of an homogeneous free magnetization. In Sec. III, we analyze the relation between the nanopillar and parametric systems. In Sec. IV we explore the inhomogeneous dynamics predicted by the parametric nature of the spin-transfer torque effect at dominant order. Finally, in Sec. V, we give the conclusions and remarks.

II. MACROSPIN DYNAMICS OF THE FREE LAYER

Consider a nanopillar device, with fixed layer magnetization $\mathbf{M}_0$ along the positive x axis as depicted by Fig. 1; this ferromagnet has a large magnetocrystalline anisotropy or it is thicker than the free layer, and therefore it acts as a polarizer for the electric current. Let us assume that the free layer is a single-domain magnet, that is, the magnetization rotates uniformly $\mathbf{m}(\mathbf{r},t) = \mathbf{m}(t)$.

Hereafter, we work with the following adimensionalization: The magnetization of the free layer $\mathbf{M} \to M_s \mathbf{m}$ and the external field $\mathbf{H_a} \to M_s \mathbf{h_a}$ are normalized by the saturation magnetization M_s; moreover, the time $t \to \gamma M_s t$ is written in terms of the gyromagnetic constant γ and M_s. For instance, in a cobalt layer of 3 nm thickness, $M_s \simeq 1.4 \times 10^6 \, A/m$, and the characteristic time scale is $(\gamma M_s)^{-1} \simeq 3.2$ ps [20].

———————
[*]aoleon@dfi.uchile.cl
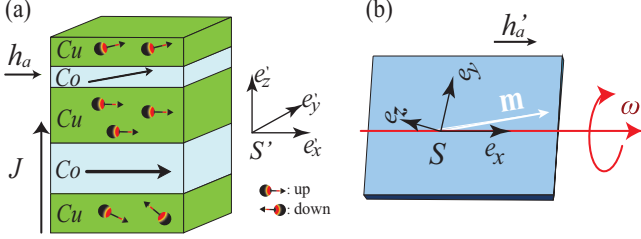[†]marcel@dfi.uchile.cl

FIG. 1. (Color online) Equivalent physical systems. (a) Schematic representation of the spin-transfer torque nano-oscillator setup. The light (blue) and dark (green) layers represent magnetic and nonmagnetic metal films, respectively. J and h_a are the electric current through the spin-valve and the external magnetic field, both effects are parallel to the easy axes of the ferromagnetic layer under study. $\mathbf{M}_o$ stands for the magnetization of the fixed layer. (b) Rotating magnetic plate with an easy axis in the rotation direction, subjected to a constant magnetic field, $\mathbf{h_a'}$.

When the free magnetization is homogeneous, the normalized magnetic energy per unit of volume is [20]

$$\frac{E}{\mu_0 M_s^2} = -\mathbf{m}\cdot\mathbf{h_a} - \frac{1}{2}\beta_x m_x^2 + \frac{1}{2}\beta_z m_z^2, \qquad (1)$$

and the external magnetic field $\mathbf{h_a} = h_a \mathbf{e}_x$ points along the x axis (see Fig. 1). The coefficients β_x and β_z are combinations of the normalized anisotropy and demagnetization constants with respect to the appropriate axes, where β_x (β_z) favors (disfavors) the free magnetization in the x axis (z axis).

The dynamic of the magnetization of the free layer is described by the dimensionless Landau-Lifshitz-Gilbert equation (LLG) with an extra term that accounts for the spin-transfer torque [2,6,7,20,21],

$$\frac{d\mathbf{m}}{dt} = -\mathbf{m}\times\mathbf{h}_{\text{eff}} + \alpha\mathbf{m}\times\frac{d\mathbf{m}}{dt} + g\,\mathbf{m}\times(\mathbf{m}\times\mathbf{e_x}). \qquad (2)$$

The first term of the right-hand side of Eq. (2) accounts for the conservative precessions generated by the effective field,

$$\mathbf{h}_{\text{eff}} \equiv -\frac{1}{\mu_0 M_s^2}\frac{\delta E}{\delta\mathbf{m}} = (h_a + \beta_x m_x)\mathbf{e}_x - \beta_z m_z\mathbf{e}_z. \qquad (3)$$

The second and third terms of Eq. (2) are the phenomenological Gilbert damping and the spin-transfer torque respectively. The dimensionless prefactor g is given by [11] $g \equiv \mathcal{P}(m_x)(\hbar/2)(J/d|e|)(1/\mu_0 M_s^2)$, and $\mathcal{P}$ describes the electron polarization at the interface between the magnet and the spacer, J the current density of electrons, d the thickness of the layer, and $e < 0$ the electric charge. The current density of electrons J and the parameter g are negative when the electrons flow from the fixed to the free layer. There are different expressions for the polarization $\mathcal{P}(m_x)$ in the literature [2,22–25]. For certain types of nanopillars, a better agreement with experimental observations is obtained if $\mathcal{P}(m_x)$ is constant, see Refs. [24,26,27] for more details.

The dynamics of LLG are characterized by the conservation of the magnetization magnitude $\|\mathbf{m}\| = 1$, since $\mathbf{m}$ and $d\mathbf{m}/dt$ are perpendicular. The LLG model, Eq. (2), admits two natural equilibria $\mathbf{m} = \pm\mathbf{e}_x$, which represent a free magnetization that is parallel (+) or antiparallel (−) to the fixed magnetization $\mathbf{M}_0$ [see Fig. 1(a)]. Both states correspond to extrema of the

free energy E. We will concentrate on the equilibrium $\mathbf{m} = \mathbf{e}_x$; nevertheless due to the symmetries of the LLG equation, the same results hold for $\mathbf{m} = -\mathbf{e}_x$ when replacing (g, h_a) with $(-g, -h_a)$.

III. EQUIVALENT PHYSICAL SYSTEMS

Let us consider a rotating magnetic plane with angular velocity $\mathbf{\Omega} = \Omega_0\mathbf{e}_x$ and an easy axis in the rotation direction, subjected to a constant magnetic field applied in the rotation direction $\mathbf{h_a'} = (h_a + \Omega_0)\mathbf{e}_x$ [see Fig. 1(b)].

This rotating ferromagnet can be described in both the co-movil frame S, defined by the vectors $\{\mathbf{e}_x, \mathbf{e}_y, \mathbf{e}_z\}$, or in the inertial frame S', defined by $\{\mathbf{e}_x', \mathbf{e}_y', \mathbf{e}_z'\}$. Note that the ferromagnetic easy axis is described by the same vector in the both frames ($\mathbf{e}_x' = \mathbf{e}_x$); nevertheless, unit vectors $\mathbf{e}_y(t) = \cos(\Omega_0 t)\mathbf{e}_y' + \sin(\Omega_0 t)\mathbf{e}_z'$ and $\mathbf{e}_z(t) = -\sin(\Omega_0 t)\mathbf{e}_y' + \cos(\Omega_0 t)\mathbf{e}_z'$ rotate together with the magnetic plate [see Fig. 1(b)]. In the co-movil system the normalized magnetic energy will be the same of Eq. (1); however, in the inertial frame the energy depends explicitly in time,

$$\frac{E'}{\mu_0 M_s^2} = -\mathbf{m}\cdot\mathbf{h_a'} - \frac{1}{2}\beta_x m_x'^2 + \frac{1}{2}\beta_{zz}'(t)m_z'^2$$
$$+ \frac{1}{2}\beta_{yy}'(t)m_y'^2 + \frac{1}{2}\beta_{yz}'(t)m_y'm_z', \qquad (4)$$

where the time varying coefficients $\beta_{zz}' = \beta_z[1 + \cos(2\Omega_0 t)]/2$, $\beta_{yy}' = \beta_z[1 - \cos(2\Omega_0 t)]/2$, and $\beta_{yz}' = -\beta_z\sin(2\Omega_0 t)$ act as a parametric forcing. Note that the frequency of the forcing is twice the frequency of the rotations. Therefore, this system presents a subharmonic parametric resonance [13].

The dynamics of the magnetic plane in the inertial frame S' is described by the Landau-Lifshitz-Gilbert equation

$$\left.\frac{d\mathbf{m}}{dt}\right|_{S'} = -\mathbf{m}\times\mathbf{h}_{\text{eff}}'(t) + \alpha\mathbf{m}\times\left.\frac{d\mathbf{m}}{dt}\right|_{S'}, \qquad (5)$$

where $\mathbf{h}_{\text{eff}}' = -(1/\mu_0 M_0^2)(\delta E'/\delta\mathbf{m})$. Let us now write the Eq. (5) in the noninertial frame S, where the time derivative operator in the rotating system takes the form $\partial_t|_{S'} = \partial_t|_S + \mathbf{\Omega}\times$ [13], thus the dynamics of the rotating magnetic plate in the noninertial frame S reads

$$\left.\frac{d\mathbf{m}}{dt}\right|_S = -\mathbf{m}\times\mathbf{h}_{\text{eff}} + \alpha\mathbf{m}\times\left.\frac{d\mathbf{m}}{dt}\right|_S$$
$$- \alpha\Omega_0\mathbf{m}\times(\mathbf{m}\times\mathbf{e}_x), \qquad (6)$$

where the effective field $\mathbf{h}_{\text{eff}}$ is the same of formula (3). Therefore, the dynamics of the rotating magnetic plate in the noninertial frame S, Eq. (6), is a time-independent equation, which is equivalent to the dynamics of a nanopillar under the effect of a spin-transfer torque generated by a uniform electric current, Eq. (2). In this equivalence, the intensity of the spin-transfer effect on the nanopillar g corresponds to the angular velocity by the dissipation parameter, $-\alpha\Omega_0$. Indeed, the two physical systems depicted in Fig. 1 are equivalent. In the next sections, we will apply the well-known understanding on parametric systems to the nano-oscillator.

Parametrically driven damped nonlinear Schrödinger equation

To obtain a simple model that permits analytical calculations around the parallel state, we use the following stereographic representation [28]:

$$\psi(\mathbf{r},t) = \frac{m_y + i m_z}{1 + m_x}, \tag{7}$$

where ψ is a complex field. This representation corresponds to consider an equatorial plane intersecting the magnetization unit sphere. The magnetization components are related with the complex field by $m_x = (1 - |\psi|^2)/(1 + |\psi|^2)$, $m_y = (\psi + \bar{\psi})/(1 + |\psi|^2)$, and $m_z = (i(\bar{\psi} - \psi))/(1 + |\psi|^2)$, where $\bar{\psi}$ stands for the complex conjugate of ψ. Notice that the parallel state $\mathbf{m} = \mathbf{e}_x$ is mapped to the origin of the ψ plane. The LLG, Eq. (2) or Eq. (6), takes the following form:

$$(i + \alpha)\frac{d\psi}{dt} = (ig - h_a)\,\psi - \frac{\beta_z}{2}(\psi - \overline{\psi})\frac{1 + \psi^2}{1 + |\psi|^2}$$
$$- \beta_x \psi \frac{1 - |\psi|^2}{1 + |\psi|^2}. \tag{8}$$

This is a complex Ginzburg-Landau-type equation, which describes the envelope of a nonlinear dissipative oscillator.

An advantage of the stereographic representation is to guarantee the magnetization normalization and to consider the appropriate degrees of freedom. Notice that the switching dynamic between parallel and antiparallel state is not well described, since the antiparallel state is represented by infinity [28]. This kind of dynamics is not considered in the present work. To grasp the dynamical behavior exhibited by the previous model, let us consider that the complex amplitude is small and that the parameters $\alpha, \beta_z/2$ are also small. Introducing the renormalized amplitude $A(\mathbf{r},t) = \psi(\mathbf{r},t)e^{i\pi/4}\sqrt{2\beta_x + \beta_z}$, after straightforward calculations, Eq. (8) is approximated at dominant order by

$$\frac{dA}{dt} = -i\nu A - i|A|^2 A - \mu A + \gamma \bar{A}, \tag{9}$$

where $\mu \equiv -g - \alpha\nu$, $\nu \equiv -h_a - (\beta_x + \beta_z/2)$, and $\gamma \equiv \beta_z/2$. Thus under the above assumptions the nanopillar resonator is described by Eq. (9), which is known as the PDNLS equation without space. This model has been used to describe parametric resonators [13].

The coefficient γ is the intensity of the forcing in usual parametric systems. For instance, it is proportional to the amplitude of the oscillation in vibrated media or the intensity of time-dependent external fields. In the case of the nanopillar $\gamma = \beta_z/2$ is not a control parameter. In the context of the PDNLS amplitude equation γ breaks the phase invariance, i.e., $A \nrightarrow Ae^{i\phi_0}$. A change of variables of the form $A = Be^{i\omega t}$ (rotating frame) permits us to restore the explicit time-dependent forcing,

$$\frac{dB}{dt} = -i(\nu + \omega)B - i|B|^2 B - \mu B + \gamma e^{-2i\omega t}\bar{B}. \tag{10}$$

Moreover, in this representation the parametric nature of the PDNLS equation is evident. The parameter $\mu > 0$ accounts for dissipation in parametric systems and it models radiation, viscosity, and friction, depending on the particular physical
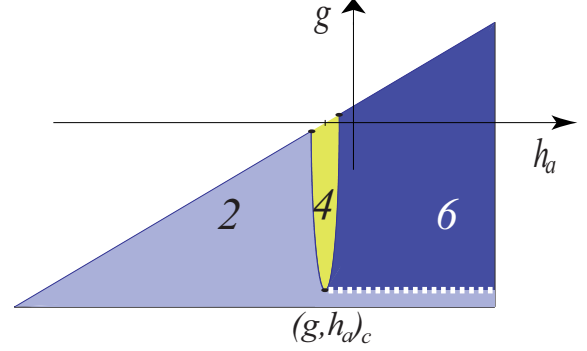

FIG. 2. (Color online) Bifurcation diagram of the parallel state $\mathbf{m} = \mathbf{e}_x$, in the dark zone $\mathbf{m} = \mathbf{e}_x$, is stable. The elliptical-like light zone delimited by $g^2 + [h_a - (\beta_x + \beta_z/2)]^2 = \beta_z^2/4$ is known as Arnold's tongue. In this region there are four equilibria and the parallel state is unstable. On the left of Arnold's tongue and above the segmented curve $g = -\beta_z/2$ there are six equilibria.

context. In our case, this dissipation is the combination of the Gilbert damping and the spin-polarized current. Finally, the detuning ν accounts for the deviation from a half of the forcing frequency. In the case of the nanopillar, ν is controlled by the external field.

To obtain Eq. (9) we have assumed that $\alpha, \beta_z/2 \ll 1$ and that the amplitude is a slowly varying amplitude ($|A| \ll 1$), that is, we have the scaling $|A|^2 \sim \nu \sim \mu \sim \gamma \sim \partial_t \ll 1$. Notwithstanding, the model, Eq. (9), is qualitatively valid outside this limit.

The parallel state $A = 0$ is always a solution of Eq. (9). Decomposing the amplitude into its real and imaginary parts $A(t) = u(t) + iv(t)$ and linearizing around them, we have

$$\frac{d}{dt}\begin{pmatrix} u \\ v \end{pmatrix} = \begin{bmatrix} \gamma - \mu & \nu \\ -\nu & -(\gamma + \mu) \end{bmatrix}\begin{pmatrix} u \\ v \end{pmatrix}. \tag{11}$$

Imposing a solution of the form $(u,v) \sim e^{\lambda_{\pm}t}(u_0,v_0)$, we obtain the growth rate relation $\lambda_{\pm} = -\mu \pm \sqrt{\gamma^2 - \nu^2}$. The stability condition, which corresponds to $\text{Re}e(\lambda_{\pm}) < 0$ is shown in dark areas in Fig. 2. The elliptical-like light zone of Fig. 2 is known as Arnold's tongue in the context of parametric systems, and it accounts for the destabilization of the parallel state for $\mu^2 + \nu^2 = \gamma^2$. The exact curve of the Arnold's tongue in terms of the original parameters can be obtain from the LLG equation without neglecting α, that is, $g^2 + [h_a - (\beta_x + \beta_z/2)]^2 = \beta_z^2/4$. Inside the Arnold's tongue this model has also the equilibria

$$A_{\pm} = \pm \left(1 - i\sqrt{\frac{\gamma - \mu}{\gamma + \mu}}\right)\sqrt{\frac{\gamma + \mu}{2\gamma}(\sqrt{\gamma^2 - \mu^2} - \nu)}. \tag{12}$$

In this region there are four equilibria (see Fig. 2); they are the parallel state $A = 0$ (equivalently $\mathbf{m} = \mathbf{e}_x$), the antiparallel state ($\mathbf{m} = -\mathbf{e}_x$) and $A_{\pm}$. Crossing the curve of the Arnold's tongue for positive detuning $\sqrt{\gamma^2 - \mu^2} = \nu > 0$, the $A_{\pm}$ states and $A = 0$ collide together through a pitchfork bifurcation. For greater values of the detuning parameter ν, only the parallel and antiparallel states exist.

For negative detuning and $\gamma > \mu$ (above the dashed curve in Fig. 2), and outside Arnold's tongue $\sqrt{\gamma^2 - \mu^2} < |\nu|$, the $A_\pm$ states exist and are stable. Since the $A = 0$ equilibrium is also stable in this region, it is necessary to have other two states $A'_\pm$ that separate them in the phases space which have the form

$$A'_\pm = \pm\left(1 + i\sqrt{\frac{\gamma - \mu}{\gamma + \mu}}\right)\sqrt{\frac{\gamma + \mu}{2\gamma}(-\sqrt{\gamma^2 - \mu^2} - \nu)}. \quad (13)$$

In this region (the darkened area in Fig. 2), there are six equilibria. Thus the PDNLS equation describes the homogeneous stationary solutions which have been studied the context of the nano-oscillator [20,29].

When $g \leq -\alpha\nu$ the coefficient that rules the dissipation becomes negative, and the magnetization oscillates and moves away from the parallel state. This instability is known as the Andronov-Hopf bifurcation [30]. When it does not saturate the magnetization switches to the antiparallel state or reaches another stationary equilibrium. Precessions or self-oscillations emerge when this instability saturates. In the past, this regime has been extensively studied experimentally and theoretically in the context of the spin-transfer torque resonator [8,10,12]. This instability does not occur in usual parametric systems since the dissipation coefficient is always positive $\mu > 0$.

In brief, the nanopillars driven by a spin-transfer torque effect are equivalent to parametric systems, and then they are well described by the paradigmatic model for parametric systems, the PDNLS equation without space. We will see in the next section the predictions of this model for the nanopillar in the case of a variable magnetization.

IV. GENERALIZATION TO AN INHOMOGENEOUS MAGNETIZATION DYNAMICS

The macrospin approximation permits us to understand several features of the magnetization dynamics driven with spin torque, but, even so, this approximation is not completely valid because in general both the precession and magnetic reversal are inhomogeneous [31]. There are several approaches to study the nonuniform magnetization dynamics; nevertheless, we use here a minimal model with a ferromagnetic exchange torque as the dominant space-dependent coupling in order to understand the emergence of a rich spatiotemporal dynamics.

In the case of an inhomogeneous magnetization $\mathbf{m}(\mathbf{r},t)$, which corresponds to a spatial extension of the nano-oscillator, the magnetic energy $E = \mu_0 M_s^2 \int \epsilon \, dx \, dy$ of the free layer is the integral of the following dimensionless density of energy [20]:

$$\epsilon = -\mathbf{m} \cdot \mathbf{h_a} - \tfrac{1}{2}\beta_x m_x^2 + \tfrac{1}{2}\beta_z m_z^2 + \tfrac{1}{2}|\nabla\mathbf{m}|^2, \quad (14)$$

where $\{x, y\}$ stands for the spatial coordinates of the free layer. The spatial coordinates have been dimensionless $\mathbf{r} \rightarrow l_{\text{ex}}\mathbf{r}$ in terms of the *exchange length* $l_{\text{ex}} \equiv \sqrt{2A/(\mu_0 M_s^2)}$, where A is the exchange coupling in the ferromagnet. The gradient operator is defined on the plane of the film as $\nabla \equiv \mathbf{e}_x\partial_x + \mathbf{e}_y\partial_y$. The β_x and β_z coefficients account for both the easy axis and the demagnetization in the thin-film approximation [20]. In this approximation, the contribution of the demagnetization effect to the magnetic energy density is local, and the shape of

the thin film is taken into account by the Neumann boundary condition for the magnetization.

The LLG equation and the effective field are

$$\frac{\partial\mathbf{m}}{\partial t} = -\mathbf{m}\times\mathbf{h}_{\text{eff}} + \alpha\mathbf{m}\times\frac{\partial\mathbf{m}}{\partial t} + g\ \mathbf{m}\times(\mathbf{m}\times\mathbf{e_x}), \quad (15)$$

$$\mathbf{h}_{\text{eff}} \equiv -\frac{1}{\mu_0 M_s^2}\frac{\delta E}{\delta\mathbf{m}} = (h_a + \beta_x m_x)\mathbf{e}_x - \beta_z m_z\mathbf{e}_z + \nabla^2\mathbf{m}. \quad (16)$$

Notice that gradients come from the ferromagnetic exchange energy, and then the spatial derivatives must be written in terms of the coordinates that label the sample, even if it rotates. Then the equation of the magnetization of the rotating plate in its co-movil frame is Eq. (6) with an extra term for the spatial dependence,

$$\frac{\partial\mathbf{m}}{\partial t}\bigg|_S = -\mathbf{m}\times\mathbf{h}_{\text{eff}} + \alpha\mathbf{m}\times\frac{\partial\mathbf{m}}{\partial t}\bigg|_S$$
$$- \alpha\Omega_0\mathbf{m}\times(\mathbf{m}\times\mathbf{e}_x), \quad (17)$$

where $\mathbf{h}_{\text{eff}} = (h_a + \beta_x m_x)\mathbf{e}_x - \beta_z m_z\mathbf{e}_z + \nabla^2\mathbf{m}$ and the $\nabla \equiv \mathbf{e}_x\partial_x + \mathbf{e}_y\partial_y$ operator is defined on the co-movil plane spanned by $(\mathbf{e}_x, \mathbf{e}_y)$. Thus the spatial dependence of $\mathbf{m}$ does not change the equivalence between the nanopillar and the rotating magnet presented in Sec. III. Using the same change of variable of Eq. (7), the LLG Eq. (15) reads

$$(i + \alpha)\partial_T\psi = (ig - h_a)\psi - \frac{\beta_z}{2}(\psi - \overline{\psi})\frac{1 + \psi^2}{1 + |\psi|^2}$$
$$- \beta_x\psi\frac{1 - |\psi|^2}{1 + |\psi|^2} + \nabla^2\psi - 2\frac{\overline{\psi}}{1 + |\psi|^2}(\nabla\psi)^2, \quad (18)$$

which describes the envelope of coupled nonlinear oscillators. Due to the complexity of this equation, we will consider a simple limit, which permits us to grasp its dynamics. Using the small amplitude that varies slowly in space $A(\mathbf{r},t) = \psi(\mathbf{r},t)e^{i\pi/4}\sqrt{2\beta_x + \beta_z}$, we obtain

$$\partial_\tau A = -i\nu A - i|A|^2 A - i\nabla^2 A - \mu A + \gamma\bar{A}, \quad (19)$$

which is the PDNLS model. The extra term with spatial derivatives describes dispersion.

Parametric textures for nanopillars

The above model, Eq. (19) has been extensively used to study the pattern formation; in particularly, this model exhibits solitons, oscillons, periodic textures, and complex behaviors, among others. To verify these predictions, we compare them with the numerical solutions of Eq. (2) in two geometrical configurations. The first is a one-dimensional free layer, that is, a nanopillar for which $\mathbf{m}(\mathbf{r},t) \approx \mathbf{m}(x,t)$, and the second is a two-dimensional nanopillar with a square cross section. Different transversal lengths are used in simulations, all of them displaying the same qualitative aspects of the solutions. The simulations are conducted using a fifth-order Runge-Kutta algorithm with a constant step size for time integration and finite differences for spatial discretization. The spatial differential operators are approximated with centered schemes

of order 6 and specular (Neumann) boundary conditions are used.

1. Dissipative solitons

Analytical solutions for the dissipative soliton are known in one dimension [18,19,32]. In two dimensions dissipative solitons are observed, however, without analytical expressions. From this result and using the stereographic change of variable, we find the following analytical form for magnetic dissipative solitons in one dimension:

$$m_x = \frac{2\beta_x + \beta_z - R(x)^2}{2\beta_x + \beta_z + R(x)^2},$$

$$\begin{pmatrix} m_y \\ m_z \end{pmatrix} = \frac{2R(x)\sqrt{2\beta_x + \beta_z}}{2\beta_x + \beta_z + R(x)^2} \begin{pmatrix} \cos\varphi_0 \\ \sin\varphi_0 \end{pmatrix}, \tag{20}$$

with $\sin(2\varphi_0) \equiv 2g/\beta_z$, $R \equiv \sqrt{2\delta}\,\mathrm{sech}[\sqrt{\delta}(x - x_0)]$, and $\delta \equiv h_a + \beta_x + \beta_z/2 + \sqrt{(\beta_z/2)^2 - g^2}$. The width of the soliton is controlled by the external field. The typical sizes are about $10 l_{\mathrm{ex}}$.

Figures 3(a) shows the analytical results compared with numerical simulations of the LLG equation, which presents a quite good agreement for small amplitude solitons, i.e., for $\delta \ll 1$. Furthermore, Fig. 3(b) illustrates the dissipative solitons observed numerically in two dimensions. We note that these solitons are well described by a hyperbolic secant function, which was obtained using variational methods [33].

Dissipative solitons are observed in the region of parameter space bounded by $\beta_z^2/2 - (|h_a| - (\beta_x + \beta_z/2))^2 = g^2$ and $\beta_z/2 = |g|$. This region is analytically inferred from the amplitude Eq. (19). Figure 4 shows the respective phase
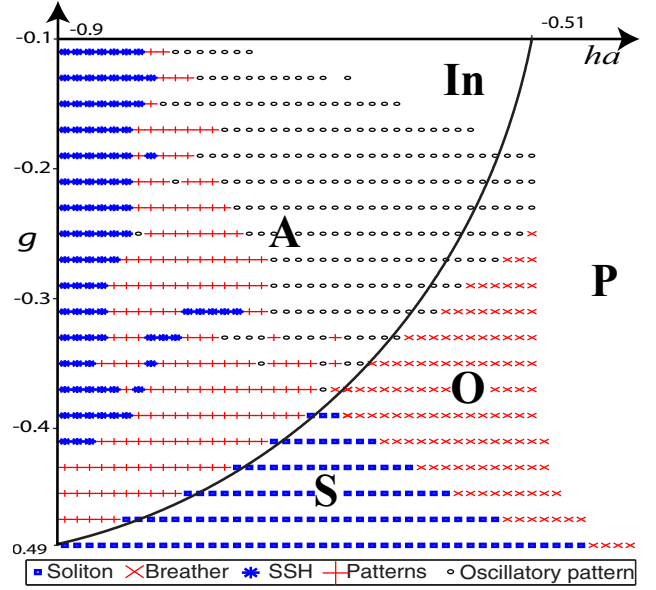

FIG. 4. (Color online) Phase diagram of LLG model, Eq. (2). "S-region" represents solitons region, "O-region" stands for breather solitons (oscillons) region, and "A-region" is the Arnold's tongue. The In-region accounts for inhomogeneous dynamical states far from the parallel configuration. In the zone P, only the parallel state is observed.

diagram of the LLG equation, and the region of dissipative solitons is denoted by "S-region."

Increasing the difference between injection and dissipation, $\gamma - \mu$, dissipative solitons undergo an Andronov-Hopf bifurcation, generating oscillatory localized states or breather solitons characterized by exhibiting shoulders in the amplitude profile [34]. Figure 5 illustrates this kind of solution. Similar solutions have also been reported in a magnetic wire forced by a transversal uniform and oscillatory magnetic field [35],

FIG. 3. (Color online) Dissipative solitons in one- and two-dimensional nanopillars (with a square cross section) with $\beta_x = 0.5$, $\beta_z = 1$, and $\alpha = 0.05$. (a) One-dimensional soliton for $g = -0.4999$, $h_a = -0.97$; the points account for the numerical integration of the LLG equation and the line accounts for the analytical solution given by Eq. (20). (b) Soliton in two-dimensions, $g = -0.49995$, $h_a = -0.99$; the three-dimensional plot shows the profile of the component m_y, while the insets show the m_x and the m_z components.
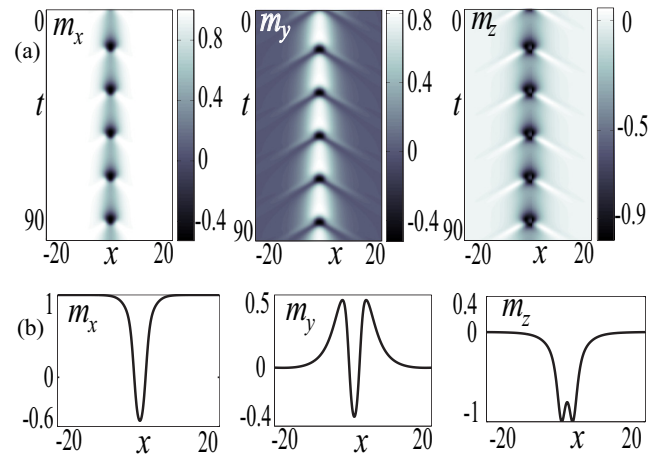

FIG. 5. (Color online) Breather or oscillon solution for $g = -0.33$, $h_a = -0.51$. (a) The spatiotemporal diagram. (b) The magnetization components at the time for which m_x reaches its minimal position. Typical oscillation periods are about $\Delta t \approx 16(\gamma M_s)^{-1}$, which is about $\Delta t \approx 51$ ps for a 3-nm-thick cobalt free layer.
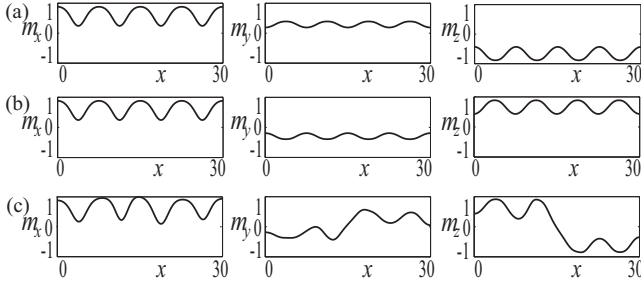
FIG. 6. Dissipative structures for $g = -0.37$, $h_a = -0.75$, inside the Arnold's tongue. [(a) and (b)] Pattern states. (c) Kink solution, this domain wall is a slowly moving front connecting the (a) and (b) patterns.

which corresponds to a parametric system. These oscillatory solutions are observed in the O-region of the bifurcation diagram shown in Fig. 4. Notice that, for spin-transfer torques that favor the parallel state, the nanopillar can also behave as a nano-oscillator.

2. Pattern states

Let us introduce the A-region of the bifurcation diagram (cf. Fig. 4), which is circumscribed by the curve $\beta_z^2/2 - [|h_a| - (\beta_x + \beta_z/2)]^2 = g^2$ in the Arnold's tongue. Inside this region the quiescent state $A = 0$ is unstable, giving rise to a nonzero uniform state and stationary and oscillatory patterns. Figures 6(a) and 6(b) show stable stationary patterns that exist inside the Arnold's tongue, and Fig. 6(c) shows a propagative wall that connects the patterns. In addition, the PDNLS model is characterized by exhibiting supercritical patterns at $\gamma = \mu$ ($\beta_z/2 = |g|$), growing with a power law $1/4$ as a function of the bifurcation parameter [36]. Recently, such dissipative structures induced by spin-transfer torques in nanopillars have been characterized numerically and theoretically [37], where the spatial textures emerge from a spatial supercritical quintic bifurcation. In one spatial dimension, the magnetic patterns read at dominant order by

$$\begin{pmatrix} m_y \\ m_z \end{pmatrix} \approx 2 \left[\frac{4\beta_z(g - g_c)}{(6\beta_x + 3\beta_z - 2k_c^2)^2} \right]^{1/4} \begin{pmatrix} \cos(k_c x) \\ -\cos(k_c x) \end{pmatrix}, \quad (21)$$

and $m_x \approx 1 - (m_y^2 + m_z^2)/2$. Figure 7 shows a pattern solution. The wavelength of the periodic structures, $2\pi/k_c = 2\pi/\sqrt{-h_a - \beta_x - \beta_z}$, is controlled by the external field $h_a < 0$. In two spatial dimensions the system shows the emergence of stripe patterns or superlattices at the onset of bifurcation [37]. The phases diagram of the textures is controlled by a single parameter that accounts for the competition between the external magnetic field, anisotropy, exchange, and the critical spin-polarized current. When the anisotropy is dominant over the external field the system exhibits striped patterns [Fig. 7(b)]; however, when the external field drives the dynamics, the system presents superlattice [Figs. 7(c) and 7(d)] as stable equilibria. Indeed, external fields pointing against the near parallel states favor the formation of more sophisticated spatial textures. Since the electric resistance $R[\mathbf{M}_0 \cdot \mathbf{m}]$ of the nanopillar depends on the relative orientation [31] of the fixed $\mathbf{M}_0$ and free $\mathbf{m}$ layers, and $\mathbf{M}_0 \cdot \mathbf{m} = m_x \approx 1 - (m_y^2 + m_z^2)/2$
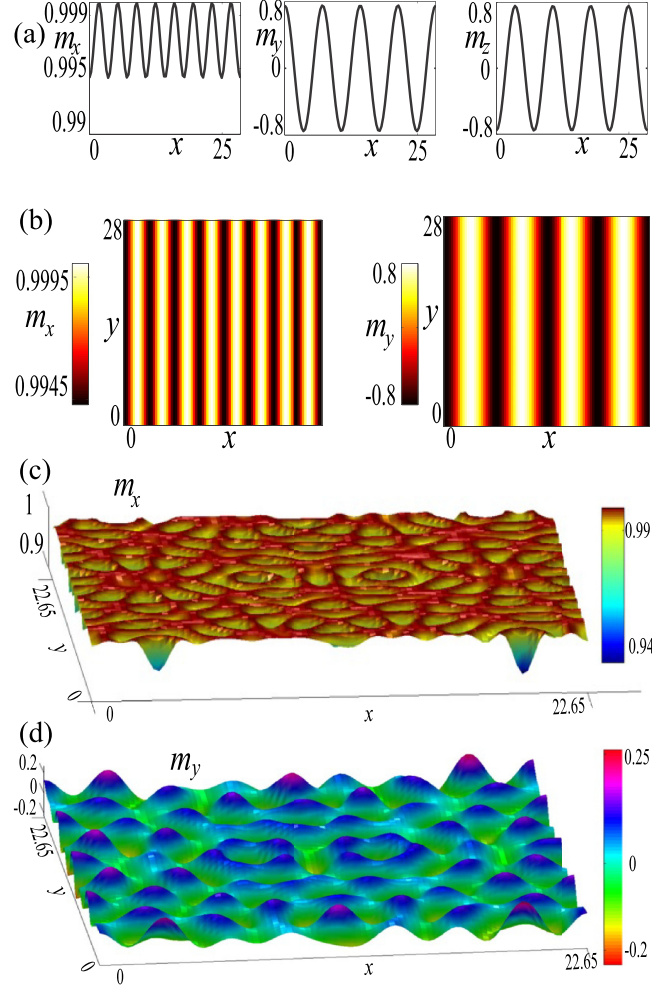

FIG. 7. (Color online) Patterns induced by the spin-polarized current. (a) One-dimensional state for $g = -0.49999$, $h_a = -1.8$, as predicted by Eq. (21), $m_y \approx -m_z$. Notice that the norm conservation implies that $m_x \approx 1 - 0.5(m_y^2 + m_z^2)$ oscillates with a half of the wavelength of the other two components. (b) Bidimensional pattern for the same parameters used in (a), and the component m_z (not shown) is the negative of m_y. (c) The magnetization component m_x for a superlattice pattern obtained with $g = -0.4999$, and $h_a = -6$. (d) The component m_y of the state of (c); the component $m_z \approx -m_y$.

the signature of the patterns is a time-independent resistance that increases a square root of the current $R = R_p + \eta(g - g_c)^{1/2}$ when g is negative and goes to zero. The parameter η contains all the information of the applied field, anisotropies, and geometry.

Notice that according to the PDNLS model, Eq. (9) and Eq. (19), the parametric resonance occurs when $\nu \approx 0$ and $\gamma \approx \mu$ or, equivalently, $(g, h_a)_c = -(\beta_z/2, \beta_x + \beta_z/2)$. For a 3-nm-thick material with saturation magnetization similar to cobalt [20], that is, $M_s \simeq 1.4 \times 10^6$ A/m, the critical current density is $J_c = J(g_c) \approx -\beta_z \times 10^9$ A/cm^{-2} for a constant $\mathcal{P}(m_x) \approx 1$ polarization function. Since localized states and patterns appear for currents that are fractions of the critical current $|J| \sim 3|J_c|/5$, the smaller the β_z parameters is, the smaller the spin-polarized currents required to observe the parametric phenomenology. Most of our results use $\beta_x = 1/2$ and $\beta_z = 1$;

nevertheless, we have conducted numerical simulations for different values of β_z for β_x in order to achieve the parametric resonance at arbitrary small currents, and the predictions of Eqs. (9) and (19) remain unchanged. The robustness of this parametric phenomenology is a characteristic of systems near their parametric resonance.

V. CONCLUSIONS AND REMARKS

We have shown that nanopillars under the effect of a direct electric current are equivalent to simple rotating magnetic plates. The latter system is characterized by displaying a parametric instability. This equivalence permits us to transfer the known results of the self-organization of parametric

systems to the magnetization dynamics induced by the spin-transfer torque effect. In particular, we have shown that for spin-polarized currents that favor the parallel state the system is governed by the PNDLS equation, and then the magnetization exhibits localized states and patterns both in one and two spatial dimensions. Numerical simulations show a quite good agreement with the analytical predictions.

[1] *Concepts in Spin Electronics*, edited by S. Maekawa (Oxford University Press, Oxford, 2006).

[2] J. C. Slonczewski, J. Magn. Mater. Magn. **159**, L1 (1996).

[3] L. Berger, Phys. Rev. B **54**, 9353 (1996).

[4] M. Tsoi, A. G. M. Jansen, J. Bass, W. C. Chiang, M. Seck, V. Tsoi, and P. Wyder, Phys. Rev. Lett. **80**, 4281 (1998).

[5] J. Z. Sun, J. Magn. Magn. Mater. **202**, 157 (1999).

[6] E. B. Myers, D. C. Ralph, J. A. Katine, R. N. Louie, and R. A. Buhrman, Science **285**, 867 (1999).

[7] J. A. Katine, F. J. Albert, R. A. Buhrman, E. B. Myers, and D. C. Ralph, Phys. Rev. Lett. **84**, 3149 (2000).

[8] S. I. Kiselev, J. C. Sankey, I. N. Krivorotov, N. C. Emley, R. J. Schoelkopf, R. A. Buhrman, and D. C. Ralph, Nature (London) **425**, 380 (2003).

[9] S. I. Kiselev, J. C. Sankey, I. N. Krivorotov, N. C. Emley, A. G. F. Garcia, R. A. Buhrman, and D. C. Ralph, Phys. Rev. B **72**, 064430 (2005).

[10] D. C. Ralph and M. D. Stiles, J. Magn. Magn. Mater. **320**, 1190 (2008).

[11] D. V. Berkov and J. Miltat, J. Magn. Magn. Mater. **320**, 1238 (2008).

[12] A. Slavin and V. Tiberkevich, IEEE Trans. Magn. **45**, 1875 (2009).

[13] L. D. Landau and E. M. Lifshiftz, *Mechanics*, Course of Theoretical Physics (Pergamon Press, Oxford, 1976), Vol. 1.

[14] J. W. Miles, J. Fluid Mech. **148**, 451 (1984); W. Zhang and J. Viñals, Phys. Rev. Lett. **74**, 690 (1995); X. Wang and R. Wei, Phys. Rev. E **57**, 2405 (1998); M. G. Clerc, S. Coulibaly, N. Mujica, R. Navarro, and T. Sauma, Phil. Trans. R. Soc. A **367**, 3213 (2009).

[15] B. Denardo, B. Galvin, A. Greenfield, A. Larraza, S. Putterman, and W. Wright, Phys. Rev. Lett. **68**, 1730 (1992).

[16] J. N. Kutz, W. L. Kath, R.-D. Li, and P. Kumar, Opt. Lett. **18**, 802 (1993).

[17] S. Longhi, Phys. Rev. E **53**, 5520 (1996).

[18] I. V. Barashenkov, M. M. Bogdan, and V. I. Korobov, Europhys. Lett. **15**, 113 (1991).

[19] M. G. Clerc, S. Coulibaly, and D. Laroze, Phys. Rev. E **77**, 056209 (2008); Int. J. Bifurcat. Chaos **19**, 3525 (2009); Physica D **239**, 72 (2010); Europhys. Lett. **97**, 30006 (2012).

[20] I. D. Mayergoyz, G. Bertotti, and C. Serpico, *Nonlinear Magnetization Dynamics in Nanosystems* (Elsevier, Oxford, 2009).

[21] J. Z. Sun, Phys. Rev. B **62**, 570 (2000); X. Waintal, E. B. Myers, P. W. Brouwer, and D. C. Ralph, *ibid.* **62**, 12317 (2000); M. D. Stiles and A. Zangwill, *ibid.* **66**, 014407 (2002).

[22] J. C. Slonczewski, J. Magn. Mater. Magn. **247**, 324 (2002).

[23] J. Xiao, A. Zangwill, and M. D. Stiles, Phys. Rev. B **70**, 172405 (2004).

[24] J. Xiao, A. Zangwill, and M. D. Stiles, Phys. Rev. B **72**, 014446 (2005).

[25] J. Barnas, A. Fert, M. Gmitra, I. Weymann, and V. K. Dugaev, Phys. Rev. B **72**, 024426 (2005).

[26] S.-W. Lee and K.-J. Lee, IEEE Trans. Magn. **46**, 2349 (2010).

[27] W. Kim, S.-W. Lee, and K.-J. Lee, J. Phys. D **44**, 384001 (2011).

[28] M. Lakshmanan, Phil. Trans. R. Soc. A **369**, 1280 (2011).

[29] Z. Li and S. Zhang, Phys. Rev. B **68**, 024404 (2003).

[30] A. A. Andronov and S. E. Khajkin, *Theory of Oscillations* (Dover, London, 1987).

[31] K. J. Lee, A. Deac, O. Redon, J. P. Nozieres, and B. Dieny, Nat. Mater. **3**, 877 (2004).

[32] M. G. Clerc, S. Coulibaly, M. A. Garcia-Nustes, and Y. Zarate, Phys. Rev. Lett. **107**, 254102 (2011).

[33] D. Anderson, M. Bonnedal, and M. Lisak, Phys. Fluids **22**, 1838 (1979).

[34] I. V. Barashenkov and E. V. Zemlyanaya, Phys. Rev. E **83**, 056610 (2011).

[35] D. Urzagasti, D. Laroze, M. G. Clerc, and H. Pleiner, Europhys. Lett. **104**, 40001 (2013).

[36] P. Coullet, T. Frisch, and G. Sonnino, Phys. Rev. E **49**, 2087 (1994).

[37] A. O. León, M. G. Clerc, and S. Coulibaly, Phys. Rev. E **89**, 022908 (2014).

Apéndice C

Alternating spin-polarized current induces parametric resonance in spin valves

This chapter presents the magnetization dynamics induced by a time-varying spin-transfer torque.

Publication details:

Title: Alternating spin-polarized current induces parametric resonance in spin valves.

Authors: Marcel G. Clerc, Saliya Coulibaly, David Laroze, Alejandro O. León, and Álvaro Núñez.

Corresponding author: Marcel G. Clerc.

Alternating spin-polarized current induces parametric resonance in spin valves

Marcel G. Clerc,[1] Saliya Coulibaly,[2] David Laroze,[3,4] Alejandro O. León,[1] and Álvaro S. Núñez[1]

[1]*Departamento de Física, Facultad de Ciencias Físicas y Matemáticas, Universidad de Chile, Casilla 487-3, Santiago, Chile*
[2]*Laboratoire de Physique des Lasers, Atomes et Molécules, Centre National de la Recherche Scientifique, Unités Mixtes de Recherche 8523, Université des Sciences et Technologies de Lille, 59655 Villeneuve d'Ascq Cedex, France*
[3]*Instituto de Alta de Investigación, Universidad de Tarapacá, Casilla 7D, Arica, Chile*
[4]*SUPA School of Physics and Astronomy, University of Glasgow, Glasgow G12 8QQ, Scotland, United Kingdom*

Ferromagnetic systems under the influence of spin-polarized currents exhibit rich spatiotemporal dynamics at nanoscales. We study spin-transfer nano-oscillators driven by the combination of alternating and direct spin-polarized electric currents. We show here that the alternating current induces parametric instabilities on spin valves, that is, the magnetization responses at half the forcing frequency. A spatial self-organization emerges as a result of the oscillatory current, which includes dissipative solitons and Faraday-type waves. The parametric regime is described analytically by means of the Landau-Lifshitz-Gilbert-Slonczewski equation, in good agreement with micromagnetic simulations including the full dipolar field.

I. INTRODUCTION

Control of magnetization in spin valves has been the subject of intense research in recent years [1–4]. In such devices, a perpendicular to plane electric current transfers spin angular momentum from one ferromagnetic film into another one. This effect is known as the spin-transfer torque [1,5,6], and it can generate magnetic switching or reversals, and stable oscillatory states in the radio-frequency domain. Furthermore, the addition of an alternating electric current, in the radio-frequency domain, affects the reversal threshold through a frequency locking mechanism. The injection of combined radio-frequency and direct electric currents induces other dynamical responses, such as synchronization, chaos [7], and stochastic resonance [8].

Although the first predictions on current-induced dynamics were made assuming a uniform magnetization (the macrospin model), it is known that usually both switching and precessional motions are nonuniform [9,10]. Moreover, a direct spin-polarized electric current can induce static spatially periodic textures in magnetic films [11,12]. Vortices are a classical example of localized magnetization states [13]. In general, vortex stability is related to the geometrical properties of the sample [14]. A spatial distribution of the applied current can also modify the magnetic states. For example, the case of metallic point contact, in which the current is applied through a small metallic cross section in contact with a continuous magnetic film, exhibits nonuniform magnetization states [15]. In addition, magnetic solitonic modes in nano-oscillators have been observed [16–18]. Recently, dissipative magnetic droplet solitons were experimentally found and studied [19], after they were theoretically predicted in Ref. [20].

The study of spatially self-organized structures is beyond the specific case of magnetization dynamics; moreover, it is a widespread topic in nonlinear science [21–30]. Among the large variety of patterns generated by out-of-equilibrium nonlinear systems, dissipative localized structures [21,22,29] have always been of great interest and extensively studied for their potential applications. In the context of spin transfer, localized states can be of great advantage, since the energy localization that they produce is independent of the geometrical

properties of the system. Usually the existence of localized structures is related to a subcritical bifurcation [31]. This is, for example, the case of parametrically driven systems [29]. Parametric driving occurs when energy or momentum is injected in a system by means of a temporal modulation of one or more parameters. Hence, resonance can produce a response frequency different from the forcing frequency. The best known case is the 2:1 resonance phenomenon, where the driving frequency is close to twice the natural frequency of the system [32]. Parametric excitation of localized states arises in a wide range of physical systems. Examples include vertically oscillating layers of water, nonlinear lattices, optical fibers, Kerr-type optical parametric oscillators, the magnetization in an easy-plane ferromagnet exposed to an oscillatory magnetic field, and a parametrically driven damped chain of pendula. In most cases parametric forcing is made by modulating one of those parameters on which the natural frequency of the system depends.

In the context of spin-transfer nano-oscillators, current-induced parametric excitations were recently observed in point-contact spin-valve nanodevices [33,34]. Point contacts inject direct and microwave currents into spin valves, thus generating oscillating spin-transfer and Oersted-field torques on magnetic moments. Both effects contribute to the parametrically excited dynamics. This inhomogeneous forcing induces a fixed vortex. As a result of inhomogeneous forcing, the dynamics of these systems corresponds to nonextended parametric systems.

In this paper, we demonstrate theoretically and numerically that a uniform alternating spin-polarized electric current can produce parametric excitation in spin-valve devices. Figure 1 shows the typical dynamical response under parametric injection, in which the magnetization oscillates at half the forcing frequency. A parametrically induced resonance occurs when the self-oscillation induced by the direct current couples with the alternating current oscillation. A minimal model describing the dynamics of the magnetization at the onset of this resonance is given. We also show that such parametrically driven spin-transfer nano-oscillators (PDSTNOs) generate self-organized magnetic structures such as dissipative solitons and Faraday-type waves. To verify the robustness of such
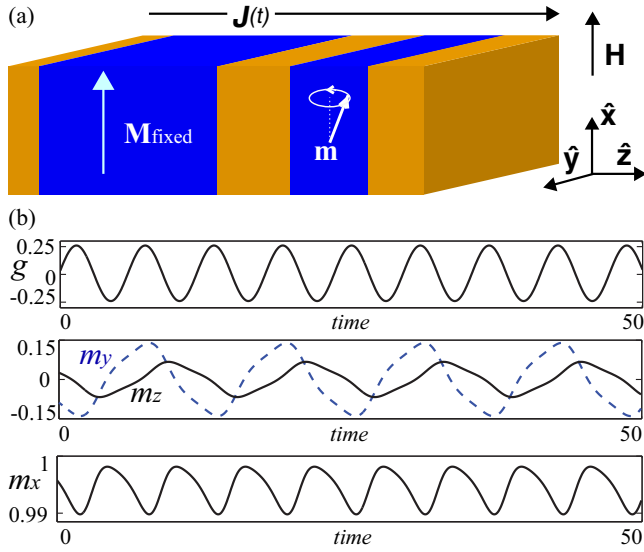
FIG. 1. (Color online) Schematic representation of the spin-transfer nano-oscillator device and typical subharmonic response. (a) A multilayer nanopillar with *free* magnetization **m**, and *fixed* magnetization along **M**$_{\text{fixed}}$. (b) Parametrically induced oscillation obtained from Eq. (1), where g is the dimensionless alternating current parameter; the dynamical variables m_y and m_z oscillate at half the frequency of the electric current, while the magnetization component $m_x \sim 1 - (m_y^2 + m_z^2)/2$ precesses at the forcing frequency.

states, we conduct micromagnetic simulations including the full dipolar field.

The paper is organized as follows. In Sec. II we investigate the effect of a time-dependent spin-polarized current under the approximation of a uniform magnetization. In Sec. III we extend our study to nonuniform magnetization dynamics. Finally, in Sec. IV we give our main conclusions and remarks.

II. PARAMETRICALLY DRIVEN SPIN-TRANSFER NANO-OSCILLATORS IN THE MACROSPIN APPROXIMATION

Let us consider a spin-valve or nanopillar device, composed by two ferromagnetic layers separated by a nonmagnetic conductor as depicted by Fig. 1(a). One magnetic film has a *fixed* magnetization along the positive $\hat{x}$ axis, while the uniform magnetization of the second magnet **M**(t) is variable or *free*. The free magnetization obeys the dimensionless Landau-Lifshitz-Gilbert-Slonczewski (LLGS) equation [5,35,37]:

$$\dot{\mathbf{m}} = -\mathbf{m} \times \mathbf{h}_{\text{eff}} + \alpha \mathbf{m} \times \dot{\mathbf{m}} + g\, \mathbf{m} \times (\mathbf{m} \times \hat{x}), \quad (1)$$

where $\mathbf{m} = \mathbf{M}/M_s$ is the normalized magnetization of the free layer, M_s is its saturation magnetization, and $\dot{\mathbf{m}}$ stands for the temporal derivative of $\mathbf{m}$. Within the macrospin approximation, the vector $\mathbf{m}(t)$ is uniform. The time is rendered dimensionless using M_s and the gyromagnetic constant γ, $t \to \gamma M_s t$. The first term of the right-hand side of Eq. (1) favors precessions around the effective field $\mathbf{h}_{\text{eff}}$:

$$\mathbf{h}_{\text{eff}} = (h_0 + \beta m_x)\hat{x} - m_z \hat{z}, \quad (2)$$

where β stands for the easy axis coefficient (in this case the x axis), and $h_0 = H_0/M_s$ is the normalized external magnetic

along the x axis. The last term of the effective field is the demagnetization field, and it disfavors configurations along the z axis. The second term of Eq. (1) accounts for the phenomenological Gilbert damping. The spin-transfer torque is modeled in Eq. (1) with the term proportional to g. The coefficient g is defined by

$$g = \frac{\hbar}{2|e|d} \frac{\mathcal{P}J}{\mu_0 M_s^2},$$

where $\mathcal{P}$ describes the electron polarization at the interface between the magnet and the spacer, J is the current density, $|e|$ is the modulus of the electric charge, and d is the thickness of the layer. In the spin-transfer theory of Slonczewski [5], the coefficient g is a function of the magnetization, $g = g(\mathbf{m} \cdot \hat{x})$. Let us focus on the small applied currents and small amplitude oscillations around the $\hat{x}$ axis; in this regime we can approximate $g(\mathbf{m} \cdot \hat{x}) \approx g(1)$; this approach is known as *sine approximation* [37].

In a linear regime the dynamics of the magnetization can be described by only one independent variable. Indeed, assuming $m_y^2 \sim m_z^2 \ll 1$, one obtains

$$m_z = \frac{1}{1+h}\left(\frac{\alpha g}{1+h} - 1\right)[\dot{m}_y + (\alpha h - g)m_y], \quad (3)$$

and

$$\ddot{m}_y = -\omega^2 m_y - 2\tilde{\mu}\dot{m}_y + \dot{g}m_y + \frac{\alpha \dot{g}}{1+h}\dot{m}_y, \quad (4)$$

with $h = h_0 + \beta$, $\omega^2 = (1 + \alpha^2)[h(1 + h) + g^2]$, and $\tilde{\mu} = \alpha(h + 1/2) - g$. Thus, the magnetization satisfies the equation of an oscillator.

In the case of a direct current ($g = g_0$), the stability analysis of Eq. (4) shows a stationary bifurcation at $(h + 1/2)^2 + g_0^2 - (1/2)^2 = 0$, and an Andronov-Hopf bifurcation at $\alpha(h + 1/2) - g_0 = 0$ [1,11]. The Andronov-Hopf instability is responsible for the self-oscillations in spin-transfer nano-oscillators. Let us consider a periodic time-dependent current injection. In the linear approximation, Eq. (4) is a *Mathieu-type equation* with a damping force. Such a model is commonly solved by means of the classical Floquet method [38], which allows the determination of the instability regions—Arnold tongues—in parameter space. Hence, parametric resonance occurs in regions where the motion of the system is unstable with respect to driving frequencies that are different from its natural frequency. In what follows we will focus on the case where the driving frequency is close to twice the natural frequency of the system. In this case, a modal decomposition method [39] has been used to solve Mathieu-type equations. More precisely, if we assume a spin-polarized current of the form $g(t) = g_0 + g_1 \sin(\omega t)$, the parametric instability region can be obtained using the following trial function (Galerkin expansion [40]):

$$m_y(t) = p_1^0 e^{i\frac{\omega}{2}t} + p_3^0 e^{i\frac{3\omega}{2}t} + \text{c.c.}, \quad (5)$$

where the coefficients $p_{1,3}^0$ are constants and the symbol c.c. means complex conjugate. Introducing the ansatz (5) into Eq. (4), we find the following solvability condition for nonzero coefficients p_1^0 and p_3^0:

$$|a|\Lambda|^2 + Lg_1^2|^2 - b^2|\Lambda|^4 g_1^2 = 0, \quad (6)$$
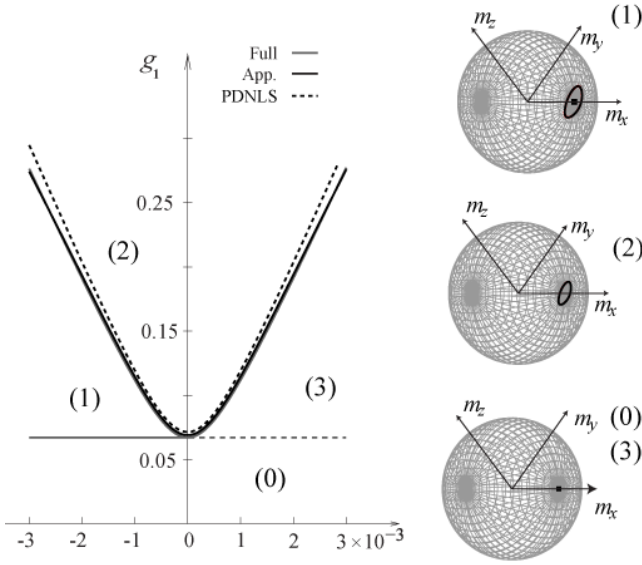
FIG. 2. (Color online) Bifurcation diagram (left) and phase portraits (right) of the parametric resonance in the macrospin limit. The parameters are $h_0 = 0.2$, $\beta = 0.05$, $g_0 = 0.018$, $\alpha = 0.025$, and $g_1 = 0.2$. The detuning parameters are $\nu = -0.005$ in region (1), -0.0005 in region (2), and 0.05 in region (3). The solid line (red curve) is given by the full equation using a trial function up to the fifth harmonic and can be considered as the exact limit in the quasireversible case. The solid black line is obtained from Eq. (6), while the black dashed line comes from the amplitude equation (8). The dashed red line gives the transition to the Faraday instability and may be taken into account only in the micromagnetic limit.

where $L = (|c|^2 - i\,\mathrm{Re}(c)b - b^2)\bar{\Lambda} - \mathrm{Re}(\Lambda)a - |\Lambda|^2/2$. Here we have set $\omega_0^2 \simeq (1 + \alpha^2)[h(h + 1) + g_0^2]$, $a \simeq 2\omega_0(\nu - i\mu)$, $b \simeq g_0 - \alpha\omega_0^2/(1 + h)$, $c \simeq -2\omega_0[1 - i\alpha\omega_0/(1 + h)]$, $\delta \simeq 4\omega_0(2\omega_0 - i\mu)$, $\mu \simeq \alpha(h + \frac{1}{2}) - g_0$, $\Lambda = a + \delta$, and $\nu = \omega/2 - \omega_0$ represents the detuning parameter. Notice that in Eq. (6) we have considered only terms up to the order of $\mu_0 \sim g_0 \sim g_1^2 \sim \nu \sim \alpha$ and $\alpha \ll 1$. The relationship (6) is depicted by the black solid line in Fig. 2. We have compared this curve with that given by the full numerical solution obtained with a trial function up to the fifth harmonic (gray line). These two curves are almost indistinguishable in this figure. Hence, our reduced approximation provides an excellent description of the boundaries of the parametric instability. The region inside the curve accounts for the Arnold tongue [41]. In this region, the steady magnetization state, $\mathbf{m} = \hat{\mathbf{x}}$, undergoes an instability, which is saturated in a stable precessional state corresponding to a limit cycle in phase space. Figure 1(b) shows the typical temporal evolution of the magnetization components inside the Arnold tongue. The right panel in Fig. 2 illustrates the precessional and uniform states in the magnetization space. Outside this tongue, in region (1) outlined in the left panel of Fig. 2, the precessional state persists and coexists with the stable uniform magnetization. The precessional state exhibits a saddle-node bifurcation when going from region (0) to region (1).

The dynamics of parametrically forced systems can be decomposed into fast and slow temporal scales at the onset of their subharmonic resonance [21]. The fast scale is given by

the oscillation frequency $\omega_0 \approx \omega/2$, while the slow scale is the evolution of the oscillation envelope. The description of the PDSTNO at the onset of resonance, in terms of the oscillation amplitude, is obtained by introducing the following ansatz:

$$m_y = m_{y,0}[A e^{i(\omega_0 + \nu)t} + \bar{A} e^{-i(\omega_0 + \nu)t}] + W_y, \qquad (7)$$

where the normalized oscillation envelope A describes the magnetization deviation from the homogeneous orientation $\mathbf{m} = \hat{\mathbf{x}}$. The normalization constant $m_{y,0} = -\sqrt{2\omega_0/(3N_1 + \omega_0^2 N_2)}$, where $N_1 \simeq [(1 + 2\beta)h + \beta]/2$, and $N_2 \simeq (1 + \beta)(h - 2)/[2(h + 1)^2] + \beta/[2(h + 1)]$ describes the characteristic scale of oscillations. W_y is a higher-order correction that depends nonlinearly on A and its complex conjugate. Introducing formula (7) in Eq. (1), linearizing W_y and applying the solvability condition, we get the *parametrically driven and damped nonlinear Schrödinger equation* (PDNLS) without space [21,29]:

$$\dot{A} = -i\nu A - i|A|^2 A - \mu A + \gamma \bar{A}, \qquad (8)$$

where $\mu = \alpha(h + \frac{1}{2}) - g_0$ stands for linear dissipation, and $\gamma = (b/2\omega_0)g_1 \approx \alpha g_1/[4\sqrt{h(1 + h)}]$ represents the forcing amplitude. In the conservative limit $\mu = \gamma = 0$, the PDNLS equation becomes the well-known *nonlinear Schrödinger equation*, which describes the amplitude of Hamiltonian oscillations. In the dissipative case $\mu, \gamma > 0$, the balance between injection and dissipation generates attracting states, and permanent behaviors such as self-sustained precessions. Note that in this representation the solutions can be obtained analytically (see Ref. [12] and references therein). Moreover, the bifurcation diagram of the PDNLS model is the same as shown in the left panel of Fig. 2.

The amplitude Eq. (8) can be derived using symmetry arguments. When there is no injection or dissipation, the magnetization dynamics are invariant under time reversal $t \to -t$ and temporal translation $t \to t + \Delta t$. Hence, the amplitude A must satisfy $(t, A) \to (-t, \bar{A})$ and $(t, A) \to (t + \Delta t, A e^{-i\Delta})$. Then, the amplitude equation at dominant order reads $\dot{A} = ic_1 A + ic_2|A|^2 A$, where c_1 and c_2 are real constants. In the presence of dissipation and parametric forcing, the time inversion and translation symmetries are broken, respectively. Taking into account these effects, the amplitude equation fulfills $\dot{A} = ic_1 A + ic_2|A|^2 A + c_3 A + c_4 \bar{A}$, where the extra terms depend on damping and driving forces. Therefore, the dynamical behaviors exhibited by PDSTNO belong to the universality class of parametrically driven systems [21].

It is worth noting that all the parameters of the PDNLS equation are controlled by the electric current. Furthermore, under the scaling $\gamma \sim \mu \sim \nu \sim |A|^2 \sim d/dt \ll 1$ in Eq. (8), the coupling between the time-varying injection γ and the oscillation envelope $A(t)$ is of the same order as the other physical effects. This makes the parametric forcing an efficient mechanism for controlling the magnetization dynamics.

III. PARAMETRICALLY INDUCED SPATIAL TEXTURES

Physical systems with a parametric forcing exhibit a large variety of spatially self-organized states [21]. Hence, the feasibility of PDSTNO devices to generate parametric instabilities offers a great advantage for pattern forming studies in the nanoscale domain with respect to other magnetic systems.

In the next subsections we study the inhomogeneous magnetic states $\mathbf{m} = \mathbf{m}(\mathbf{r},t)$ induced by the alternating current. Using a simplified magnetic model and the amplitude equation approach we predict the existence of subharmonic standing waves, or Faraday-type waves, and solitons. These predictions are in agreement with our micromagnetic simulations.

A. Analytic approach to nonuniform dynamics

A minimal model can be obtained neglecting the effects of the borders and approximating the demagnetizing energy by its leading-order contribution in terms of a shape anisotropy. The last approximation is valid when the magnetization has small deformations with respect to the uniform state and the free layer thickness is small compared with lateral sizes.

For spatially varying magnetizations $\mathbf{m}(\mathbf{r},t)$, the LLGS model and the effective field $\mathbf{h}_{\text{eff}}$ become [35]

$$\frac{\partial \mathbf{m}}{\partial t} = -\mathbf{m} \times \mathbf{h}_{\text{eff}} + \alpha \mathbf{m} \times \frac{\partial \mathbf{m}}{\partial t} + g\,\mathbf{m} \times (\mathbf{m} \times \hat{x}), \quad (9a)$$

$$\mathbf{h}_{\text{eff}} = (h_0 + \beta m_x)\hat{x} - m_z\hat{z} + \nabla^2 \mathbf{m}, \quad (9b)$$

where the last term of $\mathbf{h}_{\text{eff}}$ accounts for the ferromagnetic exchange, and it penalizes inhomogeneities in the magnetization. The spatial operator $\nabla = \hat{y}\partial_y + \hat{z}\partial_z$ is expressed in the unit of the *exchange length* $l_{\text{ex}} = \sqrt{2A_{ex}/(\mu_0 M_s^2)}$ where A_{ex} is the exchange stiffness constant.

In this scenario the oscillation envelope $A(\mathbf{r},t)$ can be described using the following ansatz in Eq. (9a):

$$m_y = m_{y,0}e^{i(\omega_0 + \nu)t}A(\mathbf{r},t) + \text{c.c.} + W_y, \quad (10)$$

After straightforward calculations, in a similar way to the previous section, we obtain the PDNLS equation:

$$\frac{\partial A}{\partial t} = -i\nu A - i|A|^2 A - \mu A + \gamma \bar{A} - i\nabla'^2 A, \quad (11)$$

where the last term of Eq. (11) accounts for the dispersion with $\nabla' = [(2h+1)/(2\omega_0)]^{1/2}\nabla$. The sign of dispersion and nonlinearity renders this equation to a focusing type [36]. Notice that the Laplacian term is the leading-order spatial coupling that accounts for spatial reflection $\mathbf{r} \to -\mathbf{r}$ and translation $\mathbf{r} \to \mathbf{r} + \Delta\mathbf{r}$ symmetries.

The amplitude equation (11) is the prototype model describing the envelope of coupled nonlinear oscillators. Furthermore the PDNLS equation allows us to relate the magnetization dynamics of PDSTNO into the same phenomenology of a wide spectrum of physical systems that ranges from nonlinear optical systems to fluids dynamics under driving forces.

The amplitude Eq. (11) is characterized by exhibiting Faraday-type waves and dissipative solitons [21]. The origin of Faraday-type waves is a spatial instability of the parallel state $A = 0$. As a result of this destabilization, the noise-induced perturbations are exponentially amplified in time. The growth rate σ of the small perturbations $A \sim e^{\sigma t + i\mathbf{k}\cdot\mathbf{r}}$ is obtained linearizing Eq. (11) around zero:

$$\sigma = -\mu \pm \sqrt{\gamma^2 - (|\mathbf{k}|^2 - \nu)^2}, \quad (12)$$

where $\mathbf{k}$ is the wave vector of the modes in which perturbations are decomposed. For alternating currents above the critical value $\gamma_c = \mu$, the modes with wave number $|\mathbf{k}| = \sqrt{\nu}$ grow and destabilize the uniform configuration. The zone where
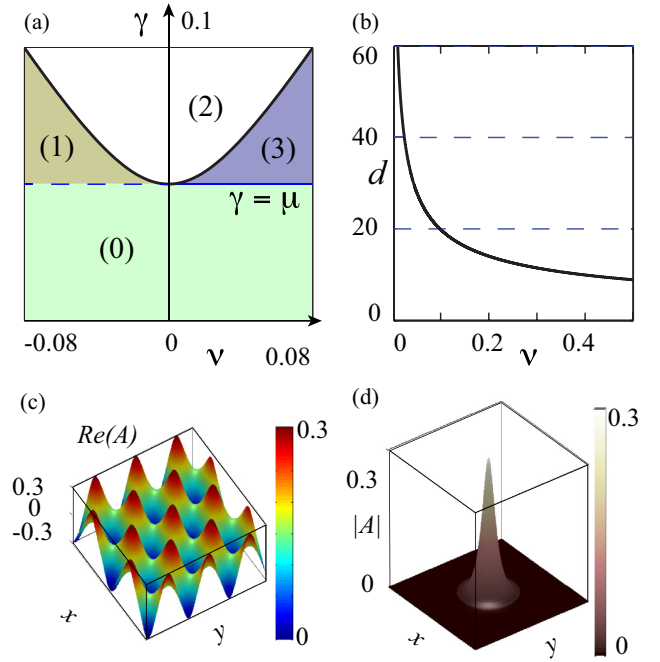

FIG. 3. (Color online) Phases diagram of the PDNLS model, Eq. (11). (a) Detuning-injection plane; in zones (1) and (3) solitons and standing waves exist. Region (2) is known as the Arnold tongue; in this zone the parallel state $A = 0$ becomes unstable, and then solitons also are unstable. Standing waves are the only steady states observed in this region. In zone (3) standing waves emerge by supercritical bifurcation. (b) Wavelength for Faraday-type waves as a function of detuning. (c) Typical Faraday-type waves obtained for $\gamma = 0.055$, $\mu = 0.05$, and $\nu = 0.075$. (d) Dissipative soliton, parameters $\gamma = 0.0505$, $\mu = 0.05$, and $\nu = -0.015$.

Faraday-type waves exist is marked as (3) in Fig. 3(a). It is worth noting that the necessary conditions $\gamma > \mu$ and $\nu > 0$ to observe Faraday-type waves, as well as their wavelength $d = 2\pi l_{\text{ex}}/\sqrt{\nu}$, are completely controlled by the electric current parameters $\{g_1, g_0, \omega\}$, or equivalently the PDNLS parameters $\{\gamma(g_1), \mu(g_0), \nu(\omega)\}$. Figure 3(b) shows the typical wavelengths, in units of the exchange length, as a function of the detuning parameter. As this figure illustrates, for positive detuning, typical wavelengths are of order $d \sim 15l_{\text{ex}}$, which is about $d_{\text{Co}} = 52(\text{nm})$ and $d_{\text{Py}} = 85(\text{nm})$ for cobalt and Permalloy, respectively. Smaller wavelengths can be obtained by increasing the forcing frequency ω.

At the onset of the spatial instability and after transients, the standing wave is composed of one or a few Fourier modes, compatible with boundary conditions and having a wave number close to the critical value $|\mathbf{k_c}| \approx \sqrt{\nu}$. Figure 3(c) shows a typical standing wave of Eq. (11). In general, the number of such modes, as well as the orientation of their wave vectors, depend on the nonlinear saturation mechanisms of the particular problem, material defects, and borders [42].

This type of instability was studied in spin valves for the case of constant external field and direct spin-polarized current [11,12]. A PDNLS model was derived [12] using an appropriate time-independent change of variables of the form $A \sim (m_y + im_z)/(1 + m_x)$. Even if the system under study in Refs. [11,12] does not have parametric forcing, the

magnetization obeys a PDNLS equation, and textures usually found in parametrically driven systems emerge [12]. This correspondence between parametric systems and spin valves with direct current was called *parametric equivalence*. In the parametric equivalence, the origin of the parametric injection (term $\gamma\bar{A}$) is related to anisotropy effects. The direct spin-polarized current was responsible for the dissipation term μA. It is worth noting that in the parametric equivalence most of the magnetic textures are static and periodic in space. In opposition, when an alternating current is applied, the magnetization oscillates both in space and time $m_y \sim e^{i\omega_0 t}\cos(i\mathbf{k}\cdot\mathbf{r}) + $ c.c. Since the anisotropies are fixed in usual setups, the only control parameters in the parametric equivalent system are the detuning (external magnetic field) and dissipation (the constant electric current). In our present case, the amplitude g_1 and frequency ω of the alternating current and the direct current g_0 are the control parameters associated to the parametric injection γ, detuning ν, and dissipation μ, respectively. In brief, the use of an alternating current permits a more adequate control of the parametric behaviors exhibited by the PDNLS model.

Dissipative solitons are another prominent example of spatial self-organization in macroscopic nonlinear systems. They can be described by particlelike attributes, such as position and width [43].

The parametric forcing induces dissipative solitons that connect asymptotically the quiescent state $A = 0$. Figure 3(d) shows a soliton state, obtained from Eq. (11). There is no analytic expression for this solution in PDNLS model, nevertheless they can be approximated using the variational method [44,45] by

$$A_{\text{soliton}}(\mathbf{r}) = a_0\sqrt{\lambda}e^{i\phi_0}\,\text{sech}(b_0\sqrt{\lambda}|\mathbf{r}|), \qquad (13)$$

where $\lambda \equiv -\nu + \sqrt{\gamma^2 - \mu^2}$, $\cos(2\phi_0) = \mu/\gamma$, $a_0 = 2.166$, and $b_0 = 0.933$. This approximation gives a characteristic amplitude $a_0\lambda^{1/2}$, and a characteristic width $b_0^{-1}\lambda^{-1/2}$. In a similar way to the Faraday-type waves wavelengths, the electric current parameters $\{g_1, g_0, \omega\}$ control the soliton typical lengths.

We can see from formula (13) that, at dominant order, the soliton decays exponentially to the parallel state $A \sim e^{-\sqrt{\lambda}|\mathbf{r}|} \to 0$ far from the center of the soliton, that is, $|\mathbf{r}| \gg \lambda^{-1/2}$. Since, soliton tails connect the homogeneous state, solitons are observed only where the parallel state is stable. These zones are labeled as (0) and (1) in Fig. 3. Hence, solitons exist for negative detuning and injection amplitudes in the range $\mu < \gamma < \sqrt{\mu^2 + \nu^2}$, which corresponds to zone (1) in Fig. 3(a).

B. Micromagnetic simulation of solitons and Faraday-type waves

To investigate the robustness of the observed textures, and to illustrate the parametric instability of spin valves, we model a $500 \times 500 \times 2$-nm^3 Permalloy free layer sample ($M_s = 800$ kA/m, $K = 14.5$ kJ/m^3) with a discretization of $127 \times 127 \times 1$ cells with a Neumann boundary condition. We use an adaptive step size fifth-order Runge-Kutta scheme. The effective field includes the full demagnetization term [46]

$$\mathbf{h}_{\text{eff}} = (h_0 + \beta m_x)\hat{x} - \nabla\Phi + \nabla^2\mathbf{m}, \qquad (14)$$

where the magnetic potential Φ is

$$\Phi(\mathbf{r}) = \frac{1}{4\pi}\int_V \frac{\rho_m(\mathbf{r}')}{|\mathbf{r}-\mathbf{r}'|}d^3r' + \frac{1}{4\pi}\int_{\partial V}\frac{\sigma_m(\mathbf{r}')}{|\mathbf{r}-\mathbf{r}'|}d^2r', \qquad (15)$$

and the charge densities in the bulk $\rho_m = -\nabla\cdot\mathbf{m}$ and at the surface $\sigma_m = \hat{n}\cdot\mathbf{m}$ are the magnetic analog of electric charge densities. The density ρ_m is induced by nonuniformly magnetic distributions, while σ_m appears if the magnetization points towards the outward normal $\hat{n}$ at the sample borders [46].

We obtain the demagnetization field using the discrete convolution [47] between the magnetization and the demagnetization tensor. The demagnetization tensor components are generated by the function included in the OOMMF code [48,49]. We use an external field $H = 0.2M_s$ and a direct current density $J_{\text{dc}} = 0.16$ A/μm^2; for a polarization factor $\mathcal{P} = 0.3$ we obtain the following reduced parameters: $h = 0.2$, $\beta = 0.03$, and $g_0 = 0.01$. That is, the critical value of the radio-frequency current for the parametric instability is $g_1 = 0.034$ ($J_{\text{ac}} = 0.55$ A/μm^2). In this configuration the natural frequency is $\omega_0 = 0.53$ ($\Omega_0 = 14.85$ GHz) and for the detunings $\nu_1 = -0.004$ (112 MHz below Ω_0) and $\nu_2 = 0.075$ (2 GHz above Ω_0) a localized state and Faraday-type waves are expected, respectively. Fixing the effective alternate current at $g_1 = 0.2$ (3.22 A/μm^2) we obtain different spatial structures that can be seen from Figs. 4(a) and 4(b) for ν_1 and ν_2, respectively. Hence, solitons and Faraday-type waves persist when the demagnetizing effects are included [50]. Since the magnetization is approximately in the x axis, the main demagnetization contribution at the in-plane borders is a surface magnetic charge of the form $\sigma_m = \pm\mathbf{m}\cdot\hat{x}$. Figure 5 shows the typical deviations induced by the effect of magnetic charges.
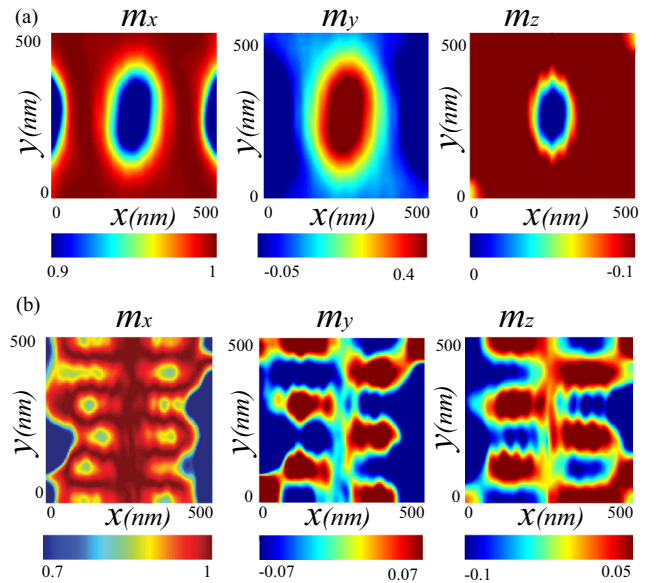

FIG. 4. (Color online) Parametrically induced textures. Dissipative solitons (a) and Faraday-type waves (b) obtained from simulations of the LLG equation with the effective field (14) for a $500 \times 500 \times 2$-nm^3 Permalloy sample with $\nu = -0.004$ and 0.075, respectively. The Gilbert damping parameter is fixed at $\alpha = 0.014$.
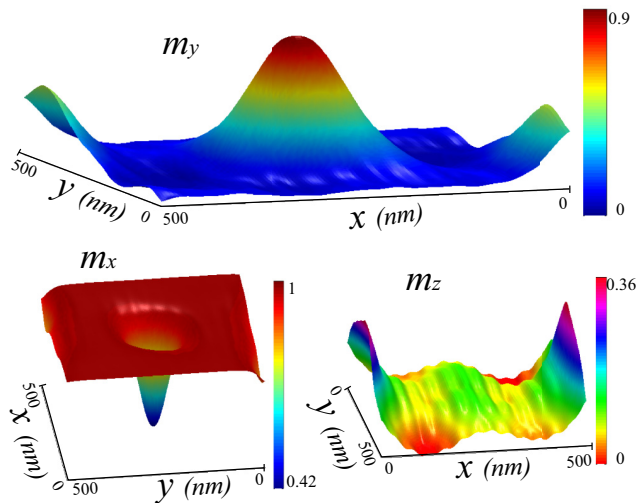
FIG. 5. (Color online) Dissipative solitons in parametrically driven spin valves obtained from Eq. (9b) using the effective field (14). Solitons persist when the sample borders and the full dipolar field are considered.

IV. CONCLUSIONS AND REMARKS

We have shown that a spin-polarized electric current, with both constant and oscillatory components, induces parametric instabilities in spin valves. In the case of macrospin approximation, additional equilibria and precessional states emerge. This scenario changes when the spatial variations of the magnetization are considered. In particular, our analysis shows that the free magnetic layer exhibits a wide class of robust self-organization phenomena observed in driven systems, such as dissipative solitons and Faraday-type waves. These states are robust when additional effects, such as the dipolar field or the sample borders, are considered. Hence, the use of alternating spin-polarized currents opens the possibility to control transitions from the parallel state to uniform precessions or dissipative solitons and Faraday-type waves. These behaviors could open novel and fresh functionality to spin-valve devices.

[1] S. I. Kiselev, J. C. Sankey, I. N. Krivorotov, N. C. Emley, R. J. Schoelkopf, R. A. Buhrman, and D. C. Ralph, Microwave oscillations of a nanomagnet driven by a spin-polarized current, Nature (London) **425**, 380 (2003); D. C. Ralph and M. D. Stiles, Spin transfer torques, J. Magn. Magn. Mater. **320**, 1190 (2008); G. Bertotti, C. Serpico, I. D. Mayergoyz, A. Magni, M. d'Aquino, and R. Bonin, Magnetization switching and microwave oscillations in nanomagnets driven by spin-polarized currents, Phys. Rev. Lett. **94**, 127206 (2005), and references therein.

[2] B. Georges, J. Grollier, M. Darques, V. Cros, C. Deranlot, B. Marcilhac, G. Faini, and A. Fert, Coupling efficiency for phase locking of a spin transfer nano-oscillator to a microwave current, Phys. Rev. Lett. **101**, 017201 (2008).

[3] Z. Yang, S. Zhang, and Y. C. Li, Chaotic dynamics of spin-valve oscillators, Phys. Rev. Lett. **99**, 134101 (2007).

[4] D. Li, Y. Zhou, C. Zhou, and B. Hu, Fractional locking of spin-torque oscillator by injected ac current, Phys. Rev. B **83**, 174424 (2011), and references therein.

[5] J. C. Slonczewski, Current-driven excitation of magnetic multilayers, J. Magn. Magn. Mater. **159**, L1 (1996).

[6] L. Berger, Emission of spin waves by a magnetic multilayer traversed by a current, Phys. Rev. B **54**, 9353 (1996).

[7] Z. Li, Y. C. Li, and S. Zhang, Dynamic magnetization states of a spin valve in the presence of dc and ac currents: Synchronization, modification, and chaos, Phys. Rev. B **74**, 054417 (2006).

[8] M. d'Aquino, C. Serpico, R. Bonin, G. Bertotti, and I. D. Mayergoyz, Stochastic resonance in noise-induced transitions between self-oscillations and equilibria in spin-valve nanomagnets, Phys. Rev. B **84**, 214415 (2011), and references therein.

[9] K. J. Lee, A. Deac, O. Redon, J. P. Nozieres, and B. Dieny, Excitations of incoherent spin-waves due to spin-transfer torque, Nat. Mater. **3**, 877 (2004).

[10] X. W. Yu, V. S. Pribiag, Y. Acremann, A. A. Tulapurkar, T. Tyliszczak, K. W. Chou, B. Bräuer, Z. P. Li, O. J. Lee, P. G. Gowtham, D. C. Ralph, R. A. Buhrman, and J. Stöhr, Images of a spin-torque-driven magnetic nano-oscillator, Phys. Rev. Lett. **106**, 167202 (2011).

[11] A. O. León, M. G. Clerc, and S. Coulibaly, Dissipative structures induced by spin-transfer torques in nanopillars, Phys. Rev. E **89**, 022908 (2014).

[12] A. O. León and M. G. Clerc, Spin-transfer-driven nano-oscillators are equivalent to parametric resonators, Phys. Rev. B **91**, 014411 (2015).

[13] S.-B. Choe, Y. Acremann, A. Scholl, A. Bauer, A. Doran, J. Stöhr, and H. A. Padmore, Vortex core driven magnetization dynamics, Science **304**, 420 (2004).

[14] K. Yu. Guslienko, Magnetic vortex state stability, reversal and dynamics in restricted geometries, J. Nanosci. Nanotechnol. **8**, 2745 (2008).

[15] Q. Mistral, M. van Kampen, G. Hrkac, Joo-Von Kim, T. Devolder, P. Crozat, C. Chappert, L. Lagae, and T. Schrefl, Current-driven vortex oscillations in metallic nanocontacts, Phys. Rev. Lett. **100**, 257201 (2008).

[16] A. Slavin and V. Tiberkevich, Spin wave mode excited by spin-polarized current in a magnetic nanocontact is a standing self-localized wave bullet, Phys. Rev. Lett. **95**, 237201 (2005).

[17] S. Bonetti, V. Tiberkevich, G. Consolo, G. Finocchio, P. Muduli, F. Mancoff, A. Slavin, and J. Akerman, Experimental evidence of self-localized and propagating spin wave modes in obliquely magnetized current-driven nanocontacts, Phys. Rev. Lett. **105**, 217204 (2010).

[18] R. K. Dumas, E. Iacocca, S. Bonetti, S. R. Sani, S. M. Mohseni, A. Eklund, J. Persson, O. Heinonen, and J. Akerman, Spin-wave-mode coexistence on the nanoscale: A consequence of the oersted-field-induced asymmetric energy landscape, Phys. Rev. Lett. **110**, 257202 (2013).

[19] S. M. Mohseni *et al.*, Spin torque generated magnetic droplet solitons, Science **339**, 1295 (2013).

[20] M. A. Hoefer, T. J. Silva, and M. W. Keller, Theory for a dissipative droplet soliton excited by a spin torque nanocontact, Phys. Rev. B **82**, 054432 (2010).

[21] M. G. Clerc, S. Coulibaly, and D. Laroze, Localized states beyond the asymptotic parametrically driven amplitude equation, Phys. Rev. E **77**, 056209 (2008); Non-variational Ising-Bloch transition in parametrically driven systems, Int. J. Bifurcation Chaos **19**, 2717 (2009); Parametrically driven instabilities in quasi-reversal systems, **19**, 3525 (2009); Localized states and non-variational Ising-Bloch transition of a parametrically driven easy-plane ferromagnetic wire, Physica D **239**, 72 (2010); Localized waves in a parametrically driven magnetic nanowire, Europhys. Lett. **97**, 30006 (2012).

[22] D. Urzagasti, D. Laroze, M. G. Clerc, S. Coulibaly, and H. Pleiner, Two-soliton precession state in a parametrically driven magnetic wire, J. Appl. Phys. **111**, 07D111 (2012).

[23] D. Urzagasti, A. Aramayo, and D. Laroze, Soliton-Antisoliton interaction in a parametrically driven easy-plane magnetic wire, Phys. Lett. A **378**, 2614 (2014).

[24] D. Urzagasti, D. Laroze, and H. Pleiner, Localized chaotic patterns in weakly dissipative systems, Eur. Phys. J. Special Topics **223**, 141 (2014).

[25] A. O. León, M. G. Clerc, and S. Coulibaly, Traveling pulse on a periodic background in parametrically driven systems, Phys. Rev. E **91**, 050901 (2015).

[26] M. Clerc, P. Coullet, and E. Tirapegui, Lorenz bifurcation: Instabilities in quasireversible systems, Phys. Rev. Lett. **83**, 3820 (1999); The stationary instability in quasi-reversible systems and the Lorenz pendulum, Int. J. Bifurcation Chaos **11**, 591 (2001).

[27] S. Fauve, in *Hydrodynamics and Nonlinear Instabilities*, edited by C. Godrèche and P. Manneville (Cambridge University Press, Cambridge, 1998), Chap. 4 and references therein.

[28] C. Elphick, E. Tirapegui, M. Brachet, P. Coullet, and G. Iooss, A simple global characterization for normal forms of singular vector fields, Physica D **29**, 95 (1987).

[29] I. V. Barashenkov, M. M. Bogdan, and V. I. Korobov, Stability diagram of the phase-locked solitons in the parametrically driven, damped nonlinear Schrödinger equation, Europhys. Lett. **15**, 113 (1991).

[30] M. G. Clerc, S. Coulibaly, M. A. Garcia-Ñustes, and Y. Zárate, Dissipative localized states with shieldlike phase structure, Phys. Rev. Lett. **107**, 254102 (2011).

[31] S. Fauve and O. Thual, Solitary waves generated by subcritical instabilities in dissipative systems, Phys. Rev. Lett. **64**, 282 (1990).

[32] M. Faraday, On a peculiar class of acoustical figures; and on certain forms assumed by groups of particles upon vibrating elastic surfaces, Philos. Trans. R. Soc. London **121**, 299 (1831).

[33] C. Wang, H. Seinige, and M. Tsoi, Current-driven parametric resonance in magnetic multilayers, J. Phys. D **46**, 285001 (2013).

[34] P. Bortolotti *et al.*, Parametric excitation of magnetic vortex gyrations in spin-torque nano-oscillators, Phys. Rev. B **88**, 174417 (2013).

[35] Z. Li and S. Zhang, Magnetization dynamics with a spin-transfer torque, Phys. Rev. B **68**, 024404 (2003); J. Z. Sun, Spin-current interaction with a monodomain magnetic body: A model study, *ibid.* **62**, 570 (2000); X. Waintal, E. B. Myers, P. W. Brouwer, and D. C. Ralph, Role of spin-dependent interface scattering in generating current-induced torques in magnetic multilayers, *ibid.* **62**, 12317 (2000); M. D. Stiles and A. Zangwill, Anatomy of spin-transfer torque, *ibid.* **66**, 014407 (2002).

[36] Y. S. Kivshar and G. P. Agrawal, *Optical Solitons: From Fibers to Photonic Crystals* (Academic Press, San Diego, 2003).

[37] J. Xiao, A. Zangwill, and M. D. Stiles, Macrospin models of spin transfer dynamics, Phys. Rev. B **72**, 014446 (2005).

[38] L. Cesari, *Asymptotic Behaviour and Stability Problems in Ordinary Differential Equations* (Springer, New York, 1962).

[39] E. I. Butikov, Subharmonic resonances of the parametrically driven pendulum, J. Phys. A **35**, 6209 (2002).

[40] C. M. Bender and S. A. Orzag, *Advanced Mathematical Methods for Scientists and Engineers* (McGraw-Hill, New York, 1978).

[41] V. I. Arnold, *Geometrical Methods in the Theory of Ordinary Differential Equations* (Springer-Verlag, New York, 1998).

[42] R. B. Hoyle, *Pattern Formation: An Introduction to Methods* (Cambridge University Press, Cambridge, 2006).

[43] M. Remoissenet, *Waves Called Solitons* (Springer, Berlin, 1999).

[44] D. Anderson, M. Bonnedal, and M. Lisak, Self-trapped cylindrical laser beams, Phys. Fluids **22**, 1838 (1979).

[45] M. G. Clerc, S. Coulibaly, and D. Laroze, Interaction law of 2D localized precession states, Europhys. Lett. **90**, 38005 (2010).

[46] J. M. D. Coey, *Magnetism and Magnetic Materials* (Cambridge University Press, Cambridge, 2010).

[47] N. Hayashi, K. Saito, and Y. Nakatani, Calculation of demagnetizing field distribution based on fast Fourier transform of convolution, Jpn. J. Appl. Phys. **35**, 6065 (1996).

[48] A. J. Newell, W. Williams, and D. J. Dunlop, A generalization of the demagnetizing tensor for nonuniform magnetization, J. Geophys. Res. Solid Earth **98**, 9551 (1993).

[49] M. Donahue and D. Porter, The Object Oriented MicroMagnetic Framework (OOMMF project at ITL/NIST), http://math.nist.gov/oommf/.

[50] See Supplemental Material at http://link.aps.org/supplemental/10.1103/PhysRevB.91.224426 for a movie that shows the spatiotemporal dynamics of these spatial structures.

Apéndice D

Traveling pulse on a periodic background in parametrically driven systems

This chapter presents a traveling pulse solution that propagates over Faraday-type patterns. This state emerges in system with a parametric injection of energy.

Traveling pulse on a periodic background in parametrically driven systems

Alejandro O. León[*] and Marcel G. Clerc[†]

Departamento de Física, Facultad de Ciencias Físicas y Matemáticas, Universidad de Chile, Casilla 487-3, Santiago, Chile

Saliya Coulibaly[‡]

Laboratoire de Physique des Lasers, Atomes et Molécules, CNRS UMR 8523,
Université des Sciences et Technologies de Lille–59655 Villeneuve d'Ascq Cedex, France, EU

Macroscopic systems with dissipation and time-modulated injection of energy, parametrically driven systems, can self-organize into localized states and/or patterns. We investigate a pulse that travels over a one-dimensional pattern in parametrically driven systems. Based on a minimal prototype model, we show that the pulses emerge through a subcritical Andronov-Hopf bifurcation of the underlying pattern. We describe a simple physical system, a magnetic wire forced with a transverse oscillatory magnetic field, which displays these traveling pulses.

Physical systems kept out of thermodynamic equilibrium exhibit pattern formation [1]. This morphogenesis, or transition from a uniform state to a pattern when a control parameter is varied, is understood in terms of a spontaneous symmetry breaking instability of the uniform state (see [1,2], and references therein). Far from the aforementioned transition, the stationary patterns can become unstable, which typically induces rich dynamical behaviors. For example, Andronov-Hopf instabilities originate vacillating-breathing states [3], while the stationary parity-breaking bifurcation induces global [4] or localized drift patterns [5]. These dynamical behaviors can coexist in a large range of parameters [3,6,7]. From a theoretical point of view, Coullet and Iooss [8] classified the generic instabilities of static periodic patterns in one spatial dimension, and described them with amplitude equations for the critical modes. This theory was generalized [9,10] to explain experimental observations, such as topological defects and localized drifting domains.

Let us consider the specific case of parametrically driven systems, that is, systems in which the injection of energy or momentum is time modulated [11]. For a forcing frequency close to twice their natural frequency, parametric systems are known to show a subharmonic resonance [11]. This instability in extended systems is characterized by the formation of subharmonic spatially periodic patterns, such as the well-known *Faraday waves* of vibrated fluids [12]. At the onset of subharmonic resonance, the dynamical evolution of the amplitude of oscillations can be described by the *parametrically driven, damped nonlinear Schrödinger* equation (PDNLS). This prototype model has been used to study self-organization in several physical systems, such as a vertically oscillating layer of water [13,14], ferromagnetic media driven by an oscillatory magnetic field [15–17], parametrically driven nonlinear oscillators [18], localized structures in nonlinear lattices [19], light pulses in optical fibers [20], optical parametric oscillators [21], and spintronic devices [22], to mention a few. Despite the success of the prototype PDNLS

model, it fails to predict localized states with damped spatial oscillations of parametrically forced ferromagnets and coupled oscillators [17,18]. To recover the dynamical properties of the original system, the PDNLS equation must be amended by taking into account higher order terms.

The instabilities of patterns in parametrically forced systems, as well as the dissipative structures and spatiotemporal behaviors induced by these bifurcations, are not entirely well understood. In the context of vertically driven granular media, the emergence of secondary drift instability of standing waves has been reported [23]. In the case of a rectangular water container subjected to vertical vibrations, preliminary observations show for forcing amplitudes above a critical value, the amplitude of Faraday waves becomes modulated by a nonpropagative localized structure [cf. Fig. 1(a)] [24]. Traveling pulses on stationary periodic structures have been observed in directional solidification [25]. Theoretically, this type of dynamical behavior has been described in a unified manner by considering the coupling of counterpropagative wave envelopes [10].

The aim of this Rapid Communication is to theoretically and numerically investigate traveling pulses immersed in a one-dimensional pattern in parametrically driven systems. The pulses over patterns are characterized by a localized increment of the amplitude of the spatially periodic background. Figures 1(b) and 1(c) show this type of solution for a parametrically driven ferromagnetic wire. Using an adequate amplitude equation, we show that pulses appear as results of a subcritical Andronov-Hopf bifurcation of the underlying pattern. This minimal approach allows us to predict this dynamical behavior in different physical systems. We show that a magnetic wire forced with a transverse oscillatory magnetic field, displays these traveling pulses.

Unified description of traveling pulses. Let us describe the envelope of the oscillations of a parametric system by a complex order parameter, $A(t,z)$, that obeys the following amended parametrically driven damped nonlinear Schrödinger equation (APDNLS),

$$\partial_t A = -i(\nu A + |A|^2 A + \partial_{zz} A) - \mu A + \gamma \bar{A} + i\delta \bar{A}(\partial_z A)^2,$$
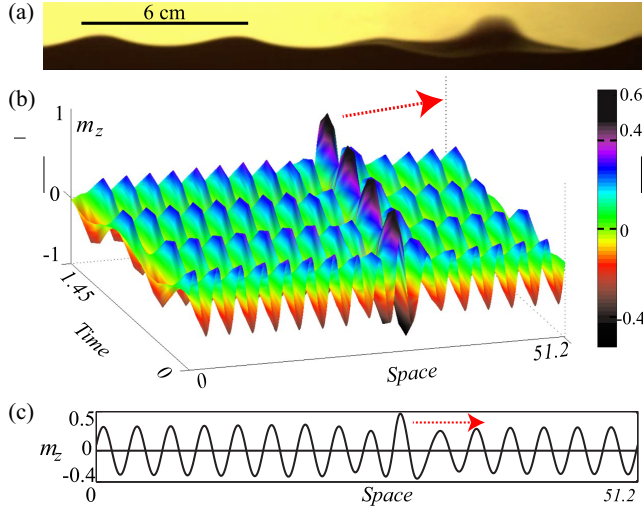
(1)

(a)

(b)

(c)

FIG. 1. (Color online) Pulses over a periodic background or pattern in parametrically driven systems. (a) Experimental snapshot of a nonpropagative hydrodynamic pulse supported by Faraday waves [24]. Numerical simulation of a magnetic wire forced with a transverse oscillatory magnetic field, Eq. (2), with $H_0 = h_0 = 2$, $\beta = 4.8$, $\alpha = 0.02$, and $\nu = 4$. (b) Spatiotemporal diagram of a slowly traveling magnetic pulse and (c) instantaneous profile of the magnetic pulse at time $t = 0$.

where t and z are the temporal and spatial coordinates. The coefficient ν accounts for the detuning between half of the forcing frequency and the response frequency, while the parameters μ and γ account for the dissipation and the parametric injection, respectively. For $\delta = 0$, Eq. (1) is the usual PDNLS model, used to describe the parametrically driven systems for small injection and dissipation of energy—*quasireversible limit* [26]. Hence, parameters and operators of the above equation scale as $\nu \sim \mu \sim \gamma \sim |A|^2 \sim \partial_{zz} \sim \partial_t$. The term proportional to δ in this limit is a higher order correction. Notice that the instabilities of the quiescent state $A = 0$ are not modified by the amending term $i\delta\bar{A}(\partial_z A)^2$, because it is nonlinear.

Numerical simulations of the APDNLS equation (1) exhibit spatially periodic patterns for a given forcing amplitude and positive detuning. When γ is increased, the model displays traveling pulses over the pattern state. Figure 2 illustrates a single left-traveling pulse, and multiple pulses. Due to the $x \rightarrow -x$ invariance, the same solutions with a right-traveling pulse exist. All numerical simulations of the above equation have been performed with a space discretization of finite differences centered schemes of sixth order, and a fifth order controlled step size Runge-Kutta scheme [27] for temporal evolution.

Multiple pulses can move in the same direction or counter-propagate. In the latter case, the result of the collisions depends on the parameters: the first possibility is that one of the pulses is destroyed after the collision, while in the second case they reemerge from collisions with their particlelike characteristics unchanged [see Fig. 2(c)]. The speed of traveling pulses decreases with the amplitude of the forcing γ following a square-root power law (see Fig. 3). For small injections of energy $\gamma < \gamma_c$, traveling pulses are not stable, and the pulselike
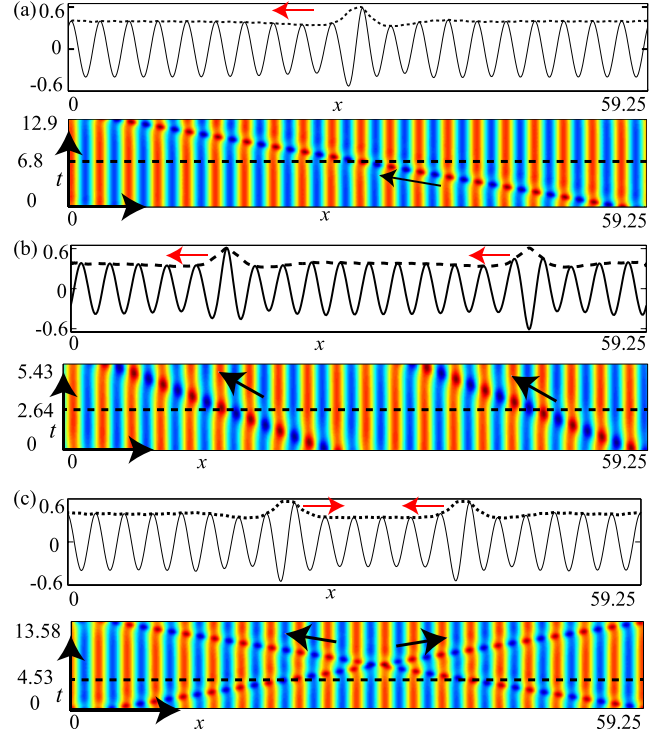
(a)

(b)

(c)

FIG. 2. (Color online) Pulse solutions obtained with different initial conditions. The top profiles of the variable $\mathrm{Re}(A)$ are taken from the dashed line of the respective spatiotemporal diagram. (a) Solitary left-traveling pulses over spatially periodic patterns. (b) Two left-traveling pulses. (c) Collision of two counterpropagative pulses. Parameters are $\gamma = 0.5$, $\mu = 0.4$, $\nu = 4.5$, and $\delta = 2$. The simulations use $N = 500$ points with a spatial step size $dx = 0.1185$.

initial conditions decay to a pattern with a characteristic time $\Delta t \sim (\gamma_c - \gamma)^{-1/2}$ (cf. inset of Fig. 3). Then, these two features allow us to conjecture that the traveling pulses appear through a saddle-node bifurcation mechanism. Likewise, increasing the parameter $\gamma > \gamma_c$, the pattern that supports the pulses becomes unstable for $\gamma \geq \Gamma_c$, and multiple pulselike structures emerge spontaneously and invade the system.
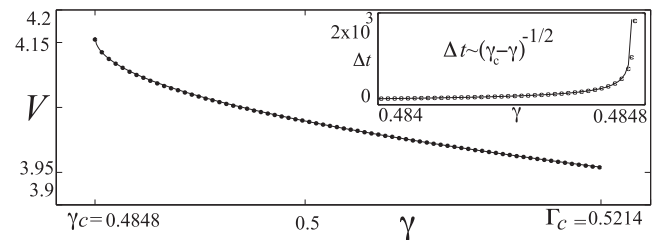

FIG. 3. Speed of the traveling pulses as a function of forcing parameter γ. Points are obtained from numerical simulations of Eq. (1) with $\nu = 4.5$, $\delta = 2.0$, and $\mu = 0.4$. The solid line $V(\gamma) = [-a_2 - \sqrt{a_2^2 - 4a_1(a_3 - \gamma)}]/(2a_1)$ fits the speed of the pulse with $a_1 = 0.9124$, $a_2 = -7.588$, and $a_3 = 16.26$. The inset shows the typical time in which a pulse decays into a pattern state for $\gamma < \gamma_c$. The solid curve $\Delta t(\gamma) = 2b_1/[-b_2 - \sqrt{b_2^2 - 4b_1(b_3 - \gamma)}]$ fits the decaying times with $b_1 = -14.227$, $b_2 = 0.0076504$, and $b_3 = 0.48476$.
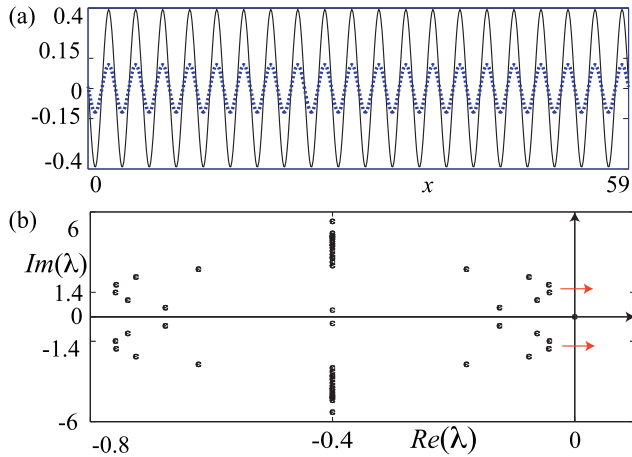
FIG. 4. (Color online) Andronov-Hopf bifurcation of patterns state of amplitude equation (1). (a) Stationary pattern for $\gamma = 0.48$, $\mu = 0.4$, $\nu = 4.5$, $\delta = 2$, and $dx = 0.1185$. The real and imaginary parts of the amplitude $A(x,t)$ are represented by a continuous and dashed curve, respectively. (b) Eigenvalues of the pattern represented in the complex plane.

The existence, stability properties, and dynamical evolution of traveling pulses immersed in patterns is closely related to the amending term of Eq. (1). Indeed, in the limit $\delta \to 0$, the APDNLS model, Eq. (1), only exhibits stationary spatially periodic patterns for positive detuning and small amplitude forcing γ, and vacillating-breathing patterns for higher values of γ. Hence, traveling pulses have not been observed in the limit of the parametrically driven nonlinear Schrödinger equation. It is worth noting that in the region where patterns exist, the gradients on the amplitude $|\partial_z A| \sim q|A|$ are not small (where q is the pattern wave number), and then the terms like $i\bar{A}(\partial_z A)^2$, $i|A|^2\partial_{zz}A$, $iA^2\partial_{zz}\bar{A}$, and $iA|\partial_z A|^2$ become relevant in the dynamics of Eq. (1). However, we have observed pulse solutions only when the amending term $i\bar{A}(\partial_z A)^2$ is included.

Formation mechanism of traveling pulses. At leading order, the pattern that supports the pulses reads $A \approx T(t,z)e^{iqz} +$ c.c., where $q = \sqrt{\nu}$ and the slowly varying amplitude of the pattern satisfies $\partial_t T = (\gamma - \mu)T - (\delta\nu - 3)^2 T|T|^4/(2\mu) + (2\nu/\mu)\partial_{zz}T$. Notice that for $\delta \to 0$ we recover the amplitude equation of patterns in parametric systems [26,28]. One of the effects of the nonlinear gradient term in the APDNLS equation (1) is to introduce a critical point at $\nu \equiv 3/\delta$ for which the quintic order saturation vanishes, changing the type of bifurcation. The dynamics of $T(t,z)$ is of relaxation type, that is, the amplitude evolves minimizing a functional. Consequently, permanent behaviors such as oscillatory patterns and traveling pulses are prohibited, and it is necessary to use the full model, Eq. (1), to understand the formation of traveling pulses.

The analytical stability analysis of the spatially periodic pattern states from Eq. (1) is a tricky task. However, its numerical study is easily accessible. Figure 4 shows the typical stationary pattern solution and its corresponding eigenvalues. When the γ parameter is increased, two complex conjugate eigenvalues cross the imaginary axis, as illustrated in Fig. 4(b). This instability corresponds to an Andronov-Hopf bifurcation. Hence, the critical modes of this instability are of the type
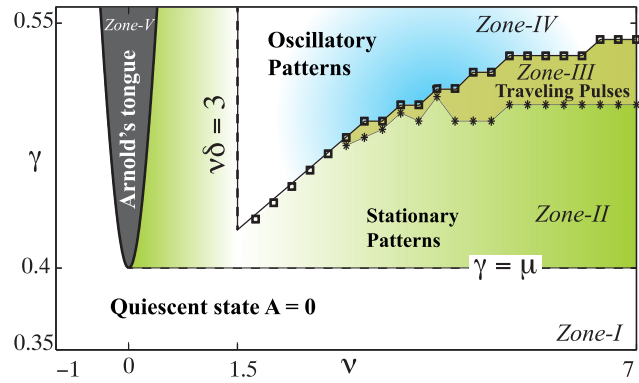

FIG. 5. (Color online) Bifurcation diagram of APDNLS equation (1). In zone I the state $A = 0$ is the only equilibrium. Zone V is Arnold's tongue; inside this region the trivial state $A = 0$ is unstable. The pattern states are observed in zones II, III, and V. The squares denote the transition from stationary patterns to oscillatory patterns. Traveling pulses are observed in zone III.

of left- and right-traveling waves, which can be written in the form $A_{c,\pm}(t,z) = B_\pm(T,Z)e^{i(\omega t \pm kz)}f_q(\pm z)$, where k is a real constant, f_q is a complex-valued q-periodic function, and $B_\pm(T,Z)$ is a slowly varying envelope in time T and space Z. When the spatially periodic pattern $[B_\pm(T,Z) = 0]$ is unstable, multiple pulselike structures emerge spontaneously and invade the system, which is equivalent to having an inhomogeneous profile in $B_\pm(T,Z)$. Uniform profiles in $B_\pm(T,Z)$ are not numerically observed. It is important to note that this parity-breaking discontinuous or subcriticalsecondary bifurcation is numerically found for $\nu > 3/\delta$. Figure 5 shows the phase diagram of APDNLS equation (1). In zone I only the quiescent state $A = 0$ is observed for positive detuning. If one increases the forcing parameter γ, the system exhibits the emergence of patterns, zone II, through a supercritical bifurcation at $\gamma = \mu$. These spatially periodic patterns correspond to subharmonic waves in original parametrically driven systems. The pattern states are observed in zones II, III and V. Furthermore, for sufficiently large values of γ and ν, patterns become oscillatory, zone IV, through a subcritical Andronov-Hopf bifurcation. In this zone the system exhibits traveling waves. As a result of the subcritical Andronov-Hopf bifurcation, traveling pulses are observed in the region of coexistence between stationary and oscillatory patterns, zone III. Decreasing δ, both regions of oscillatory patterns with broken $x \to -x$ symmetry, and traveling pulses move to larger detuning. Therefore, in quasireversible limit, $\delta = 0$, those areas vanish from the bifurcation diagram.

Parametrically driven magnetic wire. Let us consider a ferromagnetic wire along the z axis. In the continuous framework, the material is described by its normalized magnetization $\mathbf{m} = \mathbf{m}(t,z)$, where $\{z,t\}$ are the spatial coordinates along the wire and the time, respectively. The evolution of the magnetization obeys the Landau-Lifshitz-Gilbert equation [29],

$$\frac{\partial \mathbf{m}}{\partial t} = -\mathbf{m} \times \mathbf{h}_{\text{eff}} + \alpha\mathbf{m} \times \frac{\partial \mathbf{m}}{\partial t}. \quad (2)$$

The first term on the right-hand side of Eq. (2) accounts for the conservative precessions generated by the effective field,

$\mathbf{h}_{\text{eff}} \equiv h\mathbf{e}_x - \beta m_z \mathbf{e}_z + \partial_{zz}\mathbf{m}$, where $\{\mathbf{e}_x, \mathbf{e}_y, \mathbf{e}_z\}$ denote the unit vectors along the respective Cartesian axis and h is the intensity of the external field $\mathbf{h} = h\mathbf{e}_x$. The coefficient $\beta > 0$ accounts for the anisotropy of the wire and it penalizes the magnetization along the z axis. Finally, the Laplacian of the magnetization stands for the ferromagnetic exchange interaction and it favors the homogeneous magnetic configurations.

The second term of Eq. (2) is the phenomenological Gilbert damping. Equation (2) has two trivial equilibria, $\mathbf{m} = \pm\mathbf{e}_x$. For positive external field, $h > 0$, $\mathbf{m} = \mathbf{e}_x$ is the most favored state. The dynamics around this equilibrium is characterized by damped oscillations with frequency $\omega_0 = \sqrt{H_0(H_0 + \beta)}$. Considering a combination of a constant and a periodic external magnetic field, $h(t) = H_0 + h_0 \cos[2(\omega_0 + \nu)t]$, the magnetic wire behaves as a parametrically driven oscillatory medium. Therefore, in a certain range of parameters the system must exhibit traveling pulse immersed in patterns. Figure 1 shows the profile and spatiotemporal evolution of traveling pulses observed in the magnetic wire.

To understand the origin of these pulses, we consider the following ansatz:

$$\begin{pmatrix} m_y \\ m_z \end{pmatrix} = \sqrt{\frac{4\omega_0}{\beta(\omega_0^2 + 3H_0^2)}} A(t,z) e^{i\phi(t)} \begin{pmatrix} \sqrt{H_0 + \beta} \\ -i\sqrt{H_0} \end{pmatrix}$$
$$+ \text{c.c.} + \vec{W}, \tag{3}$$

with $m_x = \sqrt{1 - m_y^2 - m_z^2}$, $\phi(t) = \omega_0 t + \nu t + \pi/4$, the symbol c.c. stands for complex conjugate, and $\vec{W}$ is a small correction vector that accounts for the higher order terms in the amplitude A. Replacing the above ansatz in Eq. (2), linearizing in $\vec{W}$, and imposing a solvability condition, after straightforward calculations, we obtain

$$\partial_t A = -i(\nu A + |A|^2 A + \partial_{\xi\xi}A) - \mu A + \gamma \bar{A} + i c_1 |A|^2 \partial_{\xi\xi}A$$
$$+ i c_2 A^2 \partial_{\xi\xi}\bar{A} + i c_3 A |\partial_\xi A|^2 + i c_1 \bar{A}(\partial_\xi A)^2, \tag{4}$$

where $\mu \equiv \alpha(2H_0 + \beta)/2$, $\gamma \equiv \beta h_0/(4\omega_0)$, $c_1 = d\beta(4H_0 - \beta)/2$, $c_2 = -d(\beta^2 + 12H_0\beta + 16H_0^2)/4$, $c_3 = -d(\beta^2 + 4H_0\beta + 8H_0^2)$, $d = 4\omega_0/[\beta H_0(2H_0 + \beta)(4H_0 + \beta)]$, and the spatial coordinate ξ is related to the original coordinate by $\xi \equiv \sqrt{2\omega_0/(2H_0 + \beta)}z$. In the quasireversible limit, the last four terms in the above equation are negligible. In this limit the forcing magnetic wire is described by the PDNLS equation. This equation allows one to study different localized states such as dissipative solitons [15,30–35] and localized waves [17,36]. Both Eqs. (1) and (4) share the same pattern instability and traveling pulses. Hence, the magnetic wire forced with a transverse oscillatory magnetic field can be modeled phenomenologically by the amplitude equation (1).

In conclusion, we have studied the emergence of traveling pulses immersed in one-dimensional patterns in the context of parametric systems. As results of the subcritical parity-breaking Andronov-Hopf bifurcation of the stationary pattern, the system exhibits a coexistence region between stable stationary and unstable oscillatory patterns. Within this coexistence region, we observe traveling pulses. Depending on the initial condition, we found a single and multiple pulses solutions. A simple PDNLS-like model allows us to explain the pulses dynamics as an effect of the nonlinear gradients of the full system. This simple model also allows us to predict traveling pulses in a magnetic wire forced with an external transverse oscillatory magnetic field.

[1] G. Nicolis and I. Prigogine, *Self-Organization in Nonequilibrium Systems* (Wiley, New York, 1977).

[2] M. C. Cross and P. C. Hohenberg, Pattern formation outside of equilibrium, Rev. Mod. Phys. **65**, 851 (1993).

[3] P. Brunet, J. M. Flesselles, and L. Limat, Elastic properties of a cellular dissipative structure, Euro. Phys. J. B **35**, 525 (2003).

[4] L. Pan, and J. R. de Bruyn, Spatially uniform traveling cellular patterns at a driven interface, Phys. Rev. E **49**, 483 (1994).

[5] P. Coullet, R. E. Golstein, and G. H. Gunaratne, Parity-Breaking Transitions of Modulated Patterns in Hydrodynamic Systems, Phys. Rev. Lett. **63**, 1954 (1989).

[6] C. Counillon, L. Daudet, T. Podgorski, and L. Limat, Dynamics of a Liquid Column Array under Periodic Boundary Conditions, Phys. Rev. Lett. **80**, 2117 (1998).

[7] P. Brunet, Stabilized Kuramoto-Sivashinsky equation: A useful model for secondary instabilities and related dynamics of experimental one-dimensional cellular flows, Phys. Rev. E **76**, 017204 (2007).

[8] P. Coullet and G. Iooss, Instabilitiy of One-Dimensional Cellular Patterns, Phys. Rev. Lett. **64**, 866 (1990).

[9] L. Gil, Instabilities of one-dimensional cellular patterns: Far from the secondary threshold, Europhys. Lett. **48**, 156 (1999).

[10] L. Gil, Secondary instability of one-dimensional cellular patterns: A gap soliton, black soliton and breather analogy, Physica D **147**, 300 (2000).

[11] L. D. Landau and E. M. Lifshitz, *Mechanics*, Course of Theoretical Physics Vol. 1 (Pergamon, New York, 1976).

[12] M. Faraday, On a peculiar class of acoustical figures; and on certain forms assumed by groups of particles upon vibrating elastic surfaces, Philos. Trans. R. Soc. London **121**, 299 (1831).

[13] J. W. Miles, Parametrically excited solitary waves, J. Fluid Mech. **148**, 451 (1984).

[14] M. G. Clerc, S. Coulibaly, N. Mujica, R. Navarro, and T. Sauma, Soliton pair interaction law in parametrically driven Newtonian fluid, Philos. Trans. R. Soc., A **367**, 3213 (2009).

[15] I. V. Barashenkov, M. M. Bogdan, and V. I. Korobov, Stability diagram of the phase-locked solitons in the parametrically

driven, damped nonlinear Schrödinger equation, Europhys. Lett. **15**, 113 (1991).

[16] S. R. Woodford and I. V. Barashenkov, Stability of the Bloch wall via the Bogomolnyi decomposition in elliptic coordinates, J. Phys. A: Math. Theor. **41**, 185203 (2008).

[17] M. G. Clerc, S. Coulibaly, and D. Laroze, Localized states of parametrically driven easy-plane ferromagnetic wire, Physica D **239**, 72 (2010).

[18] M. G. Clerc, S. Coulibaly, and D. Laroze, Localized states beyond the asymptotic parametrically driven amplitude equation, Phys. Rev. E **77**, 056209 (2008).

[19] B. Denardo, B. Galvin, A. Greenfield, A. Larraza, S. Putterman, and W. Wright, Observations of localized structures in nonlinear lattices: Domain walls and kinks, Phys. Rev. Lett. **68**, 1730 (1992).

[20] J. N. Kutz, W. L. Kath, R.-D. Li, and P. Kumar, Long-distance pulse propagation in nonlinear optical fibers by using periodically spaced parametric amplifiers, Opt. Lett. **18**, 802 (1993).

[21] S. Longhi, Stable multipulse states in a nonlinear dispersive cavity with parametric gain, Phys. Rev. E **53**, 5520 (1996).

[22] A. O. León and M. G. Clerc, Spin-transfer-driven nano-oscillators are equivalent to parametric resonators, Phys. Rev. B **91**, 014411 (2015).

[23] S. Douady, S. Fauve, and C. Laroche, Subharmonic instabilities and defects in a granular layer under vertical vibrations, Europhys. Lett. **8**, 621 (1989).

[24] I. Espinoza, Control de solitones disipativos en un fluido forzado paramétricamente, Pontificia Universidad Católica de Chile, 2009.

[25] A. J. Simon, J. Bechhoefer, and A. Libchaber, Solitary Modes and the Eckaus Instability in Directional Solidification, Phys. Rev. Lett. **61**, 2574 (1988).

[26] M. G. Clerc, S. Coulibaly, and D. Laroze, Parametrically driven instabilities in quasi-reversal systems, Int. J. Bifurcation Chaos **19**, 3525 (2009).

[27] W. H. Press, S. A. Teukolsky, W. T. Vetterling, and B. P. Flannery, *Numerical Recipes in C: The Art of Scientific Computing* (Cambridge University Press, New York, 1992).

[28] P. Coullet, T. Frisch, and G. Sonnino, Dispersion-induced patterns, Phys. Rev. E **49**, 2087 (1994).

[29] I. D. Mayergoyz, G. Bertotti, and C. Serpico, *Nonlinear Magnetization Dynamics in Nanosystems* (Elsevier, Oxford, 2009).

[30] I. V. Barashenkov and E. V. Zemlyanaya, Traveling solitons in the damped-driven nonlinear Schrödinger equation, SIAM J. Appl. Math. **64**, 800 (2004).

[31] I. V. Barashenkov, E. V. Zemlyanaya, and T. C. van Heerden, Time-periodic solitons in a damped-driven nonlinear Schrödinger equation, Phys. Rev. E **83**, 056609 (2011).

[32] I. V. Barashenkov and E. V. Zemlyanaya, Soliton complexity in the damped-driven nonlinear Schrödinger equation: Stationary to periodic to quasiperiodic complexes, Phys. Rev. E **83**, 056610 (2011).

[33] D. Urzagasti, D. Laroze, M. G. Clerc, S. Coulibaly, and H. Pleiner, Two-soliton precession state in a parametrically driven magnetic wire, J. Appl. Phys. **111**, 07D111 (2012).

[34] M. G. Clerc, M. A. Garcia-Ñustes, Y. Zárate, and S. Coulibaly, Phase shielding soliton in parametrically driven systems, Phys. Rev. E **87**, 052915 (2013).

[35] D. Urzagasti, D. Laroze, M. G. Clerc, H. Pleiner, Breather soliton solutions in a parametrically driven magnetic wire, Europhys. Lett. **104**, 40001 (2013).

[36] M. G. Clerc, S. Coulibaly, and D. Laroze, Localized waves in a parametrically driven magnetic nanowire, Europhys. Lett. **97**, 30006 (2012).

Apéndice E

Alternating superlattice textures in driven nanomagnets

This chapter presents two-dimensional oscillatory pattern states.

Preprint details:

Title: Alternating superlattice textures in driven nanomagnets.

Authors: Alejandro O. León, David Laroze, Marcel G. Clerc, and Ana M. Cabanas.

Corresponding author: Alejandro O. León.

In preparation for being submitted to: Communications in Nonlinear Science and Numerical Simulation.

Alternating superlattice textures in driven nanomagnets

Alejandro O. Leon[a,*], David Laroze[b], Marcel G. Clerc[a], Ana M. Cabanas[b]

[a]*Departamento de Física, Facultad de Ciencias Físicas y Matemáticas, Universidad de Chile, Casilla 487-3, Santiago, Chile*
[b]*Instituto de Alta Investigación, Universidad de Tarapacá, Casilla 7D, Arica, Chile*

Abstract

Nanomagnets driven with uniform electric currents exhibit a wide variety of spatial textures. In the present work, we investigate alternating superlattice states in nanomagnets, which are spatially periodic textures composed by several spatial modes that oscillate in time. The magnetic system is described in the continuum approach by the Landau-Lifshitz-Gilbert-Slonczewski equation, and direct numerical simulations of this model allow us to characterize the alternating patterns. As a result of this temporal oscillation, textures alternate between different shapes. In particular, we focus on two types of textures, namely a superhexagon and a square-like pattern, which are composed by six and two dominant Fourier modes, respectively. Based on an appropriate modal decomposition, we reveal that the mechanism that originates the alternating superhexagon is a homoclinic bifurcation. In addition, we show that the oscillatory square-like texture emerges through a supercritical Andronov-Hopf bifurcation.

1. Introduction

Macroscopic systems exhibit spatial patterns as a result of the competition between dissipation and injection of energy, momentum and particles [1, 2]. Examples of patterns can be found in different branches of science and within a wide range of spatial scales, such as stripes in zebra's skin, ocean waves, vegetal population spots, sand ripples, convection rolls in fluids, to mention a few. From the mathematical point of view, regular patterns are spatially periodic states composed by spatial modes with one or a few intrinsic wavenumbers [2]. At the onset of the spatial bifurcation that originates the patterns, the dynamical evolution of the system is governed by the critical modes of the instability, while all the other degrees of freedom are slave variables and then they are functions of the critical modes. In two spatial dimensions, the most common observed patterns are stripes (one roll-like mode), squares (two roll-like modes), and hexagons (three roll-like modes). On the other hand, superlattices are an example of more sophisticated structures because they are composed by at least four interacting modes [2]. The analytical description of pattern forming systems is usually performed by means of amplitude equations [1]. This approach permits predicting the shape of the pattern and obtaining simple mathematical expressions for the mode envelopes as functions of the physical parameters of the system. In the case of stationary spatial instabilities, amplitude equations usually take the form of relaxation equations, and therefore they only predict steady states.

When the energy injection is increased, stationary patterns might become dynamic states, which is a secondary bifurcation of the system [1]. An example of dynamic textures is alternating patterns, in which the dissipative structure oscillates in time, and the envelopes of spatial modes alternate between large and small values. Alternation between simple lattices were observed in Rayleigh-Bénard experiments [3, 4], where a fluid mixture is heated from below and cooled from the top. In this case, the fluid alternates between two types of convection patterns, namely rolls and squares, as a result of a supercritical Andronov-Hopf instability of a stationary square texture. This type of secondary bifurcation is described by the well known Ginzburg-Landau equation, however the derivation of this equation requires to know the analytical expression of the stationary pattern, which is usually unknown. Therefore, the derivation of the corresponding amplitude equations is a complicated task. An alternative strategy to study secondary instabilities is by means of a truncated modal decomposition of the equations into an arbitrary number of modes, this approach is known as the Galerkin expansion. For the case of Rayleigh-Bénard experiment, the alternating patterns were studied theoretically using the Galerkin method [5]; which permitted transforming of the spatiotemporal dynamics into a set of Lorentz-type equations, where the analytical calculations and the numerical characterization become easier. During last decade, several other examples of alternating patterns have been observed and studied in the context of fluid convection [6–12]; the mechanisms that originate the oscillatory states are homoclinic bifurcations, homoclinic gluing, and Andronov-Hopf instabilities. Another example of alternating patterns appears in vertically vibrated fluids [13], where the profile of the fluid surface exhibits an hexagon-stripe-hexagon temporal sequence. Vibrated fluids are an example of parametrically driven systems, where the forcing mechanism oscillates in time.

---

[*]Corresponding author
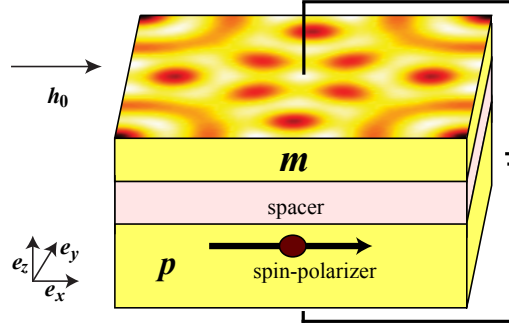   *Email address:* `aoleon@dfi.uchile.cl` (Alejandro O. Leon)

Figure 1: (Color online) Spin-valve device composed by two ferromagnets and one spacer. The thicker material with *fixed* magnetization **p** polarizes or filters the spins of the electric current, while the other ferromagnetic layer with *free* magnetization **m** interacts with the current and the external field **h₀**; we are interested in the dynamics of this magnet. The two materials are separated by a nonmagnetic metal to avoid magnetostatic interactions between them. The rest of the structure (not shown) is composed by non-magnetic metals.

Let us consider the particular case of driven magnetic systems. At nano-scales, magnetic devices can be kept out of the thermodynamic equilibrium by means of spin-transfer torques [15, 16]. The spin-transfer torque effect is based on the interaction between the spins of the magnetic medium and the spins of the electric current. The dynamical responses of nanomagnets to spin-transfer torques include limit-cycles [17–19], magnetic reversions [19], chaos [20], patterns [21–23], vortex lattices [24, 25], solitons [14, 26], among others. This versatility of the spin-transfer torque renders it the ideal effect to manipulate magnetization, read and record information, and generate micro-frequency spin-waves [27]. Recently, a relationship between parametrically driven systems and nanomagnets forced with direct electric current has been established [14]. Moreover, both systems can be described by the same normal form equations and they show similar states such as solitons and patterns, even if the electric current is constant in time for the forced magnet. Therefore, driven nanomagnets can exhibit alternating patterns which are found in vibrated fluids.

The aim of this article is to study alternating superlattice textures in nanomagnets driven by spin-transfer torques. In particular, we focus on two states, superhexagons and square-like patterns. Using an appropriate modal decomposition of the magnetization equations, we show that the alternating superhexagons emerge through a homoclinic bifurcation. In the case of square-like patterns, the origin of the oscillations is a supercritical Andronov-Hopf instability. The article is organized as follows: in the next section we describe the physical system and the spatial instability responsible for pattern formation. In Sec. 3 we describe alternating superhexagons by means of direct numerical simulations and a modal decomposition. The last approach permits us to explain the emergence of dynamical patterns in terms of low-dimensional bifurcations. In Sec. 4 we study an oscillatory square-like state that emerges through an Andronov-Hopf instability. Finally, the conclusions are presented in Sec. 5.

2. Driven nanomagnets and magnetic textures formation

Let us consider a *spin-valve* device, which is metallic structure composed by two ferromagnets and one spacer between them. A schematic setup is shown in Fig. 1. Spin-valves usually have lateral dimensions of $L \sim 100nm$. One ferromagnet is thicker than the other and it has a *fixed* magnetization that filters or polarizes the spins of the current towards the fixed magnetization direction **p**. The other ferromagnet is a thin film known as *free* layer, and it interacts with the current and external fields. The rest of the structure is composed by conducting materials. We are interested in the dynamics of the free layer, which is described by its magnetization field vector $\mathbf{M} = \mathbf{M}(T, \mathbf{R})$. We consider two forcing mechanisms, namely an external magnetic field $\mathbf{h_0} = h_0 \mathbf{e}_x$ and a spin-transfer torque generated by an electric current g that flows perpendicular to the planes of the layers. The magnetization dynamics are described by the dimensionless *Landau-Lifshitz-Gilbert-Slonczewski equation* [15, 28–30]

$$\frac{\partial \mathbf{m}}{\partial t} = -\mathbf{m} \times \left[(h_0 + \beta_x m_x)\mathbf{e}_x - \beta_z m_z \mathbf{e}_z + \nabla^2 \mathbf{m} \right] + g\mathbf{m} \times (\mathbf{m} \times \mathbf{e}_x) + \alpha \mathbf{m} \times \frac{\partial \mathbf{m}}{\partial t}, \tag{1}$$

where $\mathbf{m} = \mathbf{M}/M_s$ such that M_s is the saturation magnetization. The variables $t = T/(\gamma M_s)$ and $\mathbf{r} = \mathbf{R}/l_{ex} = x\mathbf{e}_x + y\mathbf{e}_y$ stand for the dimensionless time and space coordinates over the layer, respectively. Here the characteristic temporal γM_s and spatial l_{ex} scales are material properties. For example, for a cobalt layer of $3nm$ of thickness, $M_s \simeq 1.4\ 10^6 A/m$, and the characteristic scales are $(\gamma M_s)^{-1} \simeq 3.2ps$, and $l_{ex} \simeq 3.4nm$ [28]. The gradient operator is defined as $\nabla \equiv \mathbf{e}_x \partial_x + \mathbf{e}_y \partial_y$. The unitary vectors $\{\mathbf{e}_x, \mathbf{e}_y, \mathbf{e}_z\}$ are oriented along the corresponding Cartesian axis (see Fig. 1).

In addition, the coefficients of anisotropy β_x and β_z stand for the preferred directions of the magnetization, and they are combinations of the magnetocrystalline and demagnetizing effects, moreover β_x (β_z) favors (disfavors) configurations along the x-axis (z-axis).
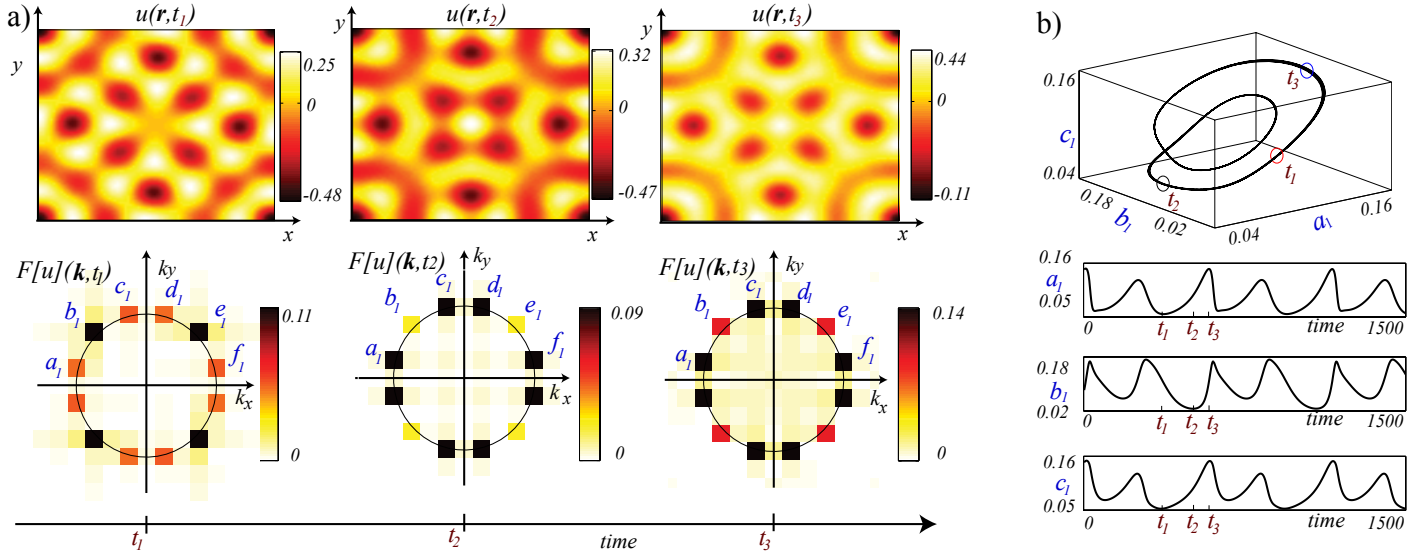
Figure 2: (Color online) Alternating superlattice state with six dominant Fourier modes (with their respective complex conjugate). (a) Three figures of a normalized magnetization component $u = m_y/(1 + m_x)$ are shown in the upper panel, while the lower panel illustrates the respective spatial Fourier spectra $F[u]$. The amplitude of the Fourier modes of u are $\{a_1, b_1, c_1, d_1, e_1, f_1\}$, we can define in a similar manner another reduced magnetization component, $v = m_z/(1 + m_x)$, and its respective Fourier amplitudes $\{a_2, b_2, c_2, d_2, e_2, f_2\}$. The modes oscillate between large and small values, moreover for the time t_2 the amplitude b_1 of the Fourier peak located on the diagonal almost disappears. (b) Trajectories $a_1(t)$, $b_1(t)$ and $c_1(t)$ are the envelopes of the modes shown in (a).

The coefficient β_z is small for devices where the perpendicular magnetocristalyne anisotropy partially cancels the demagnetization effect (see [44] and references therein). The laplacian term accounts for the ferromagnetic exchange and it smoothes nonuniformities. The spin-polarized electric current is modeled by the term proportional to g, while α is a phenomenological dissipation coefficient. The sample borders are taken into account using Neumann boundary conditions for the magnetization. Both the external field $\mathbf{h_0}$ and the polarization of the current $\mathbf{p}$ are to point along the x-axis direction, which permits one to switch the magnetization between equilibria $\mathbf{m} = \mathbf{e}_x$ and $\mathbf{m} = -\mathbf{e}_x$. We focus here on the regime in which the electric current stabilizes the state $\mathbf{m} = \mathbf{e}_x$, and the external field disfavors it; this competition of forces induces rich spatiotemporal dynamics. Let us remark that, here we only consider the dominant order physical effects, however additional terms can be included into Eq. (1), such as the full non-local demagnetizing field [41], and variable spin-transfer torque amplitude $g = g(\mathbf{m})$ [29].

Equation (1) has been extensively studied to explain and predict the emergence of limit-cycles [17–19], patterns [21–25], solitons [14, 26], among other states. Notice that the magnetization norm is a conserved quantity, $\partial_t |\mathbf{m}|^2 = \partial_t \mathbf{m} \cdot \mathbf{m} = 0$, and therefore the magnetization can be written in different representations such as spherical [23, 28], canonical [28] and stereographic [28, 31]. In the last case, the spherical surface is mapped to the equatorial plane $m_x = 0$ through the relation $A = (m_y + im_z)/(1 + m_x)$. In this representation, A is a complex amplitude that accounts for the deviations from the $\mathbf{m} = \mathbf{e}_x$ solution. After straightforward calculation one obtains the following generalized *Complex Ginzburg-Landau* equation

$$(i + \alpha) \frac{\partial A}{\partial t} = (ig - h_a) A - \frac{\beta_z}{2} \left(A - \overline{A}\right) \frac{1 + A^2}{1 + |A|^2} - \beta_x A \frac{1 - |A|^2}{1 + |A|^2} + \nabla^2 A - 2 \frac{\overline{A}}{1 + |A|^2} (\nabla A)^2, \tag{2}$$

where and $\bar{A}$ means the complex conjugate of A. The above model has been used to describe the dynamics of dissipative waves in several contexts [1, 2]. An interesting limit of Eq. (2) is obtained for the scaling $\alpha \ll |A|^2 \sim \partial_t \sim \partial_{xx} \sim \beta_z \sim |g| \sim |v| \ll 1$ and $|h_a| \sim \beta_x \sim 1$, where $-v = h_0 + \beta_x + \beta_z/2$; in this case, the generalized Complex Ginzburg-Landau equation takes the form of the well-known *parametrically driven, damped nonlinear Schrödinger* equation,

$$\frac{\partial \psi}{\partial t} = -iv\psi - i|\psi|^2\psi - i\nabla^2\psi - \mu\psi + \gamma\bar{\psi}, \tag{3}$$

where $\psi = \sqrt{2\beta_x}e^{i\pi/4}A$, $\mu = -g - \alpha v$, $\gamma = \beta_z/2$. The aforementioned equation has been used to describe several systems in presence of temporally-modulated forcings, known as parametrically driven systems. Furthermore, both driven nanomagnets and parametrically driven systems exhibit states such as localized states [32–41] and patterns [41–43]. This equivalence [14] between driven nanomagnets and parametrically forced systems suggests that the alternating textures found in vertically vibrated fluids [13] should also emerge in spin-transfer torque driven magnets.

Stationary patterns appear in spin-valves through a supercritical spatial instability of the uniform state $\psi = 0$ (see Refs. [14, 23]). In this bifurcation, small perturbations with wavenumber $q^2 = v = -(h_0 + \beta_x + \beta_z/2)$ are amplified in time when $g \geq -\beta_z/2$. The

existence of a real wavenumber $q^2 \geq 0$ is fulfilled when the external field is negative $h_0 \leq -(\beta_x + \beta_z/2) < 0$, that is, when the vector $\mathbf{h_0}$ points against the equilibrium $\mathbf{m} = \mathbf{e}_x$. Hence, patterns are the result of the competition between the spin-polarized current that stabilizes the $\psi = 0$ state and the external field that disfavours it ($h_0 < 0$). Using a normal form approach, it was obtained a general set of equations describing the critical modes compatible with the boundary conditions [23]. This analysis revealed that for applied fields above a critical value, that is $h_0 > h_0^c \equiv -4(\beta_x + \beta_z/2)$, stripes are the only stable pattern. On the other hand, when the field is below the critical value $h_0 < h_0^c$, all modes compatible with the boundary conditions grow and reach the same nonzero amplitude. In this scenario, a wide range of stationary superlattices emerges.

For negative external fields $h_0 < 0$, the electric current can switch the magnetization from $\mathbf{m} = +\mathbf{e}_x$ to $\mathbf{m} = -\mathbf{e}_x$ when g varies from negative to positive values. Hence, all the dissipative structures close to the equilibrium $\mathbf{m} = +\mathbf{e}_x$ in the phase space must become unstable when the current is increased. Indeed, increasing the control parameter g, which is equivalent to diminish dissipation [14] or increase injection, the system self-organizes into alternating superlattices (see Fig 2). The particular attractor usually depends on the external field h_0, the current g, the lateral dimension L and the initial condition. However, among the plethora of alternating textures that emerge in this system, two of them deserve special attention due to their regularity in Fourier space. The first one is the alternating superhexagon shown in Fig. 2, which is composed by six Fourier modes. We observe this texture for small applied fields close to $h_0 = -2.5$. The second alternating texture is a square-like pattern state. Square-like states exhibit a spectrum with two large peaks and several smaller peaks (cf. Fig. 7). They appear for large applied fields close to $h_0 = -6$. These states emerges through an Andronov-Hopf bifurcation of the stationary square-like texture. The next two sections are devoted to the description of such states.

3. Alternating superhexagons

Let us consider applied fields close to $h_0 = -2.5$. In this case, the typical oscillatory state is composed by six interacting modes, which gives the appearance of a temporal alternation between patterns of different shapes, namely a square, a supersquare and a superhexagon. Figure 2 illustrates this dissipative structure, which was obtained for the parameter values $g = -0.4911$, $\beta_x = 1/2$, $\beta_z = 1$, and $\alpha = 0.05$. The numerical simulation was conducted by dividing the sample into a grid of 90×90 squares of side length $dx = 0.230571$ (approximately 0.8 nm for cobalt). The spatial differential operators are approximated with centered schemes of order-6, while the time integration is performed using a fourth order Runge-Kutta algorithm with constant step-size $\Delta t = 0.01$ (approximately 0.03 ps for cobalt).

A simple physical quantity that characterizes the dynamics in time is spatial average of the magnetization, given by

$$\mathbf{m}^{av}(t) \equiv \frac{1}{L^2} \iint \mathbf{m}(t, \mathbf{r}) dx dy. \tag{4}$$

Figure 3(a) shows the temporal evolution of this average. The oscillation period is around $\Delta t \sim 350$, which is about 1 ns for common devices. The trajectories are characterized by sharp peaks, moreover, they are far from the shape of sinusoidal functions. This type of dynamical behavior suggests a homoclinic bifurcation as the creation mechanism of alternating superhexagons [45]. In systems with a homoclinic bifurcation, a limit-cycle approaches a saddle-point when a control parameter is varied, the limit-cycle eventually collides with the hyperbolic fixed point and it disappears. The signature of this bifurcation is that the oscillations evolves slowly in the vicinity of the saddle-point or stagnation point [45].
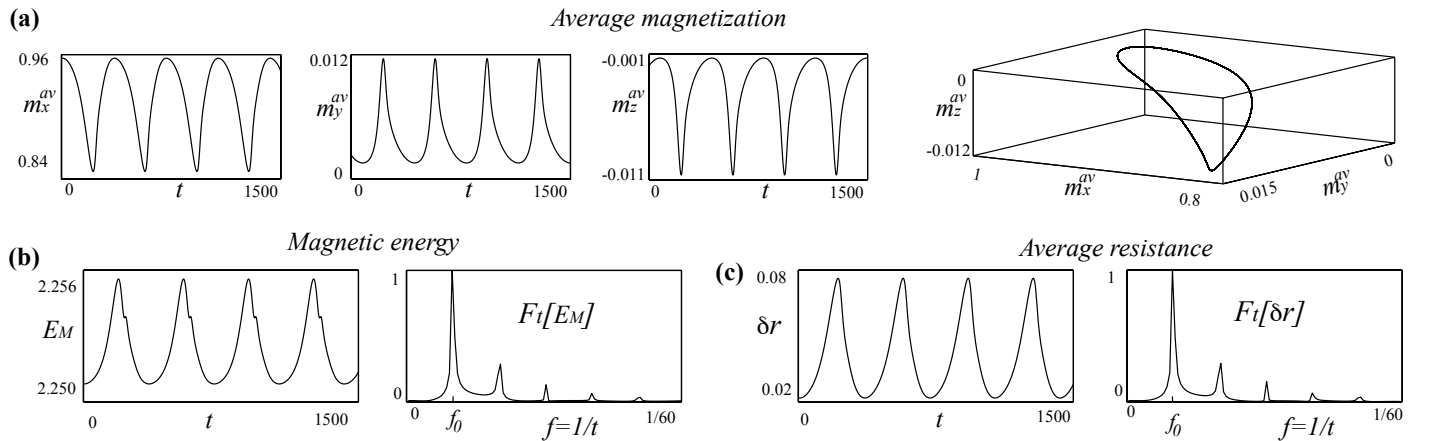

Figure 3: Temporal evolution of the average magnetization, magnetic energy, and average resistance for $g = -0.4945$. (a) Components of the average magnetization vector $\mathbf{m}^{av}$. (b) Magnetic energy. The time series $E_M(t)$ is shown on the left, while the normalized temporal Fourier transform $F_t = F[E_M - < E_M >](f)$ is shown on the right panel, where $f = 1/t$ is the frequency. (c) Average resistance profile $\delta r(t)$ (left) and its normalized temporal Fourier transform $F_t[\delta r](f)$ (right).
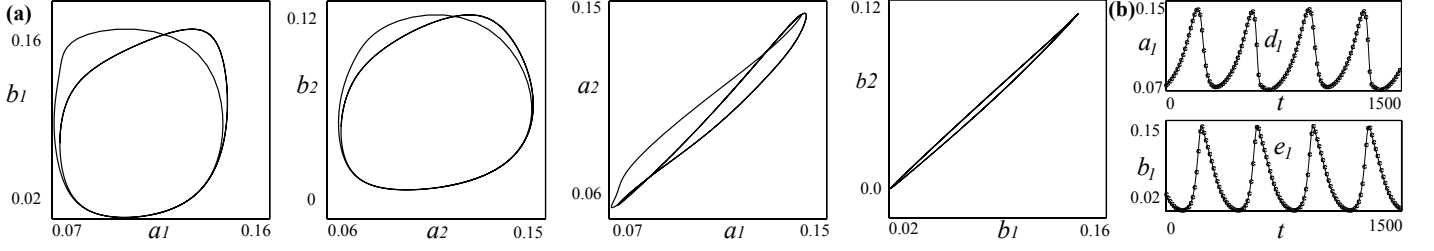
4

Figure 4: Temporal evolution of the Fourier modes of an alternating superhexagon. (a) The magnetization is projected into the three Fourier modes a, b and c (cf.2). The graph of the left panel illustrates the general form of the phase space of alternating superhexagons. (b) Temporal series of the modes envelopes. The solid lines show a_1 (up) and b_1 (down), while the points stand for d_1 (up) and f_1 (down). Thus, the amplitudes of such modes are the same.

A relevant quantity of ferromagnetic materials is the magnetic energy [28],

$$E_M = \frac{1}{L^2} \iint \left[-m_x h_0 - \frac{1}{2}\beta_x m_x^2 + \frac{1}{2}\beta_z m_z^2 + \frac{1}{2}\left(|\nabla m_x|^2 + |\nabla m_y|^2 + |\nabla m_z|^2\right)\right] dxdy. \tag{5}$$

The magnetic energy $E_M(t)$ is a global indicator that only depends in time, and then it provides information regarding the dynamics of the whole device. Figure 3(b) shows the temporal evolution of the energy. The energy remains close to the energy of films uniformly magnetized along $\mathbf{m} = +\mathbf{e}_x$, that is $E_M^{+1} = -h_0 - \beta_x/2$. Let us define the normalized Fourier spectrum of the magnetic energy as

$$F_t \equiv F_t[E_M - <E_M>](f), \tag{6}$$

where F_t is the normalized Fourier transform (that is, its maximum value is 1), and $<E_M>$ is the energy mean value. The spectra are characterized by one dominant peak at a frequency of $f_0 = 2.77 \times 10^{-3}$ (which is in the gigahertz domain for typical devices), and several harmonic peaks at frequencies nf_0, where $n = 2, 3, ...$

Another relevant dynamical indicator is the reduced magnetoresistance of the device,

$$\delta r \equiv \frac{R[m_x] - R[1]}{R[-1] - R[1]} = \frac{1}{L^2} \iint \frac{1 - m_x}{2} dxdy, \tag{7}$$

where R is the electrical resistance of the spin-valve, which can be measured experimentally. The spatial average used in formula (7) is the generalization of the magnetoresistance calculated for uniformly magnetized free layers. Figure 3(c) illustrates the behavior of the reduced resistance and its normalized Fourier spectrum (obtained with an expression similar to formula (6)). Hence, the signature of alternating super-hexagons is a dominant frequency close to f_0 in the magnetoresistance.

Let us focus on the modal decomposition of Fig. 2. In the context of nanomagnetism the device lateral dimensions are small, that is $L \sim 50 - 100nm$, and then a few wavenumbers are admitted inside the ferromagnetic layer; this favors a defect-free texture. Moreover, as the lower panel of Fig. 2 shows, the dominant Fourier peaks are close to the critical wavenumber of the spatial instability $|\mathbf{k}| \approx q$, while the amplitude of the other modes are negligible. This is because the primary and the secondary bifurcations, responsible of the emergence of stationary and oscillatory patterns respectively, occur for close values of the electric current. The Fourier spectrum is characterized by large peaks at the following wavevectors $\mathbf{q_1} = \Delta k(-4, 1)$, $\mathbf{q_2} = \Delta k(-1, 4)$, $\mathbf{q_3} = \Delta k(1, 4)$, $\mathbf{q_4} = \Delta k(4, 1)$, $\mathbf{Q_1} = \Delta k(-3, 3)$, and $\mathbf{Q_2} = \Delta k(3, 3)$, and their negative counterparts. The geometrical factor $\Delta k = 2\pi/L$ accounts for the minimal wavenumber that is admitted by the boundary conditions.

We observe that the envelopes of the pattern evolve in twin pairs, that is, $a_1 = d_1$, $b_1 = e_1$, and $c_1 = f_1$. Figure 4(b) illustrates the typical correlated trajectories. The same holds for the spectrum of the imaginary part of A, that is, $a_2 = d_2$, $b_2 = e_2$, and $c_2 = f_2$. Therefore, the effective degrees of freedom of this system are the amplitudes of three interacting square lattices. Figure 2(b) shows the temporal evolution of the envelopes of each square.

The texture oscillations become slower and more regular when the electric current approaches the value $g_c = -0.4953$. Moreover, for electric currents below the critical value g_c, the limit-cycle is not observed and the magnetization self-organizes into a stationary pattern. In this region, the numerical integration of the system is time-consuming, which makes difficult to elucidate the formation mechanism of the alternating structures. In the next subsection we obtain a reduced representation of the superhexagon by means of a Galerkin expansion.

3.1. Four-modes Galerkin expansion

The normal form approach allows one to obtain a set of amplitude equations $dA_j/dt = -\delta H/\delta\bar{A}_j$ for different types of patterns [23], where the Lyapunov function H is minimized along the evolution of the system. This method permits one to characterize stationary structures at the onset of the bifurcation, however, permanent behaviors, such as chaos and oscillations, are forbidden.
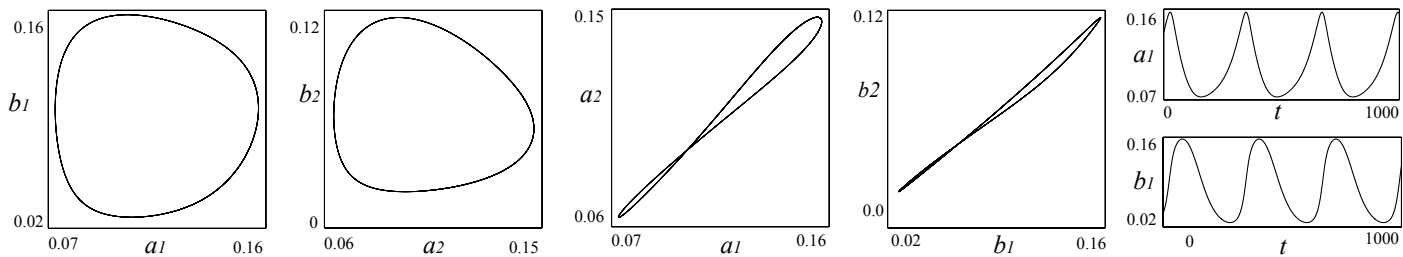
Figure 5: Phase portrait of Galerkin modes. (a) limit-cycle in the modes representation. (b) Trajectories of the Galerkin modes.

Another strategy to simplify the dynamics is to project the equations into a few relevant modes, a Galerkin expansion. This type of modal decomposition allows the study permanent dynamics, because they are not subjected to the minimization of a Lyapunov function [5].

Following the Galerkin approach of Ref. [5], we decompose the spatiotemporal magnetization dynamics into a few trajectories for the relevant observed modes, using the following ansatz for the stereographic projection $A(t, \mathbf{r}) = A_r + iA_i$

$$\begin{pmatrix} A_r \\ A_i \end{pmatrix} = \begin{pmatrix} -a_1 \\ a_2 \end{pmatrix} [\cos(\mathbf{q_1} \cdot \mathbf{r}) + \cos(\mathbf{q_2} \cdot \mathbf{r}) + \cos(\mathbf{q_3} \cdot \mathbf{r}) + \cos(\mathbf{q_4} \cdot \mathbf{r})] + \begin{pmatrix} -b_1 \\ b_2 \end{pmatrix} [\cos(\mathbf{Q_1} \cdot \mathbf{r}) + \cos(\mathbf{Q_2} \cdot \mathbf{r})], \tag{8}$$

where the real-valued functions $a_1(t)$ and $a_2(t)$ are the envelopes of the supersquare pattern given by the wavevectors $\{\mathbf{q_1}, \mathbf{q_2}, \mathbf{q_3}, \mathbf{q_4}\}$. For the sake of simplicity, we use the same amplitude for the square sub-lattices given by $\{\mathbf{q_1}, \mathbf{q_3}\}$ and $\{\mathbf{q_2}, \mathbf{q_4}\}$. The variables $b_1(t)$ and $b_2(t)$ are the real-valued amplitudes of the square pattern defined by the wavevectors $\{\mathbf{Q_1}, \mathbf{Q_2}\}$. Writing Eq. (2) into its real and imaginary parts, using expression (8), and projecting over the spatial modes (using the inner product for Fourier spaces), we obtain a simple dynamical system of the form

$$\frac{d\mathbf{X}}{dt} = \mathbf{F}(\mathbf{X}), \tag{9}$$

where $\mathbf{X} = (a_1, a_2, b_1, b_2)^T$. Due to the long expression of $\mathbf{F}$, its explicit form and the details of the projection method are given in AppendixA. In order to understand and characterize the origin mechanism of the alternating superlattice states described in Sec. 3, we integrate the set of Eqs. (9) using a fifth-order Runga-Kutta routine with variable step size and the same parameter values as in Sec. 3. Figure 4 shows the typical limit-cycle solution obtained for $g = -0.4911$. The trajectories are characterized by a slow motion in a determined region of the phase space (stagnation point, close to $a_1 = a_2 = 0$), moreover, when the current is decreased, the time that the trajectories spend in this region is increased.

Notice that we use an ansatz with only four amplitudes, which is the minimal modal decomposition that permits obtaining qualitative agreement with the magnetic equations and, at the same time, provides the possibility to identify the formation mechanism of superhexagons. A more general decomposition with more modes is required to obtain a better quantitative agreement with the magnetic equations. However, this four-modes expansion is complete enough to obtain information of the alternating superhexagons.

The characteristic limit-cycle amplitude and period are shown in Fig. 3.1. As it can be seen, the amplitude appears abruptly, which agrees with the direct numerical simulations of the magnetic equations. Moreover, decreasing the control parameter g, the oscillation
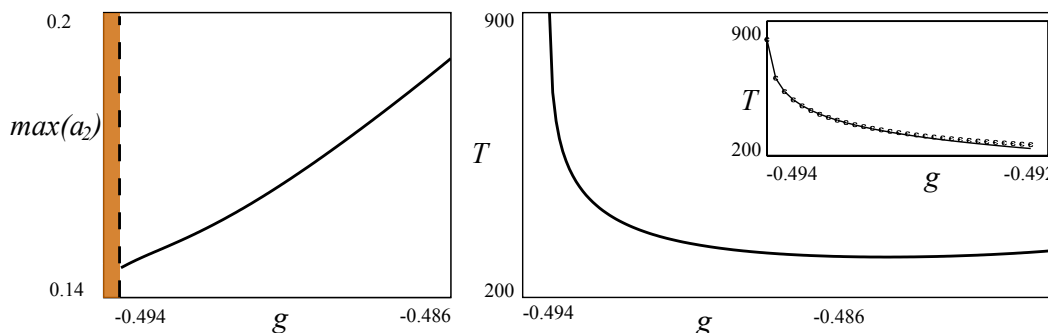

Figure 6: (Color online) Characteristic limit-cycle amplitude (left) and period (right). There is no limit-cycle for electric currents below a threshold (darker zone in the amplitude plot), the oscillations emerge abruptly for $g = -0.494$. At the onset of the emergence of the oscillations, the amplitude is finite and the period T has a logarithmic divergence. The inset shows a comparison between the data of the numerical integration (dots) and fitting curve $T \simeq 113.21 \log[1/(g + 0.49361)] - 398.54$.

6

period diverges with a logarithmic law $T \simeq 113.21 \log[1/(g - g_c)] - 398.54$, where $g_c = -0.49361$. This particular divergence law permits us to conclude that the mechanism is a homoclinic bifurcation.

The Galerkin expansion **f** will have only odd nonlinearities because model (2) is invariant under inversions of the order parameter $(A \rightarrow -A)$. According to our simulations, the quintic term is necessary to observe limit-cycles. Therefore, the relevant nonvariational interaction between modes occurs through a coupling of fifth order.

In the previously studied spin-transfer torque induced limit-cycles [17–19], the dissipation α plays an important role. Indeed, limit-cycles are the result of the balance between the dissipation α and the injection $g > 0$. However, in the case of alternating superlattices, we observe that the dissipation coefficient α does not produce relevant changes in the dynamics. Furthermore, in the limit $\alpha = 0$ the oscillatory states do not change appreciably. Hence, we conclude that the spin-transfer torque is the dominant dissipation mechanism of alternating superlattices.

4. Oscillatory square-like texture

A different scenario occurs for large applied external fields, where the alternating patterns are composed by a few dominant modes. For external fields around $h_0 = -6$, the typical oscillatory structure is a square-like pattern. Figure 7 illustrates this texture which was obtained for $g = -0.41$, and spatial and temporal step-sizes are $dx = 0.157861$ (approximately 0.51 nm) and $\Delta t = 0.004$ (approximately 0.013 ps), respectively. As it can be seen from this figure, the envelopes of the horizontal and the vertical rolls oscillate in time. The two rolls have orthogonal wavevectors $\mathbf{q_1} = q(1, 0)$, $\mathbf{q_2} = q(0, 1)$, where q is the critical wavenumber of the spatial instability found in Ref. [23]. This oscillatory state is similar to the one observed in fluids heated from bellow [3, 4], where the two-mode texture oscillates in time.

The temporal evolution of the two dominant modes is approximately sinusoidal [see Fig. 7(b)], with period around $\Delta t = 100$, which is about 0.32 ns for cobalt. In addition, the amplitude of the temporal oscillation of each mode decreases monotonically when g is decreased, until the oscillations disappear at $g'_c \approx -0.43$, see Fig. 8. These two features are the signature of a supercritical Andronov-Hopf bifurcation [45]. This instability is usually characterized by the complex Ginzburg-Landau equation, which contains the dominant order terms compatible with the symmetries of the physical system and the instability [1]

$$\frac{dH}{dt} = (g - g'_c)H - (\Gamma_0 + ic)H|H|^2, \tag{10}$$

where the order parameter $H(t)$ stands for the oscillation envelope, Γ_0 is the nonlinear coefficient, which is positive. The parameter c accounts for the coupling between the oscillation frequency and amplitude. The stationary solutions of the above model have modulus $|H| = [(g - g'_c)/\Gamma_0]^{1/2}$. Figure 8 shows the solution of the Ginzburg-Landau model using $\Gamma_0 = 4.9383$ (solid line) and the oscillation envelope obtained from direct numerical simulations of the magnetic equations (points). The agreement is fairly good.
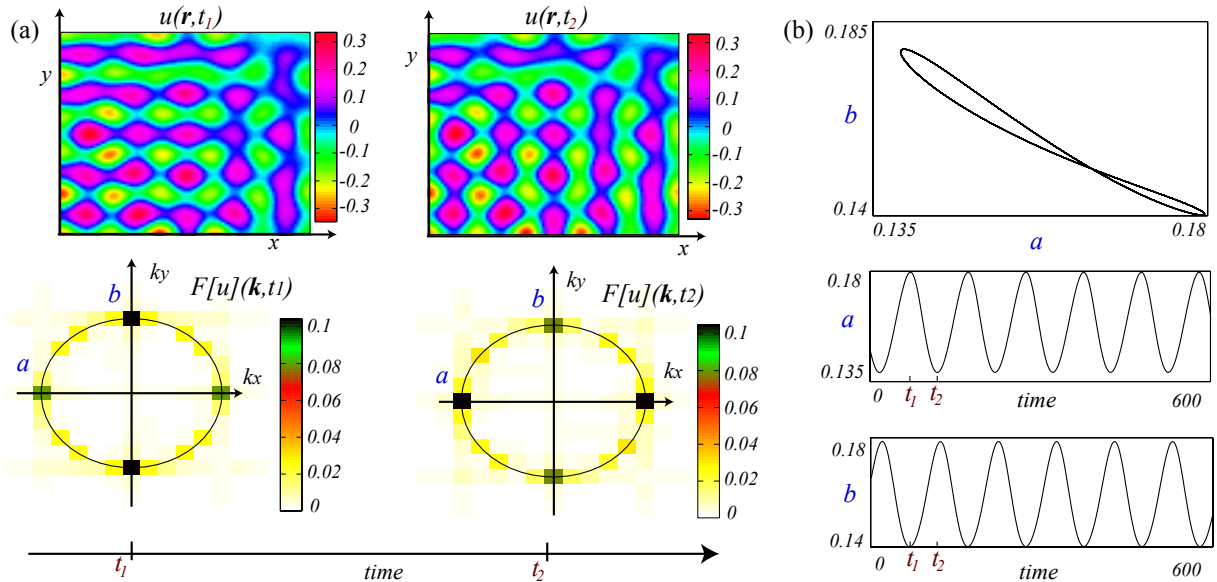

Figure 7: (Color online) Oscillatory square-like state obtained for $h_0 = -6$ and $g = -0.41$. (a) Plots of u, the real part of A (upper panel) and its respectively spatial Fourier transform (bottom panel). (b) Projection of trajectory in envelopes space and temporal evolution of the dominant envelopes.
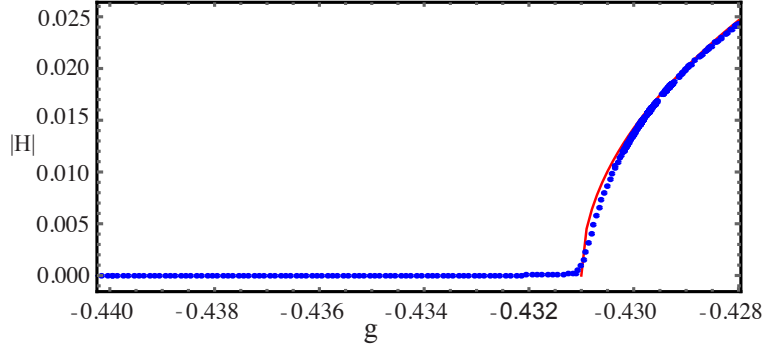
Figure 8: (Color online) Oscillation amplitude for square-like alternating texture. The oscillation envelope obeys a law $|H| = (g - g_c')^{1/2}$, this curve is plotted in solid line. Points account for the data of the direct numerical simulation.

The oscillations of the magnetization spatial average $\mathbf{m}^{av}(t)$ are shown in Fig. 9(a) and they are very close to the steady state $\mathbf{m} = +\mathbf{e}_x$. Notice that the nonlinear transformation between the dynamical variables (stereographic representation) and the Cartesian components

$$\left(m_x, m_y, m_z\right) = \frac{1}{1 + |A|^2} \left(1 - |A|^2, A + \bar{A}, i[\bar{A} - A]\right),\tag{11}$$

generates additional frequencies (harmonics) in the temporal Fourier spectrum. Hence, both the magnetic energy and the average resistance will have extra frequencies. Figure 9(b) shows the temporal evolution of the energy, which again is close to the value $E_M^{+1} = -h_0 - \beta_x/2$. The energy spectrum is characterized by two dominant peaks at a frequency of $f_1 = 0.01$ and $f_2 = 2f_1$ (which is in the gigahertz domain for typical devices), and several other peaks at frequencies nf_1, where $n = 2, 3, ..$; Figure 9(c) illustrates the behavior of the average resistance and its normalized Fourier spectrum.

5. Conclusions and remarks

In recent decades, most scientific efforts have concentrated on understanding primary spatial instabilities. However, due to the complex spatiotemporal behavior exhibited by secondary instabilities, several questions still remain unanswered. Here, we have investigated alternating superlattices—oscillatory patterns with several Fourier modes—induced by spin-transfer torques. The envelopes of the modes alternate between small and large values, which produces textures of different shapes. We focused mainly on alternating superhexagons and square-like patterns, which are oscillatory states composed by six and two dominant spatial modes, respectively. Using a simple modal decomposition, we showed that superhexagons emerge through a homoclinic bifurcation. We
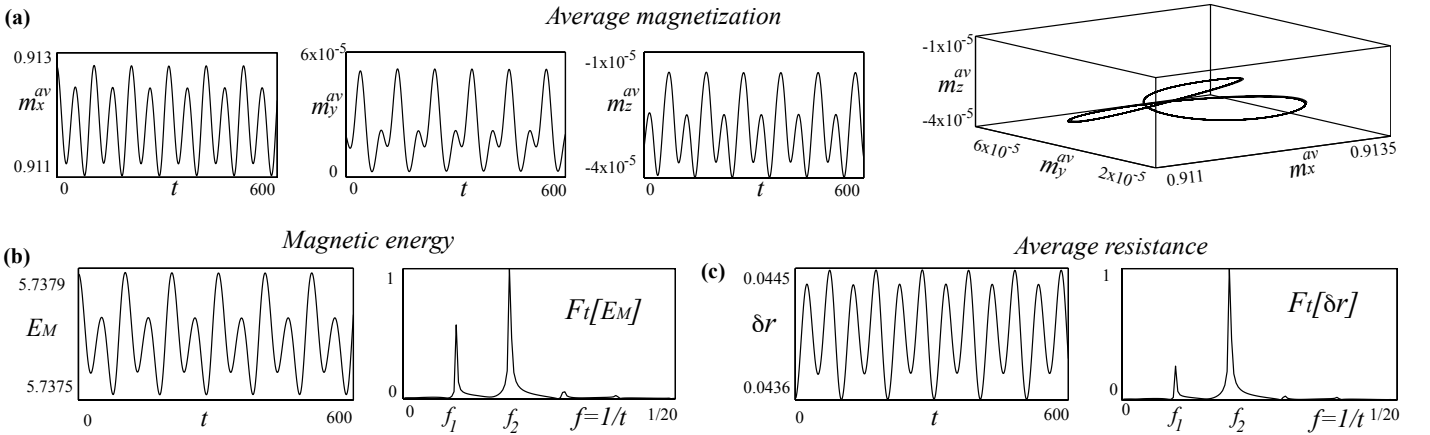
Figure 9: Temporal evolution of the average magnetization, magnetic energy, and average resistance for $g = -0.41$. (a) Components of the average magnetization vector. (b) Magnetic energy. The time series $E_M(t)$ is shown on the left, while the temporal Fourier transform $F_t = F[E_M - <E_M>](f)$ is shown on the right panel. (c) Average resistance profile $\delta r(t)$ (left) and its temporal Fourier transform $F_t[\delta r - <\delta r>](f)$ (right)

8

have considered only four modes and it provides a qualitative understanding of the dynamics. Notice that in the present case, it is necessary to use several modes to get a better quantitative agreement. Moreover, the lack of control expansion coefficient in the Galerkin method renders it a less precise strategy than amplitude equations. To have a deep unified understanding of the dynamic behavior of secondary bifurcations, novel concepts and theoretical tools are required, which represents a challenge to nonlinear science.

For large applied fields, square-like states emerge. They have two dominant Fourier modes that oscillate harmonically. The mechanism that originates the square-like patterns is a supercritical Andronov-Hopf instability. This texture is similar to the ones reported previously for the Rayleigh-Bénard experiments [3, 4]. We expect that increasing the electric current will induce complex dynamical behaviors, such as chaos and spatiotemporal chaos, in the textures. Work in this direction is in progress.

The observation of alternating patterns in nanomagnetism enforces the hypothesis regarding the equivalence between driven nanomagnets and systems with time-dependent forcing, namely parametrically driven systems. Moreover, alternating patterns offers the opportunity to generate and eventually manipulate a wide variety of spin-waves in the gigahertz domain. On the one hand, this promises to increase the technological applications of spin-valve devices, on the other hand, it becomes necessary to study alternating patterns using more general and more realistic approaches. Some generalizations include the use of circular or elliptical devices, a complete treatment of the non-local demagnetizing fields, the use of thermal torques, among others; work in this direction is left as an open problem.

Acknowledgement

AppendixA. Galerkin Expansion of the Magnetization equations

Due to the spatial regularity of the alternating superhexagons, we introduce the following ansatz

$$
\begin{aligned}
A_r &= a_1 \left[\cos(\mathbf{q_1} \cdot \mathbf{r} + \gamma_{r1}) + \cos(\mathbf{q_2} \cdot \mathbf{r} + \gamma_{r2}) + \cos(\mathbf{q_3} \cdot \mathbf{r} + \gamma_{r3}) + \cos(\mathbf{q_4} \cdot \mathbf{r} + \gamma_{r4})\right] \\
&+ b_1 \left[\cos(\mathbf{Q_1} \cdot \mathbf{r} + \Gamma_{r1}) + \cos(\mathbf{Q_2} \cdot \mathbf{r} + \Gamma_{r2})\right], \\
A_i &= a_2 \left[\cos(\mathbf{q_1} \cdot \mathbf{r} + \gamma_{i1}) + \cos(\mathbf{q_2} \cdot \mathbf{r} + \gamma_{i2}) + \cos(\mathbf{q_3} \cdot \mathbf{r} + \gamma_{i3}) + \cos(\mathbf{q_4} \cdot \mathbf{r} + \gamma_{i4})\right] \\
&+ b_2 \left[\cos(\mathbf{Q_1} \cdot \mathbf{r} + \Gamma_{i1}) + \cos(\mathbf{Q_2} \cdot \mathbf{r} + \Gamma_{i2})\right],
\end{aligned} \tag{A.1}
$$

where the functions $\{a_1(t), a_2(t), b_1(t), b_2(t)\}$ are the magnitude of the amplitude of the respective mode, and $\{\gamma_{rj}(t), \gamma_{ij}(t), \Gamma_{ik}(t), \gamma_{ik}(t)\}$ for $j = 1, 2, 3, 4$ and $k = 1, 2$, are the phases of the modes. Since we consider Neumann boundary conditions, the admissible values for the phases are 0 and π. We use here the numerically observed values of the phases:$\gamma_{r1}(t) = \gamma_{r2}(t) = \gamma_{r3}(t) = \gamma_{r4}(t) = \Gamma_{r1}(t) = \Gamma_{r2}(t) = \pi$, and $\gamma_{i1}(t) = \gamma_{i2}(t) = \gamma_{i3}(t) = \gamma_{i4}(t) = \Gamma_{i1}(t) = \Gamma_{i2}(t) = 0$. In this case, the ansatz (A.1) reduces to formula (8). Writing Eq. (2) into its real and imaginary parts, $\partial_t A = G_r + iG_i$, using ansatz (A.1) or equivalently (8), and considering the inner product for Fourier spaces, we obtain after straightforward calculations the following set of Eqs.,

$$
\begin{aligned}
8\dot{a}_1 &\equiv \frac{8}{L^2} \int \int \cos(\mathbf{q_1} \cdot \mathbf{r}) G_r(\mathbf{r}, a_1, a_2, b_1, b_2) dx dy \\
&= -\Delta k^2 [2176 b_1^5 + 6690 a_1 a_2 b_1^2 b_2 + b_1^3(-476 + 4352 a_1^2 - 649 a_2^2 + 3885 b_2^2) + 2a_1 a_2 b_2(1189 a_1^2 + 144(-2 + 3a_2^2 + 3b_2^2))] \\
&- \Delta k^2 [b_1(2176 a_1^4 + a_1^2(-476 + 1507 a_2^2 + 1729 b_2^2) - 8(17 + 27 a_2^4 + 36 b_2^2 - 81 b_2^4 - 18 a_2^2(2 + 3b_2^2)))] + 8 b_1 \beta_x \\
&- 84 a_1^2 b_1 \beta_x + 640 a_1^4 b_1 \beta_x - 16 a_2^2 b_1 \beta_x + 666 a_1^2 a_2^2 b_1 \beta_x + 36 a_2^4 b_1 \beta_x - 84 b_1^3 \beta_x + 1280 a_1^2 b_1^3 \beta_x + 222 a_2^2 b_1^3 \beta_x \\
&+ 640 b_1^5 \beta_x - 32 a_1 a_2 b_2 \beta_x + 444 a_1^3 a_2 b_2 \beta_x + 144 a_1 a_2^3 b_2 \beta_x + 1332 a_1 a_2 b_1^2 b_2 \beta_x - 48 b_1 b_2^2 \beta_x + 666 a_1^2 b_1 b_2^2 \beta_x \\
&+ 216 a_2^2 b_1 b_2^2 \beta_x + 1110 b_1^3 b_2^2 \beta_x + 144 a_1 a_2 b_2^3 \beta_x + 180 b_1 b_2^4 \beta_x + 8 b_1 \beta_z - 84 b_1^3 \beta_z + 640 a_1^2 b_1^3 \beta_z + 111 a_2^2 b_1^3 \beta_z \\
&+ 640 b_1^5 \beta_z + 666 a_1 a_2 b_1^2 b_2 \beta_z - 48 b_1 b_2^2 \beta_z + 333 a_1^2 b_1 b_2^2 \beta_z + 108 a_2^2 b_1 b_2^2 \beta_z + 1110 b_1^3 b_2^2 \beta_z + 72 a_1 a_2 b_2^3 \beta_z \\
&+ 180 b_1 b_2^4 \beta_z + 8 a_1 g + 8 b_1 h_0 - \alpha\{128 a_1^5(-17\Delta k^2 + 5\beta_x) + 6 a_1^2 a_2 b_1 b_2(-1115\Delta k^2 + 111(2\beta_x + \beta_z)) \\
&+ a_1^3(\Delta k^2(476 - 3885 a_2^2 - 4352 b_1^2 + 649 b_2^2) - 84\beta_x + 1110 a_2^2 \beta_x + (640 b_1^2 + 111 b_2^2)(2\beta_x + \beta_z)) + 8 a_1(\beta_x + h_0) \\
&+ 2 b_1(36 a_2^3 b_2(-12\Delta k^2 + 2\beta_x + \beta_z) + a_2 b_2(\Delta k^2(288 - 1189 b_1^2 - 432 b_2^2) + 2(-8 + 111 b_1^2 + 36 b_2^2)(\beta_x + \beta_z)) - 4g) \\
&+ a_1(-\Delta k^2(648 a_2^4 + 68(-2 - 7 b_1^2 + 32 b_1^4) + (288 + 1507 b_1^2) b_2^2 - 216 b_2^4 + a_2^2(-288 + 1729 b_1^2 + 432 b_2^2)) + 180 a_2^4 \beta_x \\
&+ 2(320 b_1^4 - 8 b_2^2 + 18 b_2^4 + b_1^2(-42 + 333 b_2^2))(\beta_x + \beta_z) + 3 a_2^2(2(-8 + 111 b_1^2 + 36 b_2^2)\beta_x + 3(37 b_1^2 + 12 b_2^2)\beta_z))\},
\end{aligned} \tag{A.2}
$$

9

$$4\dot{a}_2 \equiv \frac{4}{L^2}\int\int \cos(\mathbf{q_1}\cdot\mathbf{r})G_i(\mathbf{r},a_1,a_2,b_1,b_2)dxdy$$

$$
\begin{aligned}
=\quad & 72\Delta k^2 b_2 + 108a_2^2\Delta k^2 b_2 - 180a_2^4\Delta k^2 b_2 + 272\Delta k^2 b_1^2 b_2 - 396a_2^2\Delta k^2 b_1^2 b_2 - 1887\Delta k^2 b_1^4 b_2 + 108\Delta k^2 b_2^3 - 360a_2^2\Delta k^2 b_2^3 \\
-\quad & 1260\Delta k^2 b_1^2 b_2^3 - 180\Delta k^2 b_2^5 - 4a_1^3 a_2 b_1(539\Delta k^2 - 111\beta_x) + 4b_2\beta_x - 18a_2^2 b_2\beta_x + 50a_2^4 b_2\beta_x - 48b_1^2 b_2\beta_x + 216a_2^2 b_1^2 b_2\beta_x \\
+\quad & 555b_1^4 b_2\beta_x - 18b_2^3\beta_x + 100a_2^2 b_2^3\beta_x + 360b_1^2 b_2^3\beta_x + 50b_2^5\beta_x + a_1^4 b_2(269\Delta k^2 + 111\beta_x) + 4b_2\beta_z - 48b_1^2 b_2\beta_z \\
+\quad & 108a_2^2 b_1^2 b_2\beta_z + 555b_1^4 b_2\beta_z - 18b_2^3\beta_z + 50a_2^2 b_2^3\beta_z + 360b_1^2 b_2^3\beta_z + 50b_2^5\beta_z + 4a_2 g + 4b_2 h_0 \\
+\quad & a_1^2 b_2(-2\Delta k^2(136 + 234a_2^2 + 809b_1^2 - 198b_2^2) - 16\beta_x + 9(24a_2^2\beta_x + (37b_1^2 + 4b_2^2)(2\beta_x + \beta_z))) \\
-\quad & 2a_1 a_2 b_1(2\Delta k^2(-136 + 198a_2^2 + 539b_1^2 + 630b_2^2) + 16\beta_x - 3(24a_2^2\beta_x + (37b_1^2 + 36b_2^2)(2\beta_x + \beta_z))) \\
-\quad & \alpha\{a_2^5(-180\Delta k^2 + 50\beta_x) - 72a_1 a_2^2 b_1 b_2(35\Delta k^2 - 3(2\beta_x + \beta_z)) + 2a_2^3(18\Delta k^2(3 - 35a_1^2 + 11b_1^2 - 10b_2^2) - 9\beta_x + 180a_1^2\beta_x \\
+\quad & (18b_1^2 + 25b_2^2)(2\beta_x + \beta_z)) + 2b_2(2a_1 b_1(\Delta k^2(136 - 539b_1^2 - 198b_2^2) + (-8 + 111b_1^2 + 36b_2^2)(\beta_x + \beta_z)) \\
+\quad & a_1^3 b_1(-1078\Delta k^2 + 111(2\beta_x + \beta_z)) - 2g) + a_2(-\Delta k^2(1887a_1^4 - 269b_1^4 + 4b_1^2(68 + 117b_2^2) + 2a_1^2(-136 + 809b_1^2 + 198b_2^2) \\
+\quad & 36(-2 - 3b_2^2 + 5b_2^4)) + 555a_1^4\beta_x + (111b_1^4 - 18b_2^2 + 50b_2^4 + 8b_1^2(-2 + 27b_2^2))(\beta_x + \beta_z) \\
+\quad & 3a_1^2(2(-8 + 111b_1^2 + 36b_2^2)\beta_x + 3(37b_1^2 + 12b_2^2)\beta_z) + 4(\beta_x + h_0))\}, \tag{A.3}
\end{aligned}
$$

$$8\dot{b}_1 \equiv \frac{8}{L^2}\int\int \cos(\mathbf{Q_1}\cdot\mathbf{r})G_r(\mathbf{r},a_1,a_2,b_1,b_2)dxdy$$

$$
\begin{aligned}
=\quad & 128a_1^5(17\Delta k^2 - 5\beta_x) + 6a_1^2 a_2 b_1 b_2(1115\Delta k^2 - 111(2\beta_x + \beta_z)) + a_1^3(\Delta k^2(-476 + 3885a_2^2 + 4352b_1^2 - 649b_2^2) + 84\beta_x \\
-\quad & 1110a_2^2\beta_x - (640b_1^2 + 111b_2^2)(2\beta_x + \beta_z)) + b_1(2a_2 b_2(\Delta k^2(-288 + 432a_2^2 + 1189b_1^2 + 432b_2^2) + 16(\beta_x + \beta_z) \\
-\quad & 6((37b_1^2 + 12b_2^2)(\beta_x + \beta_z) + 6a_2^2(2\beta_x + \beta_z))) + 8g) + a_1(\Delta k^2(648a_2^4 + 68(-2 - 7b_1^2 + 32b_1^4) + (288 + 1507b_1^2)b_2^2 \\
-\quad & 216b_2^4 + a_2^2(-288 + 1729b_1^2 + 432b_2^2)) - 180a_2^4\beta_x - 2(320b_1^4 - 8b_2^2 + 18b_2^4 + b_1^2(-42 + 333b_2^2))(\beta_x + \beta_z) \\
-\quad & 3a_2^2(2(-8 + 111b_1^2 + 36b_2^2)\beta_x + 3(37b_1^2 + 12b_2^2)\beta_z) - 8(\beta_x + h_0)) + \alpha\{\Delta k^2(2176b_1^5 + 6690a_1 a_2 b_1^2 b_2 \\
+\quad & b_1^3(-476 + 4352a_1^2 - 649a_2^2 + 3885b_2^2)) + 2a_1 a_2 b_2(1189a_1^2 + 144(-2 + 3a_2^2 + 3b_2^2)) \\
+\quad & b_1(2176a_1^4 + a_1^2(-476 + 1507a_2^2 + 1729b_2^2) - 8(17 + 27a_2^4 + 36b_2^2 - 81b_2^4 - 18a_2^2(2 + 3b_2^2)))) - 640b_1^5(\beta_x + \beta_z) \\
-\quad & 666a_1 a_2 b_1^2 b_2(2\beta_x + \beta_z) - b_1^3(2(-42 + 640a_1^2 + 111a_2^2 + 555b_2^2)\beta_x + (-84 + 640a_1^2 + 111a_2^2 + 1110b_2^2)\beta_z) \\
-\quad & 4a_1(a_2 b_2(-8 + 111a_1^2 + 36a_2^2 + 36b_2^2)\beta_x + 18a_2 b_2^3\beta_z + 2g) - b_1(2(4 + 320a_1^4 - 8a_2^2 - 24b_2^2 \\
+\quad & 18(a_2^2 + b_2^2)(a_2^2 + 5b_2^2)a_1^2(-42 + 333a_2^2 + 333b_2^2))\beta_x + 3b_2^2(-16 + 111a_1^2 + 36a_2^2 + 60b_2^2)\beta_z + 8(\beta_z + h_0))\}, \tag{A.4}
\end{aligned}
$$

$$4\dot{b}_2 \equiv \frac{4}{L^2}\int\int \cos(\mathbf{Q_1}\cdot\mathbf{r})G_i(\mathbf{r},a_1,a_2,b_1,b_2)dxdy$$

$$
\begin{aligned}
=\quad & 10a_2^5(18\Delta k^2 - 5\beta_x) + 72a_1 a_2^2 b_1 b_2(35\Delta k^2 - 3(2\beta_x + \beta_z)) + 2a_2^3(18\Delta k^2(-3 + 35a_1^2 - 11b_1^2 + 10b_2^2) + 9\beta_x - 180a_1^2\beta_x \\
-\quad & (18b_1^2 + 25b_2^2)(2\beta_x + \beta_z)) + 2b_2(2a_1 b_1(\Delta k^2(-136 + 539b_1^2 + 198b_2^2) - (-8 + 111b_1^2 + 36b_2^2)(\beta_x + \beta_z)) \\
+\quad & a_1^3 b_1(1078\Delta k^2 - 111(2\beta_x + \beta_z)) + 2g) + a_2(\Delta k^2(1887a_1^4 - 269b_1^4 + 4b_1^2(68 + 117b_2^2) + 2a_1^2(-136 + 809b_1^2 + 198b_2^2) \\
+\quad & 36(-2 - 3b_2^2 + 5b_2^4)) - 555a_1^4\beta_x - (111b_1^4 - 18b_2^2 + 50b_2^4 + 8b_1^2(-2 + 27b_2^2))(\beta_x + \beta_z) \\
-\quad & 3a_1^2(2(-8 + 111b_1^2 + 36b_2^2)\beta_x + 3(37b_1^2 + 12b_2^2)\beta_z) - 4(\beta_x + h_0)) \\
-\quad & \alpha\{(-\Delta k^2 b_2(-72 + 180a_2^4 - 272b_1^2 + 1887b_1^4 + 36(-3 + 35b_1^2)b_2^2 + 180b_2^4 + 36a_2^2(-3 + 11b_1^2 + 10b_2^2)) + 4b_2\beta_x \\
-\quad & 18a_2^2 b_2\beta_x + 50a_2^4 b_2\beta_x - 48b_1^2 b_2\beta_x + 216a_2^2 b_1^2 b_2\beta_x + 555b_1^4 b_2\beta_x - 18b_2^3\beta_x + 100a_2^2 b_2^3\beta_x + 360b_1^2 b_2^3\beta_x + 50b_2^5\beta_x \\
+\quad & 4a_1^3 a_2 b_1(-539\Delta k^2 + 111\beta_x) + a_1^4 b_2(269\Delta k^2 + 111\beta_x) + 4b_2\beta_z - 48b_1^2 b_2\beta_z + 108a_2^2 b_1^2 b_2\beta_z + 555b_1^4 b_2\beta_z - 18b_2^3\beta_z \\
+\quad & 50a_2^2 b_2^3\beta_z + 360b_1^2 b_2^3\beta_z + 50b_2^5\beta_z + a_1^2 b_2(-2\Delta k^2(136 + 234a_2^2 + 809b_1^2 - 198b_2^2) - 16\beta_x \\
+\quad & 9(24a_2^2\beta_x + (37b_1^2 + 4b_2^2)(2\beta_x + \beta_z))) + 2a_1 a_2 b_1(-2\Delta k^2(-136 + 198a_2^2 + 539b_1^2 + 630b_2^2) - 16\beta_x + 3(24a_2^2\beta_x \\
+\quad & (37b_1^2 + 36b_2^2)(2\beta_x + \beta_z))) + 4a_2 g + 4b_2 h_0), \} \tag{A.5}
\end{aligned}
$$

where $\dot{f} = df/dt$. We remark that, the partial differential equation that describes magnetic media was reduced to a set of ordinary differential equations with four variables. This decomposition admits a geometrical description of the oscillations, and an efficient numerical characterization. A more general ansatz involving more modes might be used to obtain a better quantitative agreement with the magnetic equations. However, this four-modes expansion is complete enough to obtain a qualitative description of the alternating superhexagons.

[1] Cross MC, Hohenberg, PC. Pattern formation outside of equilibrium. Rev Mod Phys 1993; 65:851.

[2] Hoyle RB. Pattern formation:an introduction to methods. Cambridge University Press; 2006.

[3] Le Gal P, Pocheau A, Croquette V. Square versus Roll Pattern at Convective Threshold. Phys Rev Lett 1985; 54:2501-5.

[4] Moses E, Steinberg V. Competing patterns in a convective binary mixture. Phys Rev Lett 1986;57:2018-21.

[5] Müller HW, Lücke M. Competition between roll and square convection patterns in binary mixtures. Phys Rev A 1988;38:2965-74.

[6] Huke B, Lücke M. Roll, square, and cross-roll convection in ferrofluids. J Magn Mag Mater 2005; 289:264-7.

[7] Weggler S, Huke B, Lücke M. Roll and square convection in binary liquids: A few-mode Galerkin model. Phys Rev E 2010; 81:016309.

[8] Pharasi HK, and Kumar K. Oscillatory instability and fluid patterns in low-Prandtl-number Rayleigh-Benard convection with uniform rotation. Phys Fluids 2013;25:104105.

[9] Pal P, Kumar K, Maity P, Dana SK. Pattern dynamics near inverse homoclinic bifurcation in fluids. Phys Rev E 2013;87:023001.

[10] Maity P, Kumar K, Pal P. Homoclinic bifurcations in low-Prandtl-number Rayleigh-Bnard convection with uniform rotation. Eur Phys Lett 2013;103:64003.

[11] Maity P and Kumar K. Zero-Prandtl-number convection with slow rotation. Phys Fluids 2014;26:104103.

[12] Dan S, Pal P, Kumar K. Low-Prandtl-number Rayleigh-Bnard convection with stress-free boundaries. Eur Phys J B 2014;87:278.

[13] Périnet N, Juric D, Tuckerman LS. Alternating Hexagonal and Striped Patterns in Faraday Surface Waves. Phys Rev Lett 2012;109:164501.

[14] León AO, and Clerc MG. Spin-transfer-driven nano-oscillators are equivalent to parametric resonators. Phys Rev B 2015;91:01441.

[15] Slonczewski JC. Current-driven excitation of magnetic multilayers. J Magn Mag Mater 1996;159:L1.

[16] Berger L. Emission of spin waves by a magnetic multilayer traversed by a current. Phys Rev B 1996;54:9353.

[17] Kiselev SI, Sankey JC, Krivorotov IN, Emley NC, Schoelkopf RJ, Buhrman RA, Ralph DC. Microwave oscillations of a nano-magnet driven by a spin-polarized current. Nature 2003;425:380.

[18] Slavin A, Tiberkevich V. Nonlinear Auto-Oscillator Theory of Microwave Generation by Spin-Polarized Current. IEEE Trans Mag 2009;45:1875.

[19] Lee KJ, Deac A, Redon O, Nozieres JP, Dieny B. Excitations of incoherent spin-waves due to spin-transfer torque. Nature Materials 2004;3:877.

[20] Berkov D, Gorn N. Transition From the Macrospin to Chaotic Behavior by a Spin-Torque Driven Magnetization Precession of a Square Nanoelement. Phys Rev B 2005;71:052403.

[21] Volkov OM, Kravchuk VP, Sheka DD, Mertens FG, Gaididei Y. Periodic magnetic structures generated by spinpolarized currents in nanostripes. Appl Phys Lett 2013;103:222401.

[22] Kravchuk VP, Volkov OM, Sheka DD, Gaididei Y. Periodic magnetization structures generated by transverse spin current in magnetic nanowires. Phys Rev B 2013;87:224402.

[23] León AO, Clerc MG, Coulibaly S. Dissipative structures induced by spin-transfer torques in nanopillars. Phys Rev E 2014;89:022908.

[24] Volkov OM, Kravchuk VP, Sheka DD, Gaididei Y. Spin-transfer torque and current-induced vortex superlattices in nanomagnets. Phys Rev B 2011;84:052404.

[25] Gaididei Y, Volkov OM, Kravchuk VP, Sheka DD. Magnetic vortex-antivortex crystals generated by spin-polarized current. Phys Rev B 2012;86:144401.

[26] Li ZD, Li QY, Li L, Liu W. Soliton solution for the spin current in a ferromagnetic nanowire. Phys Rev E 2007;76:026605.

[27] Stiles MD, Miltat J. Spin dynamics in confined magnetic structures III, Springer; 2006.

[28] Mayergoyz ID, Bertotti G, Serpico C. Nonlinear magnetization dynamics in nanosystems. Elsevier; 2009.

[29] Xiao J, Zangwill A, Stiles M. Macrospin models of spin transfer dynamics. Phys Rev B 2005;72:014446.

[30] Ralph DC, Stiles MD. Spin transfer torques. J Magn Mag Mater 2008;320:1190.

[31] Lakshmanan M. The fascinating world of the Landau-Lifshitz-Gilbert equation: an overview. Philos Trans R Soc A 2011,369:1280.

[32] Barashenkov IV, Zemlyanaya EV. Stable complexes of parametrically driven, damped nonlinear Schrödinger solitons. Phys Rev Lett 1999;83:2568.

[33] M. G. Clerc MG, Coulibaly S, Laroze D. Nonvariational IsingBloch transition in parametrically driven systems. Int. J. Bifur Chaos 2009;19:2717.

[34] M. G. Clerc MG, Coulibaly S, Laroze D. Parametrically Driven Instability in Quasi-Reversal Systems. Int. J. Bifur Chaos 2009;19:3525

[35] M. G. Clerc MG, Coulibaly S, Laroze D. Interaction law of 2D localized precession states. Eur Phys Lett 2010;90:38005.

[36] M. G. Clerc MG, Coulibaly S, Laroze D. Effective-parametric resonance in a non-oscillating system. Eur Phys Lett 2012;98:30006.

[37] Urzagasti D, Laroze D, Clerc MG, Coulibaly S, Pleiner H. Two-soliton precession state in a parametrically driven magnetic wire. J Appl Phys 2012;111:07D111.

[38] Urzagasti D, Laroze D, Clerc MG, Pleiner H. Breather soliton solutions in a parametrically driven magnetic wire. Eur Phys Lett 2013;104:40001.

[39] Urzagasti D, Aramayo A, Laroze D. Solitonantisoliton interaction in a parametrically driven easy-plane magnetic wire. Phys Lett A 2014; 378:2614 .

[40] Urzagasti D, Laroze D, Pleiner H. Localized chaotic patterns in weakly dissipative systems. Eur Phys J S.T. 2014;223:141.

[41] Clerc MG, Coulibaly S, Laroze D, León AO, Núñez AS. Alternating spin-polarized current induces parametric resonance in spin valves. Phys Rev B 2015;91:224426.

[42] Miles JW. Parametrically excited solitary waves. J Fluid Mech 1984;148:451.T

[43] Kahouadji L, Périnet N, Tuckerman S, Shin S, Chergui J, Juric D. Numerical simulation of supersquare patterns in Faraday waves. J Fluid Mech 2015;772:R2.

[44] D C Ralph, Y T Cui, L Q Liu, T Moriyama, C Wang, and R A Buhrman. Spin-transfer torque in nanoscale magnetic devices. Philos Trans R Soc A 2011; 369:3617-30.

[45] Strogatz SH Nonlinear dynamics and chaos:with applications to physics, biology, chemistry, and engineering. Westview Press, 2001.

Apéndice F

Conference Proceedings

F.1. Stationary textures induced by spin-transfer torques: role of the angular dependence

Proceeding details:

Title: Stationary textures induced by spin-transfer torques: role of the angular dependence

Author: Alejandro O. León.

Accepted in: Journal of Physics: Conference Series.

Conference: XIX Simposio Chileno de Física 2014

Stationary textures induced by spin-transfer torques: role of the angular dependence

Alejandro O. León

E-mail: `aoleon@dfi.uchile.cl`
Departamento de Física, Facultad de Ciencias Físicas y Matemáticas, Universidad de Chile, Casilla 487-3, Santiago, Chile.

Abstract. Magnetic systems forced with external fields or electric currents exhibit a rich spatiotemporal dynamics. A well known example is the one of spin-transfer torque driven textures, which includes switching, precessions, dissipative solitons, and periodic textures. Using different expressions that model the spin-transfer torque —angular dependence of the spin-transfer— we obtain analytic solutions for static spatially periodic states, study their stability, and elucidate the role that the angular dependence plays in the formation of textures. We demonstrate that the type of bifurcations changes from supercritical to subcritical, depending on the particular type of torque. Numerical simulations confirm this scenario. Thus, magnetoresistance measurements could permit to determine the form of the torque.

1. Introduction

Ferromagnetic materials subjected to dissipation and injection of energy or momentum self-organize in dissipative structures, such as solitons, skyrmions, periodic textures, and domain walls. The usual driving mechanisms are the couplings between the magnetization of the ferromagnetic material and external magnetic fields and electric currents. In 1996, Slonczewski[1] and Berger [2] predicted that a spin-polarized (SP) electric current exerts a torque in ferromagnetic nano-layers, effect known as spin-transfer torque [3, 4, 5]. Since then, the interest on excitations driven by SP currents has grown considerably, both from the scientific and the technological viewpoints [4]. A typical configuration to study spin-transfer torques is the multilayer nanopillar, or spin-valve, that consists on ferromagnetic conducting films separated by non-magnetic conductors as shown in Fig. 1(a). When an electric current is applied, it transfers spin angular momentum from one relatively thick layer with *fixed* magnetization to a thin film with *free* magnetization [4].

Spin-transfer torques are non-conservative effects, and therefore they can destroy, stabilize or destabilize states. Moreover, in the case in which a SP current injects enough energy to counterbalance the dissipation, the free magnetization switches or precesses with microwave frequencies, both effects have been studied experimentally [6, 7, 8, 9] and theoretically [10, 11, 12, 13]. Hence, electric currents permit to manipulate small scale magnets and use them as memory devices, or spin-wave emitters. The SP current can also stabilize configurations that are energy maxima. In this scenario, the free magnetization exhibits the phenomenology of the systems subjected to time-dependent driving forces [14]. This dynamic behaviors includes solitons, domain walls, and spatially periodic textures or *patterns*. Typical spin-transfer torque
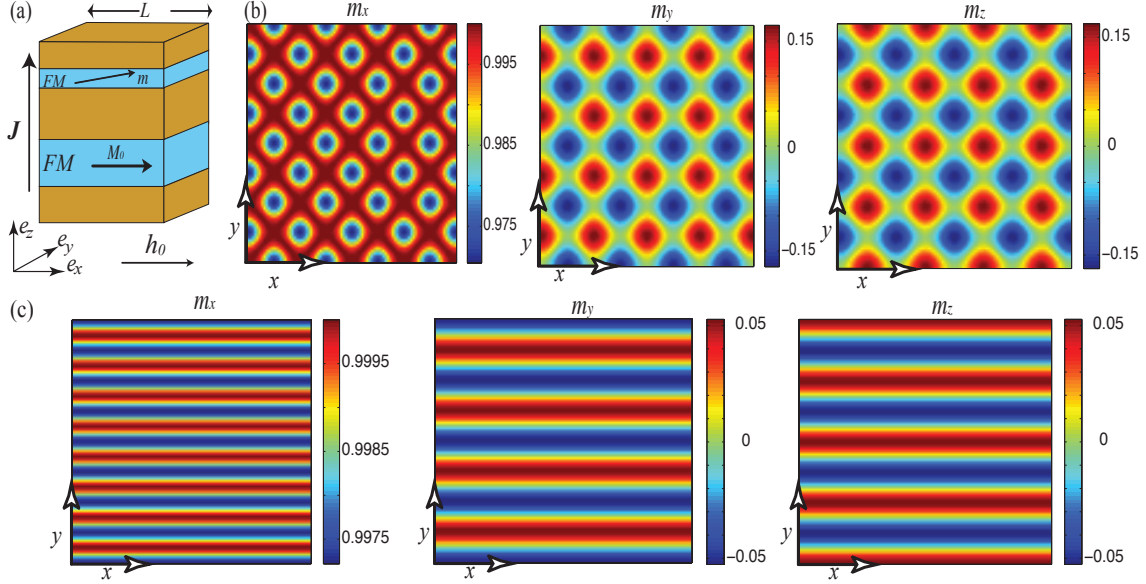
Figure 1. Nanopillar device and magnetic textures. a) Schematic spin-valve setup. The layers labeled as FM are the ferromagents, the rest of the structure is composed by nonmagnetic conductors; J is the SP electric current while h_0 is the external magnetic field, both effects are parallel to the easy-axes of the ferromagnetic layer under study. $\mathbf{M}_o$ stands for the magnetization of the fixed layer. b) Typical patterns induced by the spin-transfer torque effect. The parameters are $h_0 = -6$, $g = -0.4999$, $\beta_z = 1$, $\beta_x = 0.5$, $\alpha = 0.05$, and $dx = 0.126289$. The parameters of the torque are $\Delta = b = 0$, this is the sinus-approximation case. c) The same as b) with the Slonczewski torque, it is, $\Delta = 0$ and $b = 0.35$. Note the relation between the magnetic components $m_y \approx -m_z$. Since $m_x \approx 1 - (m_y^2 + m_z^2)/2$, the component m_x has spatial oscillations at twice the wavenumber of my and m_z.

induced patterns are shown in Figs. 1(b) and 1(c), they emerge due to an imbalance between the spin-polarized current and an external magnetic field [15]. The typical wavelength of these patterns is $20 - 30nm$.

In the classical approach, the free layer magnetization is described by the Landau-Lifshitz-Gilbert equation with an extra term that accounts for the interaction between the spin-polarized electric current and the ferromagnet [3, 4, 5]. Since the transport of the conducting electrons depends on the relative orientations of the free and fixed layers, the torque induced by the SP current can also depend on this orientation. This dependence is known as the *angular dependence of the spin-transfer torque*. Analytic expressions for this angular dependence have been proposed and studied for several geometries [1, 16, 19, 17, 18, 20]. In certain regions of the parameter space, the dynamics of the precessional states change quantitatively and qualitatively with the use of different torque terms, which permits to test the angular dependence for a given geometry [17, 18, 21, 22]. The textures predicted in Refs. [14, 15] are an alternative dynamical regime which permits to compare the predictions of the different spin-transfer models. In Ref. [15], a simplified version of the torque was used, and a more general study is required.

The aim of this article is to study the role of the angular dependence of the spin-transfer torque in pattern formation. We obtain analytic solutions for the spatially periodic patterns and elucidate their stability. It is found that the magnetic textures change strongly with the angular dependence. The manuscript is organized as follows: in Sec. 2, we describe the magnetization

dynamics of the free layer. In Sec. 3, we obtain the amplitude equation for the patterns, and analyze the role of the angular dependence. The conclusions and remarks are left to the final section.

2. Free layer magnetization dynamics

Consider a square cross-section nanopillar device, with fixed layer magnetization $\mathbf{M_0}$ along the positive x-axis, this material is thicker than the free layer, and acts as a spin filter or spin polarizer for the electric current. Lateral sizes L in the transverse directions are around 100 nanometers for typical devices. Hereafter, we adimensionalyze the magnetization of the free layer $\mathbf{M} \to M_s \mathbf{m}$ and the external field $\mathbf{H_0} \to M_s \mathbf{h_0}$ by the saturation magnetization M_s; the time $t \to \gamma M_s t$ is written in terms of the gyromagnetic constant γ, and M_s; and the spatial coordinates $(x, y) \to l_{\mathrm{ex}}(x, y)$ in terms of the *exchange length* $l_{\mathrm{ex}} \equiv \sqrt{2A/(\mu_0 M_s^2)}$ where A is the exchange coupling in the ferromagnet. For example, in a $3nm$ thick Cobalt layer, $M_s \simeq 1.4$ $10^6 A/m$, and the characteristic time and space scales are $(\gamma M_s)^{-1} \simeq 3.2 ps$ and $l_{\mathrm{ex}} \approx 3.4 nm$, respectively [5].

For thin films, the magnetic energy is given by [5]

$$E = \frac{\mu_0 M_s^2}{L^2} \int_0^L \int_0^L \left[-\mathbf{m} \cdot \mathbf{h_0} - \frac{1}{2}\beta_x m_x^2 + \frac{1}{2}\beta_z m_z^2 + \frac{1}{2}|\nabla \mathbf{m}|^2 \right] dxdy, \qquad (1)$$

an external magnetic field $\mathbf{h_0} = h_0 \mathbf{e}_x$ points along the x-axis. The coefficients β_x and β_z are combinations of the anisotropy constants with respect to the appropriate axes, where β_x (β_z) favors (disfavors) the free magnetization in the x-axis (z-axis). Since the free layer is thin, the demagnetization field can be approximated by a shape anisotropy, and it is incorporated in the β_z coefficient.

The dynamic of the free layer magnetization is modeled by the dimensionless Landau-Lifshitz-Gilbert equation (LLG) with an extra term that accounts for the spin-transfer torque [5]

$$\frac{\partial \mathbf{m}}{\partial t} = -\mathbf{m} \times \mathbf{h}_{eff} + \alpha \mathbf{m} \times \frac{\partial \mathbf{m}}{\partial t} + \eta g_0 \, \mathbf{m} \times (\mathbf{m} \times \mathbf{e_x}). \qquad (2)$$

The first term of the right hand side of Eq. (2) accounts for the conservative precessions generated by the effective field,

$$\mathbf{h}_{eff} \equiv -\frac{L^2}{\mu_0 M_s^2} \frac{\delta E}{\delta \mathbf{m}} = (h_0 + \beta_x m_x)\, \mathbf{e}_x - \beta m_z \mathbf{e}_z + \nabla^2 \mathbf{m}. \qquad (3)$$

The second and third terms of Eq. (2) are the phenomenological Gilbert damping and the spin-transfer torque, respectively. The dimensionless parameter g_0 is

$$g_0 \equiv \frac{\hbar J}{2d|e|\mu_0 M_s^2}, \qquad (4)$$

where J is the electric current density, d the thickness of the layer and $e < 0$ the electric charge. The parameters J and g_0 are negative when the electrons flow from the fixed to the free layer. The dimensionless function $\eta = \eta(\mathbf{m} \cdot \mathbf{e_x})$ is known as the spin-torque efficiency, this function depends on the relative orientation of the ferromagentic films, and the device geometry and the physical properties of the layers, it has the general form of [4, 17, 18]

$$\eta(\mathbf{m} \cdot \mathbf{e_x}) \equiv \frac{(1 - b^2)}{1 - b + \Delta(1 + b)} \left(\frac{1}{1 + bm_x} + \frac{\Delta}{1 - bm_x} \right). \qquad (5)$$

The coefficient Δ measures the anisotropy between ferromagnetic layers of the spin-valve. In the case of an symmetric structure (identical ferromagnetic layers and leads) Δ vanishes. Additionally, for short leads, Δ can be neglected. In these cases, the efficiency is just $\eta = (1+b)/(1+bm_x)$, which is term originally proposed by Slonczewski [1, 16]. The constant b accounts for the strength of the spin scattering at the free layer interface. Notice that the η function is $\eta(1) = 1$ in the parallel configuration. The approximation $\eta(m_x) \approx \eta(1) = 1$ for $m_x \approx 1$, which is equivalent to impose $b = 0$ in the formula (5), is known as the sinus spin-transfer torque, because the torque $\|\eta g_0 \mathbf{m} \times (\mathbf{m} \times \mathbf{e_x})\| \sim |\sin(\Psi)|$, where Ψ is the angle between the free and fixed magnetizations. This approximation is widely used in literature. We will compare the SP-driven dynamics in the case of a general torque $(b, \Delta > 0)$, a symmetric torque $(\Delta = 0)$, and a sinus torque $(b = 0)$.

Notice that the LLG Eq. conserves the magnetization norm $\|\mathbf{m}\| = 1$, since $\mathbf{m}$ and $\partial_t \mathbf{m}$ are perpendicular. This permits us to use a spherical representation of the free magnetization

$$\mathbf{m} = \sin(\theta)\left[\cos(\phi)\mathbf{e}_x + \sin(\phi)\mathbf{e}_y\right] + \cos(\theta)\mathbf{e}_z. \tag{6}$$

Introducing this representation in Eq. (2), one obtains the following set of equations

$$\partial_\tau \theta = -(h_0 + \alpha \eta g_0)\sin(\phi) + (\alpha h_0 - \eta g_0)\cos(\phi)\cos(\theta) + \frac{\alpha}{2}\sin(2\theta)\left[\beta_z + \beta_x \cos^2(\phi)\right]$$

$$-\frac{\beta_x}{2}\sin(\theta)\sin(2\phi) + \sin(\theta)\nabla^2\phi + 2\cos(\theta)\nabla\phi \cdot \nabla\theta + \alpha\nabla^2\theta - \frac{\alpha}{2}\sin(2\theta)\left(\nabla\phi\right)^2,$$

$$\sin(\theta)\partial_\tau \phi = (\eta g_0 - \alpha h_0)\sin(\phi) - (\alpha \eta g_0 + h_0)\cos(\phi)\cos(\theta) - \frac{1}{2}\sin(2\theta)\left[\beta_z + \beta_x \cos^2(\phi)\right]$$

$$-\alpha\frac{\beta_x}{2}\sin(\theta)\sin(2\phi) + \alpha\sin(\theta)\nabla^2\phi + 2\alpha\cos(\theta)\nabla\phi \cdot \nabla\theta - \nabla^2\theta + \frac{1}{2}\sin(2\theta)\left(\nabla\phi\right)^2, \tag{7}$$

where $\tau = t/\left(1 + \alpha^2\right)$, and $\eta = \eta(\sin(\theta)\cos(\phi))$. The simplest equilibria of Eq. (2) are $\mathbf{m} = \pm\mathbf{e}_x$, which represent a free magnetization parallel $(+)$ or anti-parallel $(-)$ to the fixed magnetization $\mathbf{M}_0$. Both states correspond to extrema of the free energy E. In spherical coordinates, the parallel and anti-parallel states are $(\theta, \phi) = (\pi/2, 0)$, and $(\theta, \phi) = (\pi/2, \pi)$ respectively. From the technological viewpoint, when both equilibria are stable, the spin-valve can be seen as a two-states system capable of saving information. Resistance measurements permit to read such data from the valve, and the spin-transfer torque induced switching allows one to write on the device. This is the basis of the spin-transfer torque based RAM memories [4].

For the rest of the manuscript we will concentrate on the parallel equilibrium $\mathbf{m} = \mathbf{e}_x$.

3. Periodic patterns

Note that the linear stability analysis around the $m_x = 1$ state is independent of the parameters b and Δ because the angular dependence is constant around the parallel state, $\eta(m_x) = \eta(1) + \mathcal{O}(m_y^2 + m_z^2) \approx 1$. The instabilities of this state have been subject of several studies the last decades [3, 4, 5, 15]. There are three main types of bifurcations: the Andronov-Hopf instability that generates self-oscillations, the stationary instability in which the system goes to other stationary equilibra, and the spatial instability (see Ref. [15] for more details); this last bifurcation is the motivation of the of this work. The spatial instability is characterized because the perturbations that destabilize the parallel state are non-uniform and generally give rise to periodic patterns. In the case of a spin-valve, when $g_0, h_0 < 0$, the SP current favors the parallel state while the external field disfavors it. The competition of these opposing effects is the physical origin of the spatial instability. Considering a critical perturbation of the form

$$\begin{pmatrix} \theta \\ \phi \end{pmatrix} \approx \begin{pmatrix} \pi/2 \\ 0 \end{pmatrix} + e^{\lambda t}\left[A_0 e^{i\mathbf{q}\cdot\mathbf{r}} + \bar{A}_0 e^{-i\mathbf{q}\cdot\mathbf{r}}\right]\begin{pmatrix} 1 \\ 1 \end{pmatrix}, \tag{8}$$

where the groth rate is $\lambda = \beta_z/2 + g_0$. The norm q of the wave-vector $\mathbf{q}$ is controlled by the external magnetic field through $q = -h_0 - \beta_x - \beta_z/2$, and it exists for $h_0 < -\beta_x - \beta_z/2 < 0$. The complex amplitude A_0 is a constant fixed by the initial conditions, and $\bar{A}_0$ is the complex conjugate of A_0. The spatially periodic perturbations are amplified on time for $g_0 > -\beta_z/2$, or decay to zero for $g_0 < -\beta_z/2$. Notice that since the nanopillar has a square cross-section, there can be several admitted modes with wave-numbers q, which will grow and interact for $g_0 > -\beta_z/2$.

In the critical situation $g_{0,c} \equiv -\beta_z/2$, there is no exponential grow or decay of the perturbations, and the modes of formula (8) exhibit a slow dynamics given by the nonlinear corrections. At the onset of the spatial bifurcation, it is possible to obtain the equations for the critical modes by introducing the following ansatz

$$
\begin{pmatrix} \theta \\ \phi \end{pmatrix} = \begin{pmatrix} \pi/2 \\ 0 \end{pmatrix} + \left[A(t)e^{iqx} + B(t)e^{iqy} + \bar{A}(t)e^{-iqx} + \bar{B}(t)e^{-iqy} \right] \begin{pmatrix} 1 \\ 1 \end{pmatrix} + \mathbf{W}(A, B, \bar{A}, \bar{B}, \mathbf{r}),
$$
(9)

where the amplitudes $A(t)$ and $B(t)$ are slowly varying functions of time, and $\mathbf{W}$ is a small correction that appears due to the nonlinear nature of the problem, and it depends nonlinearly on the amplitudes A and B. We have considered just two modes by the sake of simplicity, and the amplitudes $A(t)$ and $B(t)$ are the envelops of the spatial oscillations along the $x-$axis and $y-$axis, respectively. Replacing the above ansatz in Eq. (7), linearizing in $\mathbf{W}$, and after imposing a solvability condition [23] , we obtain

$$
\frac{dA}{dt} = (g_0 - g_{0,c})A - \Gamma A \left(|A|^2 + 2|B|^2 \right),
$$
$$
\frac{dB}{dt} = (g_0 - g_{0,c})B - \Gamma B \left(|B|^2 + 2|A|^2 \right),
$$
(10)

where the coefficient of the nonlinearity is

$$
\Gamma = \frac{3}{2} \frac{\beta_z b}{1 - b^2} \frac{(1 - b)^2 - \Delta(1 + b)^2}{1 - b + \Delta(1 + b)}.
$$
(11)

The above set of equations describes the growth of the pattern for $g_0 > g_{0,c}$, with a nonlinear interaction between modes, and a nonlinear saturation (or nonlinear gain) for $\Gamma > 0$ ($\Gamma < 0$). Let us start with the case of a nonlinear saturation $\Gamma > 0$. Notice that the set of Eqs. (10) is phase invariant, it is, they remain unchanged under transformations of the form $(A, B) \rightarrow (Ae^{i\psi_1}, Be^{i\psi_2})$ for arbitrary real constants ψ_1 and ψ_2. This motivates the use of reduced real valued variables $a_1(t) = \sqrt{\Gamma}|A(t)|$, and $a_2(t) = \sqrt{\Gamma}|B(t)|$ for the case of nonlinear saturation,

$$
\frac{da_1}{dt} = \epsilon a_1 - a_1 \left(a_1^2 + 2a_2^2 \right),
$$
$$
\frac{da_2}{dt} = \epsilon a_2 - a_2 \left(a_2^2 + 2a_1^2 \right).
$$
(12)

where $\epsilon \equiv g_0 - g_{0,c}$ For negative ϵ, the spatially periodic perturbations decay to the homogeneous solution $(a_1, a_2) = (0, 0)$, which is linearly stable. Hence, the parallel state is stabilized by the current for negative enough values of g_0.

Figure 2 shows the phase portrait of Eq. (12) for positive values of ϵ. The 4 steady states of the system are the parallel state $(a_1, a_2) = (0, 0)$, the roll patterns $(a_1, a_2) = (\sqrt{\epsilon}, 0)$ and $(a_1, a_2) = (0, \sqrt{\epsilon})$, and finally the square texture $(a_1, a_2) = (\sqrt{\epsilon/3}, \sqrt{\epsilon/3})$. Given the amplitude
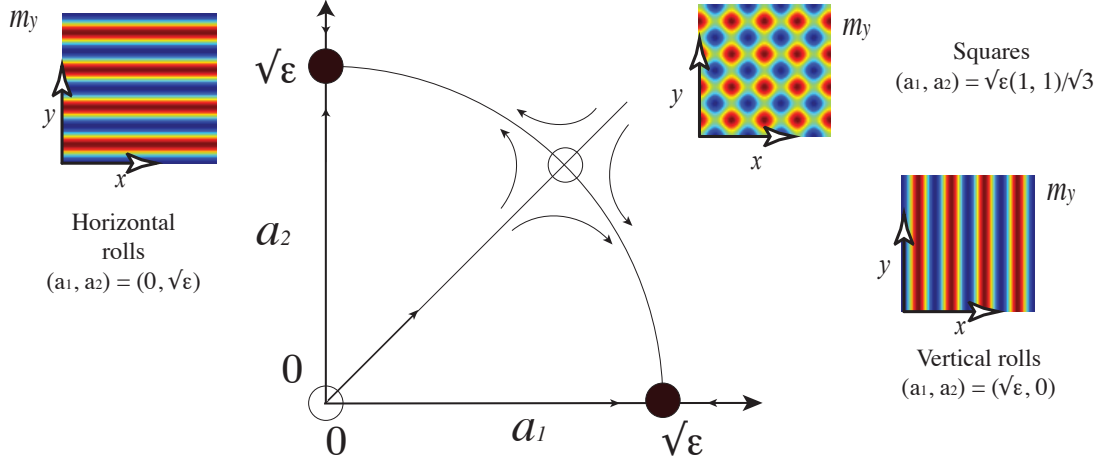
Figure 2. Phase portrait of amplitude Eq. (12), which describes the pattern formation driven by a Slonczewski spin-transfer torque. Insets show the magnetic component m_y of the equilibrium states. For $g_0 > g_{0,c}$ the vertical and horizontal roll equilibria (black circles) are stable for the Slonczewski form of the torque. The Square pattern and the uniform solution (empty circles) are unstable.

Eq. (12), the linear stability analysis of the patterns becomes a trivial task. This analysis reveals that the roll states are stable (black circles in Fig. 2) and the square is unstable (empty circle). Thus, after transients, the magnetization converges to the horizontal or vertical rolls of the form

$$m_x \approx 1 - 4\left(g_0 - g_{0,c}\right) \left[\frac{1 - b^2}{\beta_z b} \frac{1 - b + \Delta(1+b)}{(1-b)^2 - \Delta(1+b)^2} \right] \left(\frac{1 - \cos\left(\mathbf{q} \cdot \mathbf{r}\right)}{3} \right),$$

$$m_y \approx m_z \approx 2\sqrt{g_0 - g_{0,c}} \sqrt{\frac{2}{3} \frac{1 - b^2}{\beta_z b} \frac{1 - b + \Delta(1+b)}{(1-b)^2 - \Delta(1+b)^2}} \cos\left(\mathbf{q} \cdot \mathbf{r}\right), \tag{13}$$

where $\mathbf{q} \cdot \mathbf{r} = qx$ or $\mathbf{q} \cdot \mathbf{r} = qy$. Fig. 1(c) shows this state. This roll-like functions are the typical magnetic configurations for the most general spin-torque.

In the next subsections, we discuss the different types of instabilities that arise with each spin-transfer torque term. These transitions correspond to supercritical ($\Gamma > 0$), quintic supercritical ($\Gamma = 0$), and subcritical ($\Gamma < 0$).

3.1. Slonczewski limit ($\Gamma > 0$)

If the spin-valve has equal ferromagnetic films and equal leads, then $\Delta = 0$ and the $\eta(m_x)$ function is the same as proposed originally by Slonczewski in Refs. [1, 16]. In this case, the saturation coefficient takes the form

$$\Gamma = \frac{3}{2} \frac{\beta_z b}{1 + b}. \tag{14}$$

Figure 1(c) illustrates the rolls for $b = 0.35$. This type of bifurcation is known as a supercritical transition. It is worth noting that the saturation is independent of the external field h_0 and easy-axis anisotropy constant β_x. Figure 3(a) compares the numerical solution of the Landau-Lifshitz-Gilbert equation with the predicted amplitude $2|A|(\epsilon) \sim 2\left(\epsilon/\Gamma\right)^{1/2}$ of rolls $m_y \approx -m_z \approx 2|A|\cos(\mathbf{q} \cdot \mathbf{r})$. In order to integrate the LLG equation, space was discretized using a finite differences centered scheme of order six, and the temporal evolution was obtained with a fifth order variable step size Runge-Kutta.

The magnetoresistance δr permits to compare predicted textures with experimental data. Hence, it is an adequate physical quantity for characterizing magnetic configurations in spin-valves. For uniform magnetized free layers, the magnetoresistance depends only on the relative orientation between the free and fixed layers, $\delta r = \delta r(m_x)$. For nonuniform magnetic states, the average indicator $\delta r \equiv \delta r(m_x^{av})$ is commonly used [24], where m_x^{av} is the average magnetization along the x-axis. Consequently, for symmetric spin-valves the average resistance will be independent of external field and anisotropy coefficient β_x.

3.2. Sinus-aproximation ($\Gamma = 0$)

In the sinus approximation ($b = 0$), the function η is constant and the cubic coefficients of the set of Eqs. (10) vanishes. In order to quantify the saturation, it is necessary to include higher order corrections into the amplitude equation. This case was studied in detail in Ref. [15]. Let us summarize the main results of Ref. [15], and compare them with the predictions of other type of spin-transfer torques. In a similar way of the previous section, we consider a two modes ansatz of the form

$$\begin{pmatrix} \theta \\ \phi \end{pmatrix} \approx \begin{pmatrix} \pi/2 \\ 0 \end{pmatrix} + R \left[A(t) e^{i\mathbf{q_1}\cdot\mathbf{r}} + B(t) e^{i\mathbf{q_2}\cdot\mathbf{r}} + \bar{A}(t) e^{-i\mathbf{q_1}\cdot\mathbf{r}} + \bar{B}(t) e^{-\mathbf{q_2}\cdot\mathbf{r}} \right] \begin{pmatrix} 1 \\ 1 \end{pmatrix} + \mathbf{W}'(A, B, \bar{A}, \bar{B}, \mathbf{r}),$$

(15)

where the wave-vectors $\mathbf{q_1}$ and $\mathbf{q_2}$ have norm q, and their orientation is fixed by the border of the sample. The prefactor R is the characteristic scale for patterns induced by a sinus torque, which is defined as

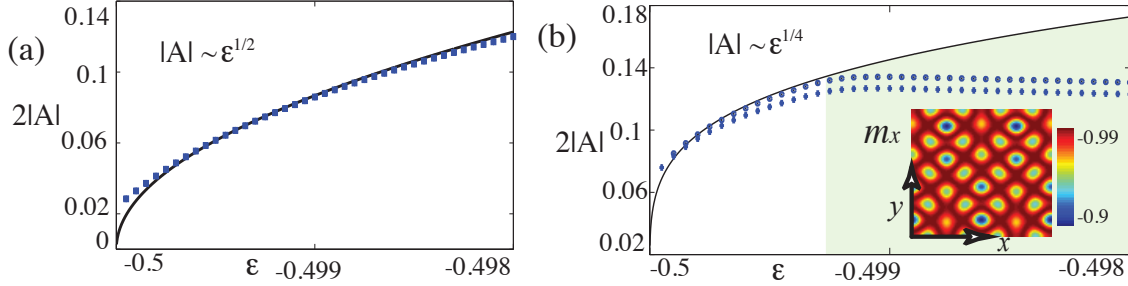$$R \equiv \sqrt[4]{\frac{4\beta_z}{(6\beta_x + 3\beta_z - 2q^2)^2}}.$$

(16)

Figure 3. Comparison between analytic calculations (solid lines) and micromagnetic simulations (crosses and circles). (a) Pattern amplitudes for the Slonczewski spin-transfer torque with $b = 0.55$, and $\Delta = 0$. The solid line is the solution roll solutions of Eq. (10), while crosses $+$ and circles $\bullet$ stand by the maximum of the Fourier transform of m_z and m_y, respectively. It is worth noting that at dominant order $|m_y| \approx |m_z| \approx |\phi| \approx |\theta - \pi/2|$. The fields (m_y, m_z) were obtained with the direct integration of the LLG Eq. (2) with $h_0 = -6$, $\beta_x = 0.5$, $\beta_z = 1$, $\alpha = 0.05$, and spatial step size $dx = 0.126289$. (b) The same as in (a) for a sinus spin-transfer torque ($b = 0$). At the onset of the spatial instability, the amplitudes of follow the law $|A| \sim \epsilon^{1/4}$ predicted by the amplitude equation (17), nevertheless far from the bifurcation the square pattern becomes unstable giving rise to the stationary pattern of the inset.

Replacing the ansatz (15) in the LLG equation and imposing solvability condition, we get

$$\frac{dA}{dt} = \epsilon A - \frac{8}{3}\frac{2-3D}{1-D}A|A|^2|B|^2 - A|A|^4 - \frac{8}{3}\frac{1}{1-D}A|B|^4,$$
$$\frac{dB}{dt} = \epsilon B - \frac{8}{3}\frac{2-3D}{1-D}B|B|^2|A|^2 - B|B|^4 - \frac{8}{3}\frac{1}{1-D}B|A|^4, \tag{17}$$

with $\epsilon \equiv g_0 - g_{0,c}$. Note that the modes interaction is mediated by quintic nonlinearities. This type of transition is known as quintic supercritical bifurcation. The parameters D accounts for the competition between the external magnetic field and the anisotropies

$$D \equiv \frac{2}{3}\frac{q^2}{2\beta_x + \beta_z} = \frac{2|h_0| - 2\beta_x - \beta_z}{6\beta_x + 3\beta_z}. \tag{18}$$

The above set of equations admits roll solutions of the form $(|A|,|B|) = (\epsilon^{1/4}, 0)$ and $(|A|,|B|) = (0, \epsilon^{1/4})$. The phase portraits of the set of Eqs. (17) are shown in Fig. 4. These solutions are linearly stable when the field $|h_0|$ is small compared with the anisotropy constants (or equivalently $D < 1$). For intense fields ($D > 1$) the rolls become unstable. In the last case, the square-like equilibrium $A = B = (\epsilon/9)^{1/4}$ is linearly stable. Figure 1(c) shows a square pattern obtained for $h_0 = -6$, where $D > 1$. The phase portrait of this case is in Fig. 4(b). For the critical value of the external field $h_{0,c} = -2(2\beta_x + \beta_z)$ the quintic saturation vanishes, and the analysis of pattern formation requires higher order corrections.

Since the saturation is given by the quintic order nonlinearities, then the equilibrium states grow as $m_y \sim m_z \sim (g_0 - g_{0,c})^{1/4}$ as illustrated in Fig. 3(b). Moreover, the m_x magnetization component follows the law $m_x \sim (g_0 - g_{0,c})^{1/2}$. Note that the square pattern of Fig. 1(c) becomes unstable when g_0 is surpasses a critical value; in this situation additional modes grow and interact. In the context of dynamical systems this bifurcation is known as a secondary instability of the underlying pattern. A different pattern appears from this instability as shown in the inset of Fig. 3(b).

In brief, the case of the sinus approximation: the equilibrium magnetization depends on the external field and the anisotropies; there is a transition for a critical value of the external field, in this transition the roll solutions interchange stability with the square-like pattern. Finally, the margnetoresistence depends on the square-root of the current $\delta r \sim (g_0 - g_{0,c})^{1/2}$.
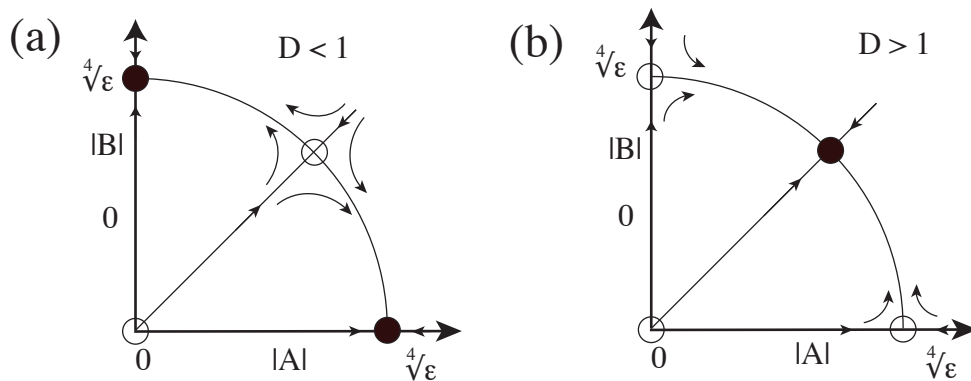

Figure 4. Phase portrait of amplitude Eq. (17), where a sinus-approximation for the spin-transfer torque has been considered. Black circles stand for stable pattern equilibria, while empty circles are for unstable states. a) Small external field ($D < 1$) favors the formation of rolls. b) High external magnetic field ($D > 1$) favors the square equilibrium.
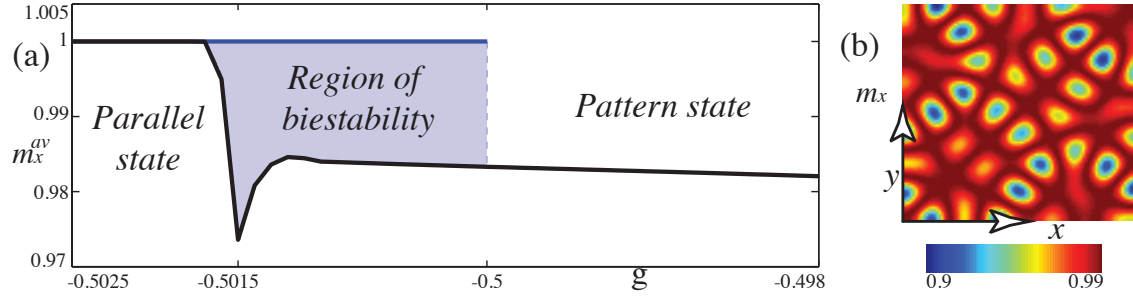
Figure 5. Hysteresis loop for asymmetric spin-valves. (a) The spatial average m_x^{av} of m_x, at equilibrium, is obtained integrating the LLG Eq. (2) with $b = 0.55$, $\Delta = 0.2$, $h_0 = -6$, $\beta_x = 0.5$, $\beta_z = 1$, $\alpha = 0.05$, and spatial step size $dx = 0.126289$. (b) m_x component of the equilibrium magnetization for $g_0 = g_{0,c}$.

3.3. Hysteresis ($\Gamma < 0$)
A completely different scenario occurs for highly asymmetric spin-valves. If the coefficient Δ surpasses the critical value $\Delta_c = (1-b)^2/(1+b)^2$, the cubic nonlinearities amplify the pattern and higher order corrections must be included in Eq. (10). In such case the spatial instability is subcritical, and patterns exist even for $g_0 < g_{0,c}$. Physical systems with subcritical spatial instabilities are characterized by an hysteresis region close to the critical point (in this case $g_0 = g_{0,c}$), it is, both the parallel state and patterns are stable. Figure 5 illustrate the hysteresis for the spatial average of the magnetization component m_x at equilibrium, m_x^{av}. Hence, in the case of asymmetric enough spin-valves, the magnetoresistence has a discontinuity.

From the viewpoint of dynamical systems, subcritical spatial instabilities generate a wide variety of states, such as domain walls, localized patterns, and interacting solitary structures [23], among others. The self-organization of highly asymmetric spin-valves forced with spin-polarized currents is an open problem, which could be interesting for memory technologies.

4. Conclusions and remarks
We have studied the formation of periodic textures in spin-valves, with a general type of spin-transfer torque. Using the weakly nonlinear analysis, we have found that the type of spatial instability changes from supercritical, to quintic supercritical and subcritical bifurcations depending on the form for the spin-transfer. The sinus approximation gives a pattern growing law of $(g_0 - g_{0,c})^{1/4}$, the magnetoresistance depends on the anisotropies and the external field. In opposition, for the Slonczewski spin-transfer torque and the general spin-transfer torque, the textures grow as $(g_0 - g_{0,c})^{1/2}$, and the magnetoresistance is independent of the external field and the easy-axis anisotropy β_x. Moreover, for highly asymmetric spin-valves, the spatial instability that creates patterns becomes subcritical, which generate hysteresis loops. Numerical simulations of the Landau-Lifshitz-Gilbert equation confirm these predictions. We expect that the formation of textures will permit to have an additional dynamical test to the spin-transfer torque terms, as well as possible application of pattern states in technology.

References
[1] Slonczewski J C, J. 1996 *Mag. Mat. Mag.* **159** L1.

[2] Berger L 1996 *Phys. Rev. B* **54** 9353.

[3] Ralph D C, and Stiles M D 2008 *J. Magn. Mag. Mater.* **320** 1190.

[4] Stiles M D, and Miltat J, in *Spin Dynamics in Confined Magnetic Structures*, edited by B. Hillebrands, A. Thiaville (Springer, Berlin, 2006) Vol. 3, Chap. 7

[5] Mayergoyz I D, Bertotti G, and Serpico C, *Nonlinear Magnetization Dynamics in Nanosystems* (Elsevier, Oxford, 2009).

[6] Katine J A, Albert F J, Buhrman R A, Myers E B, and Ralph D C 2000 *Phys. Rev. Lett.* **84** 3149.

[7] Kiselev S I, Sankey J C, Krivorotov I N, Emley N C, Schoelkopf R J, Buhrman R A, and Ralph D C 2003 *Nature (London)* **425** 380.

[8] Kiselev S I, Sankey J C, Krivorotov I N, Emley N C, Rinkoski M, Perez C, Buhrman R A, and Ralph D C 2004 *Phys. Rev. Lett.* **93** 036601.

[9] Kiselev S I, Sankey J C, Krivorotov I N, Emley N C, Garcia A G F, Buhrman R A, and Ralph D C 2005 *Phys. Rev. B.* **72** 064430.

[10] Lee K J, Deac A, Redon O, Nozieres J P, and Dieny B 2004 *Nature Materials* **3** 877.

[11] Bertotti G, Serpico C, Mayergoyz I D, Magni A, d'Aquino M, and Bonin R 2005 *Phys. Rev. Lett.* **94** 127206.

[12] Berkov D V, and Gorn N L 2008 *J. Phys. D* **41** 164013.

[13] Slavin A, and Tiberkevich V 2009 *IEEE Trans. Magn.* **45** 1875.

[14] León A O, and Clerc M G 2015 *Phys. Rev. B* **91** 014411.

[15] León A O, Clerc M G, and Coulibaly S 2014 *Phys. Rev. E* **89** 022908.

[16] Slonczewski J C 2002 *J. Mag. Mat. Mag.* **247** 324.

[17] Xiao J, Zangwill A, and Stiles M D 2004 *Phys. Rev. B* **70** 172405.

[18] Xiao J, Zangwill A, and Stiles M D 2005 *Phys. Rev. B* **72** 014446.

[19] Xiao J, Zangwill A, and Stiles M D 2007 *Eur. Phys. J. B* **59** 415.

[20] Barnas J, Fert A, Gmitra M, Weymann I, and Dugaev V K 2005 *Phys. Rev. B* **72** 024426.

[21] Kim W, Lee S-W, and Lee K-J 2011 *J. Phys. D* **44** 384001.

[22] Lee S-W, and Lee K-J 2010 *IEEE Trans. Magn.* **46** 2349.

[23] Pismen L M *Patterns and Interfaces in Dissipative Dynamics*, (Springer Series in Synergetics, Berlin Heidelberg 2006).

[24] Lee K J, Deac A, Redon O, Nozieres J P, and Dieny B 2004 *Nature Materials* **3** 877.

F.2.   Parametric Phenomena in Magnetic Nanostripes

Chapter details:

Chapter title: Parametric Phenomena in Magnetic Nanostripes.

Author: Alejandro O. León.

Published in: Springer Proceedings in Physics

Conference: 3rd Dynamics Days South America, Valparaiso 3-7 November 2014

Book title: Nonlinear Dynamics: Materials, Theory and Experiments.

Book editors: Mustapha Tlidi and Marcel Clerc.

Parametric Phenomena in Magnetic Nanostripes

Alejandro O. León

Abstract Systems with a time-modulated injection of energy self-organize into patterns and solitons. Magnetic systems forced by a direct spin-polarized current and a constant external field are equivalent to parametrically driven systems. This parametric equivalence implies that both systems are described by the same model, the *parametrically driven, damped nonlinear Schrödinger* equation, and that they exhibit the same parametric phenomena, which includes patterns and solitons. We review here recent literature on the topic, and we investigate the case of long and narrow magnets. This configuration reduces significantly the critical currents at which self-organization emerges, and it allows the formation of bound states of solitons.

1 Introduction

In the presence of external forcing, magnetic materials exhibit a wide range of dynamical responses which include self-oscillations [1, 2], chaos [3, 4], patterns [5], solitons [6, 7], skyrmions [8] and rogue-waves [9]; this versatility renders magnetic materials an ideal framework to study nonlinear dynamics and self-organization. A particularly promising scenario occurs at nanoscales, where the magnetization is manipulated by effects which are negligible in larger systems, such as the *spin-transfer torque*. This effect occurs when the spins of an electric current interact with the spins of a ferromagnetic medium [10–12]. When the spin of conduction electrons have a preferred orientation—*spin-polarized current*—the spin-transfer torque can generate self-oscillations with microwave frequencies and magnetic reversions [13].

From a dynamical systems viewpoint, spin-transfer torques are non-variational effects that can inject or dissipate the ferromagnetic energy. The first case is important for technological applications since energy injections can induce permanent behaviors such as limit cycles [2, 13] and chaos [14]. In addition, spin-polarized currents

A.O. León (✉)
Departamento de Física, Facultad de Ciencias Físicas y Matemáticas,
Universidad de Chile, Casilla 487-3, Santiago, Chile
e-mail: alejandroleonvega@gmail.com

can switch the magnetization from one equilibrium to another, which is particularly important for the development of memory technologies [12].

The presence of a dissipative spin-transfer torque permits to generate stationary patterns [5], domain walls and dissipative solitons [6]. This rich variety of magnetization textures can be understood because a magnetic medium in presence of spin-polarized direct currents obeys the same equations of macroscopic systems with a time-dependent forcing [6], known as parametrically driven systems [15]. These systems are characterized by oscillating at half the forcing frequency and exhibiting sub-harmonic resonances [15]. In several cases, these resonances induce patterns or Faraday-type waves [16] and solitons [17–20]. A few examples of parametrically driven systems are vibrating fluids [17], nonlinear lattices [21], light pulses in optical fibers [22], optical parametric oscillators [23], and ferromagnetic materials under oscillatory magnetic fields [24, 25]. Parametrically driven systems can be described in a unified manner using the *parametrically driven, damped nonlinear Schrödinger equation* (PDNLS) [26], this model is valid when the forcing frequency is close to twice the natural frequency of oscillations, and the injection and dissipation of energy are small. The PDNLS equation admits several analytic solutions for one-dimensional systems, in particular, expressions for solitons [17, 27] and patterns [28] are known. Hence, the equivalence between parametrically driven systems and magnets forced by a direct spin-polarized current, has permitted to predict a large variety of states in nanomagentism, and to use the PDNLS analytic solutions as approximations for the magnetic states [6].

We review here the parametric equivalence, and apply it to large and narrow magnets driven by spin-polarized currents. Some advantages of this configurations are the stabilization of multiple localized states for long enough magnets, the reduction of critical currents at which patterns and solitons emerge, and the simplicity of one-dimensional systems.

The chapter is organized as follows. In next section we describe the theoretical model of a ferromagnetic medium under spin-polarized currents. In Sect. 3 we review the parametric equivalence and its most important predictions. The discussions and conclusions are left to the final section.

2 Theoretical Model for Magnetization Dynamics

In the continuum approach, magnetic nanostripes are described by their magnetization vector $\mathbf{M}(x', t)$ [1]. Time $t' = \gamma_0 M_s t$ and the space coordinates $x' = l_{ex}x$, where x is the direction of the stripe, are written in terms of the following material properties: the gyromagnetic ratio γ_0, the saturation magnetization M_s and the exchange length l_{ex}. At nanoscales, the magnetization norm $||\mathbf{M}|| = M_s$ is constant within the material, and therefore the dynamical variable is the unitary vector $\mathbf{m} = \mathbf{M}/M_s$. The following phenomenological model, known as *Landau-Lifshitz-Gilbert* (LLG) dimensionless equation, describes the magnetization evolution [1]

$$\partial_t \mathbf{m} = -\mathbf{m} \times \mathbf{h}_{eff} + \alpha \mathbf{m} \times \partial_t \mathbf{m}, \tag{1}$$

where the first term of (1) accounts for precessions around the effective field $\mathbf{h}_{eff}$ defined by

$$\mathbf{h}_{eff} \equiv -\frac{L_0}{\mu_0 M_s^2} \frac{\delta E_M}{\delta \mathbf{m}} = \partial_{xx}\mathbf{m} + \mathbf{h}_0 + \mathbf{h}_D + \beta_{x0} m_x \mathbf{e}_x, \tag{2}$$

and

$$E_M = \frac{\mu_0 M_s^2}{L_0} \int_0^{L_0} \left[\frac{1}{2}|\partial_x \mathbf{m}|^2 - \mathbf{m} \cdot \mathbf{h}_0 - \frac{1}{2}\mathbf{m} \cdot \mathbf{h}_D - \frac{\beta_{x0}}{2} m_x^2 \right] dx, \tag{3}$$

the vectors $\partial_{xx}\mathbf{m}$ and $\mathbf{h}_0$ stand for the exchange and external fields, respectively. The magnetostatic field $\mathbf{h}_D$ is usually a nonlocal function of the magnetization, and it is obtained by solving Maxwell equations inside the material. The magnetocrystaline anisotropy is given by $\beta_{x0} m_x \mathbf{e}_x$, and it favors orientations along the x axis. E_M is the magnetic energy of the material. When the last term of (1) is zero, the magnetization is a Hamiltonian oscillator and the energy is conserved.

The term proportional to α in (1) models dissipation mechanisms [1]. If the external field $\mathbf{h}_0$ is independent of time, then the magnetic energy converges monotonically to its minima $dE_m/dt = -(\alpha \mu_0 M_s^2 / V_0) \int |\partial_t \mathbf{m}|^2 \leq 0$ at a rate proportional to α. Hence, magnetic materials are damped oscillators, and after transients the magnetization reaches its stable equilibrium. One possibility to break the relaxation-type dynamic of the LLG equation is by using a time-dependent external field $\mathbf{h}_0 \rightarrow \mathbf{h}_0(t)$. Under this parametric injection, ferromagnetic media exhibit Faraday-type waves [28], fronts and several types of localized states [24, 26, 27, 29–33]. The case of oscillatory fields has been extensively studied in the literature, and then we will focus on another physical effect that permits to manipulate the magnetization, namely the spin-transfer torque.

Spin-transfer torques emerge in multilayer nanopillars (see Fig. 1). This type of metallic device is composed by two conducting ferromagnetic layers separated by a nonmagnetic metal. The electric current is uniform and it flows perpendicular to the plane of the layers. One magnetic film has *fixed* magnetization and it is used
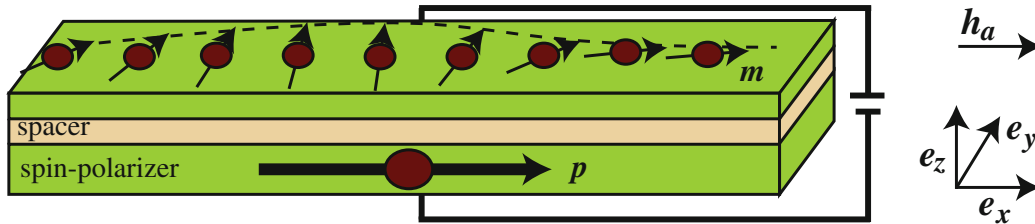

Fig. 1 Nanopillar device. This conducting structure is composed by two magnetic nanostripes and a nonmagnetic spacer. The magnetization is fixed for one ferromagnet, and it is used to polarize the electric current that flows perpendicular to the layers. We are interested on the magnetization dynamics of the second material, which are affected by the electric current and an external field $\mathbf{h}_a$

as a filter (polarizer) for the spins of the electric current. We are interested on the magnetization dynamics of the second material, which is *free* and evolves according to the LLG equation. Spin-polarized currents can be modeled as an additional torque τ_{stt} in the (1). At leading order, this term reads

$$\tau_{stt} = g'\mathbf{m} \times (\mathbf{m} \times \mathbf{p}) \,, \tag{4}$$

where $\mathbf{p}$ is the direction of the spins of the electric currents. The function $g'(\mathbf{m} \cdot \mathbf{p})$, known as *spin-transfer efficiency*, accounts for the details of the transport processes of conduction electrons. There are several expressions in literature [10, 35–40] for g', the simplest one is to approximate $g'(\mathbf{m} \cdot \mathbf{p}) \approx g'(1)$, this approach is known as *sine-approximation*. In this chapter we use this approximation. The parameter $g \equiv g'(1)$ depends on the intensity of the applied electric current and device properties [34]

$$g = \frac{\hbar}{2|e|d_z} \frac{\eta_0 J}{\mu_0 M_s^2},$$

where J is the current density of electrons, d_z the thickness of the free layer and $e < 0$ the electric charge. The current density of electrons J and the parameter g are negative when the electrons flow from the fixed to the free layer. All other transport properties of the materials are summarized in the η_0 coefficient.

2.1 Simplified Model for Magnetization Dynamics in Nanostripes

Let us focus on the nanostripe magnet of Fig. 1. A nanostripe is a large and narrow thin film, satisfying $d_x \gg d_y \gg d_z$ for the lateral dimensions along the respective Cartesian axis. We approximate the magnetostatic field by shape anisotropy terms β_{x1} and β_z, where β_{x1} (β_z) favors (disfavors) configurations along the x axis (z axis). We set both the external field direction $\mathbf{h}_0 = h_0 \mathbf{e}_x$ and the spin-current direction $\mathbf{p} = \mathbf{e}_x$ along the x axis. Under these assumptions, the LLG model simplifies to

$$\partial_t \mathbf{m} = -\mathbf{m} \times \left[(h_0 + \beta_x m_x)\mathbf{e}_x - \beta_z m_z \mathbf{e}_z + \partial_{xx}\mathbf{m}\right] + \alpha\mathbf{m} \times \partial_t\mathbf{m} + g\mathbf{m} \times (\mathbf{m} \times \mathbf{e}_x) \,, \tag{5}$$

where $\beta_x \equiv \beta_{x0} + \beta_{x1}$. This model admits two homogeneous stationary states: $\mathbf{m} = \pm\mathbf{e}_x$ in which the magnetization points parallel (+) and antiparallel (−) to the polarization direction of the current. We concentrate on the first state, however the dynamics of the antiparallel state are equivalent in the appropriate region of the parameter space, due to the symmetry $(\mathbf{h}_a, g) \rightarrow -(\mathbf{h}_a, g)$ of (5).

It is worth noting that we study time-independent forcing mechanisms, namely a direct electric current and a constant magnetic field, and then this systems is not parametrically driven. Even so, using an appropriate change of variables, the system

can be described by the PDNLS equation (as we will see in next section) and then it exhibits the phenomena usually found in parametrically driven systems, such as patterns and solitons [6].

3 Parametric Equivalence

3.1 Stereographic Projection

The Landau-Lifshitz-Gilbert equation conserves the magnetization norm $\partial_t |\mathbf{m}| = (\mathbf{m} \cdot \partial_t \mathbf{m})/|\mathbf{m}| = 0$, and then it can be written in different coordinate systems such as spherical [1, 5], canonical [1], and stereographic variables [1, 41]. In stereographic representation, the equations for magnetization dynamics take the form of a generalized *complex Ginzburg-Landau* model, which is a paradigmatic description of nonlinear oscillators. Figure 2 shows the stereographic representation, which is obtained by projecting the phase space—spherical surface—over the equatorial plane $m_x = 0$, according to [41]

$$a(x, t) = \frac{m_y + im_z}{1 + m_x}. \tag{6}$$

The complex field a represents deviations from the parallel state $\mathbf{m} = \mathbf{e}_x$. Replacing formula (6) in (5) and after straightforward calculations one obtains (the generalized *complex Ginzburg-Landau* model)

$$(i + \alpha)\, \partial_t a = (ig - h_a)\, a - \frac{\beta_z}{2}\, (a - \bar{a})\, \frac{1 + a^2}{1 + |a|^2} - \beta_x a \frac{1 - |a|^2}{1 + |a|^2} + \partial_{xx} a - 2 \frac{\bar{a}\, (\partial_x a)^2}{1 + |a|^2}, \tag{7}$$
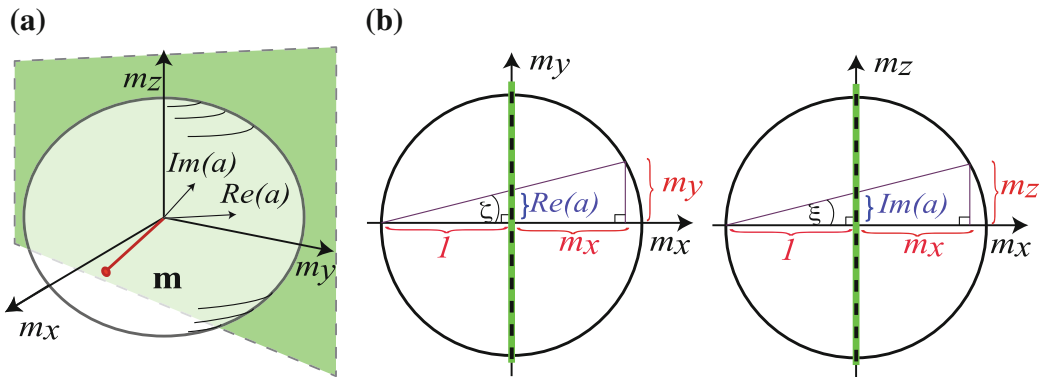
(a)   **(b)**

Fig. 2 Stereographic representation. **a** The unitary spherical surface $m_x^2 + m_y^2 + m_z^2 = 1$ is mapped to the equatorial plane defined by $m_x = 0$. **b** The projections on the complex field $a = (m_y + im_z)/(1 + m_x)$

where the term proportional to β_x is a nonlinear saturation. The term proportional to β_z breaks the phase invariant $a \rightarrow ae^{i\phi_0}$, and it is usually associated to parametric forcing. The coefficients α and g break the temporal reversion invariance $(t, a) \rightarrow (-t, \bar{a})$. Notice that in the absence of spin transfers ($g = 0$ but $\alpha \neq 0$) the (7) has the structure of a variational (relaxation type) wave equation.

3.1.1   PDNLS-Limit

A notable limit of (7) is obtained for small amplitude magnetic motions and gradients $|\partial_x a| \ll |a| \ll 1$ and small anisotropy $\beta_z \ll 1$; in this case we can replace $A \equiv ae^{i\pi/4}/\sqrt{2\beta_x + \beta_z}$ into (7) and after simplifications one obtains the *parametrically driven, damped nonlinear Schrödinger* equation

$$\partial_t A = -i \left(\nu A + A|A|^2 + \partial_{xx}A \right) - \mu A + \gamma \bar{A}, \tag{8}$$

where $\nu \equiv -h_a - \beta_x - \beta_z/2$ is the detuning between half the forcing frequency and the response frequency in usual parametrically driven systems. The dissipation and parametric injection are given by $\mu \equiv -g - \alpha\nu$ and $\gamma \equiv \beta_z/2$, respectively. The equation scales as $\nu \sim \mu \sim \gamma \sim |A|^2 \sim \partial_{xx} \sim \partial_t$, and all the higher order terms have been neglected.

It is worth noting that in the present case the dissipation is an experimental control parameter, while the injection $\gamma \equiv \beta_z/2$ is not. The nanostripe geometry is between two natural limits: the nanowire and the two-dimensional cross-section device. For the nanowires we have $d_y \sim d_z \ll d_x$ and the anisotropies are $\beta_z \approx 0$ and $\beta_x \equiv \beta_{x0} + \beta_{x1} \approx \beta_{x0} + 1$. In this case the injection γ is small and the required currents are also small. On the other hand, for two-dimensional cross-section nanopillars, we have $d_z \ll d_y \sim d_x$, and $\beta_z \approx 1$ and $\beta_x \approx \beta_{x0}$. Then, the two-dimensional magnets have a bigger parametric injection and higher electric currents are necessary to obtain the scaling $\gamma \sim \mu$.

3.2   Interpretation in Terms of Equivalent Systems

The simple stereographic projection presented above permitted us to obtain the PDNLS model in magnetic media forced by direct currents. Another approach to derive this equation is to notice that the spin-transfer torque has the form of a pseudo torque (non-inertial effect), and then the LLG equation can be transformed under an appropriate change of reference frames into a rotating system.

Let us consider a stripe rotating with constant angular velocity along the x axis direction $\Omega = \Omega_0 \mathbf{e}_x$, in presence of an external field $\mathbf{h}'_a = (h_a + \Omega_0)\mathbf{e}_x$, as shown in Fig. 3. For this system, the magnetization equations can be written in two frames: the inertial coordinate systems S' defined by $\{\mathbf{e}'_x, \mathbf{e}'_y, \mathbf{e}'_z\}$ and the co-movil coordinate system S given by the unit vectors $\{\mathbf{e}_x, \mathbf{e}_y, \mathbf{e}_z\}$, which is fixed to the stripe. In the first
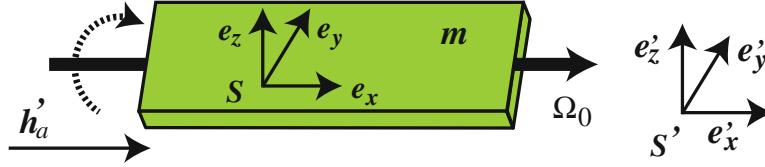
Fig. 3 Rotating magnetic stripe. The magnetization equations describe a parametrically driven device in the inertial frame S', on the other hand the magnetic equations in the co-movil frame S are the same as (5)

frame we have

$$\left(\frac{\partial \mathbf{m}}{\partial t}\right)\Big|_{S'} = -\mathbf{m} \times \mathbf{h}'_{eff}(t) + \alpha \mathbf{m} \times \left(\frac{\partial \mathbf{m}}{\partial t}\right)\Big|_{S'}, \tag{9}$$

$$\mathbf{h}'_{eff}(t) = (h_0 + \Omega_0 + \beta_x m_x)\mathbf{e}_x - \beta_z (\mathbf{m} \cdot \mathbf{e}_z(t)) \mathbf{e}_z(t) + \partial_{xx}\mathbf{m}. \tag{10}$$

Note that the projection over the fixed axis of the inertial frame produces a temporal dependence of the form

$$(\mathbf{m} \cdot \mathbf{e}_z(t)) \, \mathbf{e}_z(t) = \beta_z(-\sin(\Omega_0 t)m'_y + \cos(\Omega_0 t)m'_z)(-\sin(\Omega_0 t)\mathbf{e}'_y + \cos(\Omega_0 t)\mathbf{e}'_z).$$

Let us remark that the anisotropy field is a function of time, then, rotating stripes are parametrically driven systems. Moreover, the frequency ω of the anisotropy vector oscillations is close to twice the rotating frequency $\omega = 2(\Omega_0 + \nu)$, where ν is the detuning parameter defined in (8). Hence, the oscillation envelope of the magnetization obeys the PDNLS equation (8).

The equation (9) can be written in the co-movil system S. After transforming the temporal derivatives of vectors according to $\partial_t|_{S'} = \partial_t|_S + \Omega \times$ [15], we obtain

$$\left(\frac{\partial \mathbf{m}}{\partial t}\right)\Big|_S = -\mathbf{m} \times \mathbf{h}_{eff} + \alpha \mathbf{m} \times \left(\frac{\partial \mathbf{m}}{\partial t}\right)\Big|_S - \alpha \Omega_0 \mathbf{m} \times (\mathbf{m} \times \mathbf{e}_x), \tag{11}$$

$$\mathbf{h}_{eff} = (h_0 + \beta_x m_x)\mathbf{e}_x - \beta_z m_z \mathbf{e}_z + \partial_{xx}\mathbf{m}, \tag{12}$$

where the last term of (11) is the non-inertial torque originated in the transformation of the damping torque. The transformation of the left hand side of (9) is only a shift of the external field. Note that (11) and (12) are exactly the same LLG model of the spin-transfer driven stripe (5), where the intensity of the spin-transfer is proportional to the angular velocity $g = -\alpha \Omega_0$.

In brief, magnetic stripes driven by spin-transfer torques are equivalent to rotating stripes without spin-transfer torques. Moreover, in an appropriate reference frame both physical systems obey the same equations. Since rotating stripes are parametrically driven systems, they exhibit sub-harmonic instabilities, solitons, and patterns.

The PDNLS amplitude equation has been used to predict self-organization in several contexts. In the next subsection we review some of the solutions of this equation and compare them with the phenomena observed in (5).
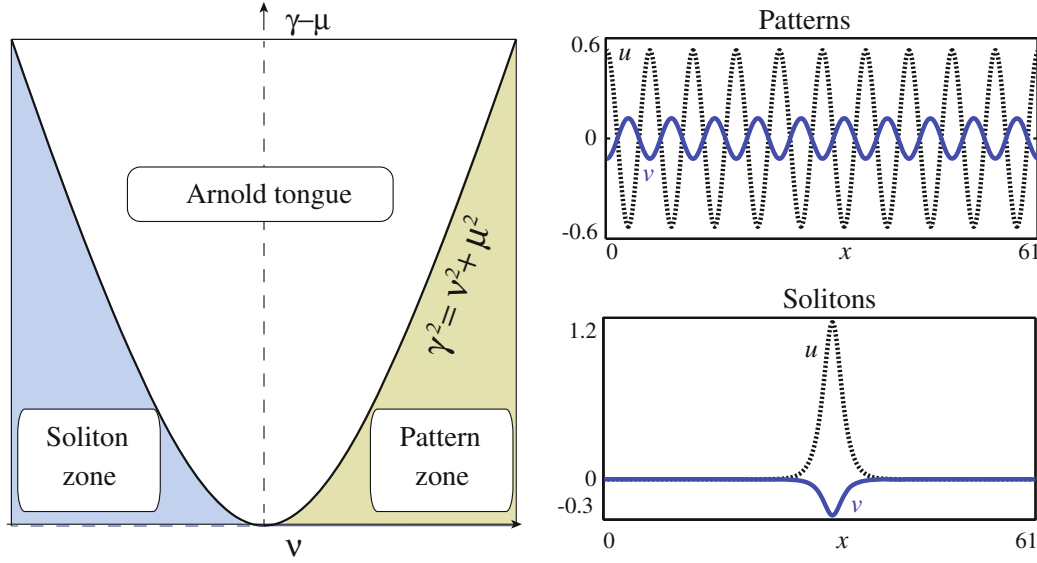
Fig. 4 Bifurcation diagram of the PDNLS model. The *right panel* shows dissipative solitons and patterns obtained from (8). Parameter values are $\gamma = 0.5$, $\mu = 0.45$, and $\nu = -0.5$ and $\nu = 1$ for solitons and patterns, respectively

3.3 Parametric Phenomena in Magnetic Nanostripes

We start writing the PDNLS equation in terms of the real and imaginary parts of the amplitude $A = u + iv$,

$$\partial_t u = (\gamma - \mu)u + (\nu + \partial_{xx})v + v(u^2 + v^2),$$
$$\partial_t v = -(\nu + \partial_{xx})u - (\gamma + \mu)v - u(u^2 + v^2). \tag{13}$$

The stability of the trivial state $u = v = 0$ is determined by its eigenvalues

$$\lambda_\pm = -\mu \pm \sqrt{\gamma^2 - (\nu - k^2)^2}, \tag{14}$$

which predict several bifurcations. The first one, is an Andronov-Hopf instability for $\mu \geq 0$. When this instability saturates, the system exhibits uniform self-oscillations [13] with frequency $\omega_0 = \sqrt{\nu^2 - \gamma^2}$. When the bifurcation is not saturated, the magnetization switches to another equilibria. In this regime, the magnetization behaves as a nonlinear oscillator with negative damping [2]. Note that the control parameter of this bifurcation requires is negative dissipation, which cannot be obtained in parametrically driven systems.

Another bifurcation predicted by expression (14) is a stationary instability when $\gamma \geq \sqrt{\nu^2 + \mu^2}$, this region is the well-known Arnold tongue (see Fig. 4). The critical curve describing the Arnold tongue in the magnetic system is $g^2 + [h_a - (\beta_x + \beta_z/2)]^2 = \beta_z^2/4$. Inside this region several states appear, such as localized states, patterns, and domain walls [6, 26].

3.3.1 Pattern Formation

The eigenvalues of expression (14) reveal a third bifurcation of the magnetic system, which occurs for $\gamma \geq \mu$ and positive detuning $\nu \geq 0$. This instability is characterized by the emergence of spatially periodic patterns with intrinsic wavenumber $\sqrt{\nu}$. At the onset of this bifurcation, a reduced description in terms of the pattern amplitude $T(t)$ is obtained using standard techniques of weakly nonlinear analysis. Moreover introducing the ansatz

$$\begin{pmatrix} u \\ v \end{pmatrix} = Te^{i\sqrt{\nu}x}\begin{pmatrix} 1 \\ 0 \end{pmatrix} - \frac{3}{2\mu}T|T|^2 e^{i\sqrt{\nu}x}\begin{pmatrix} 0 \\ 1 \end{pmatrix} + \frac{T^3}{8\nu}e^{3i\sqrt{\nu}x}\begin{pmatrix} 1 \\ 0 \end{pmatrix} + c.c. + \cdots, \quad (15)$$

in (13), one gets the following Solvability condition for the envelope $T(t)$ [28]

$$\partial_t T = (\gamma - \mu)T - \frac{9}{2\mu}T|T|^4. \quad (16)$$

This equation predicts the formation of a stable pattern for $\gamma \geq \mu$. Figure 4 shows this solution, which at leading order reads $A \approx 2(2\mu(\gamma - \mu)/9)^{1/4}\cos(\sqrt{\nu}x)$. This bifurcation was studied in detail in [5] for both the one and two-dimenssions devices. In the first case, the full solution of patterns obtained from (5) is [5]

$$m_y \approx 2\sqrt[4]{\frac{4\beta_z\,(g + \beta_z/2)}{(6\beta_x + 3\beta_z - 2\nu^2)^2}}\,\cos(\nu x), \quad (17)$$

where $m_y \approx -m_z$ and $m_x \approx 1 - (m_y^2 + m_z^2)/2$. This solution is exactly the same as the PDNLS solution in the limit $\nu \ll 1$.

Let us remark that the critical current of the spatial instability is controlled by the perpendicular anisotropy of the stripe $g = \beta_z/2$. The perpendicular anisotropy is fixed for square cross-section devices, but it can be significantly decreased for stripes by adjusting the d_y length.

3.3.2 Dissipative Solitons

The PDNLS equation (8) can be written in the terms of the modulus and phase of its order parameter $A = Re^{i\phi}$, in this case

$$\partial_t R \;\; = -\mu R + 2\partial_x R \partial_x \phi + R\partial_{xx}\phi + \gamma R\cos(2\phi), \quad (18)$$
$$R\partial_t \phi = -\nu R - R^3 - \partial_{xx}R + R(\partial_x\phi)^2 - \gamma R\sin(2\phi), \quad (19)$$

One simple solution of this equation is the uniform-phase soliton [24, 26]
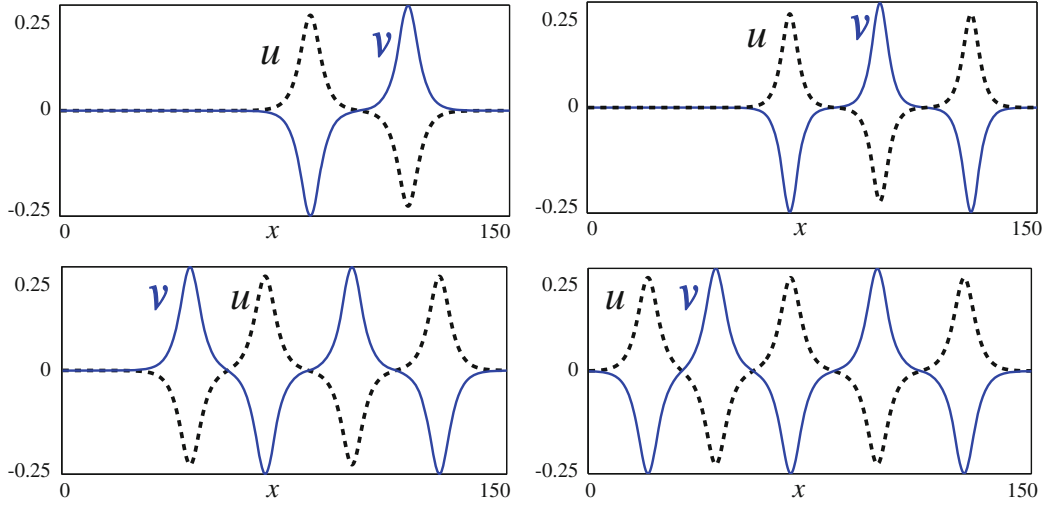
Fig. 5 Soliton-Antisoliton bound states. Snapshots of multiple localized solutions obtained from the LLG (5). Parameters are $g = -0.49781$, $h_a = -0.939895$, $\beta_x = 0.5$, $\beta_z = 1$, and $\alpha = 0.05$

$$\sin(2\phi_s) = \mu/\gamma,$$
$$R_s(x) = \sqrt{2\delta}\text{sech}(\sqrt{\delta}x), \tag{20}$$

where $\delta = -\nu + \sqrt{\gamma^2 - \mu^2}$. The right panel of Fig. 4 shows the typical profile of solitons given by the set of (20). Soliton amplitude and width are controlled by the detuning and dissipation, or equivalently by the external field and the spin-polarized current. Typical widths are about 30 nm. The uniform phase solitons $\partial_x\phi = \partial_{xx}\phi = 0$ become unstable when the size of the system surpasses a critical value, and a phase structure emerges [27, 33]. According to our simulations, nanostrips are usually small enough to ensure the stability of the uniform phase state. The magnetization components take the following form for the soliton solution

$$m_x = \frac{2\beta_x + \beta_z - R_s^2(x)}{2\beta_x + \beta_z + R_s^2(x)},$$
$$\begin{pmatrix} m_y \\ m_z \end{pmatrix} = \frac{2R_s(x)\sqrt{2\beta_x + \beta_z}}{2\beta_x + \beta_z + R_s^2(x)} \begin{pmatrix} \cos\varphi_s \\ \sin\varphi_s \end{pmatrix}, \tag{21}$$

One experimentally accessible quantity in nanopillars is the magentoresistance. The magnetoresistance depends on the magnetic configuration, and it can be approximated in terms of the average magnetization m_x^{av} along the polarization of the current, $\delta r = (1 - m_x^{av})/2$. Hence, the soliton fingerprint is a magnetoresistance similar to the one of the parallel state which increases with the square of the amplitude, it is $\delta r \sim \delta = h_a + \beta_x + \beta_z/2 + \sqrt{(\beta_z/2)^2 - g^2}$. This is a prediction of the parametric equivalence [6].

3.3.3 Soliton-Antisoliton Bound States

In parametrically driven systems, multiple coexisting solitons can emerge and interact among them [29, 42–46] and with walls [45–47]. The force between two remote solitons has been studied experimentally and theoretically in [42]. This interaction is attractive for soliton-soliton pairs [42], it is, for states that can be approximated by $R(x) \approx R_s(x_1) + R_s(x_2)$ where x_1 and x_2 are the positions of soliton cores. As a result of the attraction, solitons collapse [42, 43]. On the other hand, for solitons-antisoliton pairs, where $R(x) \approx R_s(x_1) - R_s(x_2)$, the interaction is repulsive [42, 44]. At short ranges, a third possibility exists, namely the bound states [29]. In the case of magnetic nanostripes, multiple soliton-antisoliton solutions can be found. Figure 5 illustrates these states, obtained from direct integration of (5). The multiple bumps are observed in a wide region of the parameter space, while we have not observed the soliton-soliton pair for this system. It is worth noting that this multi-stability of solitary structures makes the nanostripe a magnetoresistive memory of multiple levels.

4 Conclusions

Magnetic media forced by spin-polarized currents are equivalent to parametrically driven systems. This equivalence explains the existence of a wide variety of states in nanopillars, such as patterns and solitons. In this chapter we reviewed the parametric equivalence of [6], and we applied it to nanostripes. This configuration admits a one-dimensional description, moreover it reduces significantly the critical currents at which self-organization emerges. We found that nanostripe geometry permits the existence of soliton-antisoliton bound states. The creation and manipulation of solitary structures could be important for further developments of memory technologies and information carrying. Work in this direction is in progress.

References

1. I.D. Mayergoyz, G. Bertotti, C. Serpico, *Nonlinear Magnetization Dynamics in Nanosystems* (Elsevier, Oxford, 2009)
2. A. Slavin, V. Tiberkevich, Nonlinear auto-oscillator theory of microwave generation by spin-polarized current. IEEE Trans. Magn. **45**, 1875 (2009)
3. L.F. Álvarez, O. Pla, O. Chubykalo, Quasiperiodicity, bistability, and chaos in the Landau-Lifshitz equation. Phys. Rev. B **61**, 11613 (2000)
4. J. Bragard, H. Pleiner, O.J. Suarez, P. Vargas, J.A.C. Gallas, D. Laroze, Chaotic dynamics of a magnetic nanoparticle. Phys. Rev. E **84**, 037202 (2011)

5. A.O. León, M.G. Clerc, S. Coulibaly, Dissipative structures induced by spin-transfer torques in nanopillars. Phys. Rev. E **89**, 022908 (2014)

6. A.O. León, M.G. Clerc, Spin-transfer-driven nano-oscillators are equivalent to parametric resonators. Phys. Rev. B **91**, 014411 (2015)

7. P.-B. He, W.M. Liu, Nonlinear magnetization dynamics in a ferromagnetic nanowire with spin current. Phys. Rev. B **72**, 064410 (2005)

8. R.E. Troncoso, A.S. Núñez, Thermally assisted current-driven skyrmion motion. Phys. Rev. B **89**, 224403 (2014)

9. F. Zhao, Z.D. Li, Q.Y. Li, L. Wen, G. Fu, W.M. Liu, Magnetic rogue wave in a perpendicular anisotropic ferromagnetic nanowire with spin-transfer torque. Ann. Phys. **327**, 2085 (2012)

10. J.C. Slonczewski, Emission of spin waves by a magnetic multilayer traversed by a current. J. Magn. Mat. Mag. **159**, L1 (1996)

11. L. Berger, Emission of spin waves by a magnetic multilayer traversed by a current. Phys. Rev. B **54**, 9353 (1996)

12. M.D. Stiles, J. Miltat, in *Spin Dynamics in Confined Magnetic Structures*, edited by B. Hillebrands, A. Thiaville (Springer, Berlin, 2006) vol. 3, Chap. 7

13. S.I. Kiselev, J.C. Sankey, I.N. Krivorotov, N.C. Emley, R.J. Schoelkopf, R.A. Buhrman, D.C. Ralph, Microwave oscillations of a nanomagnet driven by a spin-polarized current. Nature (London) **425**, 380 (2003)

14. D. Berkov, N. Gorn, Transition from the macrospin to chaotic behavior by a spin-torque driven magnetization precession of a square nanoelement. Phys. Rev. B **71**, 052403 (2005)

15. L.D. Landau, E.M. Lifshiftz , *Mechanics*, vol. 1 (Course of Theoretical Physics) (Pergamon Press 1976)

16. M. Faraday, On a peculiar class of acoustical figures; and on certain forms assumed by groups of particles upon vibrating elastic surfaces. Philos. Trans. R. Soc. Lond. **121**, 299 (1831)

17. J.W. Miles, Parametrically excited solitary waves. J. Fluid Mech. **148**, 451 (1984)

18. I.V. Barashenkov, E.V. Zemlyanaya, Traveling solitons in the damped-driven nonlinear Schrödinger equation. SIAM J. Appl. Math. **64**, 800 (2004)

19. I.V. Barashenkov, E.V. Zemlyanaya, T.C. van Heerden, Time-periodic solitons in a damped-driven nonlinear Schrödinger equation. Phys. Rev. E **83**, 056609 (2011)

20. I.V. Barashenkov, E.V. Zemlyanaya, Soliton complexity in the damped-driven nonlinear Schrödinger equation: stationary to periodic to quasiperiodic complexes. Phys. Rev. E **83**, 056610 (2011)

21. B. Denardo, B. Galvin, A. Greenfield, A. Larraza, S. Putterman, W. Wright, Observations of localized structures in nonlinear lattices: domain walls and kinks. Phys. Rev. Lett. **68**, 1730 (1992)

22. J.N. Kutz, W.L. Kath, R.-D. Li, P. Kumar, Long-distance pulse propagation in nonlinear optical fibers by using periodically spaced parametric amplifiers. Opt. Lett. **18**, 802 (1993)

23. S. Longhi, Stable multipulse states in a nonlinear dispersive cavity with parametric gain. Phys. Rev. E **53**, 5520 (1996)

24. I.V. Barashenkov, M.M. Bogdan, V.I. Korobov, Stability diagram of the phase-locked solitons in the parametrically driven, damped nonlinear Schrödinger equation. Europhys. Lett. **15**, 113 (1991)

25. S.R. Woodford, I.V. Barashenkov, Stability of the Bloch wall via the Bogomolnyi decomposition in elliptic coordinates. J. Phys. A: Math. Theory **41**, 185203 (2008)

26. M.G. Clerc, S. Coulibaly, D. Laroze, Localized states beyond the asymptotic parametrically driven amplitude equation Phys. Rev. E **77**, 056209 (2008); Parametrically driven instability in quasi-reversible systems. Int. J. Bifurc. Chaos **19**, 3525 (2009); Localized states and non-variational IsingBloch transition of a parametrically driven easy-plane ferromagnetic wire. Physica D **239**, 72 (2010)

27. M.G. Clerc, S. Coulibaly, M.A. Garcia-Nustes, Y. Zárate, Dissipative localized states with Shieldlike phase structure. Phys. Rev. Lett. **107**, 254102 (2011)

28. P. Coullet, T. Frisch, G. Sonnino, Dispersion-induced patterns. Phys. Rev. E **49**, 2087 (1994)

29. D. Urzagasti, D. Laroze, M.G. Clerc, S. Coulibaly, H. Pleiner, Two-soliton precession state in a parametrically driven magnetic wire. J. Appl. Phys. **111**, 07D111 (2012)
30. D. Urzagasti, D. Laroze, M.G. Clerc, H. Pleiner, Breather soliton solutions in a parametrically driven magnetic wire. Europhys. Lett. **104**, 40001 (2013)
31. M.G. Clerc, S. Coulibaly, D. Laroze, Localized waves in a parametrically driven magnetic nanowire. Europhys. Lett. **97**, 30006 (2012)
32. A.O. León, M.G. Clerc, S. Coulibaly, Traveling pulse on a periodic background in parametrically driven systems. Phys. Rev. E. **91**, 050901 (2015)
33. M.G. Clerc, M.A. Garcia-Ñustes, Y. Zárate, S. Coulibaly, Phase shielding soliton in parametrically driven systems. Phys. Rev. E. **87**, 052915 (2013)
34. D.V. Berkov, J. Miltat, Spin-torque driven magnetization dynamics: micromagnetic modeling. J. Magn. Mag. Mater. **320**, 1238 (2008)
35. J.C. Slonczewski, Currents and torques in metallic magnetic multilayers. J. Magn. Magn. Mag. **247**, 324 (2002)
36. J. Xiao, A. Zangwill, M.D. Stiles, Boltzmann test of Slonczewskis theory of spin-transfer torque. Phys. Rev. B **70**, 172405 (2004)
37. J. Xiao, A. Zangwill, M.D. Stiles, Macrospin models of spin transfer dynamics. Phys. Rev. B **72**, 014446 (2005)
38. J. Barnas, A. Fert, M. Gmitra, I. Weymann, V.K. Dugaev, From giant magnetoresistance to current-induced switching by spin transfer. Phys. Rev. B **72**, 024426 (2005)
39. S.-W. Lee, K.-J. Lee, Effect of angular dependence of spin-transfer torque on zero-field microwave oscillation in symmetric spin-valves. IEEE Trans. Magn. **46**, 2349 (2010)
40. W. Kim, S-W. Lee, K-J. Lee, J. Micromagnetic modelling on magnetization dynamics in nanopillars driven by spin-transfer torque. Phys. D **44**, 384001 (2011)
41. M. Lakshmanan, The fascinating world of the LandauLifshitzGilbert equation: an overview. Philos. Trans. R. Soc. A **369**, 1280 (2011)
42. M.G. Clerc, S. Coulibaly, N. Mujica, R. Navarro, T. Sauma, Soliton pair interaction law in parametrically driven Newtonian fluid. Philos. Trans. R. Soc. A **367**, 3213 (2009)
43. M.G. Clerc, S. Coulibaly, L. Gordillo, N. Mujica, R. Navarro, Coalescence cascade of dissipative solitons in parametrically driven systems. Phys. Rev. E **84**, 036205 (2001)
44. D. Urzagasti, A. Aramayo, D. Laroze, Solitonantisoliton interaction in a parametrically driven easy-plane magnetic wire. Phys. Lett. A **378**, 2614 (2014)
45. X. Wang, R. Wei, Observations of collision behavior of parametrically excited standing solitons. Phys. Lett. A **192**, 1 (1994)
46. W. Wang, X. Wang, J. Wang, R. Wei, Dynamical behavior of parametrically excited solitary waves in Faraday s water trough experiment. Phys. Lett. A **219**, 74 (1996)
47. L. Gordillo, M.A. Garcia-Nustes, Dissipation-Driven Behavior of Nonpropagating Hydrodynamic Solitons Under Confinement. Phys. Rev. Lett. **112**, 164101 (2014)

.